New approach for efficient design of stainless steel RHS and SHS elements

DOCTORAL THESIS

Doctoral thesis by:
Itsaso Arrayago Luquin

Supervised by:
Esther Real Saladrigas

Barcelona, September 2016

Universitat Politècnica de Catalunya
Department of Civil and Environmental Engineering

ABSTRACT

This thesis investigates the cross-section and member behaviour of cold-formed stainless steel tubular structural elements with Rectangular and Square Hollow Sections and proposes an alternative and more efficient design approach. Combined with aesthetic appeal, exceptional mechanical properties and excellent corrosion and fire resistances, efficient design methods present stainless steel as an attractive alternative to the usual carbon steel for structural applications.

Exhaustive studies of the nonlinear stress-strain behaviour and the analytical modelling of this response are presented for different stainless steel alloys. The study was based on over 600 experimental stress-strain curves obtained from the literature and complemented with 42 tensile coupon tests. Although the material model currently included in Annex C of EN1993-1-4 (2006) was found to accurately represent the measured stress-strain curves for the different stainless steel grades and material types, revised predictive equations were proposed for the strain hardening parameters *n* and *m* and for the tensile strength and ultimate strain for ferritic stainless steels.

A comprehensive experimental programme on five different cross-sections of ferritic stainless steel grade EN1.4003 tubular elements is also described. The actual geometry and initial geometric imperfections were carefully measured and the material response of flat and corner regions of each section were characterized by conducting 20 tensile tests on coupons extracted from the cross-sections. The cross-sectional behaviour was investigated through 10 stub column tests under pure compression and 16 subjected to combined loading conditions, while 8 beams were tested under four-point bending configuration and 4 subjected to three-point bending loading conditions. At member level, the bending moment redistribution capacity of ferritic continuous beams was investigated by conducting 9 five-point bending tests. Finally, 12 tests were conducted on ferritic stainless steel columns to determine the behaviour of members subjected to concentric and eccentric compression loads. Additional data on austenitic, ferritic

and duplex stainless steel elements was generated from parametric studies based on finite element (FE) models validated from the conducted experiments.

The assessment of the codified design expressions was derived by comparing experimental and numerical strengths with the calculated resistance predictions for stainless steel cross-sections and members subjected to different loading conditions. Results demonstrated that predictions are noticeably conservative for stocky and slender cross-sections since enhanced material properties are not considered and the susceptibility of cross-sections to local buckling is underestimated. Thus, a full slenderness range Direct Strength Method (DSM) approach was proposed for stainless steel RHS and SHS cross-sections and members based on the same strength curve for all loading conditions. The proposed approach was found to be more accurate for cross-sections, columns and beam-columns since strain hardening effects are incorporated and due to the fact that the actual stress distribution of the cross-section is considered when determining the slenderness. The reliability of the approach was demonstrated by statistical analyses, enabling its use in structural design standards.

Finally, the applicability of design approaches based on global plastic analysis to stainless steel continuous beams was assessed. The analysis of continuous beam strengths demonstrated that capacity predictions based on the first hinge formation result in a considerable overconservatism and that traditional plastic design can be safely applied with the Class 1 cross-section limit provided in EN1993-1-4 (2006). However, it was also demonstrated that the best capacity predictions are obtained for design methods including both bending moment redistribution and strain hardening effects, such as the Continuous Strength Method for indeterminate structures or the proposed DSM-based approach, which were statistically validated.

ACKNOWLEDGEMENTS

This work was carried out under the supervision of Prof. Esther Real, Professor at the Department of Civil and Environmental Engineering at Universitat Politècnica de Catalunya (UPC). Her advice, help and support were essential during this project. I would like to express my sincere and special gratitude for everything I have learned from her in addition to steel structures.

The financial support received from the Ministerio de Economía y Competitividad (Spain) under the Project BIA 2012-36373 is hereby acknowledged and I would also like to highlight the financial support provided by the Universitat Politècnica de Catalunya (UPC) and the Secretaria d'Universitats i de Recerca del Departament d'Economia i Coneixement de la Generalitat de Catalunya i del Fons Social Europeu through the FI-DGR 2014 grant.

I am also really thankful to Prof. Enrique Mirambell for the help he provided and to Rolando Chacón, from the "Steel Team", who always had a helpful answer to all my questions.

Support from technicians at the Laboratori de Tecnologia d'Estructures Luís Agulló is acknowledged as well, especially the continuous help received from Tomàs. The experimental programmes would not have been possible without them.

I would also like to express my sincere gratitude to Prof. Kim Rasmussen, from the University of Sydney, not only for having hosted me for six months but for always providing the necessary guidance and patience to help me during my overseas adventure; and to Prof. Leroy Gardner, at the Imperial College London, for the coupon tests and subsequent analysis of the results.

Finally, I would like to express my heartfelt thankfulness to my family and Diego, who sincerely tried to understand what all this was about and for becoming true *stainless steel believers*. This thesis is dedicated to them with all my love for their unconditional support and continuous encouragement.

CONTENTS

CHAPTER 1

Introduction

1.1 Background

Stainless steels are iron alloys with a minimum chromium content of 10.5% that were developed from the cooperation between scientists and metallurgists around the world in the early 1910s. The alloyed chromium element in the microstructure of the different grades is responsible for the corrosion resistance property shown by stainless steels, forming a self-repairing rich oxide layer on its surface when exposed to air or any other oxidising environment. This layer protects the material from further reaction with the environment, providing thus the characteristic corrosion resistance. Including additional alloying elements such as nickel, molybdenum, titanium and copper, different mechanical and physical properties are obtained, providing a wide range of stainless steel grades suitable for several specific uses. The appropriate stainless steel grade needs to be selected for each particular application considering the aggressiveness of the environment, the fabrication route, required surface finish and the future maintenance of the structure.

Stainless steels are usually grouped into five different families according to their microscopic structure, namely austenitic, ferritic, duplex, martensitic and precipitation hardening, being austenitic and duplex stainless steels the most widely used for structural applications. Nickel is one of the principal components of austenitic stainless steels and the reason for their reasonable high cost. In opposition, the low nickel content that ferritic grades exhibit offers a lower and more stable market price while maintaining good mechanical and corrosion

resistances. This proves ferritic stainless steels to be an attractive alternative for many applications replacing austenitic grades.

1.2 Structural applications of stainless steel alloys

Stainless steel has been increasingly used in the construction industry given the combination of aesthetic appeal, favourable mechanical properties and excellent corrosion and fire resistances. Early structural applications of stainless steel can be found in the stabilisation of the dome and supporting structure of St. Paul's Cathedral in London in 1925, the cladding of the Chrysler Building in New York in 1929 or the exterior surface of the Gateway Arch in St. Louis, Missouri, in the early 1960s. However, more recent structural applications of stainless steel alloys can be found in structures situated in aggressive environments, explosion and impact resistant structures and pedestrian bridges.

Recent examples of stainless steel applications can be found in the refurbishments of the façades of two Brazilian stadiums, Governador Plácido Castelo Stadium - Castelão Arena, Fortaleza in Ceará (Brazil) and the Allianz Parque, Palmeiras Stadium in São Paulo (Brazil), made from the highly alloyed ferritic grade 444 (EN1.4521) to provide the necessary corrosion resistance of urban environments. Figure 1.1 shows the Chimpanzee Sanctuary of the Taronga Zoo in Sydney (Australia), refurbished in 2012 with a stainless steel wire mesh system made from 304 (EN1.4301) and 316 (EN1.4401) austenitic stainless steels. These grades met the required mix of strength and transparency and the corrosion resistance demand of the coastal climate.

Fig. 1.1. Enclosure structure in Taronga Zoo, Sydney (Australia). (Image by Ronstan Tensile Architecture)

One of the most recent applications of structural stainless steel in pedestrian bridges can be found in Águilas (Spain). Built in 2015, it is made from the duplex grade EN1.4462. The bridge exhibits a span length equal to 35m, it is 3.8m wide and the resisting structure consists of a steel box girder with lateral girders, as shown in Figure 1.2.

a) General view of the pedestrian bridge. (Image by http://picssr.com)

b) Bottom structural view of the pedestrian bridge. (Image by VALTER, Valenciana de Estructuras)

Fig. 1.2. Duplex stainless steel pedestrian bridge in Águilas (Spain).

1.3 Research objectives

The main objectives of the addressed thesis are to understand the general behaviour of stainless steel Rectangular and Square Hollow Section (RHS and SHS) cross-sections and members and to provide efficient design expressions that account for the specific behaviour of these corrosion resistant materials. The objectives, subdivided in general and specific objectives, are described in this section.

1.3.1 General objectives

Efficient design of structures is one of the mainstays in design practise, regardless the considered construction material. However, given the high material cost of stainless steel in comparison to carbon steel, the development of efficient design expression is more critical. Although ferritic stainless steels, with little or no nickel content, have substantially lower initial material cost compared to the more common stainless steel grades, the development of design expressions that include all its specific features is key for stainless steels to be considered as feasible alternative for structural applications. With efficient design expressions that account for the nonlinear stress-strain response and strain hardening effects, stainless steels would lead to more efficient, economic and sustainable structural designs. Thus, the different research topics considered in this thesis have been focused towards the main objective of understanding the cross-sections and member behaviour of stainless steel RHS and SHS elements in order to identify the shortcomings of the current design specifications and develop alternative guidance to overcome these limitations. More efficient design methods would lead to less tonnage use of the material for the same applied structural load levels, considerably reducing initial material costs.

1.3.2 Specific objectives

The specific objectives of this thesis are the following:

- Determination of the constitutive equation for different stainless steels grades, especially ferritics, through collected information and additional tensile tests. Identification and revision of the required expressions for the future amendments of Annex C of EN1993-1-4 (2006).

- Strengthen the available experimental data on ferritic stainless steel cross-sections and members by conducting an experimental programme that will allow a better understanding of the behaviour of these less ductile stainless steel grades.

- Development of new and efficient design approaches for the determination of the cross-sectional response of stainless steel RHS and SHS that consider strain hardening and local buckling effects. Compression, bending and combined loading conditions and different stainless steel grades will be contemplated, and the proposed approach will be statistically validated.

- Development of alternative and efficient design methods for stainless steel RHS and SHS members in compression and combined loading conditions. These new approaches need to

contemplate strain hardening effects in members stable enough to reach partial yielding of the cross-sections and they will be statistically validated.

- Assessment of the applicability of the design methods based on global plastic analysis, currently not allowed in EN1993-1-4 (2006), to stainless steel RHS and SHS continuous beams. Methods including bending moment redistribution and strain hardening effects will also be contemplated in order to define the most accurate and efficient design approach for stainless steel indeterminate structures.

1.4 Methodology

The methodology to be developed in order to reach all the objectives described in the previous section is briefly presented herein.

1) Literature review. Review of the current research in structural stainless steel, previous experimental programmes, constitutive equation, codified design guidance and alternative design methods.

2) Definition of the constitutive equation for stainless steels.

2.1) Tensile tests on different stainless steel grades.

2.2) Experimental data collection (raw stress-strain curves and key parameter values reported in the literature).

2.3) Analysis of the existing material models and predictive equations for material parameters. Development of new equations if necessary.

3) Experimental programme on ferritic stainless steel RHS and SHS cross-sections and members.

3.1) Tensile tests on flat and corner coupons.

3.2) Measurement of initial geometric imperfections and geometry.

3.3) Preliminary FE models for all specimens in order to predict ultimate capacities and deflections.

3.4) Definition of the test configurations and tests.

4) FE parametric studies. Validated FE models systematically utilized to identify the influence of the key parameters in the behaviour of stainless steel cross-sections and elements. Supplementary data to the available experimental results.

5) Analysis of the cross-sectional behaviour of stainless steel RHS and SHS.

5.1) Assessment of codified design approaches and alternative methods.

5.2) Development of a new proposal, if necessary, that captures the specific behaviour exhibited by stainless steel hollow sections. Reliability of the new proposal demonstrated according to Annex D in EN 1990 (2005) and/or AISI-S100-12 (2012).

6) Analysis of the member behaviour of stainless steel RHS and SHS.

6.1) Assessment of codified design approaches and alternative methods.

6.2) Development of a new proposal, if necessary, that captures the specific behaviour of nonlinear materials with strain hardening. Reliability of the new proposal demonstrated according to Annex D in EN 1990 (2005) and/or AISI-S100-12 (2012).

7) Analysis of stainless steel RHS and SHS continuous beams.

7.1) Assessment of codified design approaches and global plastic design methods.

7.2) Development of a new proposal, if necessary, that incorporates strain hardening and bending moment redistribution in stainless steel hollow sections. Reliability of the new proposal demonstrated according to Annex D in EN 1990 (2005) and/or AISI-S100-12 (2012).

1.5 Financial support

The different tasks leading to the research work included in this thesis have been developed in the frame of the research project BIA 2012-36373 “Estudio del comportamiento de estructuras de acero inoxidable ferrítico” from the Ministerio de Economía y Competitividad, which finances the different experimental programmes and the diffusion of the results. The author of the thesis was awarded by the Universitat Politècnica de Catalunya from December 2012 to February 2014, and by the Generalitat de Catalunya since March 2014.

1.6 Thesis outline

This chapter presents a brief introduction containing an overview of the origin of stainless steel alloys and their applications in the construction industry. Then the research objectives of the study presented in this thesis and the followed methodology are described. Finally, the financial support and the outline of the document are provided.

Chapter 2 presents a brief review of the literature that is relevant to this research. The review is intended to give an overview of important topics, with the majority of the literature being introduced and discussed at the relevant stages throughout the thesis.

The description and comparison of the different material models for the nonlinear stress-strain behaviour of stainless steel alloys is presented in chapter 3. Tensile tests and the developed software are described and a detailed evaluation of the predictive models for the key material parameters is provided. This chapter also presents the proposed expressions.

Chapter 4 presents a comprehensive experimental investigation on ferritic stainless steel cross-section and members. The experimental programme consisted of five different cross-sections, including stub column tests under compression and combined loading, simply supported and continuous beam tests and members subjected to concentric and eccentric compression loads. The implemented testing procedures and measured data are fully described for each test type.

All the relevant information regarding the Finite Element (FE) analyses conducted in this thesis using the general-purpose software ABAQUS is described in chapter 5. The validation of the FE models against experimental results is followed by the details of the conducted parametric studies.

Chapter 6 presents a comprehensive study on the cross-section behaviour of stainless steel RHS and SHS subjected to several loading conditions. Based on experimental and numerical data, codified classification limits and resistance provisions are assessed, together with the alternative design approaches. Improved full slenderness range design expressions that also account for strain hardening effects are proposed and these proposals are statistically validated.

The behaviour of stainless steel RHS and SHS members subjected to compression and combined loading is extensively investigated in chapter 7 through experimental and numerical data. The assessment of existing design approaches is presented for columns and beam-columns and an alternative full slenderness range approach that includes strain hardening and local buckling effects is proposed. The reliability of this new proposal is also statistically demonstrated.

The assessment of different design approaches based on global plastic analysis is presented in chapter 8 for stainless steel RHS and SHS continuous beams. Existing and proposed methods that incorporate bending moment redistribution and strain hardening effects are assessed and the reliability analyses of these approaches are provided.

Finally, chapter 9 summarises the findings of the research work as well as the possible areas for future research.

CHAPTER 2

Literature review

2.1 Introduction

This chapter presents a brief review of the conducted previous studies pertinent to this thesis. A brief description of the international design standards for stainless steel structures is first presented, followed by the most representative works regarding the material modelling of stainless steel. A summary of the previous research works on the cross-section resistance of stainless steel hollow sections is then provided, including previous experimental programmes, design expression codified in standards and most important alternative proposals from the literature. This is followed by a brief review of the most relevant experimental results and codified design expressions corresponding to stainless steel members, also including alternative design approaches. Finally, the literature review concerning the behaviour of stainless steel indeterminate structures is covered. Further relevant literature on each particular topic will be reviewed and provided in the following chapters.

2.2 International design standards

The first standard for the design of structural stainless steel was the “Specification for the Design of Light Gauge Cold-Formed Stainless Steel Structural Members”, published in 1968 by the American Iron and Steel Institute (AISI) and based on the research work by Johnson and Winter (1966). After some revisions issued by the American Society of Civil Engineers (ASCE) and the AISI, the latest American specification for the design of structural stainless steel was

released “Specification for the Design of Cold-Formed Stainless Steel Structural Members” SEI/ASCE 8-02 (2002) published by ASCE in 2002.

The Australian/New Zealand stainless steel design standard, titled “AS/NZS4673: 2001 Cold-Formed Stainless Steel Structures” was published in 2001 by the Joint Technical Committee and although it was developed based on the American specification, it contains some different and alternative design provisions.

The first European guidance for structural stainless steel design was the “Design Manual for Structural Stainless Steel” published in 1994 by EuroInox (1994). In 1996 the European Standards Committee CEN released the European pre-standard for stainless steel, “ENV1993-1-4: Design of Steel Structures-Supplementary rules for stainless steels”, based on the first Design Manual. This pre-standard was then converted to the current European standard EN1993-1-4 (2006). Simultaneously EuroInox published the third edition of the “Design Manual for Structural Stainless Steel” and its commentary, EuroInox (2006, 2007).

2.3 Material response and modelling of stainless steel alloys

It is widely known that the behaviour of stainless steel is considerably different from that exhibited by structural carbon steel, with a nonlinear stress-strain response even for low strain levels. Carbon steel presents an elastic region with a clearly defined yield point, usually followed by a yield plateau. In opposition to this elastic-perfectly plastic material, stainless steel presents a nonlinear stress-strain response where no clearly defined yield point is identified, which is conventionally determined as the proof stress for a 0.2% offset strain. However, the behaviour of stainless steels grades has been assumed to be similar to that exhibited by carbon steel in the existing standards and design expressions. In addition to considerably improved corrosion resistance against carbon steels, stainless steels exhibit a considerable strain hardening and high ductility, with strains at fracture reaching 40-60% for the most ductile austenitic grades. Stainless steels also present an asymmetric and anisotropic behaviour, which is substantially affected by cold-working processes (Cruise and Gardner (2008a)).

Ferritic stainless steel is one of the various available stainless steel families offering a considerably improved corrosion resistance against carbon steels, with good impact resistance although the ductility is considerably reduced if compared to austenitic grades. They also exhibit higher resistances than austenitics, lower thermic dilatation and better workability. The low nickel content in ferritic stainless steels offers a lower and more stable market price while maintaining good mechanical and corrosion resistances. This presents ferritic stainless steels as an attractive alternative for many applications replacing austenitics.

The nonlinear stress-strain behaviour exhibited by the different stainless steel grades can be analytically described by various material models. The most widely used are based on the general expression originally proposed by Ramberg and Osgood (1943) and modified by Hill (1944) and given in Eq. (2.1), where E is the Young’s modulus, $\sigma_{0.2}$ is the 0.2% proof stress conventionally considered as the yield stress, and n is the strain hardening exponent. This

formulation has been shown to be capable of accurately representing different regions of the stress-strain curve, depending on the choice of the strain hardening parameter *n*, but to be generally incapable of accurately representing the full stress-strain curve with a single value of *n*. This observation led to the development of various two-stage Ramberg-Osgood models that were capable of providing a single continuous representation of the stress-strain curve of stainless steel from the onset of loading to the ultimate tensile stress. Mirambell and Real (2000) proposed a two-stage model based on the Ramberg-Osgood expression, but defining a second curve for stresses above the 0.2% proof stress given by Eq. (2.2), with an additional strain hardening exponent *m* for the second stage. $E_{0.2}$ is the tangent modulus at the 0.2% proof stress, σ_u and ε_u are the ultimate strength and total strain and $\varepsilon_{0.2}$ is the total strain at the 0.2% proof stress.

$$\varepsilon = \frac{\sigma}{E} + 0.002 \cdot \left(\frac{\sigma}{\sigma_{0.2}} \right)^n \quad \text{for} \quad \sigma \leq \sigma_{0.2} \tag{2.1}$$

$$\varepsilon = \frac{\sigma - \sigma_{0.2}}{E_{0.2}} + \left(\varepsilon_u - \varepsilon_{0.2} - \frac{\sigma_u - \sigma_{0.2}}{E_{0.2}} \right) \cdot \left(\frac{\sigma - \sigma_{0.2}}{\sigma_u - \sigma_{0.2}} \right)^m + \varepsilon_{0.2} \quad \text{for} \quad \sigma > \sigma_{0.2} \tag{2.2}$$

In order to reduce the number of required input parameters, the two-stage Ramberg-Osgood model was simplified by Rasmussen (2003), leading to the revised expression for $\sigma \geq \sigma_{0.2}$. Rasmussen (2003) also developed predictive expressions for the determination of the second strain hardening parameter *m*, the ultimate strain and the ultimate strength, effectively reducing the number of required input parameters to the three basic Ramberg-Osgood parameters (E, $\sigma_{0.2}$ and *n)*. This proposal and the additional expressions developed by Rasmussen (2003) for the determination of some of the material parameters were included in Annex C of EN1993-1-4 (2006) for the modelling of stainless steel material behaviour.

The material model proposed by Mirambell and Real (2000) was also modified by Gardner and Ashraf (2006) in order to improve the accuracy of the model at low strains (less than approximately 10%) and to allow the model to be applied also to the description of compressive stress-strain behaviour. A further two-stage model was also proposed by Gardner et al. (2010) for application to stainless steel material modelling in fire. In the proposal, the second stage of the curve passed through the stress at 2% total strain, since this strength is widely used in structural fire design. For certain modelling scenarios, such as representing cold-forming processes and connection behaviour, an accurate material description up to very high strains is often required. This requirement led to the development of three-stage versions of the Ramberg-Osgood formulation: Quach et al. (2008), Hradil et al. (2013).

Recent studies (Real et al. (2014), Arrayago et al. (2013), Afshan et al. (2013)) have confirmed the general accuracy of the form of the EN1993-1-4 (2006) material model, but have identified some limitations in the predictive expressions for the key material parameters.

2.4 Cross-section response

2.4.1 Previous experimental programmes on tubular sections

Previous research works on stainless steel tubular sections have widely investigated the cross-sectional compression capacity from stub column tests, the flexural behaviour and rotation capacity from three and four-point bending tests and the resistance of the cross-sections under combined loading from stub column tests subjected to compression and bending moment conditions. An extensive experimental database that comprises tests on Rectangular and Square Hollow Sections (RHS and SHS) from various stainless steel grades subjected to different loading conditions has been collected through an exhaustive literature review where close to 300 experimental results have been gathered. Table 2.1 summarizes the available stub column tests in compression, while Table 2.2 gathers the different tests performed under combined loading conditions and Table 2.3 presents the available experimental data on stainless steel beams.

Table 2.1. Summary of stub column tests in compression.

Stainless steel	Material grades	Reference	No. of tests
Austenitic	1.4301	Talja and Salmi (1995)	3
	1.4301	Kuwamura (2003)	6
	1.4301	Liu and Young (2003)	4
	1.4301	Young and Liu (2003)	8
	1.4301	Gardner and Nethercot (2004a)	33
	1.4301	Young and Lui (2005)	3
	1.4306	Rasmussen and Hancock (1993a)	2
	1.4318	Kuwamura (2003)	6
	1.4318	Gardner et al. (2006)	8
	1.4301, 1.4571, 1.4307, 1.4404	Zhao et al. (2015a)	4
Ferritic	1.4003, 1.4509	Afshan and Gardner (2013)	8
	1.4003	Bock et al. (2015b)	6
	1.4509	Zhao et al. (2015c)	2
Duplex and lean duplex	1.4462	Young and Lui (2005)	6
	1.4462	Young and Ellobody (2006)	5
	1.4462	Young and Lui (2006)	6
	1.4162	Theofanous and Gardner (2009)	8
	1.4162	Huang and Young (2012)	6
	1.4162	Zhao et al. (2015a)	1

Table 2.2. Summary of stub column tests in combined loading.

Stainless steel	Material grades	Reference	No. of tests
Austenitic	1.4301, 1.4571, 1.4307, 1.4404	Zhao et al. (2015a)	20
	1.4301	Talja and Salmi (1995)	1
Ferritic	1.4509	Zhao et al. (2015c)	14
Duplex and lean duplex	1.4162	Zhao et al. (2015a)	4

Table 2.3. Summary of beam tests.

Stainless steel	Material grades	Reference	No. of tests
Austenitic	1.4318	Gardner et al. (2006)	6
	1.4306	Rasmussen and Hancock (1993b)	1
	1.4301	Real and Mirambell (2005)	2
	1.4301	Theofanous et al. (2014)	5
	1.4301	Talja and Salmi (1995)	9
	1.4301	Zhou and Young (2005)	14
	1.4301	Gardner and Nethercot (2004b)	9
	1.4301	Zhao et al. (2015a)	4
Ferritic	1.4003, 1.4509	Afshan and Gardner (2013a)	8
	1.4003	Bock et al. (2015b)	7
	1.4509	Zhao et al. (2015c)	4
Duplex and lean duplex	1.4162	Huang and Young (2013a)	10
	1.4162	Theofanous and Gardner (2010)	8
	Duplex	Zhou and Young (2005)	4
	1.4162	Zhao et al. (2015a)	1

2.4.2 EN1993-1-4 formulation for cross-sectional resistance

The Ultimate Limit State Method consists of determining the ultimate capacity of a cross-section and verifying whether the section is capable of resisting the internal forces and moments to which is subjected. Usually, each internal force or moment is considered separately, and the interaction between them is then verified. Finally, the member is verified taking into account all the relevant global instabilities. The European structural stainless steel design standard EN1993-1-4 (2006) accounts for local buckling interaction in the prediction of the ultimate capacity of stainless steel sections through the cross-section classification concept given in EN1993-1-1 (2005). However, the slenderness limits codified in EN1993-1-4 (2006) are slightly different from those provided for carbon steel.

Research works in different stainless steel specimens led to the conclusion that the cross-sectional limits currently codified in EN1993-1-4 (2006) were too conservative for austenitic and duplex stainless steel grades and revised limits were proposed by Gardner and Theofanous (2008). These new limits have been ratified by many other research works for austenitic and duplex stainless steels. Nevertheless, some recent experimental research works in ferritic stainless steel RHS and SHS reported by Ashraf and Gardner (2013a) concluded that some of the class limits proposed by Gardner and Theofanous (2008) overestimate the capacity of specimens when concerning to Class 1 cross-sections. This might be caused due to the lower ultimate strain or ductility shown by ferritic grades, which make them not as deformable as austenitic and duplex stainless steels. Nonetheless, as no plastic design is currently allowed for stainless steel members in EN1993-1-4 (2006), this limitation is not currently relevant.

Expressions given in EN1993-1-4 (2006) for the determination of the compression resistance $N_{c,Rd}$ of stainless steel cross-sections is given in Eq. (2.3), while the bending moment resistance $M_{c,Rd}$ can be calculated from Eq. (2.4).

$$N_{c,Rd} = \frac{\beta_A A \cdot \sigma_{0.2}}{\gamma_{M0}} \tag{2.3}$$

$$M_{c,Rd} = \frac{\beta_W W_{pl} \cdot \sigma_{0.2}}{\gamma_{M0}} \tag{2.4}$$

For Class 1, 2 and 3 cross-sections in compression β_A =1 needs to be adopted while β_A= A_{eff} /A is considered for Class 4 cross-sections, where A is the gross-section area and A_{eff} the effective cross-sectional area. γ_{M0} is the partial safety factor for cross-sectional resistance. In bending, β_W=1 is considered for cross-sections classified as Class 1 or 2, for Class 3 sections the elastic bending capacity is determined by considering β_W=W_{el}/W_{pl}, and finally, for Class 4 cross-sections, effective properties need to be considered through β_W=W_{eff}/W_{pl}, where W_{pl} is the plastic modulus, W_{el} is the elastic modulus and W_{eff} is the effective modulus.

When Class 4 cross-sections are analysed, the effective cross-sectional properties need to be calculated through the reduction factors given in Eqs. (2.5) and (2.6) when the cross-sectional classification codified in EN1993-1-4 (2006) is considered, and through Eqs. (2.6) and (2.7) for the Gardner and Theofanous (2008) proposal.

$$\rho = \frac{0.772}{\lambda_p} - \frac{0.125}{\lambda_p^2} \leq 1.0 \tag{2.5}$$

$$\lambda_p = \frac{\bar{b}/t}{28.4\varepsilon\sqrt{k_\sigma}} \tag{2.6}$$

$$\rho = \frac{0.772}{\lambda_p} - \frac{0.079}{\lambda_p^2} \leq 1.0 \tag{2.7}$$

Regarding axial compression and uniaxial bending interaction EN1993-1-4 (2006) refers to the corresponding equations for carbon steel in EN1993-1-1 (2005), which depend on section classification. For slender cross-sections –Class 3 and 4– a linear equation is considered, Eq. (2.8), assuming that failure occurs when the maximum stress reaches the yield stress and where N_{Ed} and M_{Ed} are the applied compression load and bending moment. Concerning stocky cross-sections –Class 1 and 2–, partial yielding of the cross-section is allowed and the interaction between compression and uniaxial bending is governed by Eq. (2.9), where n_{EN}=N_{Ed}/N_y, a is the ratio of web area to gross area, N_y is the squash load of the cross-section and M_{pl} corresponds to the plastic bending capacity.

$$\frac{N_{Ed}}{N_{c,Rd}} + \frac{M_{Ed}}{M_{c,Rd}} \leq 1.0 \tag{2.8}$$

$$M_{N,Rd} = M_{pl}\frac{1-n_{EN}}{1-0.5a} \tag{2.9}$$

2.4.3 AS/NZS4673 and SEI/ASCE 8-02 formulation for cross-sectional resistance

The codified expression for cross-sectional compression resistance in the American and Australian standards SEI/ASCE 8-02 (2002) and AS/NZS4673 (2001) are also based on the slenderness of the most slender plate element of the cross-section. For those cross-sections showing a slenderness higher than 0.673, calculated from Eq. (2.10), the effective area needs to be considered from the reduction factor ρ given in Eq. (2.11). This reduction factor is slightly higher than those introduced in Eqs. (2.5) and (2.7), and equal to that provided for carbon steel cross-sections in AISI-S100-12 (2012) and EN1993-1-5 (2006) for uniform compression. For stocky cross-sections, full cross-sectional capacity is considered as for EN1993-1-4 (2006).

$$\lambda_p = \left(\frac{1.052}{\sqrt{k}}\right)\left(\frac{b}{t}\right)\left(\sqrt{\frac{f^*}{E_0}}\right) \tag{2.10}$$

$$\rho = \frac{\left(1-0.22/\lambda_p\right)}{\lambda_p} \leq 1.0 \tag{2.11}$$

Stocky beams, particularly for stainless steel grades, have significant inelastic reserve strength and ultimate bending moments commonly reach the full plastic moment capacity. Provisions given in “Procedure II” of AS/NZS4673 (2001) and SEI/ASCE 8-02 (2002) allow the consideration of this inelastic reserve strength in bending by adopting a compression strain factor C_y to determine the maximum compressive strain and assuming an ideally elastic-plastic stress-strain curve throughout the cross-section. AS/NZS4673 (2001) also adopts the full plastic capacity for rectangular and square hollow sections.

2.4.4 Continuous Strength Method (CSM)

The ultimate resistance of stocky cross-sections subjected to axial compression can be more accurately determined through an alternative design method based on cross-section deformation capacity, the Continuous Strength Method (CSM). The method considers strain hardening effects in the calculation of the cross-sectional resistance of stocky cross-sections, providing very accurate results for stainless steels.

The method is based on the calculation of the maximum strain that a cross-section can attain ε_{CSM} evaluated in terms of its relative slenderness λ_p and the yield strain ε_y, as shown in Eq. (2.12). This curve was adjusted considering both stub column and beam test data by Afshan and Gardner (2013b) and two upper bounds on the predicted deformation capacity ε_{CSM} were also provided. The first limit corresponds to the material ductility requirements in EN1993-1-1 (2005) while the second ensures that resistances are no overpredicted due to the adopted bilinear stress-strain material model. For austenitic and duplex stainless steel grades C=0.1 was adopted, but C=0.4 was defined for ferritics, and ε_u corresponds to the ultimate strain.

$$\frac{\varepsilon_{CSM}}{\varepsilon_y} = \frac{0.25}{\lambda_p^{3.6}} \quad \text{but} \quad \frac{\varepsilon_{CSM}}{\varepsilon_y} < \min\left(15, \frac{C \cdot \varepsilon_u}{\varepsilon_y}\right) \tag{2.12}$$

The relative slenderness for each loading case can be calculated from $\lambda_p = \sqrt{\sigma_{0.2}/\sigma_{cr}}$, where σ_{cr} is the critical buckling stress, obtained from the lowest buckling mode in an eigenvalue analysis and $\sigma_{0.2}$ corresponds to the 0.2% proof stress. At the same time λ_p can be also calculated according to EN1993-1-4 (2006) for the most slender plate element in the cross-section. It should be noted that the former procedure accounts for element interaction whereas the latter does not. An additional $\lambda_p \leq 0.68$ limit is adopted given that, beyond this limit, there is no significant benefit of considering material strain hardening effects.

The cross-sectional compression resistance N_{CSM} can be calculated from Eq. (2.13) assuming an upper bound stress σ_{CSM} in the cross-section and the bending capacity M_{CSM} is obtained from Eq. (2.14). The maximum stress σ_{CSM} and the strain hardening parameter E_{sh} are obtained from a simplified bilinear material model that considers strain hardening effects developed by Ashraf and Gardner (2013b) for austenitic and duplex stainless steels. This model was found to be inaccurate for ferritics due to the lower ductility of these grades and a new bilinear material model was suggested by Bock et al. (2015a).

$$N_{CSM} = \frac{A \cdot \sigma_{CSM}}{\gamma_{M0}} \tag{2.13}$$

$$M_{CSM} = \frac{W_{pl} \cdot \sigma_{0.2}}{\gamma_{M0}} \left[1 + \frac{E_{sh}}{E} \frac{W_{el}}{W_{pl}} \left(\frac{\varepsilon_{CSM}}{\varepsilon_y} - 1 \right) - \left(1 - \frac{W_{el}}{W_{pl}} \right) \cdot \left(\frac{\varepsilon_{CSM}}{\varepsilon_y} \right)^{-2} \right] \tag{2.14}$$

A recent study on carbon steel cross-sections subjected to combined loading by Liew and Gardner (2015) proposed an alternative expression for the reduced bending capacity, given in Eq. (2.15) for uniaxial bending moment combined loading. M_{CSM} can be determined from Eq. (2.14), the definition of the different exponents *a** and *b* can be found in the original publication and $n_{CSM}=N_{Ed}/N_{CSM}$. The authors also stated that for $\varepsilon_{CSM}/\varepsilon_y$ ratios lower than 3 or slenderness values higher than $\lambda_p \geq 0.5$, interaction parameters equal to unity need to be considered, leading to a linear interaction expression.

$$M_{R,CSM} = M_{CSM}\left(1 - n_{CSM}^{a^*}\right)^{1/b} \tag{2.15}$$

Some experimental results on austenitic, lean duplex and ferritic stainless steel RHS and SHS subjected to combined loading conducted by Zhao et al. (2015a, 2015c) investigated the behaviour of RHS and SHS subjected to combined loading. It was concluded that although the equations proposed by Liew and Gardner (2015) were accurate, the best approach consisted on adopting the interaction expression codified in EN1993-1-4 (2006) for Class 1 and 2 cross-

sections (see Eq. (2.9)) but considering the fundamental capacities determined according to the CSM instead of the plastic capacities (Zhao et al. (2015b)). For slenderness higher than $\lambda_p \geq 0.6$ a linear interaction formula but with CSM endpoints was proposed.

2.4.5 Direct Strength Method (DSM)

The Direct Strength Method (DSM) is a design method developed by Schafer and Pekoz (1998) that allows the consideration of local and distortional buckling effects in an easy manner through the use of software to determine elastic buckling modes. The susceptibility of the cross-section to local buckling is determined in conjunction with strength curves depending on the slenderness of the cross-section λ_l instead of considering the effective width calculations. Although the DSM approach is currently included in the North American AISI-S100-12 (2012) specification for cold-formed carbon steel structures, it has not yet been included in stainless steel standards.

The strength curve codified for carbon steel cross-sections can be written through the general expression given in Eq. (2.16), where the nominal resistance of a carbon steel cross-section R_{nl} is calculated by reducing the gross-section capacity R_0 due to the effect of local buckling as a function of the local slenderness calculated from Eq. (2.17). The nominal R_{nl} and gross-section capacities R_0 correspond to different capacities depending on the considered loading case and R_{crl} is the critical elastic local buckling load that can be obtained from a number of numerical methods and related software programmes based on finite element and finite strip methods.

$$\frac{R_{nl}}{R_0} = \begin{cases} 1 \text{ for } \lambda_l \leq 0.776 \\ \frac{1}{\lambda_l^{0.8}} - \frac{0.15}{\lambda_l^{0.8}} \text{ for } \lambda_l > 0.776 \end{cases} \quad (2.16)$$

$$\lambda_l = \sqrt{\frac{R_0}{R_{crl}}} \quad (2.17)$$

Becque et al. (2008) investigated the local buckling behaviour of stainless steel structures through an experimental programme on lipped channel section, I-section and RHS and SHS columns. Although no differences were appreciated among the different stainless steel grades, lipped channel and I-section results highlighted the necessity of an alternative strength curve for stainless steels. This curve is presented in Eq. (2.18) and it is slightly lower than that given for carbon steel sections, with a lower limiting slenderness. However, the study also demonstrated that the former strength curve given in Eq. (2.16) was still valid for RHS and SHS. Niu et al. (2015) studied stainless steel cross-sections subjected to bending and concluded that the local buckling reduction could be also conservatively calculated from Eq. (2.18).

$$\frac{R_{nl}}{R_0} = \begin{cases} 1 \text{ for } \lambda_l \leq 0.474 \\ \frac{0.95}{\lambda_l^{0.8}} - \frac{0.22}{\lambda_l^{1.6}} \text{ for } \lambda_l > 0.474 \end{cases} \quad (2.18)$$

Recent research works by Rossi and Rasmussen (2013) on compression and distortional buckling effects of stainless steels cross-sections lead into a full slenderness DSM approach that included the effect of strain hardening in the formulation. This approach adopts a linear relationship between the resistance and the slenderness instead of the classical horizontal yield limit and the predicted capacity to the conventional yield limit ratio tends to $\sigma_u/\sigma_{0.2}$ as the slenderness approaches zero in with linear variation.

The implementation of the bending inelastic reserve strength in the DSM formulation was investigated by Shifferaw and Schafer (2012) for cold-formed carbon steel C and Z beams and this approach has already been included in the revised North American AISI-S100-16 (2016) Specification. According to Shifferaw and Schafer (2012) the inelastic reserve strength is a function of the maximum compressive strain, which is a direct function of the cross-sectional slenderness λ_l. The maximum strain in inelastic bending is limited to $3\varepsilon_y$ for carbon steel and stainless steel cross-sections in order to be consistent with the scope of AISI-S100-12 (2012), SEI/ASCE 8-02 (2002) and AS/NZS4673 (2001) specifications.

2.5 Member response in compression and combined loading

2.5.1 Previous experimental programmes on tubular section members

The behaviour of stainless steel RHS and SHS members subjected to compression and combined loading has been significantly analysed through different experimental programmes during last decades, including austenitic, ferritic, duplex and lean duplex grades. The available flexural buckling tests are presented in Table 2.4, while Table 2.5 lists the experimental programmes on members subjected to combined axial compression and bending moment.

Table 2.4. Summary of flexural buckling tests.

Stainless steel	Material grades	Reference	No. of tests
Austenitic	1.4301	Gardner and Nethercot (2004b)	22
	1.4318	Gardner et al. (2006)	12
	1.4301	Liu and Young (2003)	12
	1.4307	Rasmussen and Hancock (1993a)	4
	1.4301	Young and Liu (2003)	24
	1.4301	Talja and Salmi (1995)	12
Ferritic	1.4003, 1.4509	Afshan and Gardner (2013a)	15
	1.4003	Zhao et al. (2016a)	2
Duplex and lean duplex	Duplex	Young and Lui (2006)	20
	1.4162	Theofanous and Gardner (2009)	12
	1.4162	Huang and Young (2013b)	43
	1.4462	Lui et al. (2014)	5

Most of the tests were conducted in minor axis and under pin-ended conditions, although major axis performance was also analysed by Talja and Salmi (1995). The tested bending distributions in beam-column specimens usually correspond to constant bending moments, but Zhao et al. (2016c) reported some tests under bending moment gradient.

Table 2.5. Summary of beam-column tests.

Stainless steel	Material grades	Reference	No. of tests
Austenitic	1.4301	Hyttinen (1994)	9
	1.4301	Talja and Salmi (1995)	12
	1.4301	Zheng et al. (2015)	5
Ferritic	1.4003, 1.4512	Hyttinen (1994)	12
	1.4003	Zhao et al. (2016a)	12
	1.4003	Zhao et al. (2016c)	24
Duplex and lean duplex	1.4462	Lui et al. (2014)	15
	1.4162	Huang and Young (2014a)	37

2.5.2 EN1993-1-4 formulation for member resistance

EN1993-1-4 (2006) specification for the evaluation of the flexural buckling resistance of stainless steel members subjected to compression is based on the Perry-Robertson formulation established in EN1993-1-1 (2005) for carbon steel members, given by Eqs. (2.19)-(2.21), where χ is the reduction factor due to flexural buckling, A is the cross-sectional area (for Class 4 slender sections the effective area is used) and γ_{M1} is the instability partial safety factor. However, the particular behaviour of stainless steel members is considered by specifying different buckling curves and limiting slenderness λ_0 from the ones codified for similar carbon steel specimens in order to account for different geometric imperfections and residual stresses. Regarding stainless steel cold-formed hollow sections, EN1993-1-4 (2006) provides that the buckling curve *c* needs to be considered, with an imperfection factor of α=0.49, together with a limiting slenderness λ_0=0.4 for all stainless steel grades.

$$N_{b,Rd} = \frac{\chi A \sigma_{0.2}}{\gamma_{M1}} \tag{2.19}$$

$$\chi = \frac{1}{\phi + \sqrt{\phi^2 - \lambda_c^2}} \leq 1.0 \tag{2.20}$$

$$\phi = 0.5 \cdot \left(1 + \alpha(\lambda_c - \lambda_0) + \lambda_c^2\right) \tag{2.21}$$

Regarding design expressions for the evaluation of stainless steel beam-columns, different approaches can be found in standards and the literature. Nevertheless, compression and bending moment interaction verifications are usually presented as interaction expressions with the same general expression, given in Eq. (2.22), and a certain interaction factor *k*. The differences among these expressions basically lay on the definition of this interaction factor *k* and the calculation of the basic flexural buckling $N_{b,Rd}$ and bending moment $M_{c,Rd}$ capacities. The interaction expression codified in EN1993-1-4 (2006) is described by Eq. (2.23), where the minimum value of 1.2 is worth mentioning, which usually derives into overconservative capacity predictions since the full bending capacity of the cross-section cannot be reached for low axial compression values. The effect of the bending moment gradient is usually accounted for by including equivalent moment factors C_m in Eq. (2.22). However, EN1993-1-4 (2006) provisions

do not account for the effect of the bending moment gradient in the member behaviour and the same interaction expression is provided for uniform and non-uniform bending moment distributions.

$$\frac{N_{Ed}}{N_{b,Rd}} + C_m k \frac{M_{Ed}}{M_{c,Rk}/\gamma_{M1}} \leq 1.0 \tag{2.22}$$

$$k = 1 + 2(\lambda_c - 0.5)\frac{N_{Ed}}{N_{b,Rd}} \qquad 1.2 \leq k \leq 1.2 + 2\frac{N_{Ed}}{N_{b,Rd}} \tag{2.23}$$

2.5.3 AS/NZS4673 and SEI/ASCE 8-02 formulation for member resistance

Alternatively, SEI/ASCE 8-02 (2002) considers the nonlinear stress-strain response of stainless steel grades in the prediction of the flexural buckling resistance by allowing a gradual yielding through the use of the tangent modulus E_t corresponding to the buckling stress. However, AS/NZS4673 (2001) also considers this iterative design procedure in addition to an explicit design procedure, which is essentially the method codified in EN1993-1-4 (2006) but considering a nonlinear expression for the imperfection parameter, as described in Eqs. (2.24) and (2.25). Six different buckling curves are provided for different stainless steel grades by defining different α, β, λ_0 and λ_1 parameters.

$$\phi = \frac{1}{2}\left(1 + \eta + \lambda_c^2\right) \tag{2.24}$$

$$\eta = \alpha\left((\lambda_c - \lambda_1)^\beta - \lambda_0\right) \tag{2.25}$$

For stainless steel members subjected to combined loading conditions, SEI/ASCE 8-02 (2002) and AS/NZS4673 (2001) consider the general interaction expression presented in Eq. (2.22) but with alternative flexural buckling and bending resistances and a different interaction factor *k* given by the amplification factor defined in Eq. (2.26), where N_{cre} is the elastic critical force. The effect of the bending moment gradient is also considered through the equivalent uniform moment factor C_m.

$$k = \frac{C_m}{1 - \frac{N_{Ed}}{N_{cre}}} \tag{2.26}$$

2.5.4 Direct Strength Method (DSM)

The North American AISI-S100-12 (2012) specification for cold-formed carbon steel structures includes a DSM-based approach that determines the capacity of carbon steel members different from the traditional buckling curves. However, no similar approach has been developed for stainless steel columns and the calculation of the flexural buckling strength according to the DSM is based on the same Perry-Robertson formulation presented before. Nonetheless, the

interaction with local buckling is treated through a different procedure. Whereas the codified approaches first include the effect of local buckling and then consider the overall buckling phenomena, the DSM approach first accounts for the overall buckling of the member with a fully effective cross-section and then introduces the resistance reduction due to local buckling.

Strength curves introduced in section 2.4.5, Eqs. (2.16) and (2.18), are considered to account for overall-local buckling interaction. The nominal flexural buckling resistance $R_{nl}=N_{nl}$ can be determined by adopting R_0 equal to $N_{b,ne}$, where $N_{b,ne}$ is the resistance of the fully effective column for the considered buckling curve. The cross-section slenderness is also calculated from Eq. (2.17) adopting $N_{b,ne}$. Although the DSM concept of local and overall buckling interaction can be used for the different existing flexural buckling curves, the investigations on stainless steel columns conducted by Becque et al. (2008), from which the strength curve for stainless steel sections was derived, were based on the flexural buckling curves codified in AS/NZS4673 (2001).

AISI-S100-12 (2012) specification does not provide any specific DSM-based expression for the design of beam-columns so the general interaction expressions need to be applied with the flexural buckling and bending resistances calculated from the DSM approaches presented in previous sections. However, Rasmussen (2006) extended the existing DSM approach for flexural buckling to beam-columns by introducing different resistance parameters as radial distances in the M/M_y-N/N_y plane. In this approach the beam-column behaviour is directly tackled with a unique strength curve, considering the member and section slenderness based on the elastic instabilities of the section subjected to the actual stress distribution.

According to Rasmussen (2006) the DSM approach for beam-columns first considers the member behaviour through the general interaction expression as given in Eq. (2.22) from which the overall buckling strengths can be obtained and bending moments are expressed in terms of the axial load through a load eccentricity e, $M=e \cdot N$. The detailed outline of the method can be found in chapter 7 and assumes that the same strength curves derived for cross-sectional and column behaviour also applicable to beam-columns. The method allows the consideration of different interaction factors *k* for beam-columns, several equivalent moment factors C_m, flexural buckling resistances and bending moment capacities.

2.5.5 Modifications to codified approaches

Recent research on experimental and FE stocky stainless steel RHS and SHS beam-columns subjected to different bending moment distributions was carried out by Zhao et al. (2016b). A new expression for the interaction factor *k* which also considers the particular response of diverse stainless steel grades was proposed based on the interaction factor previously suggested by Greiner and Kettler (2008). The proposed interaction factor is given in Eq. (2.27) and the calibrated D_i parameter values for different stainless steel grades can be found in the original publication. This proposal was based on an alternative flexural buckling resistance approach proposed by Afshan et al. (2016) and the pure bending moment resistance

determined according to the Continuous Strength Method (CSM), where the effect of strain hardening is considered. The influence of the bending moment gradient was contemplated through the equivalent uniform moment factor C_m.

$$k = 1 + D_1(\lambda_c - D_2)\frac{N_{Ed}}{N_{b,Rd}} \leq 1 + D_1(D_3 - D_2)\frac{N_{Ed}}{N_{b,Rd}} \quad (2.27)$$

2.6 Response of stainless steel indeterminate structures

2.6.1 Previous experimental programmes on tubular section continuous beams

The number of available hollow section stainless steel continuous beams is very limited and restricted to the most common austenitic stainless steel EN1.4301 grade, as shown in Table 2.6.

Table 2.6. Summary of continuous beam tests.

Stainless steel	Material grades	Reference	No. of tests
Austenitic	1.4301	Mirambell and Real (2000) Real and Mirambell (2005)	4
	1.4301	Theofanous et al. (2014)	10

2.6.2 EN1993-1-4 formulation for indeterminate structures

According to EN1993-1-4 (2006) the design of stainless steel structures can be only based on global elastic calculations, as no plastic design is allowed. Hence, it is considered that the structure fails when the bending capacity is reached at the most critical section, forming a plastic hinge, but without allowing any moment redistribution. However, stainless steel indeterminate structures with stocky cross-sections possess high deformation capacity, and moment redistribution will occur prior to collapse. Therefore, EN1993-1-4 (2006) provides overly conservative capacity predictions of collapse loads, since strain hardening and moment redistribution effects are not considered.

On the contrary, the classical plastic design method is allowed in EN1993-1-1 (2005) for carbon steel indeterminate structures with cross-sections stocky enough to provide the sufficient deformation capacity for moment redistribution to occur. This deformation capacity is based on a minimum rotation capacity of R>3 in EN1993-1-1 (2005), and those cross-sections that guarantee this minimum rotation capacity are classified as Class1 cross-sections. In the case of stainless steel structures, the relevance of the rotation capacity R concept is less clear given the nonlinear stress-strain behaviour.

2.6.3 Continuous Strength Method (CSM) for indeterminate structures

Gardner et al. (2011) proposed a new design method based on the Continuous Strength Method (CSM) for a more accurate prediction of the actual response of these carbon steel

indeterminate structures through the considerations of both strain hardening and moment redistribution. In order to overcome the overconservatism of the current design provisions in EN1993-1-4 (2006) for stainless steel structures and to guarantee both safe and efficient design, the applicability of the method to stainless steel indeterminate structures was assessed by Theofanous et al. (2014).

The CSM for indeterminate structures considers the moment redistribution in the structure as in traditional plastic analysis but also accounts for strain hardening effects, providing more accurate results. The full CSM bending capacity is assigned to the critical plastic hinge (i.e. the plastic hinge subjected to the largest rotation demand), while a degree of strain hardening is also allowed for the subsequent hinges. Finally, the collapse load is determined by equating the external work done by the applied loads to the internal work resulting from the rotations of the plastic hinges, as in conventional plastic design. The method is limited to structures with cross-sections showing a minimum deformation capacity $\varepsilon_{csm}/\varepsilon_y \geq 3$ for I-sections and $\varepsilon_{csm}/\varepsilon_y \geq 3.6$ for box sections according to Theofanous et al. (2014).

CHAPTER 3

Description of stress-strain curves for stainless steel alloys

3.1 Introduction

Stainless steel alloys are characterized by a nonlinear stress-strain curve which differs from that typically exhibited by hot-finished carbon steel, but shows similarities with other construction materials such as cold-worked steel and aluminium. An accurate description of the stress-strain behaviour of stainless steel is essential for use in structural design codes and advanced analytical and numerical models, whose applications may include the simulation of section forming, the structural behaviour of members and connections, the response of structures under extreme loads, and so on.

This chapter presents a description and comparison of the different material models that have been proposed in the last few decades to model this nonlinear stress-strain behaviour. Then, tensile tests on coupons from different stainless steel grades and the collected experimental database are presented and a software that automatically determines the values of the key material parameters from any experimental stress-strain curve is described. Since recent research has shown that the parameter values derived from EN1993-1-4 (2006) are not always accurate, this chapter also presents a detailed evaluation of predictive models for the key material parameters and the proposed expressions. The description of the software has been

reported in Real et al. (2014) and tensile test results, the evaluation of the predictive models and the proposed expressions can be found in Arrayago et al. (2015).

3.2 Description of existing material models and standards

3.2.1 Existing material models

The nonlinear stress-strain behaviour exhibited by the different stainless steel grades can be analytically described by various material models. The most widely used are based on the general expression originally proposed by Ramberg and Osgood (1943) and modified by Hill (1944), as given by Eq. (3.1), where E is the Young's modulus, $\sigma_{0.2}$ is the 0.2% proof stress conventionally considered as the yield stress, and *n* is the strain hardening exponent, usually calculated from Eq. (3.2), where $\sigma_{0.01}$ is the 0.01% proof stress.

$$\varepsilon = \frac{\sigma}{E} + 0.002\left(\frac{\sigma}{\sigma_{0.2}}\right)^n \tag{3.1}$$

$$n = \frac{\ln(20)}{\ln\left(\frac{\sigma_{0.2}}{\sigma_{0.01}}\right)} \tag{3.2}$$

The basic Ramberg-Osgood formulation has been shown to be capable of accurately representing different regions of the stress-strain curve, depending on the choice of the *n* parameter, but to be generally incapable of accurately representing the full stress-strain curve with a single value of *n*. This observation led to the development of various two-stage Ramberg-Osgood models that were capable of providing a single continuous representation of the stress-strain curve of stainless steels from the onset of loading to the ultimate tensile stress. Mirambell and Real (2000) proposed a two-stage model based on the Ramberg-Osgood expression, but defining a second curve for stresses above the 0.2% proof stress with a new reference system denoted σ^*-ε^*, and presented in Figure 3.1. The transformation of the variables to the new reference system from the original one is defined in Eqs. (3.3) and (3.4), where $\varepsilon_{0.2}$ is the total strain at the 0.2% proof stress.

$$\sigma^* = \sigma - \sigma_{0.2} \tag{3.3}$$

$$\varepsilon^* = \varepsilon - \varepsilon_{0.2} \tag{3.4}$$

Hence, the second curve can be defined as established in Eq. (3.5) in terms of the new reference system (σ^* - ε^*) and according to Eq. (3.6) if the general system (σ - ε) is considered, with an additional strain hardening exponent *m* for the second stage. Eq. (3.1) continued to apply for stresses less than or equal to the 0.2% proof stress.

$$\varepsilon^* = \frac{\sigma^*}{E_{0.2}} + \varepsilon^*_{up}\left(\frac{\sigma^*}{\sigma^*_u}\right)^m \quad \text{for} \quad \sigma > \sigma_{0.2} \tag{3.5}$$

$$\varepsilon = \frac{\sigma - \sigma_{0.2}}{E_{0.2}} + \left(\varepsilon_u - \varepsilon_{0.2} - \frac{\sigma_u - \sigma_{0.2}}{E_{0.2}}\right)\cdot\left(\frac{\sigma - \sigma_{0.2}}{\sigma_u - \sigma_{0.2}}\right)^m + \varepsilon_{0.2} \quad \text{for} \quad \sigma > \sigma_{0.2} \tag{3.6}$$

where $E_{0.2}$ is the tangent modulus at the 0.2% proof stress, given by Eq. (3.7), σ^*_u and ε^*_{up} are the ultimate strength and ultimate plastic strain according to the new reference system and σ_u and ε_u are the ultimate strength and total strain in terms of the general system.

$$E_{0.2} = \frac{E}{1 + 0.002n\frac{E}{\sigma_{0.2}}} \tag{3.7}$$

Figure 3.1 shows a typical stainless steel stress-strain curve where both the general (σ - ε) and the new (σ^* - ε^*) reference systems are plotted, together with the key symbols used in the material modelling expressions. The parameter ε_{up} is the ultimate plastic strain and ε_f is the strain at fracture, both expressed in the general reference system. The remaining symbols are as previously defined.

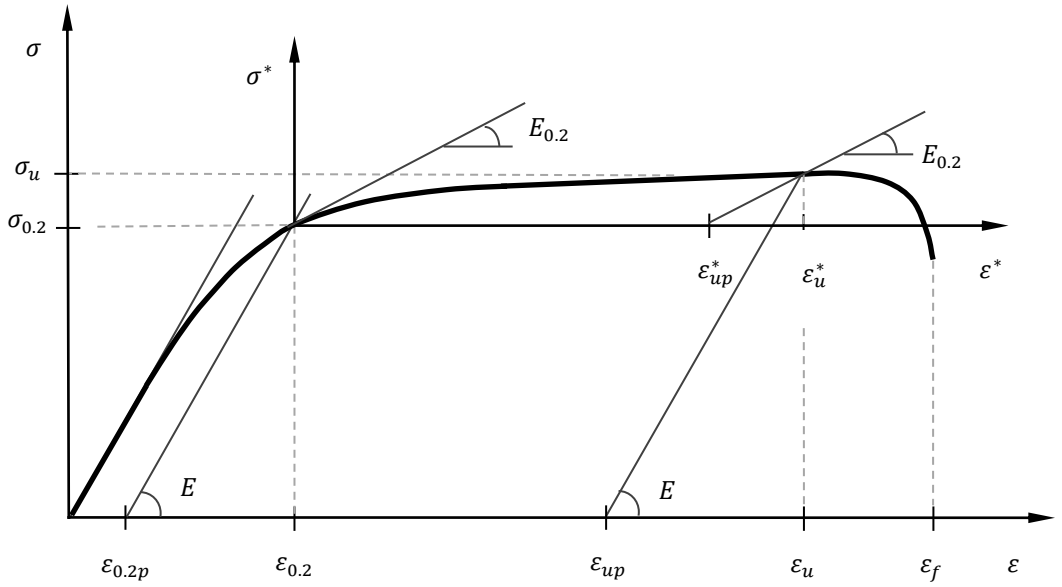

Fig. 3.1. Typical stress-strain curve with definitions of key material parameters.

In order to reduce the number of required input parameters, the two-stage Ramberg-Osgood model was simplified by Rasmussen (2003), leading to the revised expression for $\sigma > \sigma_{0.2}$ given by Eq. (3.8). This equation assumes that the ultimate plastic strain ε^*_{up} in terms of the second reference system is equal to the general ultimate total strain ε_u, as expressed in Eq. (3.9). Rasmussen (2003) also developed predictive expressions for the determination of the second

strain hardening parameter *m*, the ultimate strain and the ultimate strength, as given by Eqs. (3.10)-(3.12) respectively, effectively reducing the number of required input parameters to the three basic Ramberg-Osgood parameters (E, $\sigma_{0.2}$ and *n)*. This proposal was included in Annex C of EN1993-1-4 (2006) for the modelling of stainless steel material behaviour.

$$\varepsilon = \frac{\sigma - \sigma_{0.2}}{E_{0.2}} + \varepsilon_u \left(\frac{\sigma - \sigma_{0.2}}{\sigma_u - \sigma_{0.2}} \right)^m + \varepsilon_{0.2} \quad \text{for} \quad \sigma > \sigma_{0.2} \tag{3.8}$$

$$\varepsilon_{up}^{*} = \varepsilon_u - \varepsilon_{0.2} - \frac{\sigma_u - \sigma_{0.2}}{E_{0.2}} \cong \varepsilon_u \tag{3.9}$$

$$m = 1 + 3.5 \frac{\sigma_{0.2}}{\sigma_u} \tag{3.10}$$

$$\varepsilon_u = 1 - \frac{\sigma_{0.2}}{\sigma_u} \tag{3.11}$$

$$\frac{\sigma_{0.2}}{\sigma_u} = 0.20 + 185 \frac{\sigma_{0.2}}{E} \quad \text{for austenitic and duplex stainless steels} \tag{3.12a}$$

$$\frac{\sigma_{0.2}}{\sigma_u} = \frac{0.20 + 185 \frac{\sigma_{0.2}}{E}}{1 - 0.0375(n-5)} \quad \text{for all stainless steel alloys} \tag{3.12b}$$

The material model proposed by Mirambell and Real (2000) was also modified by Gardner and Ashraf (2006) in order to improve the accuracy of the model at low strains (less than approximately 10%) and to allow the model to be applied also to the description of compressive stress-strain behaviour. The modifications involved use of the 1% proof stress instead of the ultimate stress in the second stage of the model, leading to Eq. (3.13). Hence, the revised curve passes through the 1% proof stress $\sigma_{1.0}$ and the corresponding total strain $\varepsilon_{1.0}$, but strains are not limited to $\varepsilon_{1.0}$ and the model provides excellent agreement with experimental stress-strain data for strains up to about 10% both in tension and compression. The second strain hardening exponent was denoted $n_{0.2,1.0}$. A further two-stage model was also proposed by Gardner et al. (2010) for application to stainless steel material modelling in fire. In the proposal, the second stage of the curve passed through the stress at 2% total strain, since this strength is widely used in structural fire design.

$$\varepsilon = \frac{\sigma - \sigma_{0.2}}{E_{0.2}} + \left(\varepsilon_{1.0} - \varepsilon_{0.2} - \frac{\sigma_{1.0} - \sigma_{0.2}}{E_{0.2}} \right) \cdot \left(\frac{\sigma - \sigma_{0.2}}{\sigma_{1.0} - \sigma_{0.2}} \right)^{n_{0.2,1.0}} + \varepsilon_{0.2} \quad \text{for} \quad \sigma > \sigma_{0.2} \tag{3.13}$$

For certain modelling scenarios, such as representing cold-forming processes and connection behaviour, an accurate material description up to very high strains is often required. This requirement led to the development of three-stage versions of the Ramberg-Osgood formulation: Quach et al. (2008) proposed a material model that uses the basic Ramberg-Osgood curve (Eq. (3.1)) for the first stage, covering stresses up to the 0.2% proof stress, the Gardner and Ashraf (2006) model (Eq. (3.13)) for the second stage covering stresses up to the

2% proof stress and a straight line from the 2% proof stress to the ultimate strength for the third stage. More recently, Hradil et al. (2013) proposed an alternative three-stage model which uses the Ramberg-Osgood equation for every stage, but with different reference systems.

The comparative study presented in Real et al. (2014) highlighted that three-stage models provide the most accurate fit to experimental stress-strain curves at high strains, although a high number of parameters are needed for their definition. Therefore, considering that two-stage models representing full stainless steel stress-strain curves up to σ_u Mirambell and Real (2000) and Rasmussen (2003) also showed excellent agreement with experimental results, it was concluded that two-stage models with a reduced number of material parameters offered the best balance between accuracy and practicality.

3.1.2 EN1993-1-4 material model

The material model provided in Annex C of EN1993-1-4 (2006) for the analytical description of the stress-strain behaviour of stainless steel is based on the model proposed by Rasmussen (2003) and described by Eqs. (3.1) and (3.8). The additional expressions developed by Rasmussen (2003) for the determination of some of the material parameters are also given, including Eq. (3.10) for the second strain hardening parameter *m* and Eq. (3.11) for the ultimate strain. The strain hardening exponent *n* can be obtained either from experimental data by means of Eq. (3.2) or from Table 2.1 of EN1993-1-4 (2006). Recent studies (Real et al. (2014), Arrayago et al. (2013), Afshan et al. (2013)) have confirmed the general accuracy of the form of the EN1993-1-4 (2006) material model, but have identified some limitations in the predictive expressions for the key material parameters. These are highlighted in the following sections.

3.3 Experimental data: coupon tests and literature review

In order to evaluate the predictive models for the key material parameters given in Annex C of EN1993-1-4 (2006) and to provide revised proposals in instances where shortcomings are identified, stress-strain data were generated by conducting tensile coupon tests and experimental data were also collected. This section describes the performed tests and the gathered data.

3.3.1 Tensile coupon tests

Tensile coupon tests were conducted on selected stainless steel grades in order to supplement the existing database of results. The coupons were cut from sheet material and tested in the rolling direction at the Laboratori de Tecnologia d'Estructures Lluís Agulló at Universitat Politècnica de Catalunya (UPC). A total of 42 tensile tests were conducted; 14 on austenitic grade EN1.4301 material, 14 on ferritic grade EN1.4016 material and 14 on duplex grade EN1.4462 material. Material properties, including Young's modulus E, various proof stresses ($\sigma_{0.01}$, $\sigma_{0.05}$, $\sigma_{0.2}$ and $\sigma_{1.0}$), the ultimate tensile stress σ_u, the corresponding strain ε_u and the strain

at fracture ε_f, measured over the standard gauge length of $5.65\sqrt{A_c}$ were recorded, where A_c is the cross-sectional area of the coupon.

All tested coupons had a nominal thickness of 3mm and a nominal width of 12mm in the necked region. A gauge length of 50mm was adopted in accordance with ISO6892-1 (2009). Figure 3.2 shows a typical coupon prior to and subsequent to testing. The tensile tests were conducted under strain control in an INSTRON 8805 500kN machine and the strain rates were defined in accordance with ISO6892-1 (2009): 0.1mm/min for the initial part of the tests, up to approximately 1% strain increasing to 2.2mm/min thereafter.

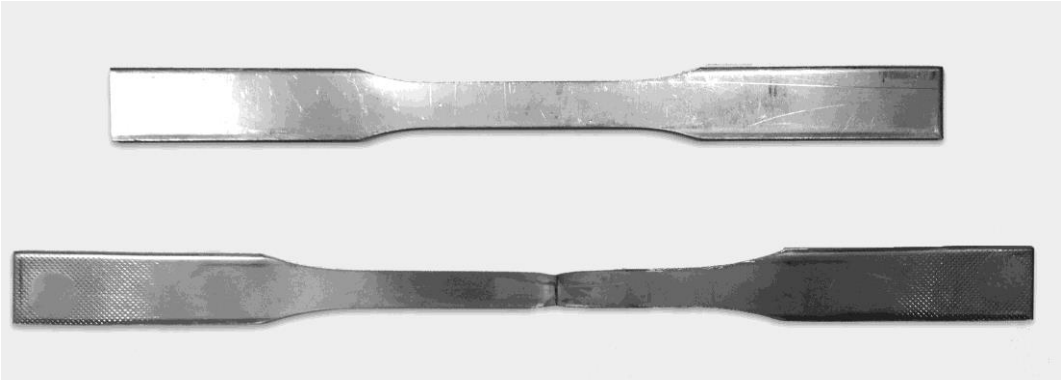

Fig. 3.2. Austenitic stainless steel coupons before and after testing.

The longitudinal strain was measured using an MTS extensometer with two contact points, and was mounted directly onto the coupons (see Figure 3.3). Two additional linear electrical resistance strain gauges were attached to the centre part of each specimen, in order to ensure an accurate measurement of the Young's modulus and to confirm the data obtained from the extensometer in the initial part of the tests. The mean values of the key measured material parameters for the different studied stainless steel grades are reported in Table 3.1.

Table 3.1. Average experimental material properties from reference and corroborating tests.

	Family	E [MPa]	$\sigma_{0.1}$ [MPa]	$\sigma_{0.2}$ [MPa]	σ_u [MPa]	ε_u [%]	ε_f [%]
Reference tests (UPC)	Austenitic	207600	280	295	668	56.1	68.2
	Ferritic	213800	301	316	502	15.6	29.7
	Duplex	213600	589	634	830	21.8	40.7
Corroborating tests (IC)	Austenitic	202900	285	302	653	--	67.3
	Ferritic	213300	303	324	520	--	27.8
	Duplex	208800	611	652	854	--	41.3

Fig. 3.3. Tensile coupon tests conducted at UPC and Imperial College London.

An example of a measured stress-strain curve for each of the tested stainless steel grades is also shown in Figure 3.4. For some of the specimens, repeated coupon tests were performed, for corroboration purposes, at Imperial College London (IC). These tests were carried out in a 150kN INSTRON machine, shown in Figure 3.3, under displacement control and using similar testing procedures to those described above.

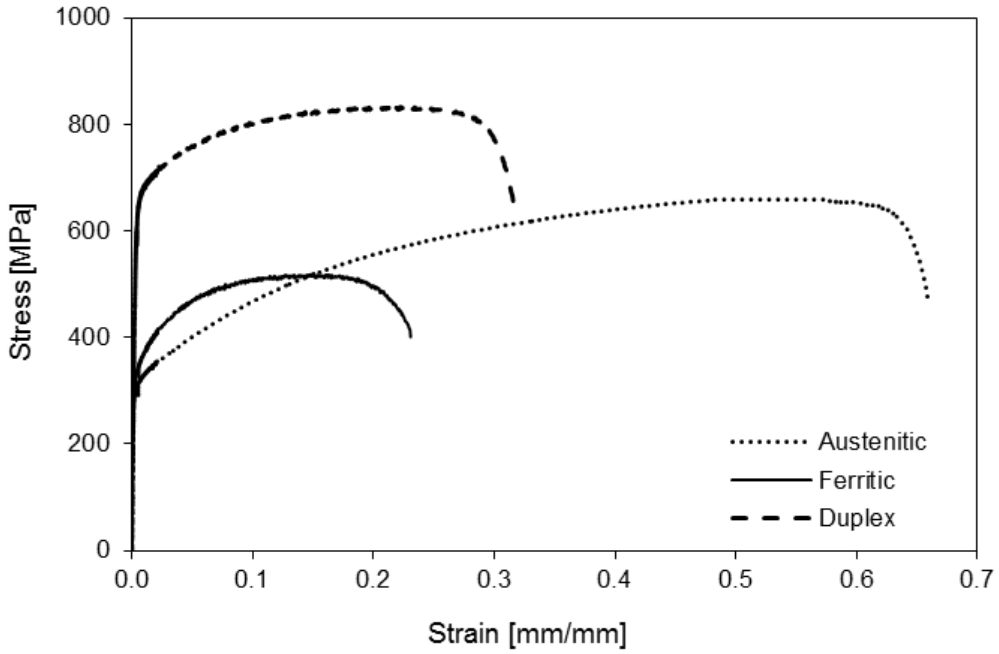

Fig. 3.4. Measured stress-strain curves for each of the studied stainless steel grades.

The reference (UPC) and corroborating (IC) test results are compared in Table 3.1 and Figure 3.5, where a maximum discrepancy between the measured strengths of less than 3% may be observed. The influence of the testing machine may therefore be considered to be small. Similar conclusions were also reached by Huang and Young (2014b).

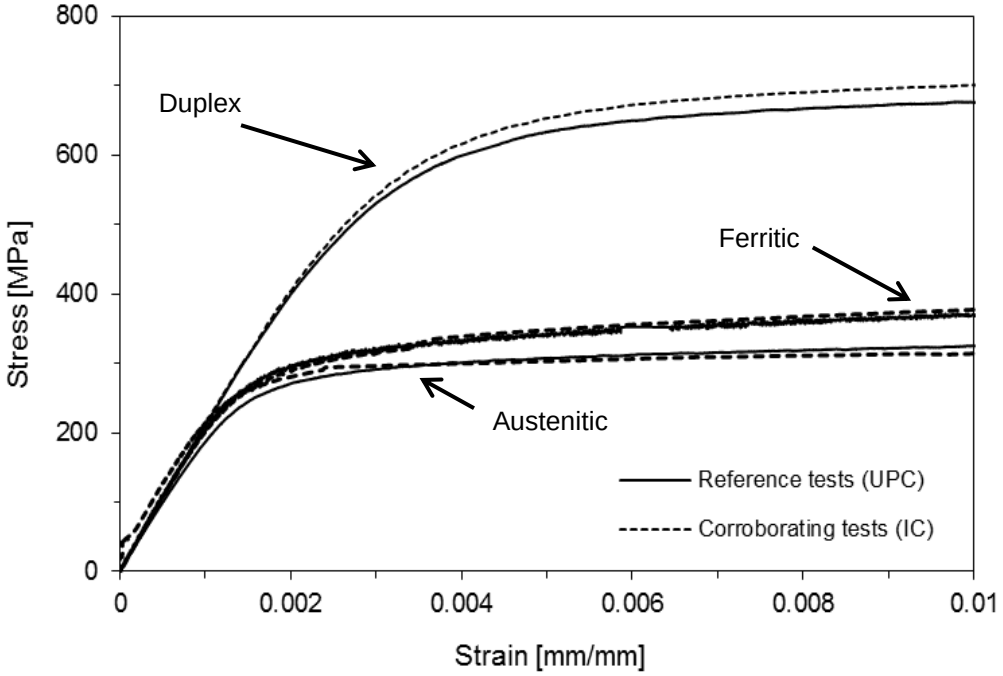

Fig. 3.5. Comparison of measured stress-strain curves up to 1% strain for the three stainless steel families.

3.3.2 Additional data collected from the literature

After the preliminary analysis of the coupon test results was conducted and the assessments of the material modelling provisions of EN1993-1-4 (2006) were made, the need for further work was highlighted. Hence, in order to enable an extensive analysis of the current provisions, a comprehensive database of experimental results has been assembled from the literature. The database, referred to as Database I in this document to differentiate it from a second database introduced later, consists of more than six hundred measured stress-strain curves, supplied as raw data by international research groups, and covering a range of stainless steel grades and products.

Note that the majority of the collected results were from coupons tested in the rolling direction (RD) but a limited number were tested in the transverse and 45º directions (TD and 45º respectively); both tensile (T) and compressive (C) behaviour of the material was also considered. A summary of the assembled results is given in Tables 3.2 to 3.4 for austenitic, ferritic and duplex and lean duplex stainless steels respectively. Note also that when “cold-formed” (CF) is specified as the type of material in Tables 3.2 to 3.4, this covers both flat and corner coupons extracted from cold-formed sections. In all tables, the following abbreviations have been considered: RD: Rolling direction, TD: Transverse direction; 45º: 45º from the rolling direction; T: Tension, C: Compression; CF: Cold-Formed; HSA: High Strength Austenitic, HSD: High Strength Duplex.

Table 3.2. Summary of the assembled austenitic stainless steel experimental stress-strain curves (Database I).

Grade	No. of curves	Product type	RD/TD/45º	T/C	Thickness range [mm]	Reference
1.4301	14	Sheet	RD	T	3	Tensile tests
1.4301	6	Sheet	RD	T	4-8	Estrada et al. (2005) Real et al. (2007)
1.4301, 1.4435, 1.4541, 1.4307	18	Sheet	RD	T	1-3	Outokumpu
1.4301	8	CF	RD	T	3-4	Nip et al. (2010)
1.4301	9	Sheet	RD	T	2-5	Xu and Szalyga (2011)
1.4301, 1.4571, 1.4404	42	CF	RD	T	2-8	Afshan et al. (2013)
1.4301	59	CF	RD	T	2-8	Gardner (2002) Gardner and Nethercot (2004a)
1.4301	57	CF, sheet	RD	C	2-8	Gardner (2002) Gardner and Nethercot (2004a)
1.4301	52	CF	RD	T	2-6	Talja (1997)
1.4318, 1.4301	87	CF	RD	T	3	Talja (2002)
1.4301	8	CF	RD	T	2-5	Zhou and Young (2007)
HSA	4	CF	RD	T	2-5	Zhou and Young (2007)

Table 3.3. Summary of the assembled ferritic stainless steel experimental stress-strain curves (Database I).

Grade	No. of curves	Product type	RD/TD/45º	T/C	Thickness range [mm]	Reference
1.4016	15	Sheet	RD	T	3	Tensile tests
1.4003, 1.4016, 1.4509, 1.4521	30	Sheet	RD	T	1.5-3.5	Manninen (2011)
1.4003, 1.4016, 1.4509, 1.4521	27	Sheet	TD	T	1.5-3.5	Manninen (2011)
1.4003	10	CF, sheet	RD	T	0.8	Real et al. (2012)
1.4003, 1.4509	20	CF	RD	T	3	Afshan and Gardner (2013a)
1.4003, 1.4509	14	CF	RD	T	2-8	Afshan et al. (2013)
1.4003	9	Sheet	RD,TD,45º	T	1.5	Rossi (2010)
1.4509	21	CF	RD	T	1-3	Talja and Hradil (2011)

Table 3.4. Summary of the assembled duplex and lean duplex stainless steel experimental stress-strain curves (Database I).

Grade	No. of curves	Product type	RD/TD/45º	T/C	Thickness range [mm]	Reference
1.4462	14	Sheet	RD	T	3	Tensile tests
1.4462	7	CF	RD	T	2-8	Afshan et al. (2013)
1.4462	6	CF	RD	T	2-6	Talja (1997)
1.4462	5	CF	RD	T	2-5	Zhou and Young (2007)
1.4162	18	CF	RD	T	3-4	Theofanous and Gardner (2010)
1.4162	48	Sheet	RD, TD	T,C	4-20	Saliba and Gardner (2013a,b)
1.4162	12	CF	RD	T	1.5-2.5	Huang and Young (2012)

In addition to the experimental results summarized in Tables 3.2 to 3.4, which were available to analyse in the form of raw data, further results reported and analysed by others were also collected. This additional collection of results, referred to as Database II, consists of more than 400 tests and is presented in Tables 3.5 to 3.7 for ferritic, austenitic, duplex and lean duplex stainless steels respectively. The results in this second database show a higher dispersion than Database I since the methodology for the calculation of the parameters will differ slightly between authors. The database comprises tests on different stainless steel families, cross-sectional shapes, thicknesses and testing directions. Not all material parameters were reported for all specimens, so some expressions could only be evaluated against a sub-set of the database.

Table 3.5. Summary of additional ferritic stainless steel experimental stress-strain curves (Database II).

Grade	No. of curves	Product type	RD/TD/45º	T/C	Thickness range [mm]	Reference
1.4003	18	CF	RD, TD, 45	T,C	1-2	Becque and Rasmussen (2009a)
404	6	CF	RD, TD, 45	T,C	1.2	Becque and Rasmussen (2009c)
1.4003, 1.4016	8	CF	RD, TD	T,C	1.2-2	Lecce and Rasmussen (2006)
1.4521	7	CF	RD	T,C	1.2-2	Niu et al. (2014)
1.4003	12	Sheet	RD	T	2-10	Rasmussen (2001)
1.4003	2	CF	RD	T	3	Tondini et al. (2013)
1.4003	5	CF	RD	T	3-4	Islam and Young (2012)
1.4509	21	CF	RD	T	1-3	Talja and Hradil (2011)

Table 3.6. Summary of additional austenitic stainless steel experimental stress-strain curves (Database II).

Grade	No. of curves	Product type	RD/TD/45º	T/C	Thickness range [mm]	Reference
1.4301	4	CF	RD, TD, 45	T,C	2	Becque and Rasmussen (2009a)
1.4301	6	CF	RD, TD, 45	T,C	8.5	Becque and Rasmussen (2009c)
1.4301	7	CF	RD	T,C	1.2-2	Niu et al. (2014)
1.4301, 1.4435	139	Sheet	RD, TD	T,C	2-10	Rasmussen (2001)
1.4301	8	CF	RD	T,C	3	Rasmussen and Hancock (1993a)
1.4301	2	CF	RD	T	3	Rasmussen and Hasham (2001)
1.4301	3	CF	RD	T	3	Rasmussen and Young (2001)
1.4301	2	CF	RD	T	5	Yousuf et al. (2013)
1.4301	16	CF	RD	T	2-3	Fan et al. (2014)
1.4301	12	CF	RD	T	1.2-4.8	Uy et al. (2011)
1.4301	3	CF	RD	T	5	Han et al. (2013)
1.4401	6	CF	RD	T	2-3	Theofanous et al. (2009)
1.4301	2	CF	RD	T	2	Liu and Young (2003)

Table 3.7. Summary of additional duplex and lean duplex stainless steel experimental stress-strain curves (Database II).

Grade	No. of curves	Product type	RD/TD/45º	T/C	Thickness range [mm]	Reference
1.4462	93	Sheet	RD, TD	T,C	2-12	Rasmussen (2001)
1.4462	6	Sheet	RD	T,C	3	Rasmussen et al. (2003)
HSD	8	CF	RD	T	1.5-3	Ellobody and Young (2005)
1.4462	5	CF	RD	T	3-6	Ellobody and Young (2006)
HSD	4	CF	RD	T	2-3	Young and Lui (2006)
1.4162	7	CF	RD	T,C	1.5	Niu et al. (2014)

3.4 Development of analysis software

With the aim of simplifying the calculation of the material parameters from every analysed experimental stress-strain curve and moreover, carry out the complex calculation needed for the optimization of the strain hardening exponents *n* and *m*, a software which automates all the required processes was developed. The developed software is described in this section.

3.4.1 Young's modulus and proof stress calculation

The software first obtains the Young's modulus for each experimental curve from a linear regression analysis of a representative set of data. This data set has to be carefully defined, since the elastic modulus is sensitive to the range of data considered. Hence, the software first determines this representative set of points removing the initial data recorded during the machine-coupon settlement, as well as any points on the nonlinear branch of the curves.

Initial experimental data sets are usually not representative due to machine-coupon settlement, and do not have to be considered in the definition of the Young's modulus. In order to establish when this settlement finishes, a r_k parameter is computed for each experimental point. r_k represents the slope corresponding to a group of 15 points from point *k* to *k+14*. The next step consists on the calculation of slope variations, $\Delta r_k=(r_k-r_{k-1})/r_{k-1}$. The first point *i* of the set of representative points is defined as the first experimental point for which the three following conditions regarding slope variations are satisfied: $\Delta r_i < 0.5\%$, $\Delta r_{i+1} < 0.5\%$, and $\Delta r_{i+2} < 0.5\%$.

The last representative point of the set used to estimate the elastic modulus has to be chosen so as to ensure the number of points of this set is high enough to obtain a representative value of the Young's modulus but also taking into consideration that all the points have to belong to the linear branch of the experimental stress-strain curve. This balance is obtained by defining the last representative point *j* as the first point which fulfils the following conditions: number of points of the set ≥ 15, $\Delta\sigma = \sigma_j-\sigma_i \geq 60$ and $\sigma_j \leq \min(\sigma_u/5, 125)$. Once the group of representative points is defined, the Young's modulus corresponding to the tensile test experimental data is determined by linear regression of these points. The goodness of this fit is systematically controlled using the correlation factor.

The proof stresses, including the 0.2% proof stress conventionally used as the yield stress, corresponding to a plastic strain *p* σ_p are then obtained by determining the intersection point between a line with the same slope as the initial Young's modulus but passing through the offset strain *p* and the measured stress-strain curve. The ultimate strength σ_u and the corresponding ultimate strain ε_u are also captured.

3.4.2 Strain hardening parameter calculation

Determination of the strain hardening exponents is carried out by a least square adjustment approach, providing values of *n* and *m* that closely match the experimental curves to the considered material model. Since the calculated values of the strain hardening parameters

depend on the considered material model, assessment of two-stage models is presented in the next section in order to determine the most appropriate for further analysis.

The strain hardening exponent optimization is carried out by a least square adjustment that minimizes the error between the experimental curve and the analytical models, providing the best curve fitting. The considered partial error represents the minimum distance between experimental and analytical curves for each data point and is given in Eq. (3.14), where both strain and stress terms are involved. Since the testing-rate changes during the performance of the tests result in different data density along the recorded strain values, C_i weights are also considered in the error definition to contemplate this fact. The total error, defined as the sum of the partial errors, is finally minimized by the least squares optimization in order to calculate the strain hardening parameters, *n* and *m*.

$$e_i = C_i \cdot \min_{k \in A} \left\{ \sqrt{\left(\frac{\varepsilon_m(\sigma_i) - \varepsilon(\sigma_k)}{0.01} \right)^2 + \left(\frac{\sigma_i - \sigma_k}{\sigma_{1.0}} \right)^2} \right\} \tag{3.14}$$

It is important to highlight that the optimization range is different for each strain hardening parameter: while *n* is optimized for stresses up to the yield stress, *m* parameters are determined for stresses between the yield stress and the ultimate strength σ_u for those material models reaching the ultimate strain of the stress-strain behaviour.

3.5 Analysis of results and recommendations

The aforementioned data are analysed in this section in order to obtain the key material and strain hardening parameters for different stainless steel families and material types, after which the accuracy of the different expressions set out in EN1993-1-4 (2006) and proposed in previous research for the determination of the key parameters, is assessed.

3.5.1 Analysis approach

Full stress-strain curves were not available for all the supplied data, since in some cases only strain gauge measurements up to about 1% strain were provided. For the calculation of the material parameters related to the initial part of the stress-strain behaviour (i.e. Young's modulus E, first strain hardening exponent *n* and initial proof stresses $\sigma_{0.01}$, $\sigma_{0.05}$, $\sigma_{0.2}$), all the collected curves (denoted Group I) have been analysed. However, when the ultimate characteristics of the material (i.e. second strain hardening parameter *m*, ultimate strain ε_u, ultimate strength σ_u) were under consideration, only the curves reaching the ultimate strain have been utilised in the analysis; these curves are denoted Group II. Table 3.8 shows the number of experimental stress-strain curves considered in the different analyses for the studied stainless steel families.

Table 3.8. Number of curves considered in the different analyses for Database I.

Family	Group I	Group II
Austenitic	367	171
Ferritic	126	94
Duplex and lean duplex	110	50
All	603	315

3.5.2 General assessment of two-stage models

As established in section 3.2, different approaches are available for the modelling of stainless steel material behaviour. The two-stage models that can represent full stainless steel stress-strain curves up to σ_u are those of Mirambell and Real (2000) and Rasmussen (2003). The main difference between these two models is the simplification that the latter considers, presented in Eq. (3.9), which assumes that the ultimate plastic strain in the second reference system ε_{up}^{*} is equal to the total ultimate strain ε_u, by neglecting the $\varepsilon_{0.2} + \frac{\sigma_u - \sigma_{0.2}}{E_{0.2}}$ term. This simplification is likely to be reasonable for the more ductile stainless steel grades (austenitic and duplex), which were originally studied by Rasmussen (2003), where the neglected term is small compared to ε_u but needs to be assessed for the less ductile ferritic grades, particularly if the material has been cold-worked. Table 3.9 evaluates the implications of the simplification defined in Eq. (3.9) for the different stainless steel families by presenting the mean, minimum and maximum values of the ratio of ultimate strains with and without the neglected term. Mean values of ultimate strain ε_u for the different stainless steel families are also presented.

Table 3.9. Assessment of Eq. (3.9) for the different stainless steel families.

Family	ε_u [mm/mm]	$\varepsilon_{0.2} + \frac{\sigma_u - \sigma_{0.2}}{E_{0.2}}$ [mm/mm]	$\frac{1}{\varepsilon_u}\left(\varepsilon_u + \varepsilon_{0.2} + \frac{\sigma_u - \sigma_{0.2}}{E_{0.2}}\right)$		
	Mean	Mean	Mean	Min.	Max.
Austenitic	0.42	0.018	1.04	1.02	1.08
Ferritic	0.13	0.015	1.20	1.02	1.81
Duplex and lean duplex	0.20	0.012	1.05	1.03	1.19

Comparisons of the Mirambell-Real (MR) model and Rasmussen (R) model with measured stress-strain curves of austenitic and (cold-formed) ferritic stainless steel are shown in Figures 3.6 and 3.7, respectively.

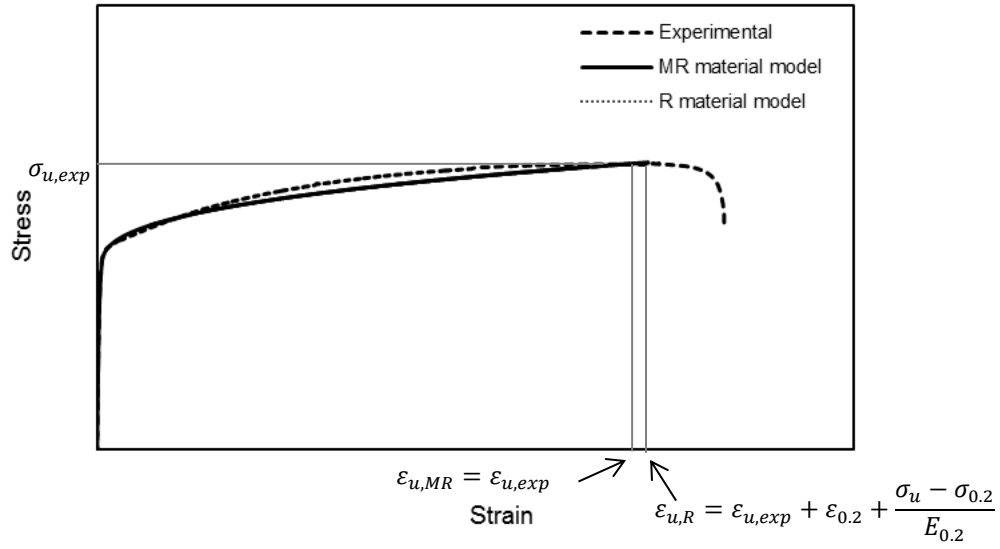

Fig. 3.6. Comparison of Mirambell-Real (MR) and Rasmussen (R) material models with an experimental austenitic stainless steel stress-strain curve.

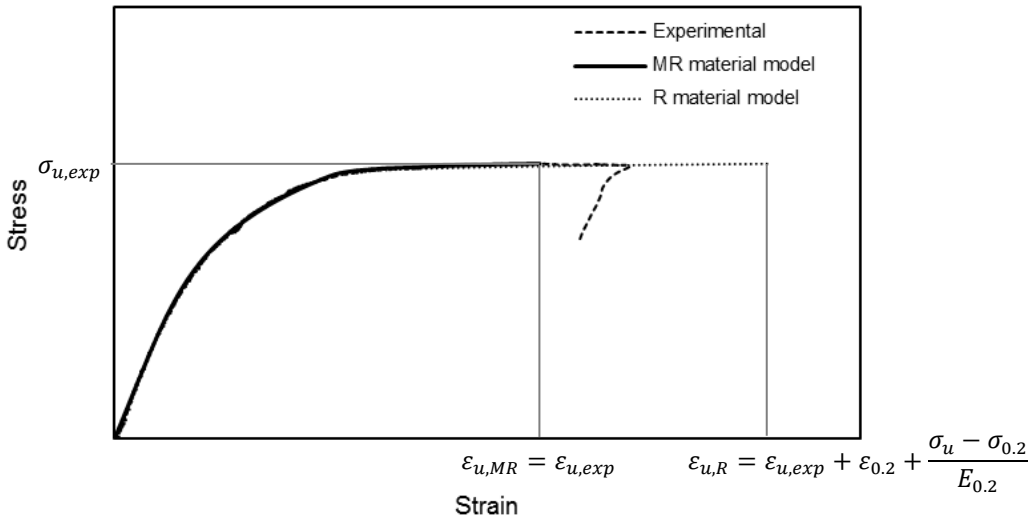

Fig. 3.7. Comparison of Mirambell-Real (MR) and Rasmussen (R) material models with an experimental ferritic stainless steel stress-strain curve.

The Figures show that while the ultimate experimental stress and strain ($\sigma_{u,exp}$ and $\varepsilon_{u,exp}$) coincide precisely with the predicted ultimate stress and strain $\varepsilon_{u,MR}$ in the case of Mirambell-Real model, this is not the case for the Rasmussen model. In the later model, the predicted ultimate strain $\varepsilon_{u,R}$ will always be greater than the experimental value, and by a larger proportion of the full curve for the less ductile materials, as indicated in Table 3.9. However, both models may be seen to accurately capture the overall stress-strain response of the two materials, and the discrepancies associated with the approximation of ultimate strain in the Rasmussen model are restricted to the latter portion of the curves. It is therefore concluded that both models are applicable to all stainless steel grades. It may also be noted that if the Rasmussen model is

curtailed at $\varepsilon_{u,exp}$ and the corresponding stress, which will be marginally below $\sigma_{u,exp}$, improved accuracy in the prediction of the ultimate region of the stress-strain response is achieved.

3.5.3 Analysis of first strain hardening exponent n

The accuracy of the classical expression proposed by Ramberg-Osgood (1943) for the first strain hardening exponent *n*, as given by Eq. (3.2), is assessed herein. This constant is traditionally calculated by imposing that the analytical curve passes through the 0.01% and the 0.2% proof stresses. This is also the approach recommended in EN1993-1-4 (2006). Different authors (Mirambell and Real (2000), Rasmussen and Hancock (1993b)) have already suggested that using the 0.05% proof stress instead of 0.01%, as given by Eq. (3.15), may provide a better representation of stainless steel experimental stress-strain curves.

$$n = \frac{\ln 4}{\ln\left(\frac{\sigma_{0.2}}{\sigma_{0.05}}\right)} \tag{3.15}$$

Assessment of the two expressions (Eq. (3.2) and Eq. (3.15)) for the determination of *n* is presented in Table 3.10 and Figure 3.8, where comparisons with the values of *n* obtained from experimental curves are shown. The predicted values of *n* are referred to as n_{pred}, while those obtained from the experiments through the described least squares optimisation process are denoted n_{exp}.

Table 3.10. Prediction of strain hardening exponent *n* for different stainless steel families.

Family		n_{exp}/n_{pred}	
		EN1993-1-4 (2006) Eq. (3.2)	Proposal Eq. (3.15)
Austenitic	Mean	1.19	1.02
	COV	0.224	0.080
Ferritic	Mean	1.35	0.95
	COV	0.171	0.133
Duplex and lean duplex	Mean	1.47	1.05
	COV	1.301	0.146
All	Mean	1.28	1.01
	COV	0.661	0.113

The results clearly demonstrate that Eq. (3.15) provides considerably more accurate predictions of the measured *n* values than Eq. (3.2), which is currently specified in Annex C of EN1993-1-4 (2006). It is therefore recommended that EN1993-1-4 (2006) is modified to reflect this finding and that authors report the 0.05% proof stress $\sigma_{0.05}$ from their experimental studies in the future.

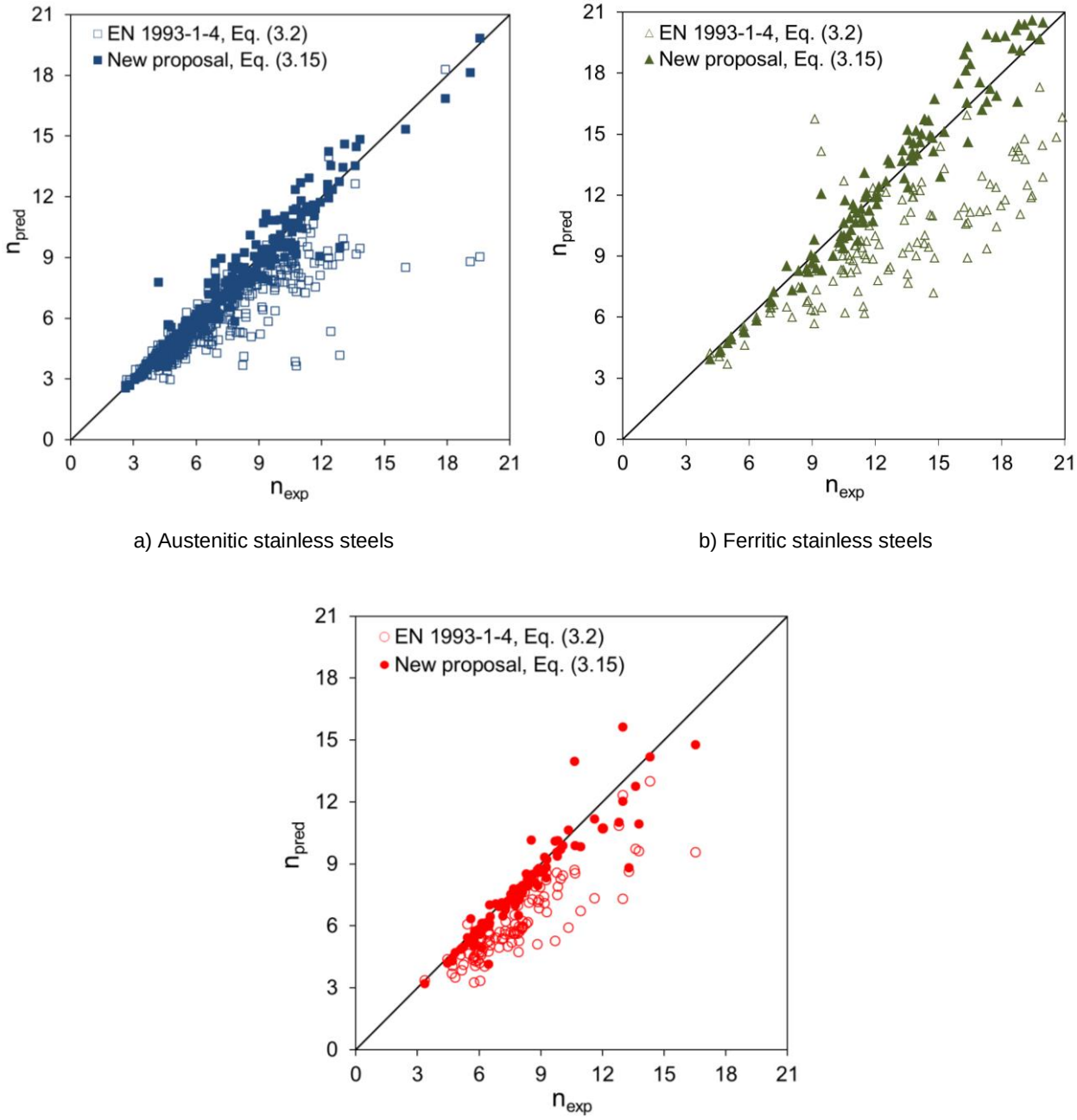

a) Austenitic stainless steels

b) Ferritic stainless steels

c) Duplex and lean duplex stainless steels

Fig. 3.8. Prediction of strain hardening parameter n for different stainless steel families.

The mean values of the measured strain hardening parameters (*n* and *m*) for different stainless steel grades, section types and testing directions are presented in Table 3.11. The lowest *n* values were obtained for the austenitic and duplex grades, reflecting the more rounded stress-strain behaviour, while the ferritic grades exhibited the sharpest yield response and therefore the highest *n* values. The results also showed that the *n* values generally decrease as the level of cold-work increases, and that higher *n* values arose for material tested in the transverse direction than the longitudinal direction.

Table 3.11. Summary of measured strain hardening exponents (*n* and *m*) for Database I.

Family	Grade	Product type	RD/TD/45º	T/C	*n*	*m*
Austenitic	1.4301	Sheet	RD	T	10.2	2.2
		Sheet	RD	C	11.8	--
		CF	RD	T	7.9	3.7
		CF	RD	C	4.8	--
	1.4435	Sheet	RD	T	11.8	2.6
	1.4541	Sheet	RD	T	10.7	2.3
	1.4307	Sheet	RD	T	11.8	2.5
	1.4571	CF	RD	T	6.8	3.2
	1.4404	CF	RD	T	7.2	3.7
	1.4318	CF	RD	T	5.2	--
Ferritic	1.4016	Sheet	RD	T	13.6	3.0
		Sheet	TD	T	17.8	2.6
	1.4003	Sheet	RD	T	17.4	2.7
		Sheet	TD	T	16.9	2.6
	1.4509	CF	RD	T	9.8	4.8
		Sheet	RD	T	15.5	2.8
		Sheet	TD	T	21.6	2.9
		CF	RD	T	11.8	--
	1.4521	Sheet	RD	T	18.5	2.6
Duplex and lean duplex	1.4462	Sheet	RD	T	8.1	3.9
		CF	RD	T	6.9	3.9
	1.4162	Sheet	RD	T	9.6	3.5
		Sheet	TD	T	10.6	3.4
		CF	RD	T	8.3	4.7
		Sheet	RD	C	7.2	--
		Sheet	TD	C	7.9	--

As noted earlier, in addition to providing formulae for the determination of *n* from experimental stress-strain data, the various stainless steel design standards (EN1993-1-4 (2006), AS/NZS4673 (2001) and SEI/ASCE 8-02 (2002)) also provide numeric values for *n* for the different stainless steel grades. Differentiation is sometimes made between the material type (annealed or cold-formed), orientation of loading (rolling direction or transverse direction) and sense of loading (tension and compression). While EN1993-1-4 (2006) only distinguishes between transverse or longitudinal directions, the Australian/New Zealand standard AS/NZS4673 (2001) considers both the orientation of loading (transverse or longitudinal) and the sense of loading (tension or compression). The North American specification SEI/ASCE 8-02 (2002) considers not only the loading sense and orientation, but also the material's level of cold-work. Following careful analysis of the collated *n* values, recommendations for values of the *n* parameter are presented in Table 3.12, where the number of curves from which the recommended values have been derived is also provided.

Table 3.12. Codified and recommended values for strain hardening parameter *n*.

Family	Grade	RD/TD	T/C	Codified *n*			Recom. *n*
				EN1993-1-4 (2006)	AS/NZS4673 (2001)	SEI/ASCE-8 (2002)	
Austenitic	1.4301	RD	T	6	7.5	8.3	7
		RD	C	6	4.0	4.1	
	1.4435	RD	T	7	--	--	
	1.4541	RD	T	6	--	--	
	1.4307	RD	T	6	7.5	--	
	1.4571	RD	T	7	--	--	
	1.4404	RD	T	7	7.5	--	
	1.4318	RD	T	6	--	--	
	No. of curves:		367				
Ferritic	1.4016	RD	T	6	8.5	8.4	14
	1.4003	RD	T	7	9.0	--	
	1.4509	RD	T	--	--	--	
	1.4521	RD	T	--	11.0	--	
	No. of curves:		117				
	1.4016	TD	T	14	14.0	14.1	
	1.4003	TD	T	11	11.5	--	
	1.4509	TD	T	--	--	--	
	No. of curves:		32				
Duplex and lean duplex	1.4462	RD	T	5	5.5	--	8
	1.4162	RD	T	--	--	--	
		RD	C	--	--	--	
	No. of curves:		92				
	1.4162	TD	T	--	--	--	
		TD	C	--	--	--	
	No. of curves:		22				

These recommended values are close to those proposed by Afshan et al. (2013), but benefit from a larger database of results, including all those considered by Afshan et al. (2013). Note that the *n* values proposed herein are slightly higher than those recommended by Afshan et al. (2013). This is attributed to the different data sets that were analysed and the fact that the data set considered herein included a higher proportion of sheet material. This is relevant because cold-working of the sheet material, which would be experienced in the cold-forming of structural sections, produces a slightly more rounded stress-strain response i.e. lower *n* values.

It should also be noted that it is proposed that no distinction is made between loading directions (transverse or longitudinal), sense of loading (tension or compression) or cold-worked level in assigning the values of *n*. This is for the following reasons: (1) simplicity, (2) there are insufficient data to enable a meaningful distinction to be drawn for many grades, (3) influence of the above parameters is generally relatively small in terms of the effect on the shape of the stress-strain curve, (4) a designer will not typically know whether the material will be orientated in the transverse or longitudinal direction, (5) the same structural element can be subjected to tension and compression depending on the load case under consideration, and (6) the level of cold-work (i.e. the amount of plastic strain to which the material has been subjected) will depend on the section geometry, the forming process and so on.

3.5.4 Analysis of second strain hardening exponent m

Annex C of EN1993-1-4 (2006) provides Eq. (3.10) for the determination of the second strain hardening exponent *m*. Recent studies involving the examination of austenitic and ferritic stainless steel stress-strain curves found that this expression provides higher values for the second strain hardening exponent *m* than those obtained from curve fitting. A revised expression, given by Eq. (3.16), is therefore proposed for all stainless steel grades, based on least squares regression. This issue is explored further herein, utilising the assembled database. Figure 3.9 shows the experimental second strain hardening exponents *m* (obtained through the described curve fitting process) plotted against $\sigma_{0.2}/\sigma_u$ for the different stainless steel grades. The codified expression and new proposal are also depicted in Figure 3.9.

$$m = 1 + 2.8\frac{\sigma_{0.2}}{\sigma_u} \tag{3.16}$$

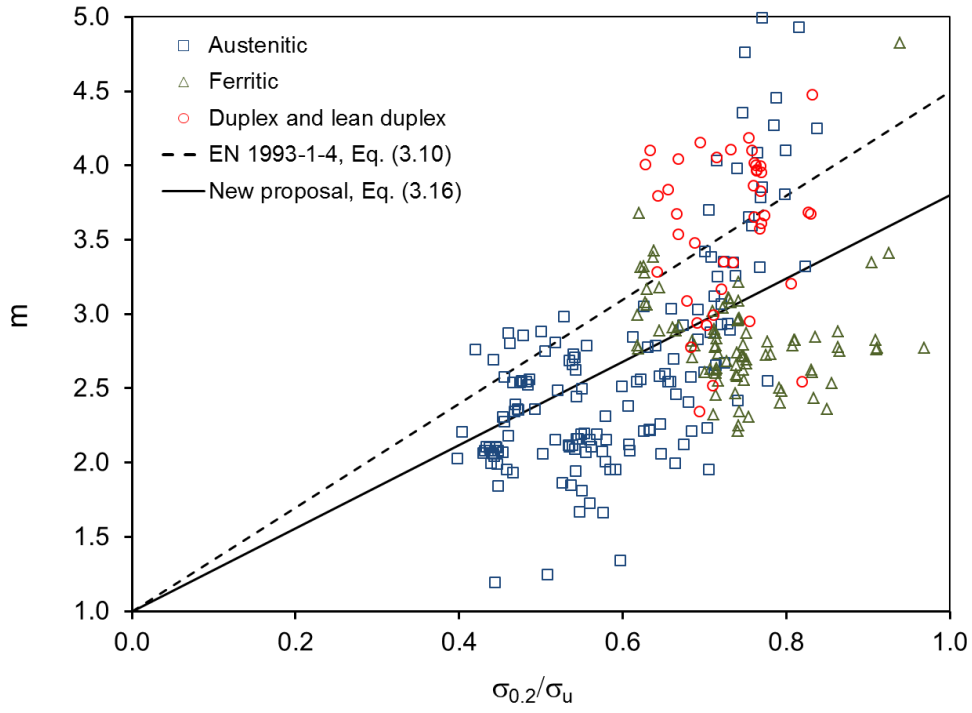

Fig. 3.9. Assessment of strain hardening parameter *m* for different stainless steel families.

Table 3.13 presents the mean experimental-to-predicted ratios of the second strain hardening parameters m_{exp}/m_{pred} for the contemplated predictive expressions. All stainless steel stress-strain curves that reached the ultimate strain, referred to as Group II in Table 3.8 have been studied. The mean m_{exp}/m_{pred} ratios calculated for Eq. (3.10) are low for the majority of the analysed data, particularly the austenitic and ferritic grades. Overall, the new proposal given in Eq. (3.16) provides more accurate predictions for the second strain hardening parameter *m* than the existing formula and is therefore recommended for code inclusion. Same results can be also observed in Figure 3.9.

Table 3.13. Assessment of strain hardening exponent *m* for different stainless steel families.

Family		m_{exp}/m_{pred}	
		EN1993-1-4 (2006) Eq. (3.10)	Proposal Eq. (3.16)
Austenitic	Mean	0.84	0.98
	COV	0.196	0.196
Ferritic	Mean	0.79	0.93
	COV	0.153	0.150
Duplex and lean duplex	Mean	1.03	1.19
	COV	0.264	0.148
All	Mean	0.85	1.00
	COV	0.191	0.193

3.5.5 Analysis of σ_u

Rasmussen (2003) developed an expression to predict the ultimate strength σ_u in terms of two of the basic Ramberg-Osgood parameters, $\sigma_{0.2}$ and E. The accuracy of this expression is assessed herein against the assembled test data, as shown in Figure 3.10, where $\sigma_{0.2}/\sigma_u$ ratios have been plotted against $\sigma_{0.2}$/E for the Group II data. The experimental results have been compared to different predictive models: Eq. (3.12a) proposed by Rasmussen (2003) for the austenitic and duplex grades and the new expression that is proposed in this thesis for ferritic grades Eq. (3.17).

$$\frac{\sigma_{0.2}}{\sigma_u} = 0.46 + 145\frac{\sigma_{0.2}}{E} \tag{3.17}$$

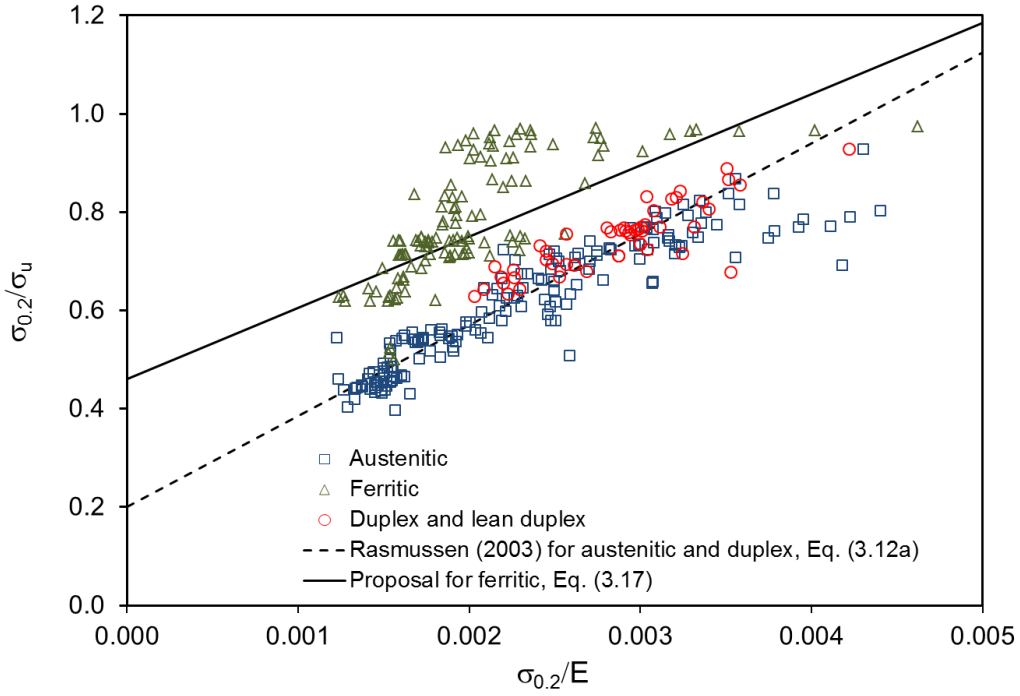

Fig. 3.10. Assessment of ultimate strength σ_u for different stainless steel families.

Figure 3.10 and Table 3.14 show that the original expression for the determination of σ_u for austenitic, duplex and lean duplex stainless steels proposed by Rasmussen (2003) provides very good predictions of the assembled data set, so the validity of Eq. (3.12a) is confirmed. However, for ferritic stainless steels, Eq. (3.12b), which was proposed by Rasmussen for all stainless steel grades, provides inaccurate results. The accuracy of the revised expression proposed for the ferritic grades has been confirmed by the experimental data and the additional data studied herein.

Table 3.14. Assessment of ultimate strength σ_u for different stainless steel families.

Family		$\sigma_{u,exp}/\sigma_{u,pred}$	
		Rasmussen (2003) Eqs. (3.12a) and (3.12b)	Proposal Eqs. (3.12a) and (3.17)
Austenitic	Mean	1.03	1.03
	COV	0.126	0.126
Ferritic	Mean	1.41	0.97
	COV	0.403	0.109
Duplex and lean duplex	Mean	0.98	0.98
	COV	0.067	0.067

3.5.6 Analysis of ε_u

Assessment of the predictive expressions for ultimate strain is presented in Figure 3.11, where the experimental ultimate strain ε_u is plotted against $\sigma_{0.2}/\sigma_u$ ratios for data from 171 austenitic, 94 ferritic and 50 duplex and lean duplex stainless steel tensile tests. Together with the experimental data, the expression for the determination of the ultimate strain provided in Annex C of EN1993-1-4 (2006), given by Eq. (3.11), is also plotted.

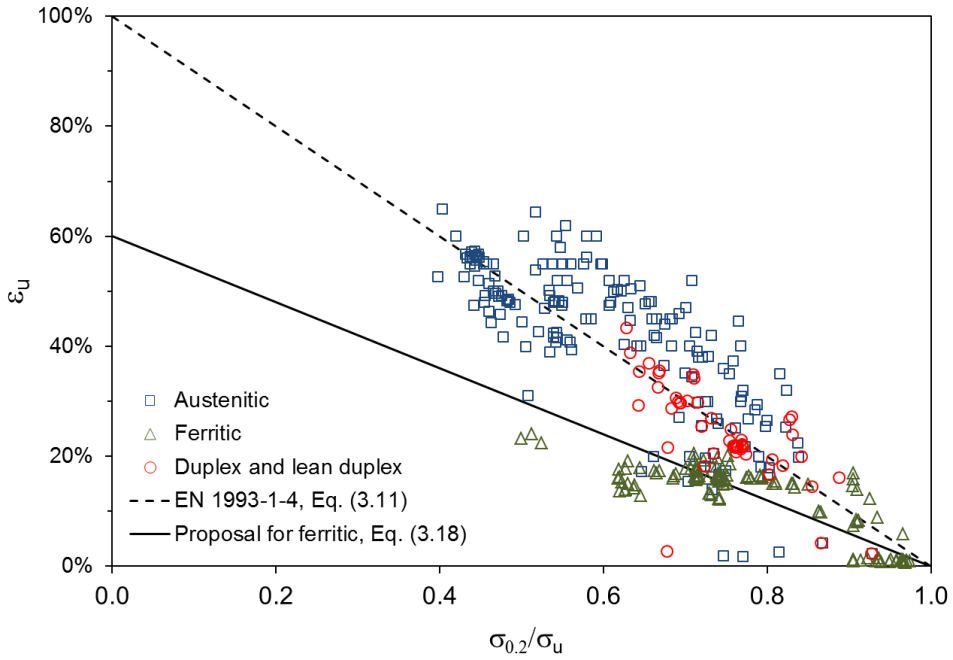

Fig. 3.11. Assessment of ultimate strain ε_u for different stainless steel families.

From Figure 3.11, the expression given by Eq. (3.11) may be seen to provide very good predictions for the austenitic, duplex and lean duplex materials, so its accuracy is confirmed for these stainless steel families. However, ferritic stainless steels exhibit less ductile behaviour than the austenitic and duplex grades, and Eq. (3.11) yields unconservative predictions of ε_u. After conducting a detailed study of the prediction of ε_u for ferritic stainless steel, a revised expression described by Eq. (3.18) is proposed. This equation was also adopted by Bock et al. (2015a). As shown in Figure 3.11 and Table 3.15, Eq. (3.18) provides good predictions for the assembled ferritic stainless steel data set.

$$\varepsilon_u = 0.6 \cdot \left(1 - \frac{\sigma_{0.2}}{\sigma_u}\right) \tag{3.18}$$

Table 3.15. Assessment of ultimate strain ε_u for different stainless steel families.

Family		$\varepsilon_{u,exp}/\varepsilon_{u,pred}$	
		EN1993-1-4 (2006) Eq. (3.11)	Proposal Eqs. (3.11) and (3.18)
Austenitic	Mean	1.09	1.09
	COV	0.280	0.280
Ferritic	Mean	0.59	0.98
	COV	0.565	0.565
Duplex and lean duplex	Mean	0.96	0.96
	COV	0.275	0.275

3.6 Additional validation

This section presents a final evaluation of the proposed equations through an independent experimental database gathered from the literature. In addition to the experimental results summarised in Tables 3.2 to 3.4, which were available to the authors to analyse in the form of raw data, further results reported and analysed by others were also collected. This additional collection of results, referred to as Database II, and presented in Tables 3.5 to 3.7, consists of more than 400 tests. As mentioned before, the results in this second database show a higher dispersion than Database I since the methodology for the calculation of the parameters slightly differs between authors. In addition, some expressions could only be evaluated against a sub-set of the database since not all material parameters were reported for all specimens.

Tables 3.16 to 3.18 compare the mean experimental-to-predicted ratios for the experimental results of Database II for m, σ_u and ε_u respectively, where the accuracy of the recommended expressions is assessed.

Table 3.16. Assessment of the second strain hardening exponent *m* for different stainless steel families for Database II.

Family		m_{exp}/m_{pred}	
		EN1993-1-4 (2006) Eq. (3.10)	Proposal Eq. (3.16)
Austenitic	Mean	0.92	1.06
	COV	0.186	0.190
Ferritic	Mean	0.67	0.78
	COV	0.458	0.456
Duplex and lean duplex	Mean	--	--
	COV		

Table 3.17. Assessment of the ultimate strength σ_u for different stainless steel families for Database II.

Family		$\sigma_{u,exp}/\sigma_{u,pred}$	
		Rasmussen (2003) Eqs. (3.12a) and(3.12b)	Proposal Eqs. (3.12a) and (3.17)
Austenitic	Mean	1.03	1.03
	COV	0.097	0.097
Ferritic	Mean	1.28	0.98
	COV	0.620	0.093
Duplex and lean duplex	Mean	0.99	0.99
	COV	0.064	0.064

Table 3.18. Assessment of the ultimate strain ε_u for different stainless steel families for Database II.

Family		$\varepsilon_{u,exp}/\varepsilon_{u,pred}$	
		EN1993-1-4 (2006) Eq. (3.11)	Proposal Eqs. (3.11) and (3.18)
Austenitic	Mean	1.02	1.02
	COV	0.253	0.253
Ferritic	Mean	0.71	1.06
	COV	0.335	0.237
Duplex and lean duplex	Mean	1.04	1.04
	COV	0.298	0.298

The results show that the prediction of the key material parameters is more accurate when the proposals (when relevant) are considered, as the mean experimental-to-predicted ratios get closer to the unity, although the scatter of the data is generally maintained, in line with the dispersion presented by the analysed data. The new expressions proposed are found to accurately predict the material parameters reported by other authors: the strain hardening exponent *m* for austenitic, ferritic and duplex stainless steels and the ultimate strength and strain for ferritics. The original expressions seem to correctly estimate the experimental values of σ_u and ε_u for austenitic and duplex grades.

3.7 Summary of proposals and concluding remarks

A comprehensive study of the nonlinear stress-strain response of stainless steel alloys and the modelling thereof is presented in this chapter. A total of over 600 experimental stress-strain curves, including austenitic, ferritic and duplex grades has been collected and analysed. The collected data have been used for the assessment of existing two-stage material models and the expressions for the prediction of the key material parameters. The material model proposed by Rasmussen (2003), and currently included in Annex C of EN1993-1-4 (2006), was found to accurately represent the measured stress-strain curves for the different stainless steel grades and material types, including ferritic stainless steels for which the model had not previously been fully verified.

Based on the assembled data set, values and predictive expressions for the key material parameters of the Rasmussen model were re-evaluated. A revised predictive equation and revised numeric values for the strain hardening parameter *n* have been recommended for all stainless steel families. A new expression for the prediction of the second strain hardening parameter *m* for all stainless steel grades has also been proposed. Finally, revised predictive expressions for ultimate tensile stress and strain for ferritic stainless steels have been proposed. It is recommended that these proposals are incorporated into future revisions of EN1993-1-4 (2006). The proposed predictive expressions and the recommended modifications to made to Annex C of EN1993-1-4 (2006) are summarised as follows:

$$n = \frac{\ln 4}{\ln\left(\frac{\sigma_{0.2}}{\sigma_{0.05}}\right)} \qquad \text{for all grades} \qquad (3.15)$$

$$m = 1 + 2.8\frac{\sigma_{0.2}}{\sigma_u} \qquad \text{for all grades} \qquad (3.16)$$

$$\frac{\sigma_{0.2}}{\sigma_u} = \begin{cases} 0.20 + 185\frac{\sigma_{0.2}}{E} & \text{for austenitic, duplex and lean duplex} \quad (3.12a) \\ 0.46 + 145\frac{\sigma_{0.2}}{E} & \text{for ferritic grades} \quad (3.17) \end{cases}$$

$$\varepsilon_u = \begin{cases} 1 - \frac{\sigma_{0.2}}{\sigma_u} & \text{for austenitic, duplex and lean duplex} \quad (3.11) \\ 0.6 \cdot \left(1 - \frac{\sigma_{0.2}}{\sigma_u}\right) & \text{for ferritic grades} \quad (3.18) \end{cases}$$

Additionally, the revised values for the first strain hardening parameter *n*, presented in Table 3.12, are recommended for inclusion in EN1993-1-4 (2006). The numeric values of Young's modulus for stainless steel proposed by Afshan et al. (2013) are also recommended herein.

CHAPTER 4

Experimental programme on ferritic stainless steel RHS and SHS elements

4.1 Introduction

This chapter presents a comprehensive experimental investigation on ferritic stainless steel tubular cross-section and members. A total of five different cross-sections were analysed, comprising three Rectangular Hollow Sections (RHS) and two Square Hollow Sections (SHS). The cross-sections were named as follows: S1–80x80x4, S2–60x60x3, S3–80x40x4, S4–120x80x3 and S5–70x50x2, which will be used throughout the document. An experimental programme including 38 cross-section tests and 21 member tests is described.

The measurement of the material properties of the different cross-sections and initial geometric imperfections is firstly described, followed by the experimental programme on cross-sections and members subjected to different loading conditions. All the tests were conducted at the Laboratori de Tecnologia d'Estructures Luis Agulló, at the Department of Civil and Environmental Engineering at Universitat Politècnica de Catalunya (UPC). Cross-sectional resistance tests comprise stub column tests subjected to pure compression and combined loading conditions, and beams tested under three-point and four-point bending conditions. Regarding member tests, continuous beams, column and beam-column configurations were investigated.

Results of this experimental programme have been reported in Arrayago and Real (2015), Arrayago and Real (2016) and Arrayago et al. (2016a). These tests were conducted together with some additional compression and simply supported bending tests on slender ferritic

stainless steel RHS and SHS, reported in Bock et al. (2015b) and complement the study on the flexural behaviour of ferritic members with stockier cross-sections.

4.2 Material and initial imperfection characterization

An accurate characterization of the basic material and geometric parameters is essential for the correct analysis and modelling of the tests. This section describes the tensile tests conducted on coupons extracted from the specimens, the determination of the actual dimensions of the specimens and the measurement of the initial geometric imperfections.

4.2.1 Material characterization: tensile tests

The investigated specimens were made from the ferritic stainless steel grade EN1.4003 and were cold-rolled and seam welded. The chemical composition and tensile properties of the original coil material provided by the manufacturer and stated in the mill certificates are presented in Tables 4.1 and 4.2 respectively. $\sigma_{0.2}$ and $\sigma_{1.0}$ are the proof stresses corresponding to 0.2% and 1.0% plastic strains, σ_u is the ultimate tensile strength and ε_f is the strain at fracture.

Table 4.1. Chemical composition from mill certificates for grade EN1.4003 stainless steel.

Section	C [%]	Si [%]	Mn [%]	P [%]	S [%]	Cr [%]	Ni [%]	N [%]	Co [%]
S1	0.010	0.360	1.410	0.032	0.000	11.300	0.400	0.009	0.030
S2	0.015	0.350	1.470	0.028	0.000	11.100	0.400	0.013	0.030
S3	0.010	0.300	1.430	0.028	0.001	11.400	0.400	0.010	0.020
S4	0.012	0.260	1.390	0.025	0.001	11.300	0.400	0.013	0.010
S5	0.012	0.290	1.440	0.030	0.001	11.200	0.400	0.009	0.010

Table 4.2. Key mechanical properties from mill certificates.

Section	$\sigma_{0.2}$ [MPa]	$\sigma_{1.0}$ [MPa]	σ_u [MPa]	ε_f [%]
S1	389	419	545	27
S2	343	367	495	35
S3	366	389	501	29
S4	357	377	492	35
S5	350	370	490	39

Cold-forming processes affect cross-sectional behaviour, particularly in the corner regions, with increasing plastic deformation resulting in significant material property enhancement. Hence, the material behaviour of the different cross-sections was characterized by conducting tensile tests on coupons extracted both from the flat (F) and corner (C) regions of the cross-sections, as presented in Figure 4.1. Two flat and two corner coupons were tested for each cross-section, resulting in a total of 20 tensile tests. The machining and testing of the coupons were conducted in the technical laboratories of Acerinox, in accordance with ISO6892-1 (2009), as shown in Figure 4.2.

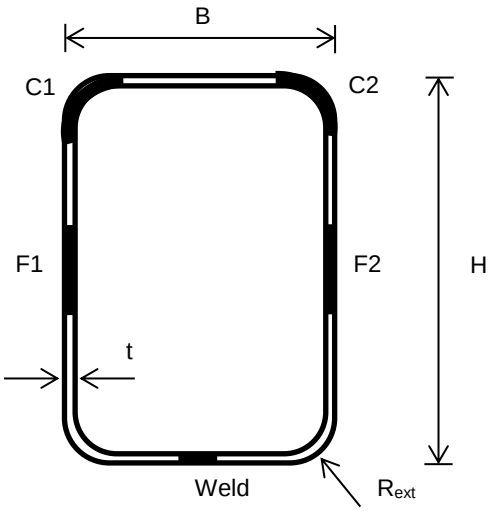

Fig. 4.1. Location of flat and corner coupons and definition of cross-section symbols.

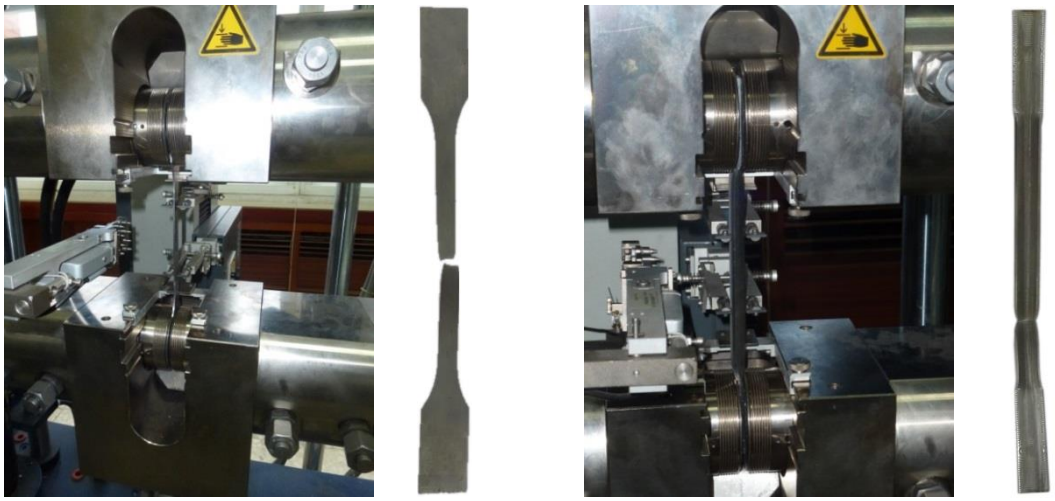

(a) Testing of S3-F coupon and tested flat coupon

(b) Testing of S2-C coupon and tested corner coupon

Fig. 4.2. Tensile coupon tests on flat and corner coupons.

Coupons were tested under an initial strain rate of $0.00025s^{-1}$ for the determination of the Young's modulus and the yield stress and then increased to $0.008s^{-1}$. Coupons extracted from the corner regions were strips with constant cross-sectional area along their entire length, and were extended two times the thickness of the cross-section into adjacent flat faces according to Cruise and Gardner (2008a), since corner properties affect regions beyond the curved portions. The area was calculated by considering the mass of each coupon and the density of the grade EN1.4003 ferritic stainless steel from EN10088 (2009). The flat coupons were machined to the usual dogbone shape, with a nominal width of 15mm over the reduced area length, and strains at fracture were measured over the standard gauge length of $5.65\sqrt{A_c}$ where A_c is the cross-sectional area of the coupon.

Averaged key material properties of the flat and corner regions of each cross-section are presented in Table 4.3, where E is the Young's modulus, $\sigma_{0.05}$ and $\sigma_{0.2}$ are the proof stresses corresponding to 0.05% and 0.2% plastic strains respectively, σ_u is the ultimate tensile strength, ε_u is the corresponding ultimate strain and ε_f is the strain at fracture. Strain hardening exponents *n* and *m* corresponding to the material model proposed by Mirambell and Real (2000) are also reported. The material properties have been obtained through the software described in chapter 3.

Table 4.3. Average tensile test results for different cross-sections.

	E [MPa]	$\sigma_{0.05}$ [MPa]	$\sigma_{0.2}$ [MPa]	σ_u [MPa]	ε_u [%]	ε_f [%]	*n*	*m*
S1 – F	173992	465	521	559	8.2	21.7	12.4	2.3
S1 – C	170049	441	577	645	1.1	7.9	5.0	5.4
S2 – F	186896	433	485	505	6.8	20.9	12.2	2.6
S2 – C	178049	459	555	587	1.0	10.1	7.9	5.2
S3– F	181632	467	507	520	3.6	21.0	16.4	2.5
S3 – C	183684	434	558	601	1.0	7.0	5.9	4.5
S4 – F	176704	391	430	490	12.6	27.1	14.6	2.3
S4 – C	194611	457	540	583	1.0	10.1	7.6	4.8
S5 – F	179568	381	418	480	13.8	26.8	15.3	2.4
S5 – C	186026	466	552	575	1.1	6.5	8.0	4.6

Full measured stress-strain curves for the flat and corner regions corresponding to S1 and S5 cross-sections are presented in Figure 4.3. This Figure, together with Table 4.3, clearly shows the effect of the cold-forming effect on the stress-strain behaviour of stainless steel specimens: both the 0.2% proof stress $\sigma_{0.2}$ and the ultimate tensile strength σ_u increase due to the cold-forming effect, while the ductility decreases considerably, as ε_u and ε_f reduce.

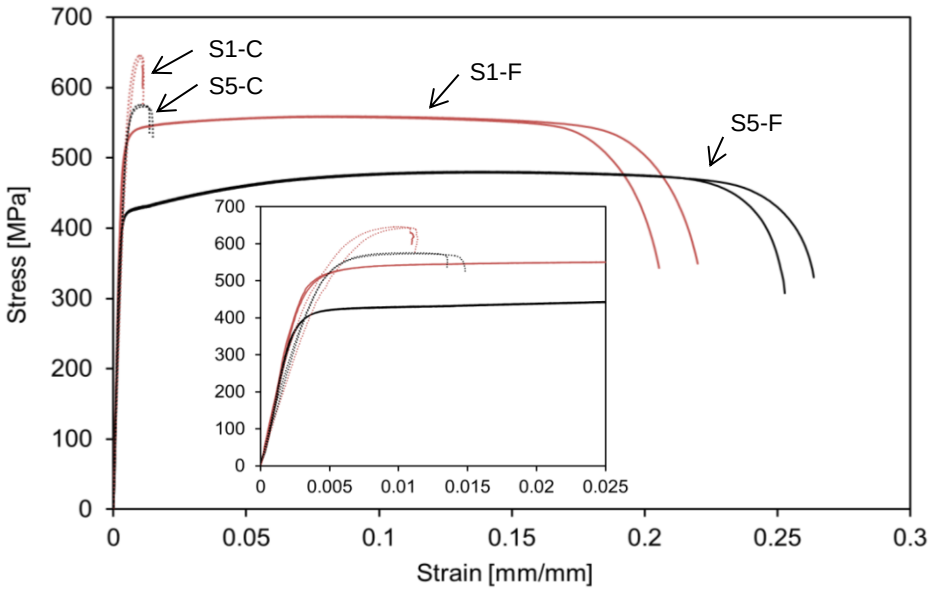

Fig. 4.3. Measured stress-strain curves for S1 and S5 flat and corner coupons.

The different behaviour of flat and corner regions of cross-sections can be considered in the analysis of the experimental results by determining the weighted average material properties as established by Hradil and Talja (2013). The parameters are weighted according to the area of the considered flat or corner region compared to the total area of the cross-section, assigning the value of the corresponding material parameter to each region. The key weighted average material properties of the different cross-sections are summarized in Table 4.4.

Table 4.4. Weighted average tensile material properties.

	E [MPa]	$\sigma_{0.05}$ [MPa]	$\sigma_{0.2}$ [MPa]	σ_u [MPa]	ε_u [%]	*n*	*m*
S1	172615	456	539	587	5.8	8.8	2.6
S2	183667	442	509	533	4.8	11.0	3.2
S3	182637	451	529	554	2.5	12.9	2.7
S4	188482	406	453	509	10.0	13.8	2.6
S5	181030	400	449	502	10.8	14.7	2.4

4.2.2 Initial imperfection measurement

Initial geometric imperfections have an important influence on thin-walled structures and thus the initial imperfections of all specimens tested in this experimental programme were measured prior to testing. Overall imperfections are not relevant in stub columns and beams since cross-section failure is expected, and therefore, only local imperfections were measured in these specimens. The determination of these local imperfections was conducted by placing each specimen on a milling machine and measuring the imperfections of the faces of the specimen at 90º and 180º angles from the weld while moving the milling machine (see Figure 4.4a). The deviations were measured by a Linear Variable Differential Transformer (LVDT) and recorded through a data acquisition system. All the obtained imperfections exhibited a half sine wave shape as demonstrated in Figure 4.4b. The local imperfection amplitudes w_0 reported in Tables 4.5, 4.7 and 4.9 are the average values of the maximum imperfections from both faces. Imperfection amplitudes of the stub column specimens to be tested under combined loading conditions were measured before the end plates were carefully welded, since the influence of the welding process was expected to be much smaller than the play in the testing system.

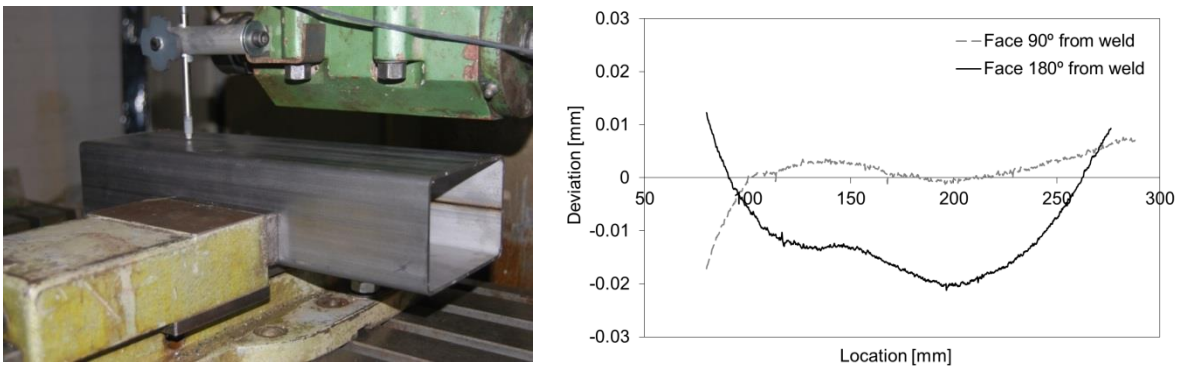

a) Local imperfection measurement setup b) Typical measured local imperfection distribution

Fig. 4.4. Local geometric imperfection measurement.

However, the initial global imperfections of the long specimens have a big influence on the ultimate strength exhibited by the members and they were carefully determined prior to the tests. They are also an important aspect to be considered when defining the adequate position of each specimen during the tests and validate future finite element models. Thus, the magnitude and distribution of the initial bow of each specimen was carefully measured by a laser device. Columns were supported onto two fixed points at both ends and the imperfections were measured by moving the laser device over a completely horizontal surface, recording measurements every 100mm and at mid-height section, as shown in Figure 4.5. The maximum global imperfection amplitudes w_g of each specimen are reported in Table 4.15.

Fig. 4.5. Global geometric imperfection measurement setup.

4.3 Stub column tests under compression and combined loading

Tests conducted on ferritic stainless steel RHS and SHS cross-sections subjected to compression and combined loading are presented in this section, where the test setups and procedures are described and the obtained experimental results are reported.

4.3.1 Stub column tests under compression

Ten stub column tests were conducted on ferritic stainless steel RHS and SHS subjected to compression for the determination of the pure compression resistance of the five investigated cross-sections. Two tests were performed for each cross-section in order to verify the repeatability of the obtained experimental values. Each stub column had a nominal length determined according to Annex A of EN1993-1-3 (2006), being 3 to 3.125 times the width of the widest plate element, in order to avoid any overall buckling phenomena while guaranteeing representative patterns of local geometric imperfections and residual stresses. The real geometry of the specimens was determined prior to the tests and local initial imperfections were also accurately measured. Table 4.5 presents the key geometrical parameters for the stub columns tested under pure compression (labelled as C), where L is the total length of the specimens, H is the total height, B is the total width, t is the thickness, R_{ext} is the external corner radius as defined in Figure 4.1 and w_0 is the maximum amplitude of the measured local imperfections.

Table 4.5. Measured dimensions of compression stub column specimens.

Specimen	L [mm]	H [mm]	B [mm]	t [mm]	R_{ext} [mm]	w_0 [mm]
S1 – C1	249.8	79.9	79.9	3.8	8.6	0.023
S1 – C2	250.0	79.9	79.9	3.8	8.9	0.027
S2 – C1	179.8	60.3	60.2	2.9	6.6	0.059
S2 – C2	180.0	60.1	60.1	2.9	6.3	0.058
S3 – C1	249.5	80.0	39.9	3.9	7.6	0.043
S3 – C2	249.0	80.0	40.0	3.9	7.6	0.035
S4 – C1	359.5	119.7	79.7	2.9	7.0	0.021
S4 – C2	359.5	119.9	79.7	2.9	6.6	0.011
S5 – C1	210.0	70.1	49.9	2.0	4.3	0.025
S5 – C2	210.0	70.0	49.8	2.0	4.2	0.022

Stub column tests were performed at the Laboratori de Tecnologia d'Estructures Lluís Agulló, at Universitat Politècnica de Catalunya (UPC), in a 1000kN INSTRON machine where a uniform compression was introduced to the specimens through two parallel platens. All stub columns were tested under pure compression and displacement control, at a constant rate of 0.5mm/min in order to reproduce the post-buckling behaviour of the specimens. The applied load was measured by the load cell of the testing machine, while the end shortening of the specimens was determined through three LVDT. One of the tests of each cross-section type was also instrumented by strain gauges: two strain gauges were attached to the widest faces of the RHS specimens, at mid-height and at a distance of four times the thickness from the external part of the elements; for SHS specimens, the four faces were instrumented. The information was recorded by an MGCPlus data acquisition system at $2s^{-1}$ intervals.

The experimental results for all compression tests are summarized and reported in Table 4.6, where N_u is the achieved ultimate compression load, δ_u is the end shortening at N_u and $N_u/A\sigma_{0.2}$ compares the ultimate compression resistance of the cross-section with the corresponding squash load, calculated considering the weighted average material properties given in Table 4.4. All the specimens failed by local buckling, as presented in Figure 4.6.

Table 4.6. Summary of test results for compression stub column specimens.

Specimen	N_u [kN]	δ_u [mm]	$N_u/A\cdot\sigma_{0.2}$
S1 – C1	654.6	2.7	1.09
S1 – C2	655.2	2.9	1.11
S2 – C1	342.6	2.7	1.07
S2 – C2	342.8	2.0	1.05
S3 – C1	465.2	3.0	1.05
S3 – C2	465.1	2.8	1.05
S4 – C1	443.1	1.3	0.89
S4 – C2	450.4	1.3	0.91
S5 – C1	190.1	0.9	0.94
S5– C2	190.1	0.9	0.94

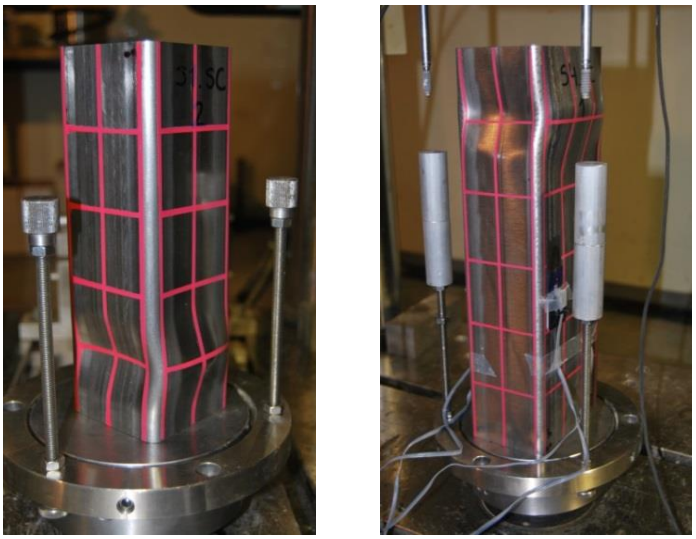

Fig. 4.6. Compression failure modes for S1 – C and S4 – C specimens.

The measured strains provided the necessary information to remove the effect of the elastic deformation of the end platens and to correct the measured end shortening data during the tests, as recommended in (Centre for Advanced Structural Engineering, 1990). The full load-corrected end shortening curves representing the pure compression response of the tested specimens are shown in Figure 4.7, where a minimum scatter between the repeated tests corresponding to the same cross-section indicate the reliability of the conducted tests. The consideration of the normalized load-end shortening response of each specimen, as depicted in Figure 4.8, highlights the different behaviour of stocky cross-sections (S1, S2 and S3), with a more ductile post-buckling response, against the slender ones (S4 and S5), where the descending part of the diagram is steeper.

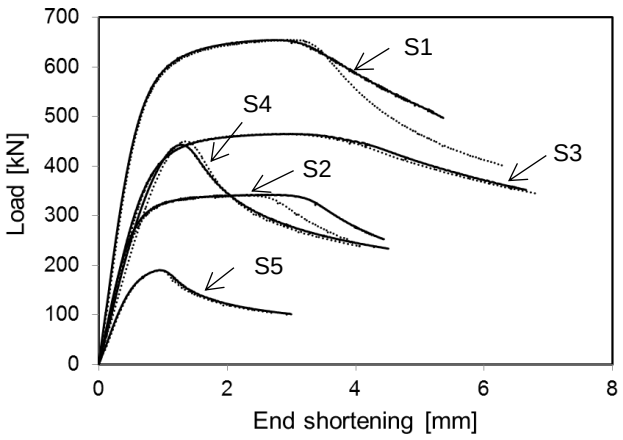

Fig. 4.7. Load end-shortening curves for stub column tests in compression.

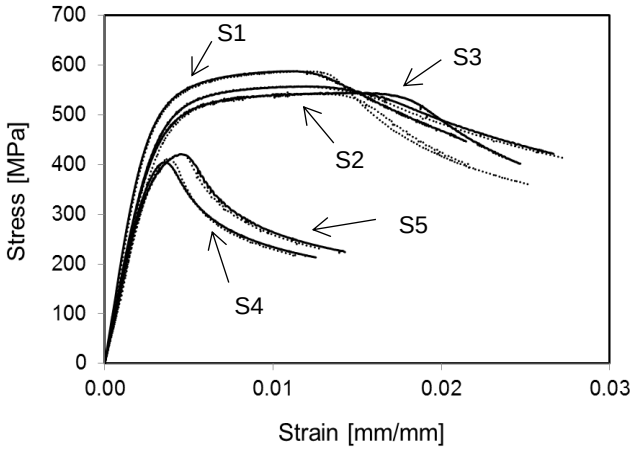

Fig. 4.8. Normalized load-end shortening response for stub column tests in compression.

4.3.2 Stub columns tests under combined loading

The ultimate cross-section resistance of ferritic stainless steel RHS and SHS subjected to combined axial compression and uniaxial bending loading conditions was also investigated in the conducted experimental programme. A total of 16 stub columns were tested under combined loading, two specimens for each cross-section and loading condition. While two specimens were tested for SHS, four specimens were considered for RHS as both bending axes were studied. The measured dimensions of the specimens are reported in Table 4.7, where the symbols are as previously defined. Specimens presented nominal lengths between 3 and 6.25 times the width of the corresponding plate element depending on the studied axis. Combined loading tests around major axis (M_j) have been labelled as CL1 and CL2, while CL3 and CL4 refer to tests conducted around minor axis (M_i).

Table 4.7. Measured dimensions of combined loading stub column specimens.

Specimen	L [mm]	H [mm]	B [mm]	t [mm]	R_{ext} [mm]	w_0 [mm]
S1 – CL1	249.8	79.9	79.9	3.9	8.3	0.026
S1 – CL2	250.0	80.2	80.3	3.8	8.5	0.024
S2 – CL1	180.0	60.1	60.1	2.9	6.5	0.028
S2 – CL2	180.0	60.1	60.1	2.9	6.4	0.024
S3-Mj – CL1	249.3	80.0	39.9	3.8	7.6	0.006
S3-Mj – CL2	249.0	80.0	40.0	3.8	7.7	0.023
S3-Mi – CL3	249.8	79.9	39.9	3.8	7.7	0.031
S3-Mi – CL4	249.8	80.0	40.0	3.8	8.1	0.030
S4-Mj – CL1	359.5	119.9	79.7	3.0	6.5	0.020
S4-Mj – CL2	359.5	119.8	79.7	2.9	6.6	0.016
S4-Mi – CL3	360.0	119.9	79.7	2.9	7.0	0.018
S4-Mi – CL4*	360.0	119.9	79.9	3.0	7.7	0.014
S5-Mj – CL1	210.0	70.0	49.8	2.0	4.2	0.027
S5-Mj – CL2	210.0	70.0	49.8	2.0	4.2	0.037
S5-Mi – CL3	209.5	70.2	49.8	2.0	4.2	0.038
S5-Mi – CL4	210.0	70.0	49.8	2.0	4.3	0.035

All tests were also conducted in a 1000kN INSTRON machine and the compressive load was eccentrically introduced into the specimens through two parallel platens, subjecting the cross-sections to a combination of axial compression and bending moment. The compression platens of the testing machine were fixed against all rotations, and the required degrees of freedom were arranged separately. Two steel end plates were welded to each specimen at both ends with the adequate eccentricity and these end plates were connected to knife edges, allowing rotations about the studied axis. Triangular-shaped grooves with a depth of 9mm were machined in order to guarantee pin-ended boundary conditions, with a groove showing an angle of 100º and a triangular bar with an angle of 60º, as presented in Figure 4.9. The axial load was introduced to the outer faces of the specimens, since the considered nominal eccentricity was equal to the half of the height or width (H/2 or B/2, respectively), depending on the studied axis (see Figure 4.9a). Tests were carried out under displacement control in order to reproduce the post-buckling behaviour, at a testing rate of 0.25mm/min.

The instrumentation used during eccentrically loaded stub column tests is presented in Figure 4.9a and consisted of one LVDT measuring the end shortening at the loading line and a load cell for the measurement of the applied load. Strain-gauges were also affixed for the determination of the compressive and tensile strains at the extreme fibres and two inclinometers fixed to both steel end plates were also included to measure the end rotations. In order to obtain the second order effects for each specimen, the lateral deflections of the compressed faces at mid-height were measured by means of an additional LVDT. Strain gauges were placed at the mid-height section, at a distance of four times the cross-sectional thickness from the corners, similar to those presented for compression stub column tests. All specimens failed by local buckling of the flat elements at mid-height section, as shown in Figure 4.9b for the S2-CL1 specimen.

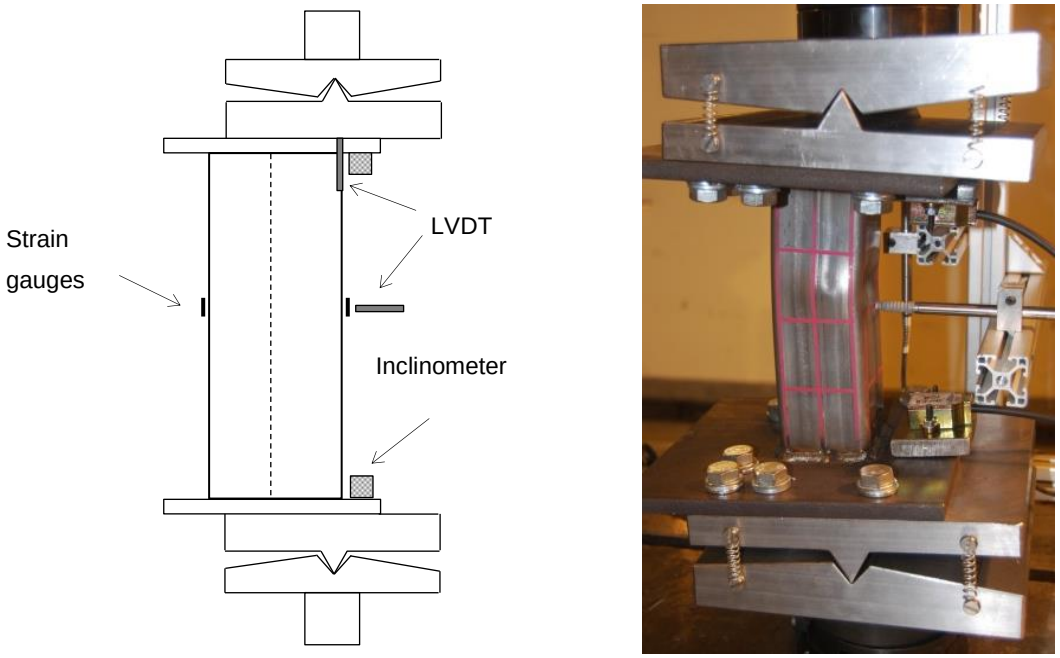

a) Schematic diagram of the test setup. b) Testing of the S2-CL1 specimen.

Fig. 4.9. Combined loading stub column test setup.

As mentioned before, some of the specimens tested under combined loading conditions were instrumented with strain gauges measuring the strains at the extreme fibres of the cross-sections at the mid-height section. These strain measurements allowed for the calculation of the axial and flexural strains (Eq. (4.1) and (4.2) respectively), and therefore, the determination of the actual load eccentricities e_0 introduced into the specimens. This calculated load eccentricities e_0 can be then compared with the corresponding measured eccentricities.

$$\varepsilon_N = \frac{\varepsilon_{max} + \varepsilon_{min}}{2} \tag{4.1}$$

$$\varepsilon_M = \frac{\varepsilon_{max} - \varepsilon_{min}}{2} \tag{4.2}$$

ε_{max} is the measured strain at the maximum compressed fibre and ε_{min} the measured maximum tensile or minimum compressive strain at the other extreme fibre. If the bending moment at each loading step is considered to be a function of both the initial eccentricity e_0 and the lateral deflection or second order eccentricity d and the applied axial load N, and the expression relating the total bending moment with the flexural strain is considered, $M_T = N(e_0 + d) = EI\kappa$, the actual load eccentricity can be determined. The curvature is given by $\kappa = \varepsilon_M / 0.5D$, where D is the outer dimension of the cross-section, equal to the height H when major axis tests are considered and equal to B for minor axis tests; E is the Young's modulus and I the relevant second moment of area. Therefore, the determination of the actual load eccentricity can be derived through Eq. (4.3). Note that since Eq. (4.3) is only applicable in the elastic range of the material, the actual eccentricities have been calculated as the average values of the eccentricities obtained while the material behaved elastically, for low load values.

$$e_0 = \frac{EI(\varepsilon_{max} - \varepsilon_{min})}{D \cdot N} - d \tag{4.3}$$

Results of combined loading stub column tests are reported in Table 4.8, where the ultimate compression load N_u is reported together with the corresponding end-shortening δ_u, end rotation θ_u and the lateral deflection at failure d_u. The measured e_m and calculated actual load eccentricities e_0 are also included, which are in good agreement.

Table 4.8. Summary of test results for uniaxial bending plus compression specimens.

Specimen	N_u [kN]	δ_u [mm]	θ_u [deg]	d_u [mm]	e_m [mm]	e_0 [mm]	M_T [kNm]	M_1 [kNm]	M_2 [kNm]
S1 – CL1	282.0	4.2	1.80	2.6	38.9	38.1	11.5	10.7	0.7
S1 – CL2	278.3	4.4	1.93	2.7	39.7	--	11.8	11.0	0.8
S2 – CL1	150.4	4.3	2.01	3.5	29.5	29.4	4.9	4.4	0.5
S2 – CL2	152.6	4.5	2.05	3.6	28.7	--	4.9	4.4	0.5
S3-Mj – CL1	198.2	7.5	3.40	5.2	39.0	37.0	8.4	7.3	1.0
S3-Mj – CL2	200.3	8.0	3.22	5.9	38.5	--	8.9	7.7	1.2
S3-Mi – CL3	188.1	3.7	2.19	4.4	19.9	18.3	4.3	3.4	0.8
S3-Mi – CL4	189.9	3.5	2.10	4.2	19.5	--	4.5	3.7	0.8
S4-Mj – CL1	192.6	3.2	1.12	1.7	59.4	57.5	11.4	11.1	0.3
S4-Mj – CL2	192.9	3.1	0.98	1.8	59.6	--	11.8	11.5	0.3
S4-Mi – CL3	196.3	2.7	0.90	2.2	39.3	37.4	7.8	7.3	0.4
S4-Mi – CL4*	181.1	2.6	1.19	2.0	38.7	--	7.4	7.0	0.4
S5-Mj – CL1	89.6	2.8	1.10	2.2	35.5	37.1	3.5	3.3	0.2
S5-Mj – CL2	90.4	2.6	0.93	2.0	35.1	--	3.4	3.2	0.2
S5-Mi – CL3	81.2	1.7	0.75	1.4	23.4	22.8	2.0	1.8	0.1
S5-Mi – CL4	80.9	1.6	0.83	1.3	23.7	--	2.0	1.9	0.1

Three different bending moment values associated to the ultimate loads are provided for each specimen in Table 4.8: M_1 represents the first order bending moment due to the eccentricity of the applied force, calculated as $M_1=N_u \cdot e_0$, while M_2 represents the bending moment due to second order effects, determined from $M_2=N_u \cdot d_u$. M_T represents, therefore, the total bending moment, being $M_T=M_1+M_2$. For those specimens where strain gauge measurements were

available, M_1 moments were calculated by using the calculated actual load eccentricities e_0, but for the others the measured eccentricities e_m were considered. The full experimental load-end rotation curves for each cross-section under uniaxial bending plus compression are presented in Figures 4.10 and 4.11.

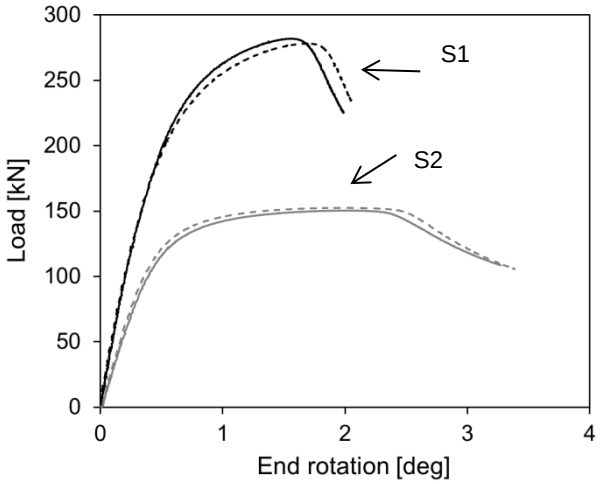

a) Test curves for S1 and S2

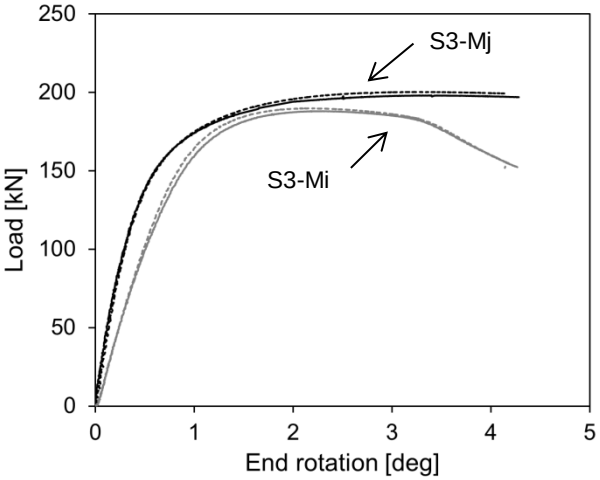

b) Test curves for S3-Mj and S3-Mi

Fig. 4.10. Measured load-end rotation curves for specimens S1,S2 and S3 for uniaxial bending plus compression tests.

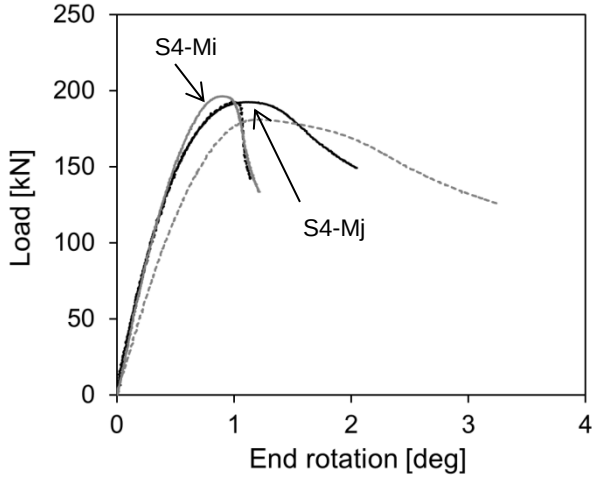

c) Test curves for S4-Mj and S4-Mi

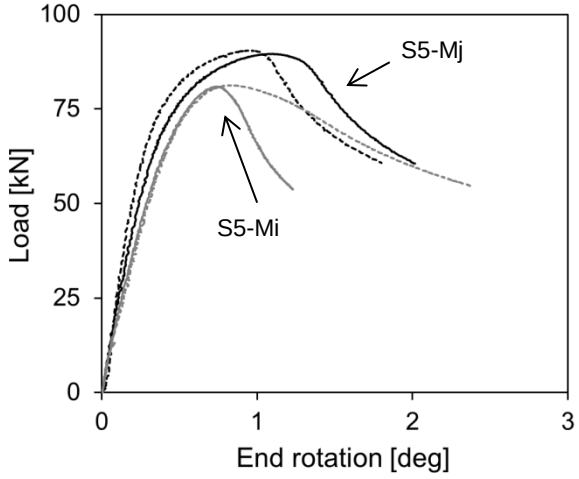

d) Test curves for S5-Mj and S5-Mi

Fig. 4.11. Measured load-end rotation curves for S4 and S5 specimens for uniaxial bending plus compression tests.

4.4 Simply supported beam tests

This section describes the three-point and four-point bending tests conducted on ferritic stainless steel RHS and SHS simply supported beams in order to determine the bending moment resistance and rotation capacity of the different cross-sections. The comparison between three-point and four-point bending tests will highlight the effect of the bending moment gradient and shear upon the cross-sectional resistance capacity. Although web crippling was

not prevented at the loading and support sections in three-point bending tests, these sections were stiffened in four-point bending tests by inserting wooden blocks in order to investigate the influence of stiffening these sections against web buckling caused by local transverse forces.

A total of twelve simply supported beams were tested, eight four-point bending tests (labelled as 4P) covering the five studied cross-sections and considering both major (denoted as Mj) and minor (Mi) bending axes for RHS and four three-point (3P) bending tests. The nominal total length of the specimens tested as simply supported beams was 1700mm, with a span length of 1500mm. The average values of the measured key geometrical parameters for the beam specimens are presented in Table 4.9, where L is the total length of the specimens, H is the height, B is the width, t is the thickness, R_{ext} is the external corner radius, as defined in Figure 4.1 and w_0 is the maximum amplitude of the measured local imperfections.

All tests were conducted in a 1000kN capacity MTS hydraulic machine under displacement control so the post-failure behaviour of the beams could be captured, at a testing rate of 2mm/min. Data was acquired with the MGCPlus system.

Table 4.9. Measured dimensions of short beam specimens.

	L [mm]	H [mm]	B [mm]	t [mm]	R_{ext} [mm]	w_0 [mm]
S1 – 3P	1700.0	80.0	79.9	3.8	8.0	0.069
S2 – 3P	1700.0	60.1	60.2	3.0	6.1	0.078
S3-Mj – 3P	1700.0	79.9	39.9	3.9	6.6	0.078
S4-Mj – 3P	1700.0	119.8	79.9	2.6	7.0	0.060
S1 – 4P	1700.0	80.3	80.3	4.0	7.2	0.073
S2 – 4P	1700.0	60.2	60.1	2.9	6.3	0.057
S3-Mj – 4P	1700.0	79.9	39.8	3.8	7.2	0.062
S3-Mi – 4P	1700.0	79.9	39.9	3.9	6.9	0.034
S4-Mj – 4P	1700.0	119.8	79.9	2.9	7.1	0.062
S4-Mi – 4P	1700.0	119.7	80.0	2.9	7.1	0.077
S5-Mj – 4P	1700.0	70.1	49.8	1.9	4.4	0.067
S5-Mi – 4P	1700.0	70.1	49.9	2.0	4.2	0.075

4.4.1 Four-point bending tests

Eight four-point bending tests on ferritic stainless steel RHS and SHS were conducted in order to investigate the pure bending response of the cross-sections. The adopted test configuration is presented in Figure 4.12, where the loads were applied at a distance of 510mm from both supports, being separated by 480mm. Loading and support sections were stiffened to prevent web crippling by inserting wooden blocks and reactions at both supports were measured in order to verify the symmetry of the system. In addition, the deflections at the midspan were measured with a string potentiometer and at loading points by two displacement transducers for the determination of the curvature of the specimens at each load step. Two inclinometers recording end rotations were placed at the support points and strain-gauges were also attached

to the top and bottom flanges of the cross-sections at a distance of 60mm from the midspan section.

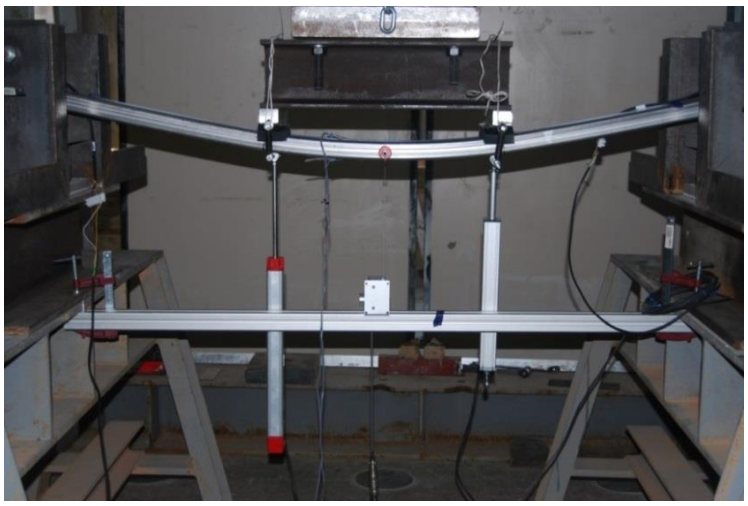

Fig. 4.12. General view of the S3-Mi – 4P test under four-point bending conditions.

All specimens failed by local buckling of the compressed flange at the loading sections for four-point bending tests (see Figure 4.13a) since wooden blocks inserted at these positions prevented web crippling.

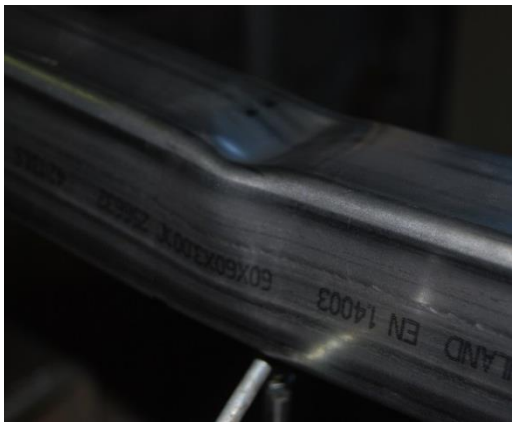

a) Four-point bending loading conditions (wooden blocks)

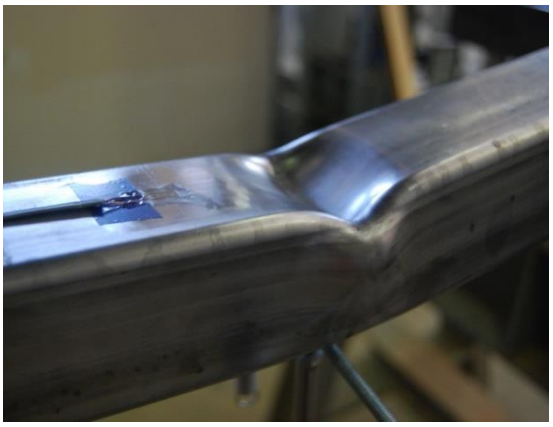

b) Three-point bending loading conditions (no wooden blocks)

Fig. 4.13. Detailed view of the failed sections at loading section for S2 specimens.

Four-point bending test results are summarised in Table 4.10, where the reached ultimate loads F_u are reported together with the corresponding midspan deflection u_u, and the ultimate bending moment M_u calculated from the measured support reactions. Additionally, the comparison of the bending resistances against elastic (M_{el}) and plastic (M_{pl}) bending moment capacities is also presented, and finally, the rotation capacity R is provided for those beams showing a M_u/M_{pl} ratio greater than 1. The rotation capacity R is a measure of the rotation between the point where the moment-curvature curve reaches the plastic bending capacity M_{pl} and the point where the moment falls below M_{pl}. For four-point bending tests, the rotation capacity R is determined according to $R=\kappa_u/\kappa_{pl}-1$, where κ_u is the curvature corresponding to the ultimate load

and defined as given in Eq. (4.4), and κ_{pl} is the elastic curvature corresponding to M_{pl} in the ascending branch, defined as $\kappa_{pl}=M_{pl}/EI$. E is the Young's modulus, I is the relevant second moment of area, u_{av} is the average value of the deflections at the loading sections (u_1 and u_3), u_2 is the deflection at the midspan section and L^* is the distance between applied loads, as defined in Figure 4.14.

$$\kappa = \frac{8 \cdot (u_2 - u_{av})}{4 \cdot (u_2 - u_{av})^2 + L^{*2}} \tag{4.4}$$

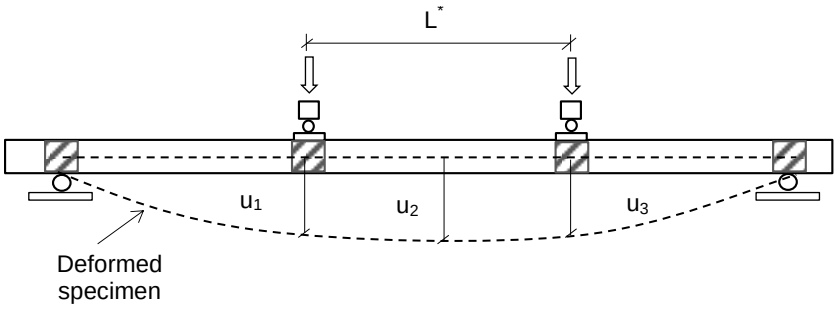

Fig. 4.14. Symbol definition for the determination of the curvature in a four-point bending test.

Table 4.10. Summary of test results for four-point bending specimens.

	F_u [kN]	u_u [mm]	M_u [kNm]	M_u/M_{el}	M_u/M_{pl}	R	Experimental classification
S1 – 4P	66.1	42.4	16.9	1.18	0.96	--	Class 3
S2 – 4P	27.2	59.6	6.9	1.23	1.00	1.4	Class 2
S3-Mj – 4P	43.2	63.8	11.0	1.36	1.02	1.8	Class 2
S3-Mi – 4P	26.3	104.4	6.7	1.26	1.01	2.1	Class 2
S4-Mj – 4P	64.1	16.3	16.3	1.03	0.84	--	Class 3
S4-Mi – 4P	48.6	22.5	12.4	0.97	0.83	--	Class 4
S5-Mj – 4P	19.2	48.0	4.9	1.26	1.03	1.9	Class 2
S5-Mi – 4P	13.9	49.9	3.5	1.09	0.94	--	Class 3

The cross-section classification of each specimen, based upon the experimental results, is also reported in Table 4.10. Cross-sections not reaching the elastic bending capacity have been experimentally classified as Class 4, while those with ultimate bending resistances between elastic and plastic moments have been considered as Class 3. A minimum rotation capacity of R≥3 is adopted for guaranteeing the moment redistribution capacity of carbon steel cross-sections and since no specific limit is provided for stainless steels, the same limit is usually adopted, as in Theofanous et al. (2014). Therefore, specimens reaching the plastic bending capacity but with a rotation capacity lower than 3 have been defined as Class 2, while those with R≥3 have been classified as Class 1. As Table 4.10 demonstrates, a single cross-section can be experimentally adopted as Class 4, S4-Mi, while none of them can be considered Class 1, and the rest are classified either as Class 2 and Class 3.

The full normalized bending moment-curvature curves are presented in Figure 4.15 for those beams tested under four-point bending conditions. The weighted average material properties

presented in Table 4.4 have been used in the calculation of κ_{pl} and M_{pl} for the normalization. No curves are presented for section S4 due to data acquisition issues making the curvature calculations impossible, although ultimate loads were recorded.

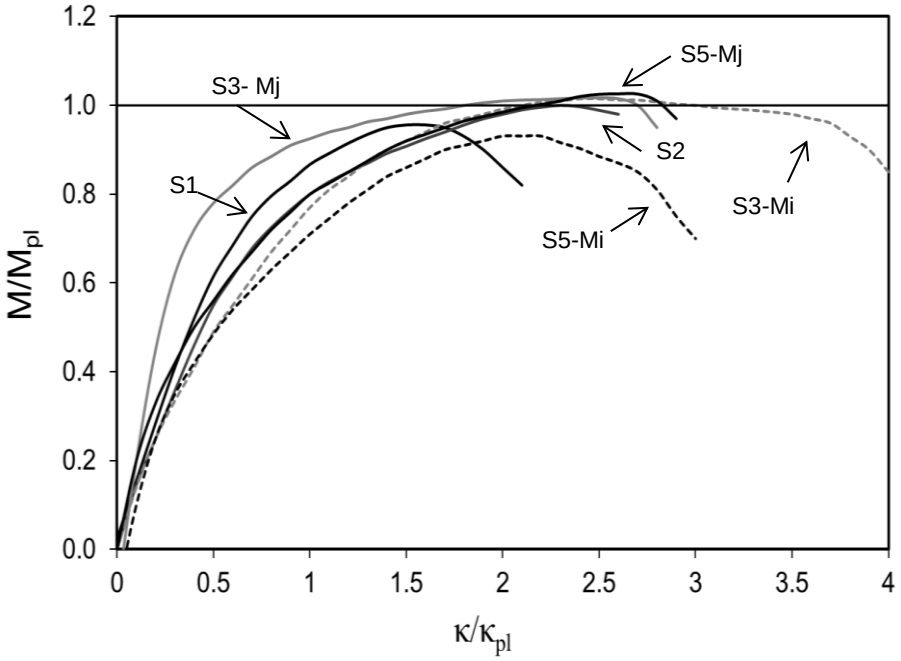

Fig. 4.15. Normalized bending moment-curvature curves for four-point bending tests.

The typical behaviour of stocky and slender cross-sections can be better understood from the analysis of the recorded strain gauge data. Figure 4.16 shows both the load-deflection and load-strain curves for the S2 and S5-Mj specimens tested under 4P loading conditions. The loads and stresses at which the beams do not behave elastically have been identified for both specimens, indicating some nonlinearity occurred during the tests. The loads and stresses at which the strain gauges measuring the extreme tensile and compressive strains do not behave identically have also been identified, which indicates local buckling of the compressed flange. In the load-deflection curves stresses have been determined through elastic calculations, while in load-strain curves the stresses corresponding to the strains at which a different behaviour is observed have been considered from the average material curve of each cross-section.

The comparison between these four Figures clearly shows the different behaviour exhibited by stocky and slender cross-sections. For the S2 specimen the loss of linearity in Figure 4.16a can be attributed to the nonlinear stress-strain behaviour of the material, since the local buckling of the compressed flange does not start until higher load levels are reached (see Figure 4.16b). The load at which the strain gauges diverged was defined as the load at which the difference between the compressive and tensile strains reached 1% of the maximum strain. For the S5-Mj specimen the loss in linearity and the local buckling of the compressed flange occurred at the same load, as shown in Figures 4.16c and 4.16d, which indicates that buckling took place while the material was still elastic and the nonlinearity in the curves is due to pre-yielding local buckling, which is typical of slender cross-sections.

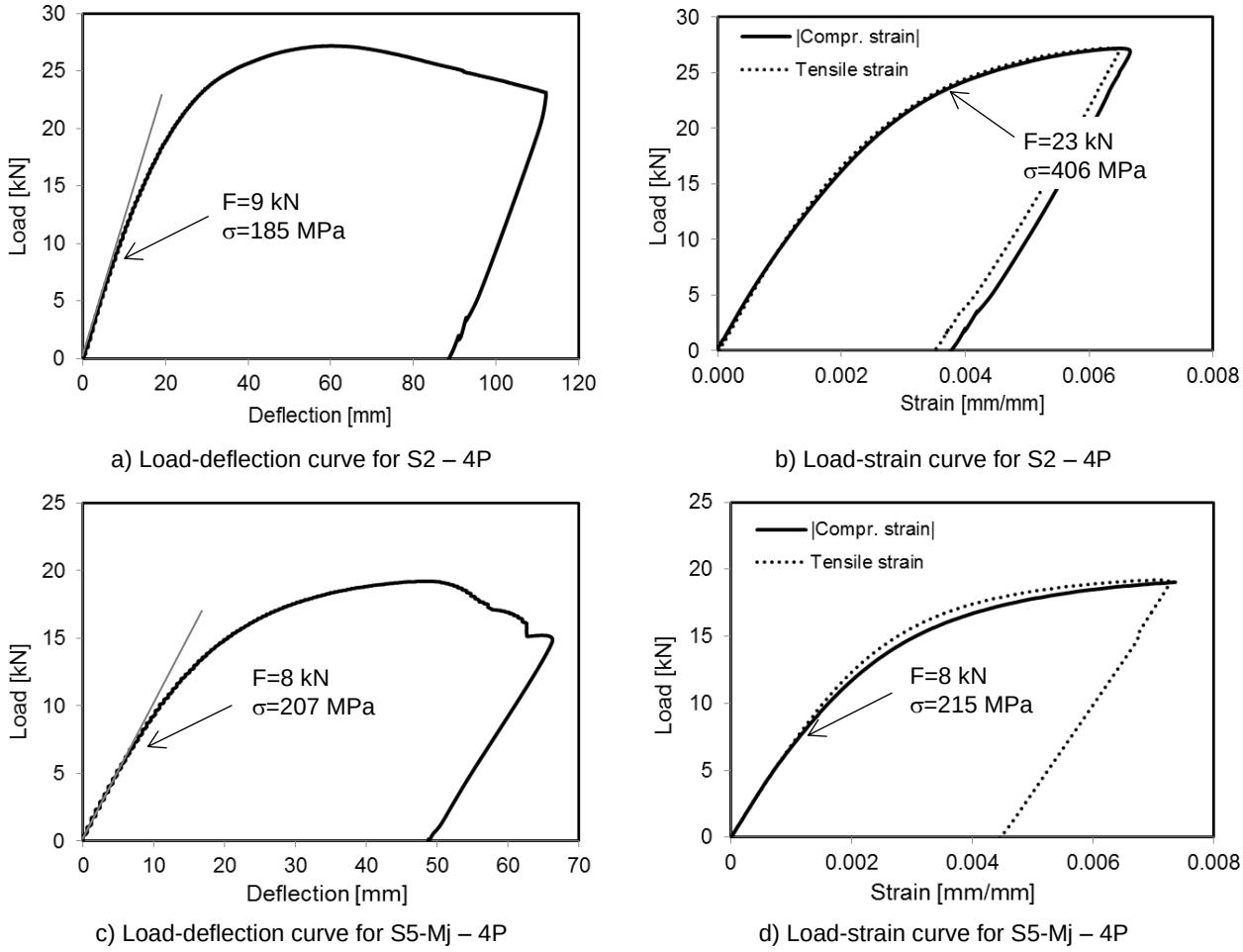

a) Load-deflection curve for S2 – 4P

b) Load-strain curve for S2 – 4P

c) Load-deflection curve for S5-Mj – 4P

d) Load-strain curve for S5-Mj – 4P

Fig. 4.16. S2 – 4P (stocky) and S5-Mj – 4P (slender) cross-section behaviour in bending.

4.4.2 Three-point bending tests

Four simply supported beam tests subjected to three-point bending conditions were tested under the setup shown in Figure 4.17, but not for all cross-sections and bending axis. Only S1, S2, S3-Mj and S4-Mj cross-sections were tested under bending moment gradient conditions. The load was introduced as a line load through neoprene elements at the midspan and the deflection at the loading point was measured using displacement transducers. The rotation at the loading section was measured using two inclinometers placed at the supports along with load cells to measure the support reactions. The instrumentation also included two strain-gauges measuring the maximum compressive and tensile strains of the cross-section situated at 60mm from the loading point. All specimens failed by a combination of buckling of the compressed flange and web crippling at the loading points (see Figure 4.13b), since they were not stiffened. This needs to be considered when analysing the experimental results as the ultimate bending capacity of the specimens subjected to both bending and local transverse force is smaller than for those with stiffened loading sections, where no interaction occurs.

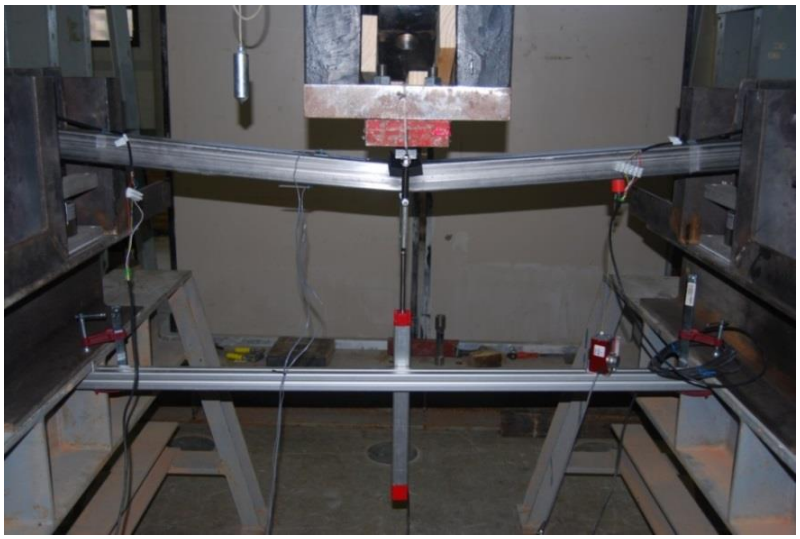

Fig. 4.17. General view of the S2-3P test under three-point bending conditions.

Three-point bending test results are summarised in Table 4.11, where the reached ultimate loads F_u are reported together with the corresponding midspan deflections u_u, and ultimate bending moments M_u. The comparison of the bending resistances against elastic (M_{el}) and plastic (M_{pl}) bending capacities is also presented, as well as the rotation capacity R of those beams reaching the plastic bending moment capacity. For three-point bending test, the rotation capacity is calculated according to $R=\theta_u/\theta_{pl}-1$, where θ_u is the total rotation at the midspan section corresponding to the ultimate load, which can be calculated as the sum of the rotations at both support sections. θ_{pl} is the elastic rotation corresponding to the plastic moment capacity M_{pl} in the ascending branch, $\theta_{pl}=L\cdot M_{pl}/2EI$, where L is the span length, E is the Young's modulus and I is the relevant second moment of area.

Table 4.11. Summary of test results for three-point bending specimens.

	F_u [kN]	u_u [mm]	M_u [kNm]	M_u/M_{el}	M_u/M_{pl}	R
S1 – 3P	40.4	44.7	15.2	1.06	0.86	--
S2 – 3P	26.4	26.4	6.2	1.11	0.90	--
S3-Mj – 3P	30.2	30.9	11.3	1.40	1.04	0.99
S4-Mj – 3P	34.1	10.0	12.8	0.80	0.65	---

Figure 4.18 shows the normalized moment-rotation curves for the specimens tested under three-point bending conditions, where rotations were calculated as the sum of the measured rotations at the supports and the material properties reported in Table 4.4 were used in M_{pl} and θ_{pl} calculations. The behaviour of the beams tested under three-point bending conditions can be appreciated in Figure 4.18, clearly different from that exhibited by the four-point bending specimens, which showed greater ductility apparent from a higher load maintained with increasing curvatures.

As web crippling was not prevented in these specimens, the behaviour of all of these 3P beams were similar, showing peak-shape moment-rotation curves as the cross-sections were not capable of rotating while maintaining the achieved ultimate loads, due to web failure.

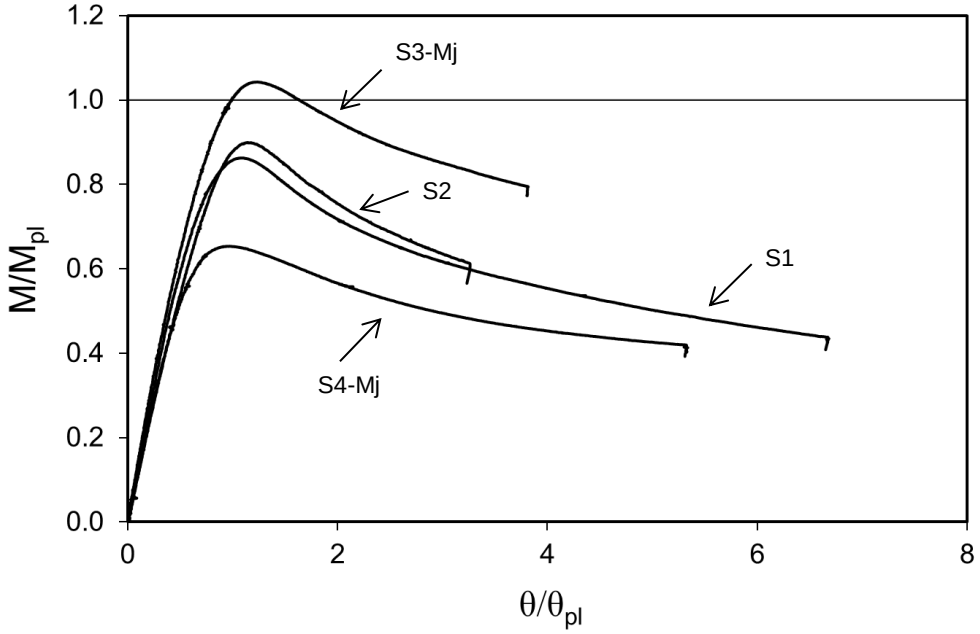

Fig. 4.18. Normalized moment-rotation curves for three-point bending tests.

EN1993-1-4 (2006) provisions regarding the interaction of local transverse force and bending moment refer to EN1993-1-3 (2006) standard for carbon steel cold-formed sections and it is considered through Eq. (4.5).

$$\frac{F_{Ed}}{R_{w,Rd}} + \frac{M_{Ed}}{M_{c,Rd}} \leq 1.25 \tag{4.5}$$

where F_{Ed} and M_{Ed} are the design local transverse force and bending moment respectively, $R_{w,Rd}$ is the web crippling resistance and $M_{c,Rd}$ is the bending moment resistance. EN1993-1-3 (2006) provides several expressions for the determination of the web crippling resistance of cross-sections, although Bock et al. (2013) proposed a more accurate expression for stainless steel RHS and SHS sections. The local transverse force and bending moment interaction expression given in Eq. (4.5) has been evaluated by comparing the 3P experimental loads with those calculated from Eq. (4.6). For this analysis, the bending moment resistances M_u obtained from the 4P tests have been considered, together with the two different approaches for the calculation of the web crippling resistance $R_{w,Rd}$. L_s refers to the span length, equal to 1500mm in the 3P tests.

$$F_{pred} = 1.25\left[\frac{1}{R_{w,Rd}} - \frac{L_s/2}{M_u}\right]^{-1} \tag{4.6}$$

Table 4.12 presents the comparison of the measured ultimate experimental loads F_u with those predicted from Eq. (4.6) and the different approaches of calculating $R_{w,Rd}$. This Table demonstrates that results obtained for the web crippling resistances given in EN1993-1-3 (2006) are overly conservative, while the predictions using the Bock et al. (2013) formulation can be seen to be substantially improved over the current codified method.

Table 4.12. Assessment of local force-bending moment interaction for the 3P tests.

		F_{pred}/F_u	
	F_u [kN]	$R_{w,Rd}$ according to EN1993-1-3 (2006)	$R_{w,Rd}$ according to Bock et al. (2013)
S1 – 3P	40.4	0.53	0.96
S2 – 3P	26.4	0.58	0.94
S3-Mj – 3P	30.2	0.51	0.94
S4-Mj – 3P	34.1	0.52	1.01
	Mean	0.53	0.96
	COV	0.059	0.035

4.5 Continuous beam tests

The behaviour of stainless steel RHS and SHS members subjected to bending was investigated by conducting nine five-point bending or continuous beam tests (labelled as 5P), which were performed in order to determine the redistribution capacity of ferritic stainless steel beams. The objective of these tests was to assess whether plastic design, which is not currently allowed in EN1993-1-4 (2006), is applicable to ferritic stainless steel cold-formed members. The same cross-sections analysed under four-point bending conditions were investigated, with RHS tested in both major and minor bending axes. The measured key geometrical properties of these long beams are reported in Table 4.13.

Table 4.13. Measured dimensions for long beam specimens.

	L [mm]	H [mm]	B [mm]	t [mm]	R_{ext} [mm]
S1 – 5P1	3200.0	80.0	79.8	4.0	8.1
S1 – 5P2	3200.0	79.6	79.8	4.0	8.1
S2 – 5P	3200.5	60.2	60.2	3.1	6.4
S3-Mj – 5P	3199.5	80.1	40.0	4.1	8.6
S3-Mi – 5P	3199.5	79.9	39.8	4.0	8.1
S4-Mj – 5P	3200.0	119.4	79.9	2.9	7.5
S4-Mi – 5P	3200.0	119.6	80.5	3.0	7.4
S5-Mj – 5P	3200.5	70.1	49.9	2.0	4.3
S5-Mi – 5P	3200.0	70.0	49.7	2.0	3.8

All specimens tested under five-point bending configuration presented a nominal length of 3200mm, and were tested over a two span structural configuration. The test setup is shown in Figure 4.19 with the two loaded 1500mm spans, each subjected to a concentrated midspan load. All support reactions were measured using load cells in order to evaluate the reaction redistribution during the tests, midspan deflections were recorded by two displacement

transducers and rotations were also measured using inclinometers at the right span outer support and at a distance of 250mm from the internal support within the left span. Strains at the top and bottom flanges were measured by several strain gauges at a distance of 60mm from the loading sections and the internal support and all loading and support points were stiffened with wooden blocks in order to prevent web crippling.

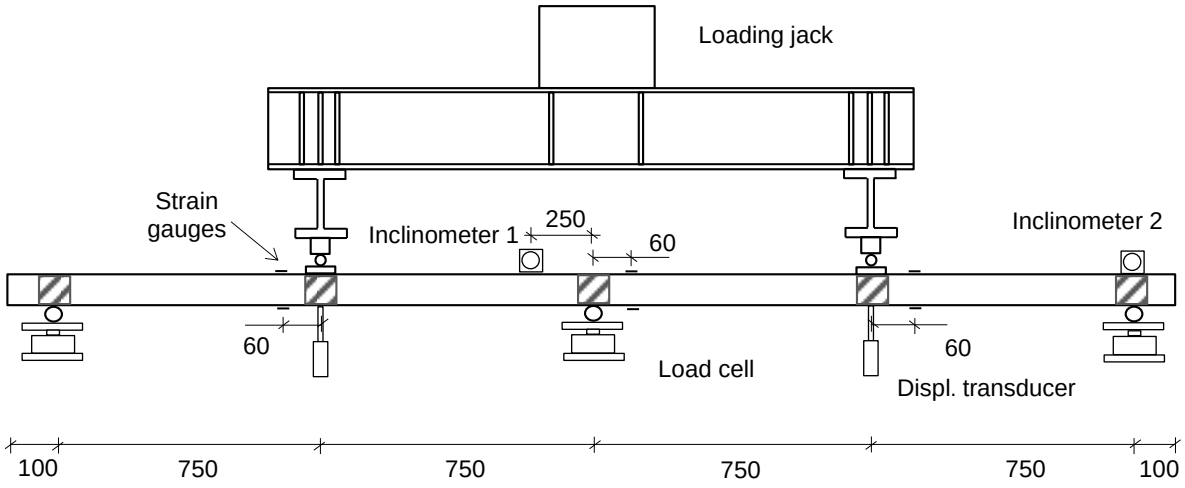

Fig. 4.19. Schematic diagram of the test setup for five-point bending tests. Dimensions in mm.

Full load-average midspan deflection curves for the conducted five-point bending tests are presented in Figure 4.20 and the key test results are reported in Table 4.14 with the ultimate loads F_u, corresponding u_u midspan deflections, reaction forces at the middle support R_u and corresponding rotations at inclinometers 1 and 2, θ^1_u and θ^2_u (see Figure 4.19) presented. Continuous bending tests on S1 cross-section were repeated in order to demonstrate the reliability of the test results, with the differences as shown in Figure 4.20 and Table 4.14 being minimal.

Table 4.14. Summary of test results for five-point bending specimens.

	F_u [kN]	u_u [mm]	R_u [kN]	θ^1_u [rad]	θ^2_u [rad]
S1 – 5P1	117.2	25.1	77.7	0.050	0.022
S1 – 5P2	119.5	24.6	79.8	0.047	0.025
S2 – 5P	51.7	29.1	34.0	0.053	0.038
S3-Mj – 5P	84.2	23.5	56.1	0.048	0.025
S3-Mi – 5P	52.4	47.4	34.6	0.068	0.047
S4-Mj – 5P	106.5	11.4	69.5	0.022	0.010
S4-Mi – 5P	87.4	16.7	58.7	0.029	0.012
S5-Mj – 5P	34.4	20.6	22.5	0.038	0.025
S5-Mi – 5P	26.7	27.8	17.6	0.055	0.033

The specimens were tested in a 1000kN MTS hydraulic machine under displacement control at a rate of 2mm/min, and failed by local buckling of the compressed flange at the internal support and loading points (see Figure 4.21).

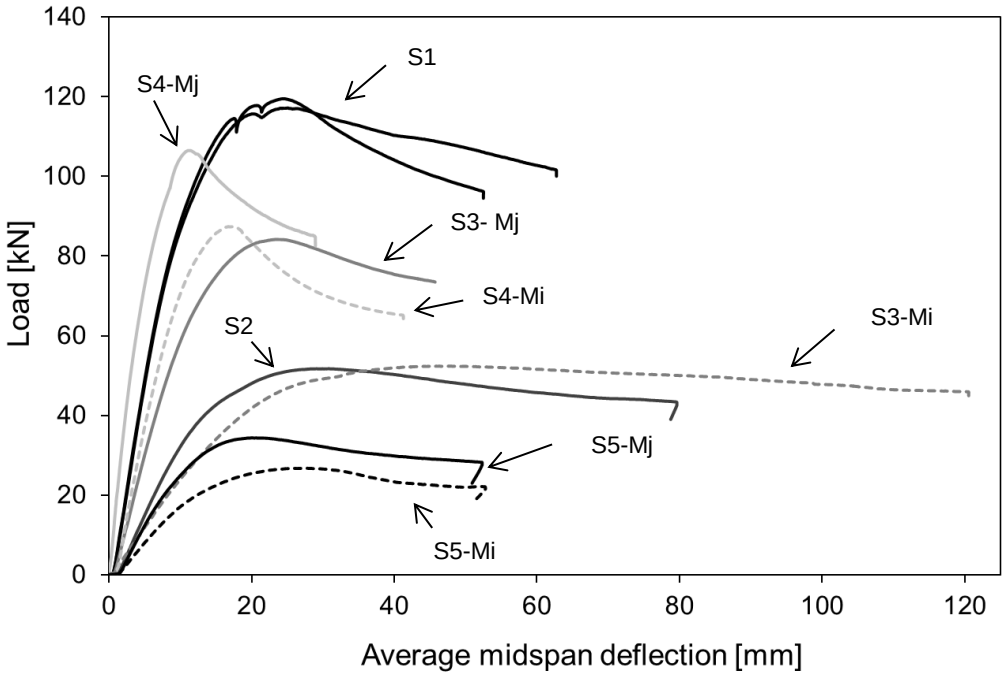

Fig. 4.20. Load-midspan deflection curves for five-point bending tests.

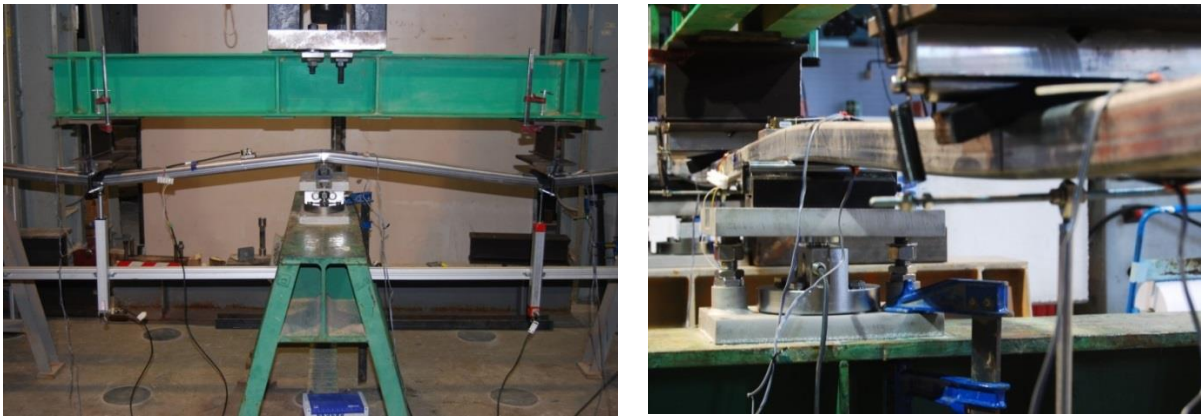

Fig. 4.21. Detailed views of the failed sections for the S1-5P specimen.

The analysis of the experimental results of S1 and S2 cross-section continuous beams based on the reaction and strain gauge measurements is presented in order to illustrate the behaviour of ferritic stainless steel RHS indeterminate beams. For both cross-sections the experimental bending moment at the internal support and span sections, calculated from the measured support reactions, has been plotted against the applied total load as continuous lines in Figures 4.22a and 4.22c, together with the elastically predicted bending moment values as slashed lines. Additionally, the elastic and plastic bending capacities are shown, with the experimental bending resistances from the previous simply supported tests. Ultimate bending values corresponding to the 3P tests $M_{u,3P}$ have been considered since the bending moment distribution in support sections is similar. The measurements obtained from the different strain gauges attached at the internal support sections are also presented (Figures 4.22b and 4.22d) in order to evaluate the load level at which the compressed flange of the cross-section buckles.

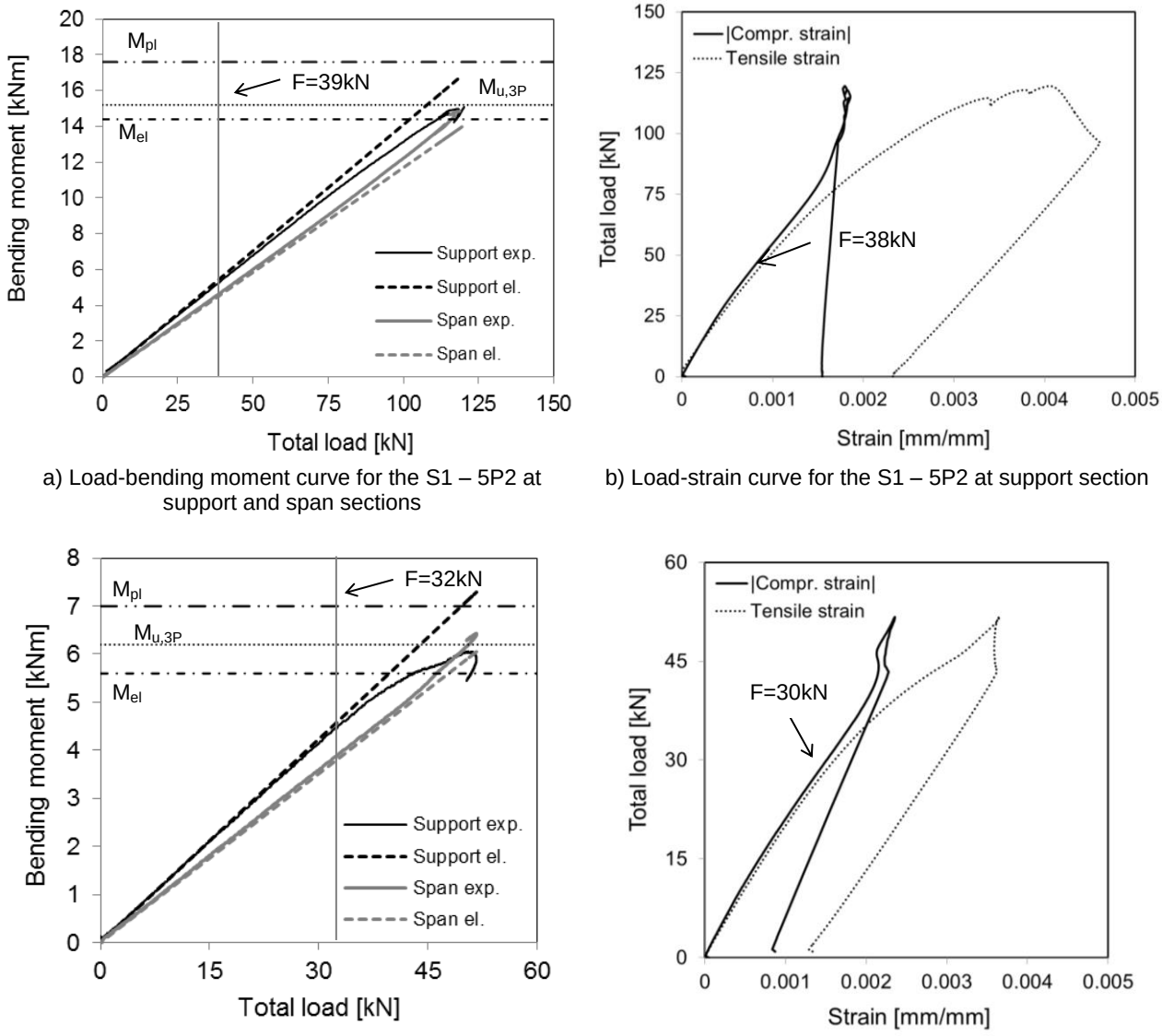

a) Load-bending moment curve for the S1 – 5P2 at support and span sections

b) Load-strain curve for the S1 – 5P2 at support section

c) Load-bending moment curve for the S2 – 5P at support and span sections

d) Load-strain curve for the S2 – 5P at support section

Fig. 4.22. S1 – 5P2 and S2 – 5P cross-section behaviour as continuous beams.

Figure 4.22 demonstrates that for both cross-sections when the load at which the compressive and tensile strains begin to differ the experimental and elastic bending moments also start diverting, indicating the buckling of the compressed flange. Beyond this point, the experimental bending moment at the support increases in a lower rate than the elastic moment while the bending moment at the midspan section increases faster, until the value of the ultimate bending moment for 3P tests $M_{u,3P}$ is reached and the beam fails.

4.6 Member tests under compression and combined loading

Flexural buckling and beam-column tests were conducted in order to investigate the behaviour of ferritic stainless steel members. Five ferritic RHS and SHS members with a nominal length of 1500mm were tested under pure compression and seven beam-column tests under combined compression and uniform bending moment were also performed. All column and beam-column

tests were performed under pin-ended boundary conditions and minor axis buckling was considered in RHS specimens.

The actual geometry of all specimens was carefully determined by the measurement of all the relevant dimensions, which are summarized in Table 4.15. L is the total length of the specimens, H is the total height, B is the total width, t is the thickness and R_{ext} is the external corner radius, as defined in Figure 4.1. For every cross-section, a flexural buckling (i.e. concentric compression) test, labelled CC, was conducted, together with one or two beam-column (i.e. eccentric compression) tests, named EC1 and EC2 respectively. The maximum global imperfection amplitude w_g of each specimen is also reported in Table 4.15, measured as described in section 4.2.2.

Table 4.15. Measured dimensions for the tested specimens.

Specimen	L [mm]	H [mm]	B [mm]	t [mm]	R_{ext} [mm]	w_g [mm]
S1 – CC	1495	79.6	80.2	3.9	7.0	0.81
S1 – EC1	1495	80.1	80.3	3.9	7.3	1.25
S1 – EC2	1498	79.9	80.3	4.0	7.5	1.38
S2 – CC	1500	60.3	60.2	2.9	5.9	0.66
S2 – EC1	1500	60.0	60.2	3.0	5.9	0.69
S3 – CC	1500	80.0	40.0	3.8	6.8	0.85
S3 – EC1	1500	80.0	40.2	3.8	6.5	0.89
S4 – CC	1500	119.8	79.8	2.9	7.2	1.21
S4 – EC1	1500	119.8	79.6	3.0	7.2	1.58
S5 – CC	1500	70.0	49.6	2.0	4.4	1.09
S5 – EC1	1500	70.0	49.9	2.0	4.2	1.32
S5 – EC2	1500	70.1	49.9	2.0	4.3	1.35

Pin-ended conditions were guaranteed by two pin-ended bearings, which allowed free rotations about minor axis and fixed conditions about the orthogonal axis, as presented in Figure 4.23.

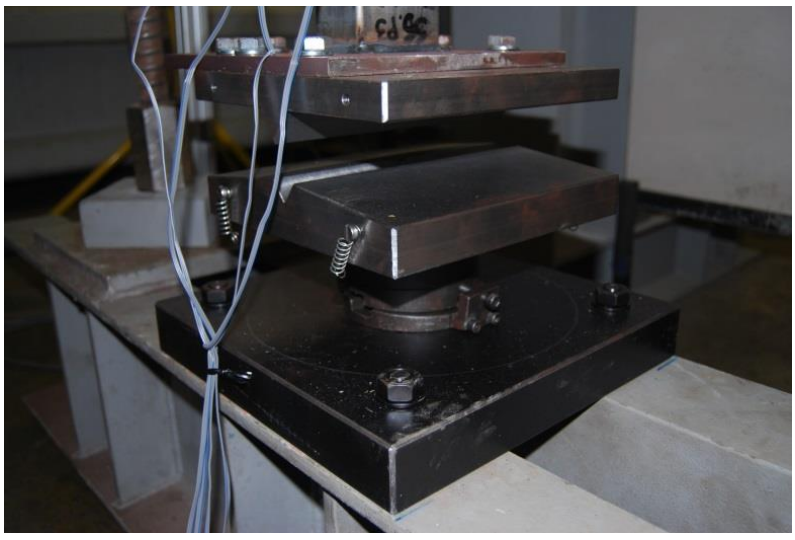

Fig. 4.23. Lower pin-ended bearing.

These bearings were specially mechanized and consisted on plates with a knife edged wedges and plates containing a V-shaped pits. The lower pit plates were connected to the end supports, while the upper ones were connected to the hydraulic jack. Two steel end plates were welded to each specimen at both extremes, at a specified eccentricity, and the end plates were bolted to the wedged plates.

Although the nominal length L of each specimen was 1500mm, the effective length of the system L_e equal to the distance between knife-edges will be considered in further analysis. The thickness of both end plates and the bearing plates need to be added to the length of the specimens, which leads to an effective length of L_e=1600mm. Thus, the member slenderness λ_c spectrum of the specimens ranged from 0.65 to 1.72, calculated according to Eq. (4.7) given in EN1993-1-4 (2006), where A is the cross-sectional area (effective area has been considered for Class 4 cross-sections), $\sigma_{0.2}$ is the 0.2% proof stress and N_{cr} is the Euler elastic critical load for flexural buckling.

$$\lambda_c = \sqrt{\frac{A\sigma_{0.2}}{N_{cr}}} \tag{4.7}$$

The instrumentation of the specimens consisted on two laser devices measuring the lateral horizontal deflections about the minor axis at mid-height, two inclinometers on the welded steel plates measuring end rotations and string potentiometers determining end shortenings, as shown in Figures 4.24 to 4.26. The applied load was directly measured from the loading machine. Four linear electrical resistance strain gauges were affixed to the extreme tensile and compressive fibres of the mid-height sections in the axial direction, at a distance of four times the cross-section thickness from the corners, to determine the actual load eccentricity. All the information was recorded by an MGCPlus data acquisition system at $2s^{-1}$ intervals.

Fig. 4.24. In detail instrumentation setup at mid-height section.

Regarding the testing procedure, the specimens, together with the bolted edge plates, were placed into the machine and the actuator was then slowly moved closer until they were in contact. To ensure full contact and avoid settlement effects, a compression load about 3kN was applied, which was negligible compared to the achieved ultimate loads. The tests were then conducted under displacement control at a testing rate of 0.2mm/min, in order to reduce any possible dynamic effects, and allowing the test to continue to post-ultimate stage. The general test setup of flexural buckling and beam-column tests is presented in Figures 4.25 and 4.26, where the most relevant instrumentation is indicated, together with a photograph of the S1 – CC specimen prior to testing.

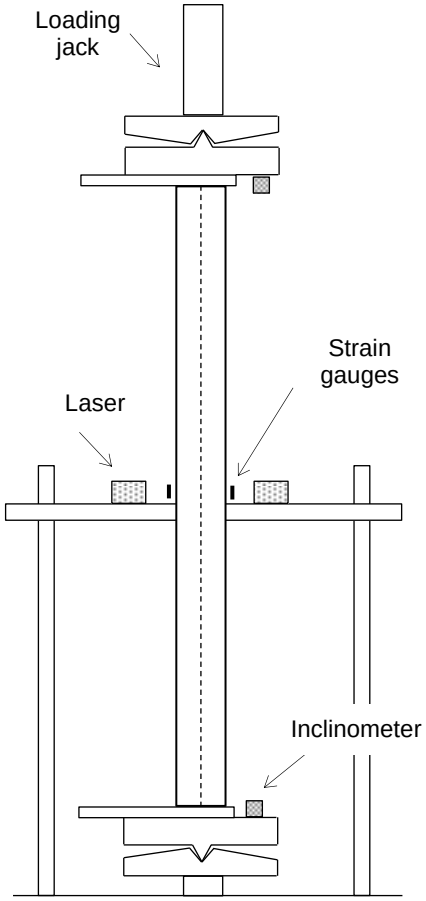

Fig. 4.25. Schematic diagram of the test setup for flexural buckling and beam-column tests.

Fig. 4.26. S1 – CC specimen prior to testing.

Measured load eccentricities e_m are compared with those calculated from strain gauge measurements e_0 in Table 4.16. The determination of the experimental load eccentricities has been derived through Eq. (4.8) following a similar procedure to that described for stub columns subjected to combined loading in section 4.3.2. ε_{max} is the measured strain at the maximum compressed fibre and ε_{min} the measured maximum tensile or minimum compressive strain at the other extreme fibre, B is the width of the cross-section, E is the Young's modulus, I is the relevant second moment of area, d is the lateral deflection at each loading step N and w_g is the initial global imperfection amplitude.

$$e_0 = \frac{EI(\varepsilon_{max} - \varepsilon_{min})}{B \cdot N} - d - w_g \quad (4.8)$$

Experimental results of ferritic RHS and SHS members tested under pure compression and combined loading are reported in Table 4.16, where N_u is the ultimate compression load, M_u is the bending moment when N_u is reached, d_u and θ_u are the lateral deflection and the total rotation corresponding to N_u, respectively. M_u represents the total bending moment, comprising the first order bending moment due to load eccentricity e_0 ($M_1=N \cdot e_0$) and second order effects caused by the lateral deflection of the members ($M_2=N \cdot d$). The similarity between the measured load eccentricities e_m and the calculated actual values e_0 indicate the reliability of the conducted tests. Note that the experimental eccentricities provided in Table 4.16 have been calculated as the average values of the eccentricities calculated at those loading steps where the material behaved elastically, with a constant Young's modulus.

Table 4.16. Summary of test results for column and beam-column specimens.

Specimen	N_u [kN]	M_u [kNm]	d_u [mm]	θ_u [rad]	e_m [mm]	e_0 [mm]
S1 – CC	447.5	2.7	5.5	0.028	0	0.6
S1 – EC1	256.0	10.3	23.0	0.104	20	17.3
S1 – EC2	193.5	12.4	29.2	0.127	40	34.7
S2 – CC	173.1	2.0	9.9	0.044	0	1.4
S2 – EC1	79.9	4.9	31.2	0.135	30	29.7
S3 – CC	130.2	2.6	18.6	0.078	0	1.1
S3 – EC1	76.4	4.7	38.6	0.167	20	22.7
S4 – CC	364.5	2.7	6.6	0.034	0	0.8
S4 – EC1	222.8	7.7	16.7	0.076	20	17.9
S5 – CC	97.4	0.9	8.4	0.032	0	1.2
S5 – EC1	62.4	2.3	25.2	0.103	12.5	11.3
S5 – EC2	44.3	2.6	28.8	0.123	25	29.4

Full measured experimental curves for all the conducted tests are presented in Figures 4.27 to 4.32 for increasing load eccentricities. The evolution of the total bending moment M_{tot} is plotted against the applied total axial load, comparing the behaviour for different load eccentricities in each cross-section. Additionally, the first order bending moment due to the actual load eccentricity e_0 has also been plotted ($M_1=N \cdot e_0$) in order to evaluate the effect of second order effects caused by the lateral deflection of the members ($M_2=N \cdot d$), which are shown not to be negligible. Therefore, M_{tot} gathers first and second order moments, being $M_{tot}=N \cdot (e_0+d)$. Besides, axial compression loads are also presented against the lateral deflections of the members, measured at the mid-height section.

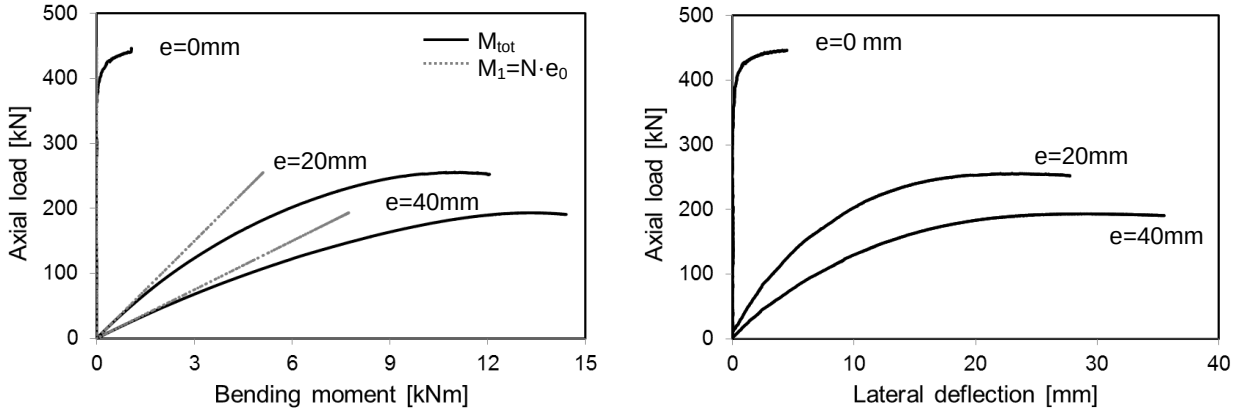

Fig. 4.27. Load-bending moment and load-lateral deflection curves for S1 specimens.

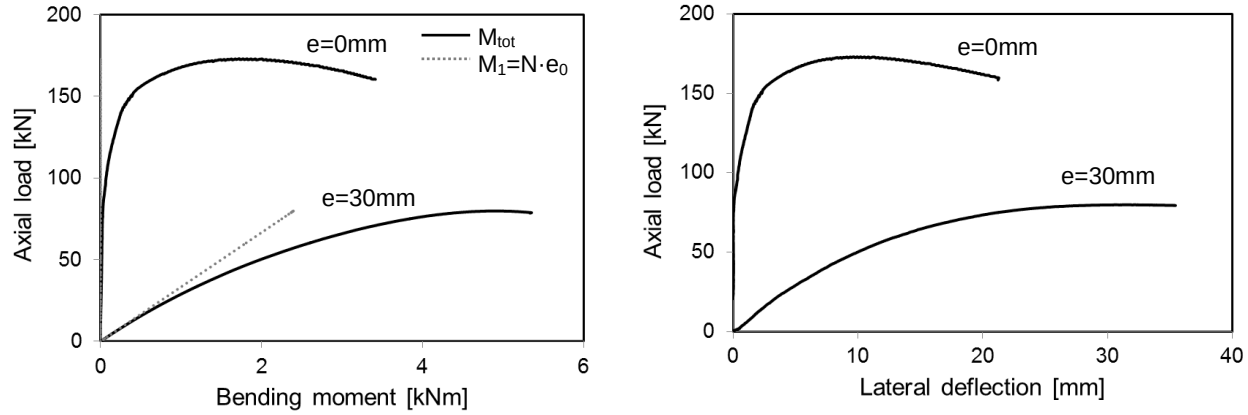

Fig. 4.28. Load-bending moment and load-lateral deflection curves for S2 specimens.

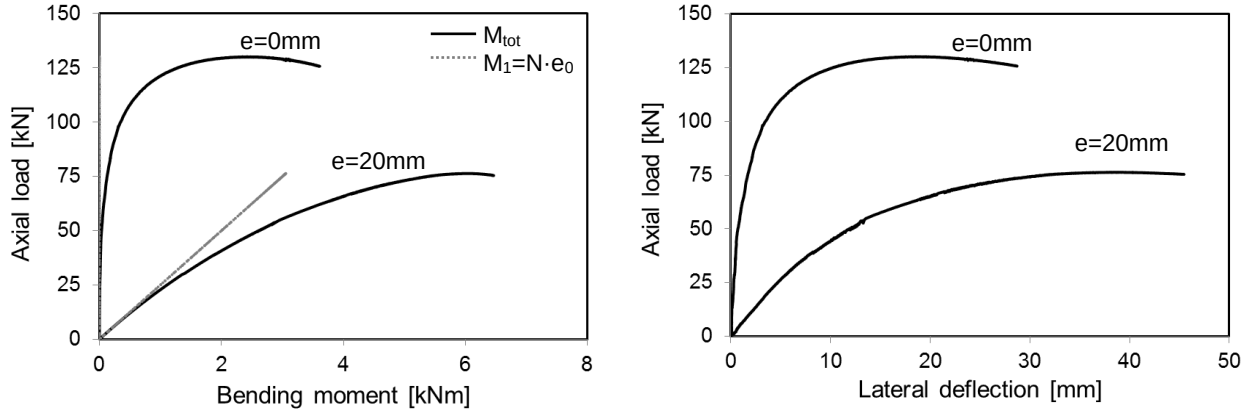

Fig. 4.29. Load-bending moment and load-lateral deflection curves for S3 specimens.

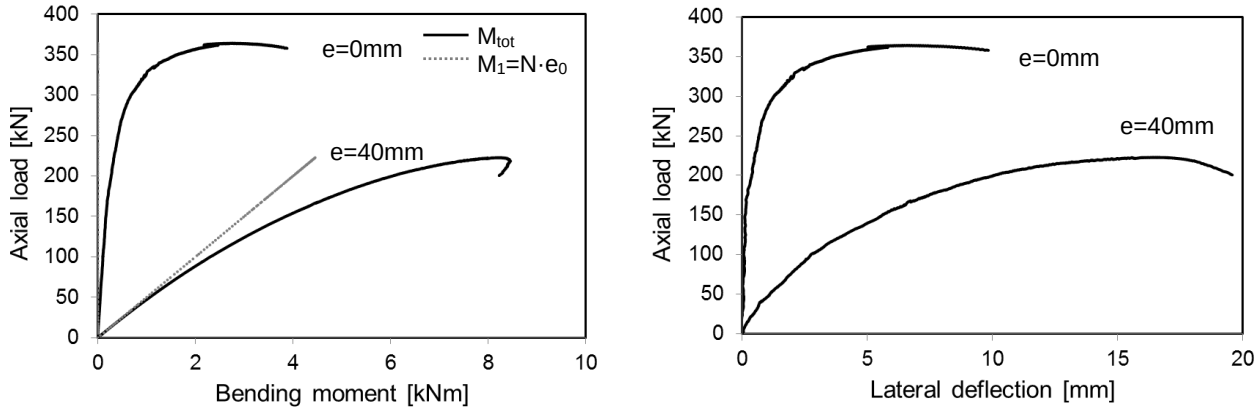

Fig. 4.30. Load-bending moment and load-lateral deflection curves for S4 specimens.

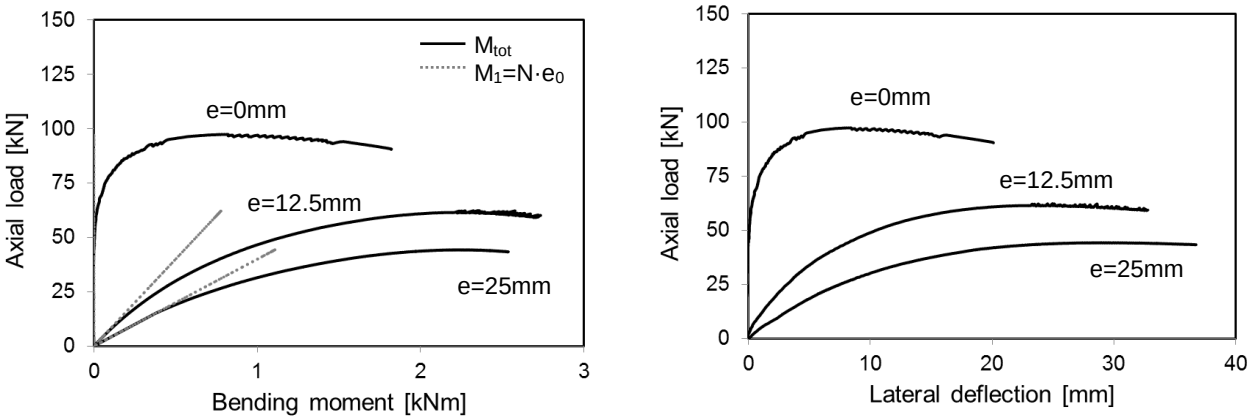

Fig. 4.31. Load-bending moment and load-lateral deflection curves for S5 specimens.

Figures 4.32 and 4.33 present the evolution of the stresses against the applied compression load for the S1 and S3 columns tested under concentric compression as indicative of typical stocky and slender cross-sections. The strains measured from the strain gauges attached to the specimens have been turned into stresses through the average stress-strain curves of each cross-section, whose parameters are defined in Table 4.4. σ_1 and σ_2 represent the average stresses at the analysed faces, while the slashed line depicts the lineal stress for each load level. In addition, the elastic critical stress σ_{cr} and the 0.2% proof stress $\sigma_{0.2}$ have been included for each specimen. Figure 4.32 shows the typical behaviour of stocky columns, where the failure of the specimen (350kN) starts after the elastic behaviour is lost (300kN) and the lateral displacement is different to zero (see Figure 4.27), which indicates that the material nonlinearity appears before the geometric nonlinearity. Alternatively, Figure 4.33 presents the typical behaviour of slender columns, where the load at which the first lateral displacement is observed coincides with both the load corresponding to the loss of the elastic behaviour and the start of the failure (around 25kN), as the elastic critical load of S3 cross-section is much lower than the corresponding 0.2% proof stress $\sigma_{0.2.}$

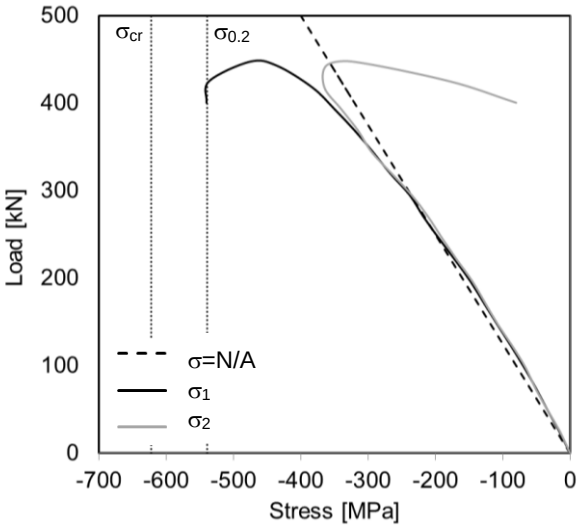

Fig. 4.32. Load-stress curves for S1 – CC specimen.

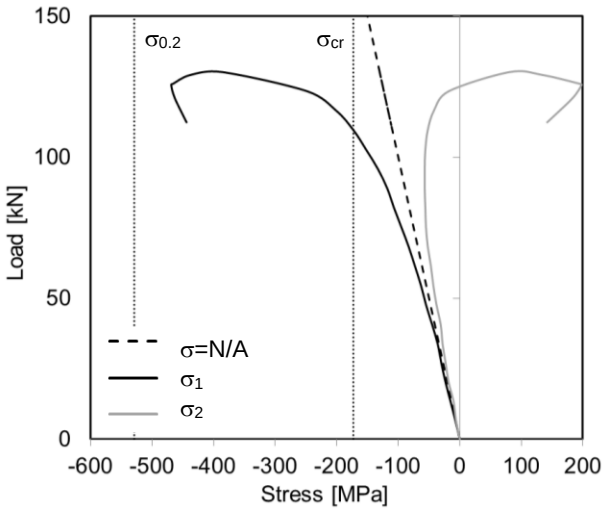

Fig. 4.33. Load-stress curves for S3 – CC specimen.

The failure modes observed in the specimens involved overall flexural buckling for every specimen but for S4, which failed by combined overall and local buckling for both compression and combined loading configurations. Figures 4.34, 4.35 and 4.36 show the failure modes of specimens S3 – EC1 and S4 – CC, where the influence of local buckling can be appreciated.

Fig. 4.34. Overall flexural buckling failure of specimen S3 – EC1.

Fig. 4.35. Interaction of local and overall flexural buckling of specimen S4 – CC.

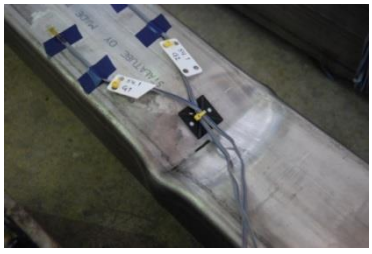

Fig. 4.36. Detailed view of the local failure of specimen S4 – EC1.

CHAPTER 5

Finite element models

5.1 Introduction

This chapter describes all the relevant information regarding the Finite Element (FE) analysis conducted in this thesis using the general-purpose package ABAQUS (ABAQUS, 2012). These numerical investigations have been used to replicate the different tests presented in chapter 4 and after the FE models were validated, several parametric studies have been conducted to generate supplementary data on different structural behaviours to complement the available experimental results. First, the basic modelling assumptions are presented, followed by the comparison of the numerical and experimental results for the validation of the different tests. Finally, the details of the conducted parametric studies are provided.

5.2 General assumptions

The Finite Element (FE) models used in this study were performed by the general-purpose software ABAQUS (ABAQUS, 2012). The mid-surfaces of the cross-sections were modelled by using the four-node shell elements with reduced integration S4R, widely used when modelling cold-formed stainless steel cross-sections (Theofanous and Gardner (2009), Huang and Young (2014a), Becque and Rasmussen (2009b)). After a mesh convergence study, and in order to guarantee computational efficiency, the analyses were conducted with 5mm long shell elements. The numerical models utilized in this study were first validated against the experimental results presented in chapter 4, where the measured amplitudes of the initial

imperfections and element dimensions were considered, together with the actual material properties. The nonlinear analyses were performed conducting modified Riks analyses, where initial imperfections according to the first buckling mode shapes obtained from linear eigenvalue analyses were introduced.

Residual stresses are introduced into cold-formed specimens from the cold-working and welding processes and may have a significant effect on their structural behaviour. Several investigations (Rasmussen and Hancock (1993a), Cruise and Gardner (2008b), Huang and Young (2012)) on residual stresses concluded that the magnitude of the bending residual stresses is much higher than the magnitude of the membrane residual stresses in cold-formed sections. Therefore, membrane residual stresses are usually neglected when modelling residual stresses in cold-formed sections. In addition, and according to different research works (Rasmussen and Hancock (1993a), Cruise and Gardner (2008b), Jandera el al. (2008)), the effect of the through-thickness bending residual stresses is inherently present in the stress-strain curves obtained from coupons cut from the original tubes, since during tensile tests the coupons straighten and the bending residual stresses are reintroduced. Hence, residual stresses do not need to be explicitly reincorporated in the numerical simulations.

Two different material definitions have been considered during the validation of the FE models. Initially, the flat and corner regions of the cross-sections were differentiated and the corresponding stress-strain properties were assigned to each region. Corner regions were extended also to the adjacent flat parts by a length equal to two times the thickness of the cross-section, according to Theofanous and Gardner (2009). Additionally, the weighted average material properties were also considered in FE models, where the same behaviour was assigned to the entire cross-section as suggested by Hradil and Talja (2013) in order to evaluate the accuracy of this simplification for further FE analyses. The material parameters describing the behaviour of flat parts, corner parts and weighted average behaviour can be found in chapter 4.

The effect of the geometric initial imperfections in thin-walled structures is also an important issue to be considered, since they also may have a significant effect on the strength of the cross-section or member. Therefore, these initial imperfections need to be considered in the FE models. An imperfection pattern according to the first buckling mode shape is usually considered in numerical simulations (Becque et al. (2008), Theofanous and Gardner (2009), Huang and Young (2014c)), which is determined by conducting an elastic eigenvalue analysis before the nonlinear problem is considered. For short specimens (i.e. stub columns subjected to compression or combined loading) only local initial imperfections are relevant since cross-section failure is expected, although for long specimens (i.e. members subjected to compression or combined loading) both overall and local imperfections need to be considered. In the validation of the FE models the measured imperfection amplitudes were considered, while for the parametric studies predicted amplitudes were adopted.

5.3 Validation of the numerical models in compression and combined loading

The numerical models representing stainless steel RHS and SHS cross-sections and members subjected to pure compression and combined loading conditions have been conducted following similar procedures and are therefore presented together. The accuracy of these models is investigated by comparing the experimental ultimate loads and load-deflection histories to those predicted by the FE models, as well as the failure mode shapes.

The edge elements at the ends of the specimens were kinematically coupled and connected to two reference points, where the relevant degrees of freedom were defined. For stub columns subjected to compression all degrees of freedom were fixed at the lower reference point while only longitudinal displacement was set free at the upper one.

Tests on stub columns subjected to combined loading and members subjected to both pure compression and combined loading conditions were conducted under pin-ended boundary conditions. In these models the ends of the specimens were also coupled to two reference points, set 50mm away from each specimen end as described in the test setups, and assuming the effective length of the columns equal to the distance between knife-edges. All degrees of freedom except the rotation around the relevant axis were restrained at the lower reference point, while longitudinal displacement and relevant rotations were set free in the upper one. Loads were introduced as imposed displacements at the upper reference points in all the models and no restrictions were defined in the rest of the nodes.

The behaviour of ferritic stainless steel stub columns subjected to compression and combined loading conditions was reproduced from numerical models by performing a nonlinear analysis with a modified Riks analysis, where local geometric imperfections, considering imperfection amplitudes equal to those measured from each specimen, were introduced. The comparison of the results derived from the FE models with the experimental results is presented in Tables 5.1 and 5.2 for stub columns subjected to compression and combined loading conditions respectively. These Tables report the numerical-to-experimental normalized loads $N_{u,FE}/N_{u,exp}$ for each specimen, together with the mean and coefficients of variation (COVs). The comparison between the predicted and experimental end shortenings and end rotations at N_u are also provided. Results corresponding to the two material definitions contemplated in the FE model validation have been included in Tables 5.1 and 5.2, those corresponding to the measured constitutive laws in flat and corner regions and to the weighted average material behaviour in the entire cross-section. Results demonstrate that although the most accurate results are obtained when the measured stress-strain curves are considered, the adoption of the simplified weighted average material properties still provides excellent results for both compression and combined loading conditions.

Table 5.1. Comparison of the stub column test results with FE results.

Specimen	Flat and corner material		Weighted average material	
	$N_{u,FE}/N_{u,exp}$	$\delta_{u,FE}/\delta_{u,exp}$	$N_{u,FE}/N_{u,exp}$	$\delta_{u,FE}/\delta_{u,exp}$
S1 – C	0.99	0.83	0.94	0.92
S2 – C	0.99	0.84	0.94	0.80
S3 – C	0.98	0.97	0.91	0.92
S4 – C	0.97	0.84	0.95	0.74
S5 – C	1.00	0.94	1.01	1.02
Mean	0.99	0.88	0.95	0.88
COV	0.012	0.072	0.040	0.125

Table 5.2. Comparison of the stub column combined loading test results with FE results.

Specimen	Flat and corner material		Weighted average material	
	$N_{u,FE}/N_{u,exp}$	$\theta_{u,FE}/\theta_{u,exp}$	$N_{u,FE}/N_{u,exp}$	$\theta_{u,FE}/\theta_{u,exp}$
S1 – CL	1.02	1.03	0.98	1.03
S2 – CL	0.97	0.90	0.96	0.81
S3-Mj – CL	0.99	0.96	0.96	0.86
S3-Mi – CL	1.00	0.95	0.96	0.89
S4-Mj – CL	1.03	0.99	0.98	1.01
S4-Mi – CL	1.02	0.96	1.01	0.98
S5-Mj – CL	1.01	1.05	0.99	0.85
S5-Mi – CL	0.99	1.03	1.01	0.91
Mean	1.00	0.98	0.98	0.92
COV	0.019	0.053	0.022	0.089

Figures 5.1a and 5.2a present the comparison of the experimental and FE load-end shortening histories (end rotation for the combined loading test) for the measured (FE) and weighted average (FE,average material) material definitions, while the comparison of the local failure modes for typical specimens are presented in Figure 5.1b and Figure 5.2b for compression and combined loading conditions respectively. Tables 5.1 and 5.2, together with Figures 5.1 and 5.2, demonstrate that in addition to provide excellent ultimate load predictions, the conducted FE models accurately capture the stiffness and the general shape of the response of the specimens. The obtained local buckling failure modes are also found to be in good agreement with those observed after the tests.

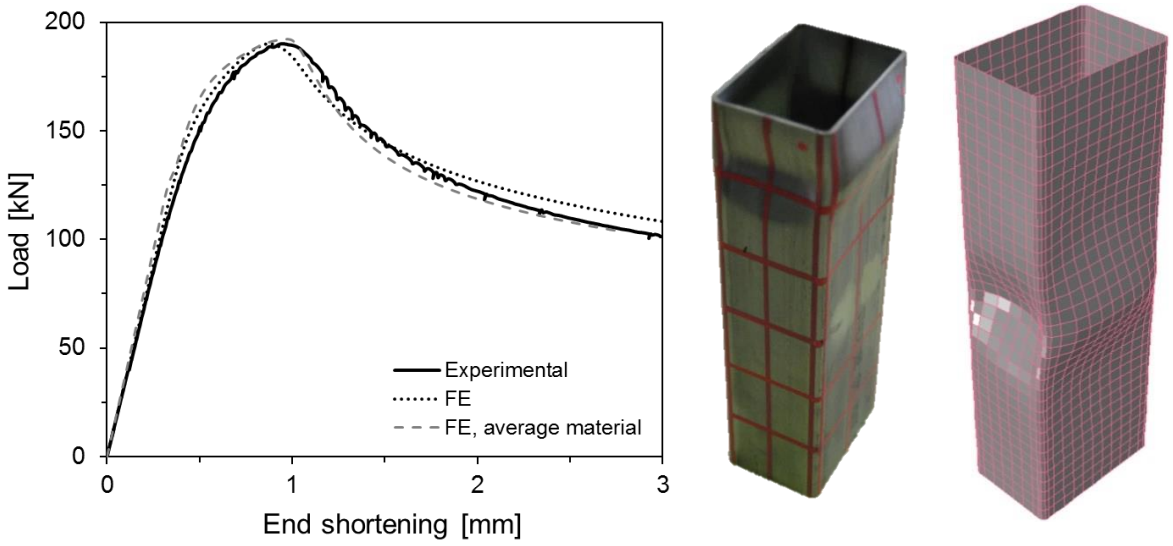

a) Experimental and numerical load-end shortening curves b) Experimental and FE failure modes

Fig. 5.1. Comparison of experimental and FE results for typical specimens in compression.

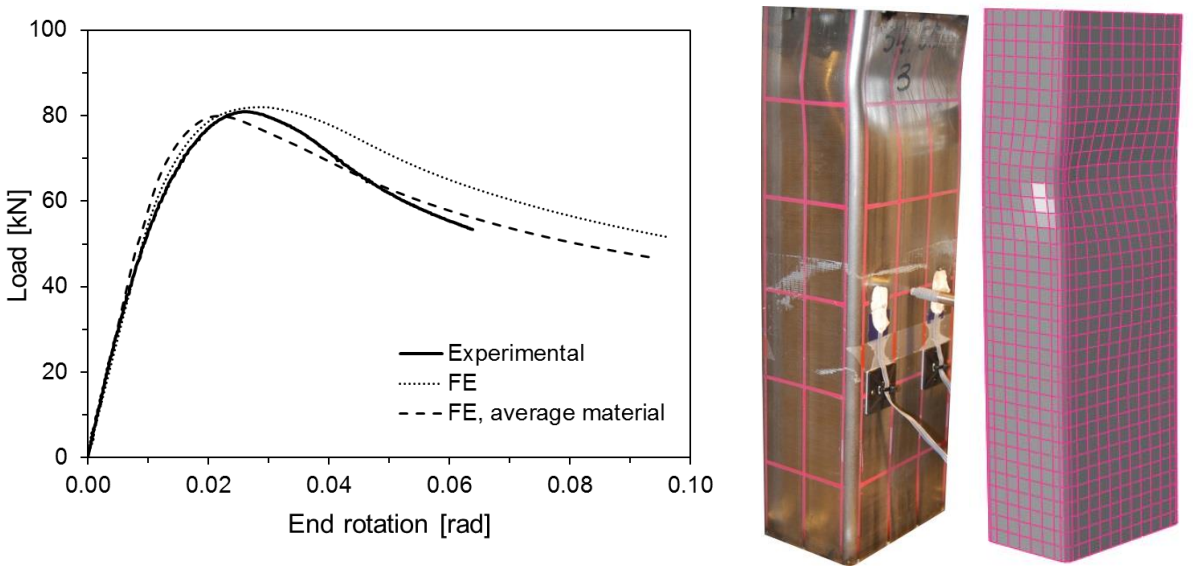

a) Experimental and numerical load-end rotation curves b) Experimental and FE failure modes

Fig. 5.2. Comparison of experimental and FE results for typical specimens under combined loading.

Regarding the tests conducted on ferritic stainless steel members subjected to compression and combined loading, experimental curves have also been compared to the corresponding FE results considering the two different material definitions. Load-lateral deflections corresponding to the measured constitutive laws in flat and corner regions (FE) and the weighted average material properties in the entire cross-section (FE, average material) are compared with the experimental curves in Figure 5.3 for typical column and beam-column specimens.

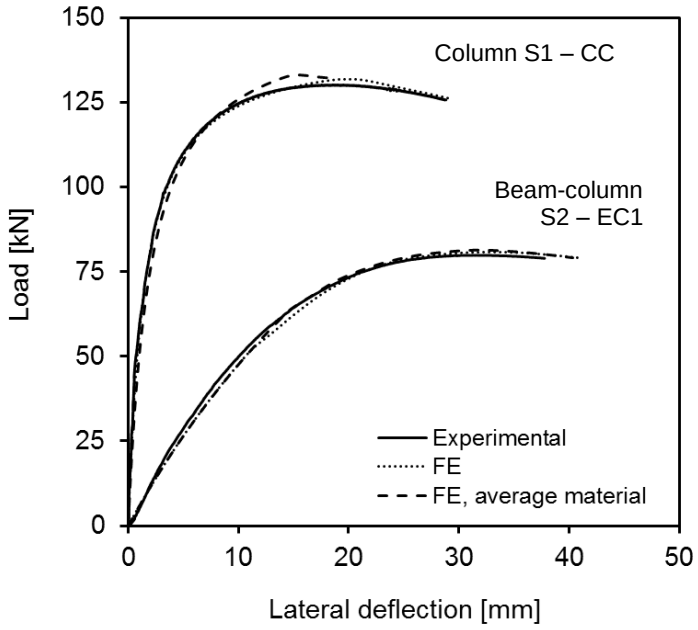

Fig. 5.3. Experimental and FE load-lateral deflection curves for typical column and beam-column specimens.

Table 5.3 reports the mean values and COVs of the numerical-to-experimental ratios of the ultimate loads and the corresponding lateral deflections, showing excellent results for both material definitions considered. It is also remarkable that the failure modes of the obtained FE models are in good agreement with experimental results, as demonstrated in Figure 5.4. Therefore, these comparisons demonstrate that the derived numerical analyses are capable of accurately predicting the ultimate loads, the full experimental histories and the failure modes of ferritic columns and beam-columns when measured material properties are adopted, but also when the weighted average material is considered.

Table 5.3. Comparison of the column and beam-column test results with FE results.

Specimen	Flat and corner material		Weighted average material	
	$N_{u,FE}/N_{u,exp}$	$d_{u,FE}/d_{u,exp}$	$N_{u,FE}/N_{u,exp}$	$d_{u,FE}/d_{u,exp}$
S1 – CC	1.00	0.93	1.04	1.07
S1 – EC1	1.02	1.08	0.99	0.94
S1 – EC2	1.02	1.04	0.99	1.05
S2 – CC	1.02	0.99	1.03	0.88
S2 – EC1	1.01	1.02	1.02	1.02
S3 – CC	1.01	1.03	1.02	0.85
S3 – EC1	1.03	1.03	1.04	0.96
S4 – CC	0.97	0.80	1.00	0.83
S4 – EC1	0.99	0.87	0.99	1.02
S5 – CC	1.02	1.00	1.02	1.00
S5 – EC1	1.01	0.96	0.99	0.98
S5 – EC2	1.04	1.03	1.05	1.02
Mean	1.01	0.98	1.01	0.97
COV	0.019	0.082	0.022	0.080

Fig. 5.4. Comparison of the experimental and numerical deformed shapes for S3 and S4 specimens.

5.4 Validation of the numerical models in bending

Simply supported beams subjected to four-point bending conditions and two span continuous beams were modelled in order to reproduce the experimental tests on ferritic stainless steel RHS and SHS described in chapter 4. Hence, same loading and boundary conditions were considered: those regions corresponding to support and loading sections stiffened by wooden blocks were modelled as kinematic coupling interaction. The bottom faces of the support and loading regions were forced to move as a solid rigid referred to their centre points, where the boundary conditions were defined. For simply supported beams the longitudinal displacement of one of the supports was fixed as well as for the middle supports in continuous beams. Loads were introduced as imposed vertical displacements in both configurations.

The suitability of the developed FE models for representing the behaviour of ferritic stainless steel simply supported and continuous beams is demonstrated in Tables 5.4 and 5.5 respectively, where the numerical-to-experimental ratios of the ultimate loads and the corresponding midspan deflections are presented, together with the mean values and COVs. As for the longitudinally loaded specimens, two different material definitions have been considered, the measured constitutive laws in flat and corner regions and the weighted average material

properties in the entire cross-section. The global and local failure modes compared in Figures 5.5 and 5.6 also demonstrate that the obtained failure shapes are also similar for experimental and FE models.

Table 5.4. Comparison of the four-point bending test results with FE results.

Specimen	Flat and corner material		Weighted average material	
	$F_{u,FE}/F_{u,exp}$	$d_{u,FE}/d_{u,exp}$	$F_{u,FE}/F_{u,exp}$	$d_{u,FE}/d_{u,exp}$
S1 – 4P	1.03	1.03	0.97	0.89
S2 – 4P	1.02	1.13	0.95	1.07
S3-Mj – 4P	1.02	1.16	0.93	1.23
S3-Mi – 4P	0.94	0.97	0.89	0.87
S4-Mj – 4P	1.03	1.02	0.94	0.92
S4-Mi – 4P	1.00	1.10	0.94	1.00
S5-Mj – 4P	0.96	0.98	0.88	0.92
S5-Mi – 4P	0.94	0.83	0.92	0.73
Mean	0.99	1.03	0.93	0.95
COV	0.038	0.104	0.032	0.157

Table 5.5. Comparison of the continuous beam test results with FE results.

Specimen	Flat and corner material		Weighted average material	
	$F_{u,FE}/F_{u,exp}$	$d_{u,FE}/d_{u,exp}$	$F_{u,FE}/F_{u,exp}$	$d_{u,FE}/d_{u,exp}$
S1 – 5P	0.97	1.01	1.00	1.39
S2 – 5P	1.01	0.88	0.95	1.00
S3-Mj – 5P	0.99	1.07	0.99	1.26
S3-Mi – 5P	1.01	0.95	0.93	0.95
S4-Mj – 5P	0.98	1.57	0.99	1.56
S4-Mi – 5P	0.99	1.03	0.98	1.10
S5-Mj – 5P	0.99	0.85	0.94	0.66
S5-Mi – 5P	1.01	0.83	0.97	0.64
Mean	0.99	1.02	0.97	1.07
COV	0.015	0.233	0.028	0.308

Fig. 5.5. Comparison of experimental and numerical deformed global shapes for a typical continuous beam.

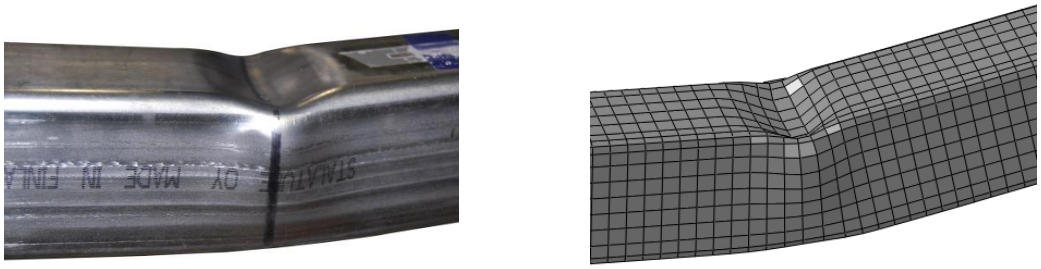

Fig. 5.6. Comparison of experimental and numerical deformed local shapes for a typical continuous beam.

Experimental load-midspan deflection curves have been, therefore, compared to the corresponding FE results, considering different constitutive laws in flat and corner regions (FE) and the weighted average material behaviour in the entire cross-section (FE, average material). Figure 5.7 presents the comparison between experimental and FE results for typical simply supported and continuous beam configurations. It is therefore demonstrated that the results derived from the numerical analyses are in good agreement with the considered experimental results for ferritic stainless steel beams when measured material properties are adopted, but also when the weighted average material is considered.

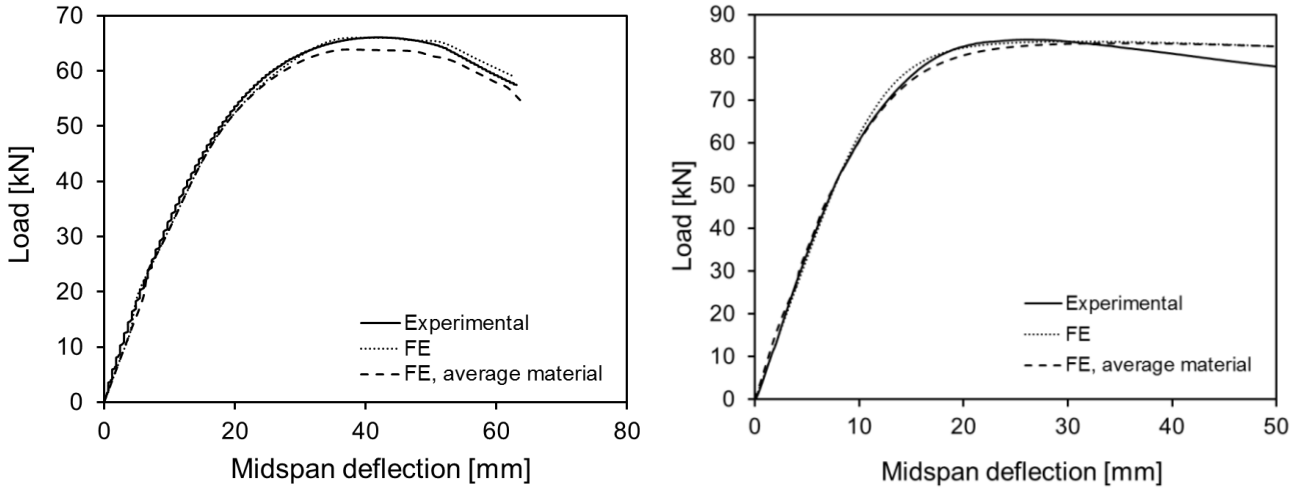

a) Typical four-point bending test

b) Typical continuous beam test

Fig. 5.7. Experimental and FE load-midspan deflection curves for typical beam specimens.

5.5 Parametric studies

The behaviour of stainless steel RHS and SHS cross-sections and members subjected to different loading conditions is investigated in this thesis. Since the available experimental data is limited, several parametric studies have been conducted in order to obtain supplementary strength data after the validation of the FE models. All the information regarding the parametric studies carried out is presented herein.

5.5.1 General assumptions

The capability of the developed FE models to accurately represent the behaviour of stainless steel RHS and SHS cross-sections and members subjected to different loading conditions has been demonstrated in the previous sections. Based on these models, several parametric studies have been conducted over a wide range of cross-sectional and member slendernesses and load combinations to supplement the existing experimental data. The parametric analyses have been developed through a combination of Phyton and Abaqus tools using the parametr.combine(MESH) option for combining the different parameters in the Python script. The basic modelling assumptions described in sections 5.3 and 5.4 have also been adopted in the parametric analyses, although few supplementary details are provided herein.

The parametric studies focus primarily on ferritic stainless steel, though comparative results are also presented for austenitic and duplex grades. A wide variety of RHS and SHS were modelled considering both stocky and slender cross-sections, covering the full cross-sectional slenderness range. As demonstrated in previous sections, the assignment of the weighted average material properties for the entire cross-section as suggested by Hradil and Talja (2013) is an adequate and simplified approach to define material properties in FE models, and it has been adopted for the conducted parametric studies.

Material properties were obtained from the tensile coupon test results reported in chapter 4 for ferritics, while those used in the parametric studies by Zhao et al. (2016b) were considered for austenitic and duplex stainless steels. The most relevant material parameters are presented in Table 5.6, where E is the Young's modulus, $\sigma_{0.2}$ is the proof stress corresponding to 0.2% plastic strain, σ_u is the tensile strength and ε_u is the corresponding ultimate strain. Strain hardening exponents *n* and *m* are also provided. The stress-strain curves used for the numerical analyses were obtained using the stress-strain curve formulation presented in chapter 3 in combination with the parameters shown in Table 5.6.

Table 5.6. Material parameter definition for parametric studies.

Stainless steel	E [GPa]	$\sigma_{0.2}$ [MPa]	σ_u [MPa]	ε_u [%]	*n*	*m*
Austenitic	197.8	417	651	35.9	5.5	3.7
Ferritic	185.7	490	533	4.8	11.0	3.2
Duplex	201.3	707	874	19.1	5.6	4.9

5.5.2 Parametric studies on cross-section behaviour

An extensive variety of RHS and SHS cross-sections covering a wide range of cross-sectional slendernesses have been modelled in the different parametric studies representing compression, bending and combined loading conditions.

The total length of stub columns subjected to compression and combined loading was set equal to three times the widest outer dimension, while all specimens modelled under four-point bending conditions presented a span length of 1500mm and a total length of 1700mm. The

outer heights H and widths B of the considered RHS and SHS ranged from 50mm to 150mm, having aspect ratios H/B equal to 1.2, 1.5 and 2 for the modelled RHS. The adopted thicknesses ranged between 2mm and 6mm to guarantee that both stocky and slender cross-sections were analysed. For combined loading FE models, the nominal load eccentricities e_0 were defined as function of the outer width B, considering e_0/B ratios equal to 0.25, 0.5 and 1.5. For pure compression 30 stub columns were conducted for each considered stainless steel grade, while 80 four-point bending tests were modelled. Regarding combined loading behaviour, more than 350 stub columns subjected to uniaxial bending plus compression conditions were modelled considering different compression-to-bending loading ratios.

Local initial imperfections were introduced in the models adopting an imperfection pattern along the member length in the form of the lowest buckling mode shape by conducting a previous elastic eigenvalue buckling analysis. The imperfection amplitudes were predicted from the modified Dawson and Walker model (Dawson and Walker, 1972) proposed by Gardner and Nethercot (2004c) given in Eq. (5.1), where $\sigma_{cr,min}$ is the minimum elastic buckling stress of all the plate elements conforming the cross-section and t is the thickness of the cross-section.

$$w_0 = 0.023\left(\frac{\sigma_{0.2}}{\sigma_{cr,min}}\right)\cdot t \tag{5.1}$$

5.5.3 Parametric studies on members under compression and combined loading

The parametric studies on stainless steel members comprised an extensive variety of different RHS and SHS considering both stocky and slender cross-sections. Minor axis flexural buckling behaviour was investigated and all the models were defined according to the general assumptions described in section 5.3. For SHS outer widths B ranging from 60mm to 200mm were considered, while for RHS the widths varied between 60mm and 100mm with aspect ratios H/B equal to 1.2, 1.5 and 2, and thicknesses ranged between 2mm and 6mm. For each ferritic stainless steel cross-section 12 different slendernesses were modelled, ranging from 0.25-3.0 every 0.25, leading to more than 1200 FE models. For austenitic and duplex stainless steels the conducted parametric study was more limited, since the parametric studies focus primarily on ferritic grades, and 160 models were conducted for each grade.

Initial global imperfection amplitudes have an important influence on the flexural buckling behaviour of stainless steel columns and the values considered for the parametric studies need to be carefully defined, although different values have been considered in the parametric studies conducted during this last decade. When FE models excluded the consideration of residual stresses, high imperfection amplitudes, L/750, were considered by Hradil et al. (2012) to compensate this effect, where L is the length of the member. However, when residual stresses are considered into the FE models lower amplitudes representing only the geometrical imperfections, similar to those measured in specimens, are usually defined. Imperfection amplitudes equal to L/1500 were considered in the numerical analyses conducted by Theofanous and Gardner (2009) and Becque and Rasmussen (2009b), while L/2000 amplitudes

were defined in Gardner et al. (2006), Huang and Young (2014c), Jandera and Machacek (2014). Alternatively, an additional imperfection magnitude of L/1000 was considered in the studies reported by Lopes et al. (2007), Greiner and Kettler (2008) and Jandera and Syamsuddin (2014). Considering that the measured initial imperfection amplitudes of the members tested in the experimental programme reported in chapter 4 ranged between L/1000 and L/2000 and that residual stresses are implicitly incorporated in the models through the measured stress-strain material definition according to Rasmussen and Hancock (1993a), the L/1500 magnitude has been considered as imperfection amplitude for the parametric study. Local initial imperfections were also included with amplitudes predicted from the modified Dawson and Walker model given in Eq. (5.1).

In addition, the minor axis strength of stainless steel hollow beam-columns was analysed through a comprehensive FE parametric study, considering three different bending moment distributions with several variations of the load eccentricity of 30 cross-sections. Similar cross-section geometries to those defined in the column parametric study were considered with four member slendernesses, leading to more than 1350 FE models for ferritic stainless steels and 430 for the austenitic and duplex grades. As for combined loading stub columns, several load eccentricities e_0 providing different compression-to-bending ratios were considered. The adopted e_0/B ratios were 0.1, 0.3, 0.75 and 1.5. The initial imperfections were defined following the procedure described for the column models.

Since the majority of the available experimental results were tested under uniform bending moment distributions plus compression loads, bending moment diagrams corresponding also to triangular (ψ=0) and bitriangular (ψ=-1) distributions were considered in the parametric study in addition to the uniform distribution (ψ=1). ψ is the ratio of the smaller to the larger moment at member ends, adopted as negative when the member is bent in reverse curvature and positive when it is bent in single curvature, according to the EN1993-1-1 (2005) definition.

5.5.4 Parametric study on continuous beams

The applicability of the different plastic design approaches to stainless steel structures was assessed through an extensive FE parametric study, where several stocky cross-sections and structural configurations were considered. The parametric study consisted on more than 550 different FE models, including a variety of stocky RHS and SHS considered Class 1 cross-sections according to the cross-sectional classification limits defined by both EN1993-1-4 (2006) and Gardner and Theofanous (2008). More slender cross-sections were also included in the analysis in order to identify the transition between Class 1 and Class 2 cross-sections and determine the limit from which global plastic analysis is applicable.

Austenitic, ferritic and duplex continuous beams with around 50 different cross-sections were considered in the parametric study, with wall thicknesses ranging between 2mm and 6mm. The outer height of the cross-sections ranged from 30mm to 80mm, while widths between 30mm and 80mm were considered.

For each cross-section, several structural configurations requiring different rotation capacities were studied. Two span continuous beams similar to those tested were modelled, with span lengths L_s (according to Figure 5.8) equal to 1500mm. The position of the applied load was varied with L_1 adopting values around 33%, 50%, 66% and 75% of the considered L_s.

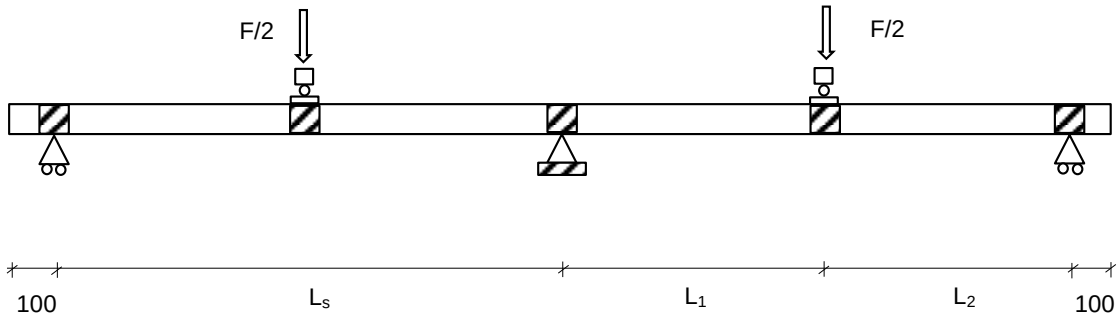

Fig. 5.8. Structural configuration definition for continuous beam parametric study.

CHAPTER 6

Cross-section behaviour of stainless steel RHS and SHS elements

6.1 Introduction

This chapter presents a comprehensive study on the cross-section behaviour of stainless steel Rectangular and Square Hollow Sections (RHS and SHS) subjected to several loading conditions. Resistance provisions codified in different standards and alternative design approaches are assessed by comparing the predicted capacities with those obtained experimentally and from numerical analysis for the compression and bending resistances of cross-sections, as well as for combined loading. The experimental results presented in chapter 4 and numerical parametric studies described in chapter 5 have been considered in the analysis of the cross-sectional behaviour of austenitic, ferritic and duplex stainless steel RHS and SHS together with additional experimental data collected from the literature.

First, the assessment of the cross-sectional classification limits codified in EN1993-1-4 (2006) and the revised limits proposed by Gardner and Theofanous (2008) is presented, followed by the assessment of the expressions codified in different international standards (e.g. EN1993-1-4 (2006), SEI/ASCE 2-08 (2002) and AS/NZS 4673 (2001)) for cross-sectional resistance under different loading conditions. It is found that since these expressions do not account for strain hardening effects, the predicted capacities of stocky cross-sections are too conservative and alternative design methods are analysed. Continuous Strength Method (CSM) design provisions are found to be more accurate for stocky cross-sections and an improved design expression is

proposed for stainless steel cross-sections under combined loading conditions, which is statistically validated.

Finally, a full slenderness Direct Strength Method (DSM) approach based on a unique strength curve is proposed for stainless steel RHS and SHS cross-sections subjected to compression, bending and combined loading. This proposal accounts for strain hardening and local buckling effects and provides accurate predictions of the cross-section strengths for both stocky and slender cross-sections. The reliability of the proposed approach has also been demonstrated by means of statistical analyses. The findings of this research work can be found in Arrayago and Real (2015), Arrayago and Real (2016) and Arrayago et al. (2016b).

6.2. Assessment of cross-sectional classification limits

The European standard EN1993-1-4 (2006) for the design of structural stainless steel elements accounts for the effect of local buckling through the cross-section classification concept given in EN1993-1-1 (2005). Cross-sections are divided in different categories depending upon their susceptibility to local buckling by comparing predetermined limits with the c/εt value of the most slender constituent plate element, considering both geometrical and material properties of the studied element. c is the width or depth of the relevant part of a cross-section, t is the element thickness and ε considers the material properties, defined as in Eq. (6.1), where $\sigma_{0.2}$ is the 0.2% proof stress and E the Young's modulus. Class limits are currently codified in EN1993-1-4 (2006), although revised limits were proposed by Gardner and Theofanous (2008) for austenitic and duplex stainless steel cross-sections due to the over-conservatism of the current limits. Table 6.1 summarizes the class limits currently codified in EN1993-1-4 (2006) and the corresponding revised limit suggested by Gardner and Theofanous (2008) for internal elements in compression, bending and compression and bending. α is the depth of the compressed part of the considered element and k_σ is the buckling factor corresponding to the appropriate stress ratio, defined in EN1993-1-5 (2006).

$$\varepsilon = \sqrt{\frac{235}{\sigma_{0.2}} \cdot \frac{E}{210000}} \tag{6.1}$$

Table 6.1. Summary of codified and revised classification limits for internal elements.

	Classification	Compression	Bending	Compression and bending	
				α>0.5	α≤0.5
Class 1	EN1993-1-4	25.7ε	56ε	$308\varepsilon/(13\alpha-1)$	$28\varepsilon/\alpha$
	Revised limits	33ε	72ε	$396\varepsilon/(13\alpha-1)$	$36\varepsilon/\alpha$
Class 2	EN1993-1-4	26.7ε	58.2ε	$320\varepsilon/(13\alpha-1)$	$29.1\varepsilon/\alpha$
	Revised limits	35ε	76ε	$420\varepsilon/(13\alpha-1)$	$38\varepsilon/\alpha$
Class 3	EN1993-1-4	30.7ε	74.8ε	$15.3\sqrt{k_\sigma}$	$15.3\sqrt{k_\sigma}$
	Revised limits	37ε	90ε	$18.5\sqrt{k_\sigma}$	$18.5\sqrt{k_\sigma}$

Stub column and four-point bending tests from the experimental programme described in chapter 4 and the numerical strengths from the parametric studies presented in chapter 5 are used in the assessment of both classifications. Other experimental results on austenitic, ferritic and duplex stainless steels reported by several authors and summarized in Tables 2.1 and 2.3 in chapter 2 have also been included in the analysis.

The assessment of the Class 3 limit for internal elements in compression is undertaken by comparing the experimental ultimate resistances of the different cross-sections with the corresponding squash loads and elastic bending capacities. Normalized experimental and FE results are plotted against the $c/\varepsilon t$ slenderness of the most slender constituent element of the cross-section subjected to compression. Figure 6.1 presents results corresponding to stub columns in compression, where compression resistances have been normalized by the corresponding squash loads $N_y=A\cdot\sigma_{0.2}$. Figure 6.2 also presents the assessment of the Class 3 limit considering the experimental and FE beam results tested under four-point bending conditions normalized by the elastic bending capacities $M_y=W_{el}\cdot\sigma_{0.2}$. The codified and revised $c/\varepsilon t$ ratios have also been included in the Figures. Cross-sections attaining the corresponding squash load or elastic bending moment capacity can be defined as Class 3 or better.

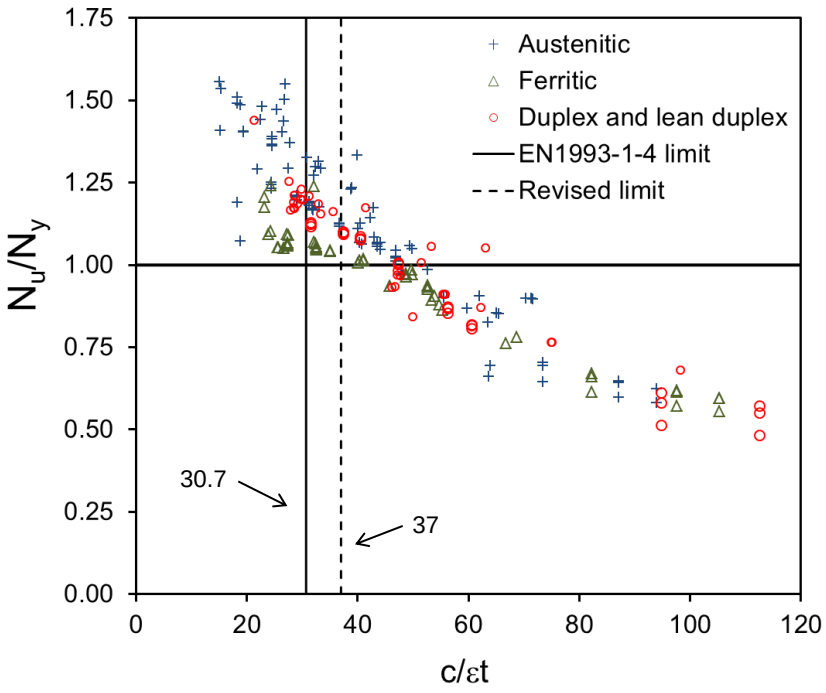

Fig. 6.1. Class 3 limit assessment for elements in compression for stub columns.

The highest N_u/N_y and M_u/M_y ratios are obtained for austenitic stainless steel stub columns and beams since these stainless steel grades usually show the highest strain hardening effects, followed by duplex and ferritic grades. However, it can be deduced from Figures 6.1 and 6.2 that all three stainless steel families show a similar behaviour so the same Class 3 limit can be considered. It can be also concluded that while EN1993-1-4 (2006) limits provide safe results, the revised limits proposed by Gardner and Theofanous (2008) are more accurate for the analysed RHS and SHS cross-sections.

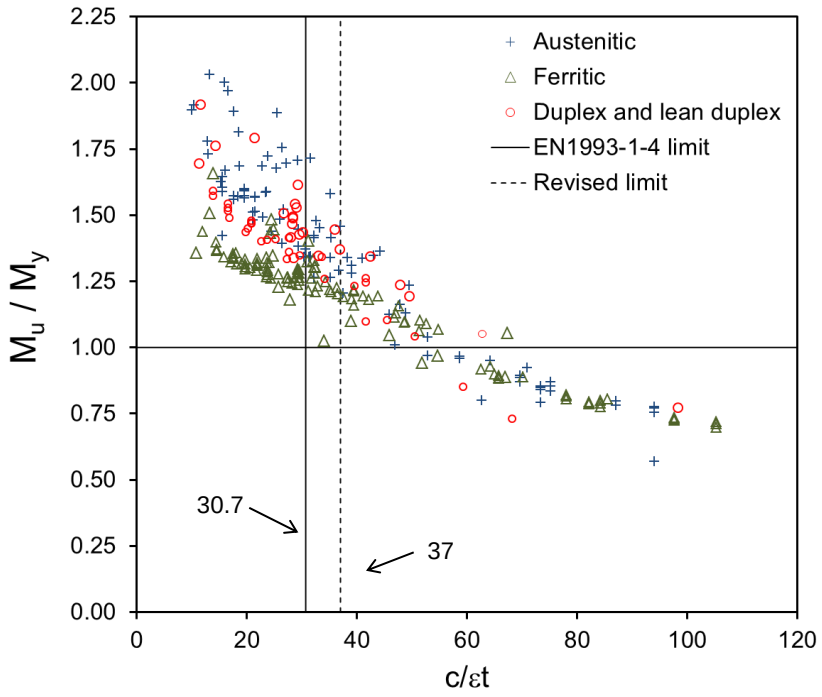

Fig. 6.2. Class 3 limit assessment for elements in compression for simply supported beams.

The Class 2 limit assessment is presented in Figure 6.3, where the ultimate bending moment resistances normalized by the plastic capacities $M_{pl}=W_{pl}\cdot\sigma_{0.2}$ are plotted against the corresponding c/tε slenderness of the compressed elements.

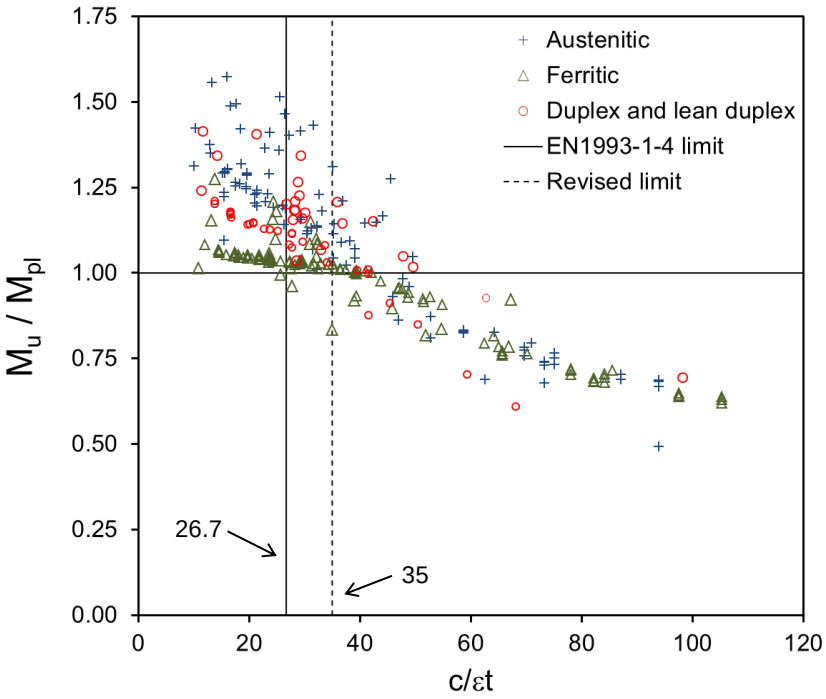

Fig 6.3. Class 2 limit assessment for elements in compression for simply supported beams.

It is apparent that the adoption of the revised cross-sectional Class 2 limit proposed in Gardner and Theofanous (2008) is more appropriate, whereas the current EN1993-1-4 (2006) Class 2

limit provides safe but overly conservative results. Again, stainless steel grades showing greater strain hardening effects such as austenitic and duplex present higher M_u/M_{pl} ratios and the predicted ultimate capacities therefore present a higher overconservatism.

The distinction between Class 2 and Class 1 cross-sections is derived from the rotation capacity developed by the beams and it is related to the $c/\varepsilon t$ slenderness parameter in EN1993-1-4 (2006). However, since Class 1 cross-sections are associated with the global plastic analysis of structures, the assessment of this limit cannot be dissociated from the study of stainless steel members. Thus, the study of the Class 1 limit is presented in chapter 8, where the behaviour of stainless steel continuous beams is investigated.

6.3 Assessment of EN1993-1-4, SEI/ASCE 8-02 and AS/NZS4673 provisions

This section presents the assessment of the expressions codified in the different international standards (i.e. EN1993-1-4 (2006), SEI/ASCE 8-02 (2002) and AS/NZS4673 (2001)) for cross-sectional resistance under different loading conditions. Stub column and four-point bending experimental results presented in chapter 4 have been analysed together with the FE strengths obtained from the parametric studies and the gathered experimental results reported in Tables 2.1 to 2.3 in chapter 2. Ultimate capacities of stainless steel RHS and SHS cross-sections subjected to compression, bending and combined compression and uniaxial bending are compared to the predicted capacities calculated according to the codified provisions.

6.3.1 Cross-sections subjected to compression

The approach in European EN1993-1-4 (2006) standard for the determination of the ultimate resistance capacity of a cross-section, as mentioned before, depends on the cross-sectional classification, and is given in Eqs. (6.2)-(6.3) for pure compression. Regarding uniform compression, cross-sections attaining the corresponding squash load before failure are considered to be fully effective, and are considered to be Class 3 or better. For cross-sections classified as Class 4, the effective cross-sectional area needs to be considered for the calculation of the compression resistance (Eq. (6.3)).

$$N_{c,Rd} = \frac{A \cdot \sigma_{0.2}}{\gamma_{M0}} \text{ for Class 1 to 3 cross-sections} \quad (6.2)$$

$$N_{c,Rd} = \frac{A_{eff} \cdot \sigma_{0.2}}{\gamma_{M0}} \text{ for Class 4 cross-sections} \quad (6.3)$$

where $\sigma_{0.2}$ is the 0.2% proof stress, A is the cross-sectional area and A_{eff} is the effective cross-sectional area. γ_{M0} is the partial safety factor for cross-sectional resistance, set to unity to allow suitable comparison with the test data. When Class 4 cross-sections are analysed, the effective area needs to be calculated through the reduction factors given in Eqs. (6.4) and (6.5) when the cross-sectional classification codified in EN1993-1-4 (2006) is considered, and through Eqs. (6.5) and (6.6) for the Gardner and Theofanous (2008) proposal.

$$\rho = \frac{0.772}{\lambda_p} - \frac{0.125}{\lambda_p^2} \leq 1.0 \tag{6.4}$$

$$\lambda_p = \frac{\bar{b}/t}{28.4\varepsilon\sqrt{k_\sigma}} \quad \text{and} \quad k_\sigma = 4 \quad \text{for compression} \tag{6.5}$$

$$\rho = \frac{0.772}{\lambda_p} - \frac{0.079}{\lambda_p^2} \leq 1.0 \tag{6.6}$$

American and Australian standards SEI/ASCE 8-02 (2002) and AS/NZS4673 (2001) usually specify same design provisions for cross-sectional resistance calculations. The cross-sectional compression resistance rules are also based on the slenderness of the most slender plate element of the cross-section. For those cross-sections showing a slenderness higher than $\lambda_p \geq 0.673$, the effective area needs to be considered when calculating the cross-sectional compression capacity by the reduction factor ρ given in Eq. (6.7). This reduction factor is slightly higher than those introduced in Eqs. (6.4) and (6.6), and equal to that provided for carbon steel cross-sections in AISI-S100-12 (2012) and EN1993-1-5 (2006) for uniform compression. For stocky cross-sections, full cross-sectional capacity is considered as for EN1993-1-4 (2006).

$$\rho = \frac{\left(1 - 0.22/\lambda_p\right)}{\lambda_p} \leq 1.0 \tag{6.7}$$

The comparison of the predicted capacities from codified approaches and the ferritic stainless steel stub column test results reported in chapter 4 is presented in Table 6.2, where the material and geometric properties reported in Tables 4.4 and 4.5 have been considered in the assessment. The predicted-to-experimental ratios for the expressions codified in EN1993-1-4 (2006) assuming both cross-sectional classifications are presented, and results for SEI/ASCE 8-02 (2002) and AS/NZS4673 (2001) are also reported. N_{EN} represents the predicted compression resistance considering the current classification in EN1993-1-4 (2006) whereas $N_{EN,rev}$ considers the revised class limits proposed by Gardner and Theofanous (2008) and $N_{SEI/AS}$ refers to SEI/ASCE 2-08 (2002) and AS/NZS4673 (2001) design rules.

Table 6.2. Comparison of experimental results with predicted capacities for compression tests.

Specimen	N_{EN}/N_u	$N_{EN,rev}/N_u$	$N_{SEI/AS}/N_u$
S1 – C1	0.89	0.89	0.92
S1 – C2	0.88	0.88	0.91
S2 – C1	0.90	0.90	0.95
S2 – C2	0.92	0.92	0.95
S3 – C1	0.91	0.91	0.95
S3 – C2	0.91	0.91	0.95
S4 – C1	0.99	1.00	1.00
S4 – C2	0.96	0.98	0.99
S5 – C1	0.96	0.98	1.01
S5 – C2	0.95	0.97	1.01
Mean	0.93	0.93	0.96
COV	0.038	0.047	0.038

As it is demonstrated in Table 6.2, predicted ultimate loads are equal for both the original classification limits and the revised ones proposed by Gardner and Theofanous (2008) for S1, S2 and S3 cross-sections, as none of the tested specimens presents a $c/\varepsilon t$ ratio between 30.7 and 37, providing safe but quite conservative results. However, slightly different values are obtained for S4 and S5, since the considered classification approaches provide different effective area calculations through Eqs. (6.4) and (6.6). Table 6.2 also suggests that for the tested ferritic cross-sections the best results are obtained when design provisions codified in SEI/ASCE 8-02 (2002) and AS/NZS4673 (2001) are considered. This is probably because the stress-strain behaviour of cold-formed ferritic stainless steels is more similar to that exhibited by carbon steels and since the approach given in SEI/ASCE 8-02 (2002) and AS/NZS4673 (2001) is that also codified for carbon steel cross-sections, better results are obtained than for a lower reduction curve.

The assessment of these design provisions for different stainless steel grades is presented in Table 6.3, where the compression strengths of the collected tests summarized in Table 2.1 in chapter 2 and the FE results from the parametric study are compared with the predicted capacities. Mean values and coefficients of variation (COVs) of the predicted-to-experimental (or FE) ratios are reported for the same design approaches assessed in Table 6.2, and results for stocky and slender cross-sections have been evaluated separately in order to make the comparison with design approaches assessed in the following sections easier. These alternative design approaches consider the effect of strain hardening in stocky cross-sections and local buckling effects are accounted through an alternative method for slender cross-sections, different from the reduction factors ρ studied herein.

Table 6.3. Assessment of design approaches for cross-sections in compression.

Grade		N_{EN}/N_u		$N_{EN,rev}/N_u$		$N_{SEI/AS}/N_u$	
		Stocky	Slender	Stocky	Slender	Stocky	Slender
Austenitic	Mean	0.76	0.85	0.77	0.89	0.77	0.96
	COV	0.106	0.116	0.117	0.105	0.122	0.121
Ferritic	Mean	0.91	0.91	0.92	0.95	0.93	1.02
	COV	0.049	0.056	0.050	0.053	0.051	0.072
Duplex	Mean	0.83	0.90	0.85	0.94	0.86	1.02
	COV	0.046	0.102	0.052	0.098	0.056	0.117
All	Mean	0.81	0.89	0.83	0.92	0.83	1.01
	COV	0.110	0.094	0.116	0.093	0.119	0.106

Results presented in Table 6.3 are in line with those reported for the test results in Table 6.2. For stocky cross-sections, results corresponding to the provisions given in different standards are found to be safe but conservative, obtaining marginally better predictions for SEI/ASCE 8-02 (2002) and AS/NZS4673 (2001) and for EN1993-1-4 (2006) with the revised classification limits. The overconservatism is highest for austenitic stainless steel cross-sections, which is the stainless steel grade with most important strain hardening effects, followed by duplex and ferritic grades. Regarding slender cross-sections, results in Table 6.3 demonstrate that although the highest N_{pred}/N_u ratios are obtained for the SEI/ASCE 8-02 (2002) and AS/NZS4673 (2001)

approach, the reduction factor considered in Eq. (6.7) substantially overestimates the actual capacity of a number of austenitic and duplex specimens by more than 20%. However, regarding ferritic stub columns, the mean N_{pred}/N_u ratio close to unity and the low scatter prove the accuracy of the results. This indicates that the reduction function given in Eq. (6.7) is valid for ferritic stainless steel sections, more similar to carbon steel, but unconservative for the austenitic and duplex grades. Therefore, when all stainless steel grades are considered, it can be concluded that the most accurate predictions of the ultimate compression resistance of slender stainless steel RHS and SHS are obtained for the EN1993-1-4 (2006) approach with the revised limits and reduction factor proposed by Gardner and Theofanous (2008).

6.3.2 Cross-sections subjected to bending

The assessment of the codified design expressions predicting the bending moment resistance has been conducted by comparing experimental and FE strengths with the predicted resistances. Since EN1993-1-4 (2006) predictive expressions depend on cross-sectional classification, the cross-sectional classifications currently coded in EN1993-1-4 (2006) and the revised limits proposed by Gardner and Theofanous (2008) have been assessed. Expressions for the determination of the bending moment capacity according to EN1993-1-4 (2006) are given in Eqs. (6.8)-(6.10). For cross-sections classified as Class 1 or 2, the plastic bending capacity given in Eq. (6.8) needs to be considered, for Class 3 sections the elastic bending capacity is assumed from Eq. (6.9), and finally, for Class 4 cross-sections, effective properties need to be considered through Eq. (6.10), where W_{pl} is the plastic modulus, W_{el} is the elastic modulus and W_{eff} is the effective modulus, calculated from the reduction factors ρ given in Eqs. (6.4) or (6.6).

$$M_{c,Rd} = \frac{W_{pl} \cdot \sigma_{0.2}}{\gamma_{M0}} \text{ for Class 1 or 2 cross-sections} \quad (6.8)$$

$$M_{c,Rd} = \frac{W_{el} \cdot \sigma_{0.2}}{\gamma_{M0}} \text{ for Class 3 cross-sections} \quad (6.9)$$

$$M_{c,Rd} = \frac{W_{eff} \cdot \sigma_{0.2}}{\gamma_{M0}} \text{ for Class 4 cross-sections} \quad (6.10)$$

AS/NZS4673 (2001) and SEI/ASCE 8-02 (2002) allow the consideration of the inelastic reserve strength as described in “Procedure II” of the standards. An ideally elastic-plastic stress-strain curve is assumed throughout the cross-section and a compression strain factor C_y is adopted to determine the maximum compressive strain, which is limited to a maximum value of $3\varepsilon_y$. AS/NZS4673 (2001) also adopts the full plastic capacity M_{pl} for tubular sections but considering that for doubly symmetric cross-sections the $3\varepsilon_y$ limit provides bending moment predictions very close to M_{pl}, only the strength predictions based on the $3\varepsilon_y$ limit are considered when SEI/ASCE 8-02 (2002) and AS/NZS4673 (2001) provisions are assessed, which therefore produce the same design strengths. For slender cross-sections, the effective modulus needs to be calculated through the reduction factor ρ given in Eq. (6.7). The comparison of the

experimental results obtained from the four-point bending tests on ferritic stainless steel RHS and SHS beams reported in chapter 4 with the bending resistance predictions codified in EN1993-1-4 (2006) assuming both cross-section classification limits is presented in Table 6.4, together with capacities predicted using AS/NZS4673 (2001) and SEI/ASCE 8-02 (2002) provisions. M_{EN} is the predicted bending resistance considering the currently codified classification in EN1993-1-4 (2006), $M_{EN,rev}$ utilizes the revised class limits proposed by Gardner and Theofanous (2008) and $M_{SEI,AS}$ is the predicted bending resistance from AS/NZS4673 (2001) and SEI/ASCE 8-02 (2002).

Table 6.4. Comparison of experimental results with predicted capacities for the 4P tests.

Specimen	M_{EN}/M_u	$M_{EN,rev}/M_u$	$M_{SEI,AS}/M_u$
S1 – 4P	0.85	1.04	1.02
S2 – 4P	1.00	1.00	0.99
S3-Mj – 4P	0.98	0.98	0.96
S3-Mi – 4P	0.79	0.99	0.96
S4-Mj – 4P	0.95	0.98	0.98
S4-Mi – 4P	0.81	0.84	0.95
S5-Mj – 4P	0.79	0.97	0.94
S5-Mi – 4P	0.79	0.82	0.92
Mean	0.87	0.95	0.97
COV	0.107	0.081	0.032

Table 6.4 demonstrates that Eqs. (6.8)-(6.10) provide safe although very conservative results when the current codified EN1993-1-4 (2006) classification limits are considered, while for the revised limits proposed by Gardner and Theofanous (2008) more accurate results are obtained, with only the bending capacity of the S1 – 4P specimen being overestimated. Again, the best prediction of the experimental bending capacities of ferritic stainless steel beams is obtained for the design provisions given in AS/NZS4673 (2001) and SEI/ASCE 8-02 (2002).

Table 6.5 presents the assessment of the different design approaches predicting the bending resistance of stainless steel RHS and SHS cross-sections. The experimental and numerical bending strengths from Table 2.3 and the conducted parametric studies have been compared to the predicted capacities for the different approaches. Table 6.5 presents the mean values and COVs of the predicted-to-experimental (or FE) capacities for stocky and slender cross-sections and different stainless steel families.

Table 6.5. Assessment of design approaches for bending.

Grade		M_{EN}/M_u		$M_{EN,rev}/M_u$		$M_{SEI,AS}/M_u$	
		Stocky	Slender	Stocky	Slender	Stocky	Slender
Austenitic	Mean	0.74	0.92	0.78	0.93	0.77	0.89
	COV	0.093	0.080	0.097	0.076	0.097	0.147
Ferritic	Mean	0.87	0.92	0.93	0.93	0.93	0.93
	COV	0.096	0.092	0.063	0.085	0.041	0.107
Duplex	Mean	0.77	0.96	0.85	0.98	0.84	0.96
	COV	0.105	0.129	0.080	0.123	0.067	0.165
All	Mean	0.80	0.93	0.86	0.95	0.85	0.93
	COV	0.122	0.106	0.109	0.100	0.104	0.142

With respect to stocky cross-sections, the overconservatism observed in Table 6.5 for austenitic and duplex stainless steel RHS and SHS cross-sections in bending can be attributed to the fact that strain hardening effects are not accounted when predicted strengths are calculated according to the different standards. Best results are obtained for the “Procedure II” approach in AS/NZS4673 (2001) and SEI/ASCE 8-02 (2002) since the consideration of the inelastic strength reserve is allowed, while for the cross-sections classified as Class 3 in EN1993-1-4 (2006) only elastic bending capacities are assigned. For slender cross-sections, very similar and accurate strength predictions are obtained for all the codified approaches.

6.3.3 Cross-sections subjected to combined loading

The analysis of the expressions codified in the different standards for stainless steel RHS and SHS sections subjected to combined axial compression and uniaxial bending moment is presented in this section. Specifications in EN1993-1-4 (2006) for the verification of cross-sections subjected to combined loading refer to the corresponding equations for carbon steel cross-sections in EN1993-1-1 (2005). For axial and bending moment interaction in slender cross-sections, Class 3 and 4, a linear equation is adopted, Eq. (6.11), assuming that failure occurs when the maximum stress reaches the yield stress. N_{Ed}, $M_{y,Ed}$ and $M_{z,Ed}$ are the applied compression load and bending moments; $N_{c,Rd}$ is the axial compression resistance, $M_{y,c,Rd}$ and $M_{z,c,Rd}$ are the moment resistances about the principal axes, calculated from Eqs. (6.2)-(6.3) and Eqs. (6.8)-(6.10), respectively. Concerning stocky cross-sections, Class 1 and 2, some plastic response is allowed and the interaction between axial force and bending moment is governed by Eq. (6.12), with $n_{EN}=N_{Ed}/N_{y.}$ The parameter $a=a_w=(A-2bt)/A$ needs to be considered when calculating the major axis strength, while for minor axis bending $a=a_f=(A-2ht)/A$ is defined, where b and h are the internal width and height of the cross-section respectively.

$$\frac{N_{Ed}}{N_{c,Rd}}+\frac{M_{y,Ed}}{M_{y,c,Rd}}+\frac{M_{z,Ed}}{M_{z,c,Rd}}\leq 1.0 \tag{6.11}$$

$$M_{N,Rd}=M_{pl}\frac{1-n_{EN}}{1-0.5a} \tag{6.12}$$

No specific design expression is given in AS/NZS4673 (2001) and SEI/ASCE 8-02 (2002) to consider the interaction of compression and bending at cross-section level and the interaction equation for member design given in Eq. (6.13) applies. N_n, $M_{n,y}$ and $M_{n,z}$ correspond to the cross-sectional compression and bending resistances and $C_{m,y}$ and $C_{m,z}$ are the equivalent uniform moment factors, equal to unity when the bending moment is constant along the member. $\alpha_{n,y}$ and $\alpha_{n,z}$ are the magnification factors, equal to $(1-N_{Ed}/N_{cre})$, which can be approximated to unity for cross-sections as the critical elastic column load for flexural buckling N_{cre} is much higher than N_{Ed}. Thus, the resulting expression when this equation is particularized for cross-sections, presented in Eq. (6.14), coincides with the linear interaction given in Eq. (6.11) but considering different compression and bending resistances.

$$\frac{N_{Ed}}{N_n} + \frac{C_{m,y}M_{y,Ed}}{\alpha_{n,y}M_{n,y}} + \frac{C_{m,z}M_{z,Ed}}{\alpha_{n,z}M_{n,z}} \leq 1.0 \quad (6.13)$$

$$\frac{N_{Ed}}{N_n} + \frac{M_{y,Ed}}{M_{n,y}} + \frac{M_{z,Ed}}{M_{n,z}} \leq 1.0 \quad (6.14)$$

The comparison of the experimental results presented in chapter 4 for ferritic stainless steel stub columns subjected to combined loading with the predicted strengths for the different codified approaches is presented in Table 6.6 and the mean values and COVs are also reported. This Table reports the r_{pred}/r_u ratios by which design interaction curves exceed or fall short of the corresponding test (or FE) data, calculated in the M/M_y-N/N_y plane as shown in Figure 6.4.

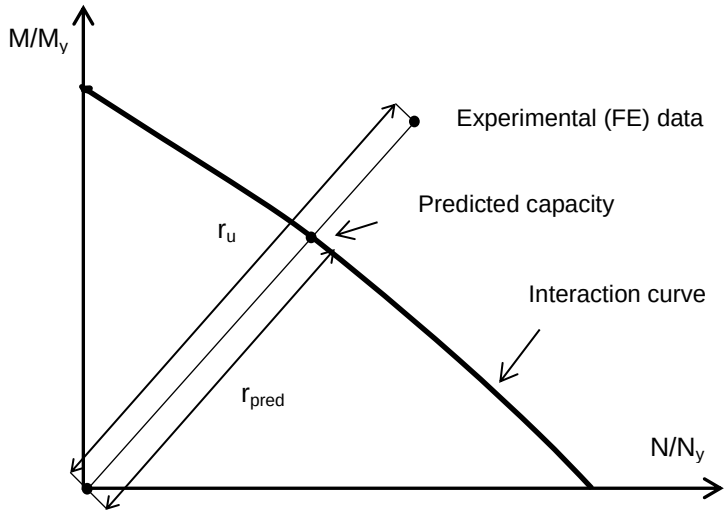

Fig. 6.4. Graphic definition of the r_{pred}/r_u ratio for the assessment of design approaches.

Table 6.6. Comparison of experimental results with predicted capacities for the combined loading tests.

Specimen	r_{EN}/r_u	$r_{EN,rev}/r_u$	$r_{SEI/AS}/r_u$
S1 – CL1	0.79	1.04	0.88
S1 – CL2	0.77	1.02	0.86
S2 – CL1	0.98	0.98	0.83
S2 – CL2	0.99	0.99	0.83
S3-Mj – CL1	0.98	0.98	0.79
S3-Mj – CL2	0.94	0.94	0.75
S3-Mi – CL3	0.83	1.06	0.90
S3-Mi – CL4	0.80	1.03	0.87
S4-Mj – CL1	0.80	1.28	1.03
S4-Mj – CL2	0.78	1.22	0.87
S4-Mi – CL3	0.77	0.79	0.92
S4-Mi – CL4	--	--	--
S5-Mj – CL1	0.72	1.01	0.83
S5-Mj – CL2	0.74	1.03	0.85
S5-Mi – CL3	0.89	0.91	0.95
S5-Mi – CL4	0.86	0.89	0.94
Mean	0.84	1.01	0.87
COV	0.108	0.120	0.078

As for compression and bending, r_{EN} represents the predicted capacity according to EN1993-1-4 (2006) with the codified classification limits, while $r_{EN,rev}$ refers to the revised limits and $r_{SEI/AS}$ corresponds to AS/NZS4673 (2001) and SEI/ASCE 8-02 (2002) provisions. According to the results presented in Table 6.6, Eqs. (6.11)-(6.12) in EN1993-1-4 (2006) with the current cross-sectional classification provide quite accurate previsions of the ultimate loads for the conducted tests. Nevertheless, when the revised cross-sectional classification is considered, the average ultimate capacity prediction is considerably better, although the classification of several cross-sections, such as S1, S3 – Mi, S4 – Mj and S5 – Mj, is too optimistic. For AS/NZS4673 (2001) and SEI/ASCE 8-02 (2002) accurate results are obtained for the tested slender cross-sections, while for the most stocky sections the linear interaction results in overly-conservative strength predictions.

The assessment of the design approaches predicting the cross-section combined loading strength is presented in Table 6.7 for austenitic, ferritic and duplex stainless steel RHS and SHS. In the analysis test results described in chapter 4 are considered together with experimental results presented in Table 2.2 in chapter 2 and the FE strengths from the parametric studies. Results are reported separately for stocky and slender cross-sections for future comparisons. Table 6.7 demonstrates that among the codified design provisions the best results for stocky cross-sections are obtained for the EN1993-1-4 (2006) specification since a nonlinear interaction curve is considered, where marginally better results are observed for the revised classification limits. As AS/NZS4673 (2001) and SEI/ASCE 8-02 (2002) adopt a linear interaction, results are less accurate for stocky cross-sections than for EN1993-1-4 (2006). For slender cross-sections the best mean r_{pred}/r_u ratios are obtained for the reduction factor ρ codified in the AS/NZS4673 (2001) and SEI/ASCE 8-02 (2002) specifications, although the capacity of a number of austenitic and duplex specimens is also substantially overestimated.

Table 6.7. Assessment of design approaches for combined loading.

Grade		r_{EN}/r_u		$r_{EN,rev}/r_u$		$r_{SEI/AS}/r_u$	
		Stocky	Slender	Stocky	Slender	Stocky	Slender
Austenitic	Mean	0.81	0.85	0.82	0.91	0.72	0.96
	COV	0.049	0.127	0.055	0.064	0.061	0.042
Ferritic	Mean	0.80	0.82	0.84	0.86	0.73	0.94
	COV	0.087	0.159	0.100	0.141	0.110	0.126
Duplex	Mean	0.88	0.86	0.89	0.93	0.76	0.93
	COV	0.047	0.159	0.045	0.113	0.045	0.149
All	Mean	0.82	0.84	0.84	0.89	0.73	0.94
	COV	0.071	0.153	0.078	0.120	0.084	0.118

Similar results can be observed in Figure 6.5 for the design expressions codified in EN1993-1-4 (2006), where ultimate strengths have been normalized by the codified pure compression and bending resistances and presented together with the interaction expressions given in EN1993-1-1 (2005), Eqs. (6.11)-(6.12). Although Eq. (6.12) depends on the shape of the cross-sections through the parameter *a*, only the maximum (a=0.5) interaction expression has been depicted for simplicity.

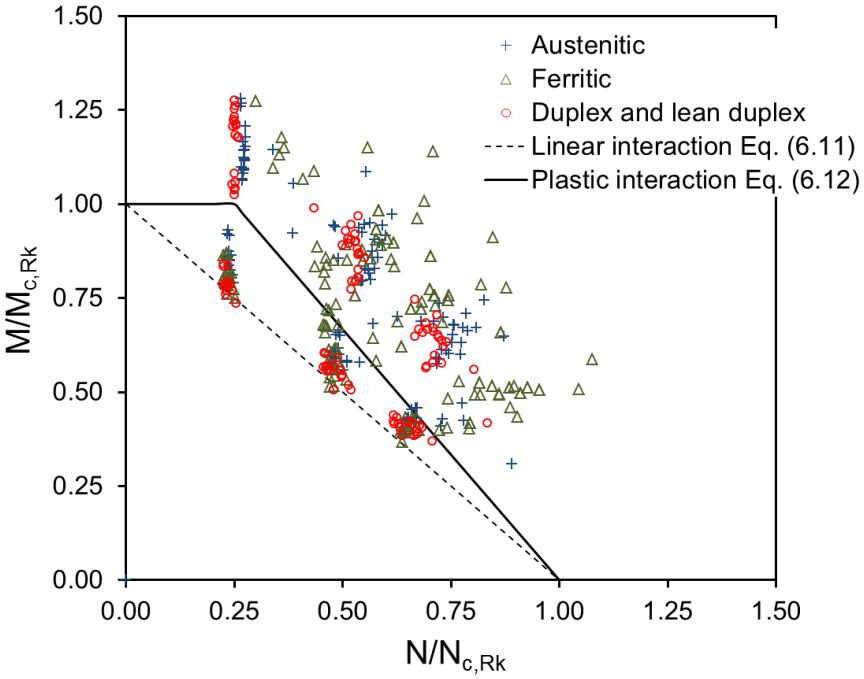

Fig. 6.5. Assessment of the EN1993-1-4 (2006) approach for combined loading.

6.4 Assessment of CSM resistance provisions

The Continuous Strength Method (CSM) is an alternative design method based on cross-section deformation capacity that considers strain hardening effects in the calculation of the cross-sectional resistance of stocky cross-sections, providing more accurate strength predictions than the current codified provisions. The method was first developed for austenitic and duplex stainless grades by Afshan and Gardner (2013b) and then adapted to the less ductile ferritic grades by Bock et al. (2015a).

The method is based on the calculation of the maximum strain that a cross-section can reach ε_{CSM} evaluated in terms of its relative slenderness λ_p and the yield strain ε_y, as shown in Eq. (6.15). This curve was adjusted considering both stub column and beam test data by Afshan and Gardner (2013b) and two additional upper bounds on the predicted deformation capacity ε_{CSM} were provided. The first limit corresponds to the material ductility requirements in EN1993-1-1 (2005) while the second ensures that resistances are not overpredicted due to the adopted bilinear stress-strain material model. For austenitic and duplex stainless steel grades C=0.1 was adopted, but C=0.4 was defined for ferritics, and ε_u corresponds to the ultimate strain.

$$\frac{\varepsilon_{CSM}}{\varepsilon_y} = \frac{0.25}{\lambda_p^{3.6}} \text{ but } \frac{\varepsilon_{CSM}}{\varepsilon_y} < \min\left(15, \frac{C \cdot \varepsilon_u}{\varepsilon_y}\right) \tag{6.15}$$

The relative slenderness for each loading case can be calculated from Eq. (6.16), where σ_{cr} is the critical buckling stress, obtained from the lowest buckling mode in an eigenvalue analysis

and $\sigma_{0.2}$ corresponds to the 0.2% proof stress. At the same time λ_p can be also calculated according to EN1993-1-4 (2006) for the most slender plate element in the cross-section as described in section 6.3.1. It should be noted that the former procedure accounts for element interaction whereas the latter does not. The $\lambda_p \leq 0.68$ limit is adopted given that, beyond this limit, there is no significant benefit of considering material strain hardening effects. Note that all the cross-sectional slendernesses considered in the analysis presented in this section are based on σ_{cr} values derived from CUFSM (Schafer and Ádány, 2006).

$$\lambda_p = \sqrt{\frac{\sigma_{0.2}}{\sigma_{cr}}} \text{ but } \lambda_p \leq 0.68 \tag{6.16}$$

Cross-sectional capacities are derived from the maximum strain ε_{CSM} or the corresponding stress σ_{CSM} calculated from Eq. (6.17). This equation is based on a simplified bilinear material model that includes strain hardening effects, where E_{sh} is the strain hardening modulus calculated from Eq. (6.18) for the different stainless steel grades.

$$\sigma_{CSM} = \sigma_{0.2} + E_{sh}\varepsilon_y\left(\frac{\varepsilon_{CSM}}{\varepsilon_y} - 1\right) \tag{6.17}$$

$$E_{sh} = \begin{cases} \dfrac{\sigma_u - \sigma_{0.2}}{0.45\varepsilon_u - \varepsilon_y} & \text{if } \dfrac{\varepsilon_y}{\varepsilon_u} \leq 0.45 \\ 0 & \text{if } \dfrac{\varepsilon_y}{\varepsilon_u} > 0.45 \end{cases} \quad \text{for ferritic grades} \tag{6.18a}$$

$$E_{sh} = \frac{\sigma_u - \sigma_{0.2}}{0.16\varepsilon_u - \varepsilon_y} \quad \text{for austenitic and duplex grades} \tag{6.18b}$$

The compression resistance of stocky stainless steel cross-sections according to the CSM can be calculated from Eq. (6.19) and the parameters defined above, where A is the gross cross-sectional area and γ_{M0} is the partial safety factor, also set to unity.

$$N_{CSM} = \frac{A \cdot \sigma_{CSM}}{\gamma_{M0}} \tag{6.19}$$

The assessment of the CSM approach for cross-section compression resistance is presented in Table 6.8, where results from Table 6.3 in section 6.3.1 corresponding to stocky cross-sections have also been included for comparison. Results clearly demonstrate the improvement introduced by the CSM when strain hardening effects are considered in ultimate load predictions, and the scatter of the obtained results is also considerably reduced, particularly for austenitic and duplex stainless steel grades.

Table 6.8. Assessment of the CSM design approach for compression and comparison with standards.

Grade		N_{CSM}/N_u	N_{EN}/N_u	$N_{EN,rev}/N_u$	$N_{SEI/AS}/N_u$
Austenitic	Mean	0.83	0.76	0.77	0.77
	COV	0.082	0.106	0.117	0.122
Ferritic	Mean	0.94	0.91	0.92	0.93
	COV	0.035	0.049	0.050	0.051
Duplex	Mean	0.88	0.83	0.85	0.86
	COV	0.036	0.046	0.052	0.056
All	Mean	0.87	0.81	0.83	0.83
	COV	0.082	0.110	0.116	0.119

The bending resistance of stainless steel cross-sections according to the CSM can be calculated from Eq. (6.20) as provided in Afshan and Gardner (2013b), where strain hardening effects and the inelastic strength reserve of the cross-sections are included. The comparison of the predicted capacities with the experimental and FE bending strengths is presented in Table 6.9 for the CSM, where results corresponding to the standards for stocky cross-sections reported in section 6.3.2 have also been included. The improvement introduced by the CSM approach is evident from results in Table 6.9 for austenitic and duplex stainless steel cross-sections, since strain hardening effects have greater influence in these grades. For ferritics, where the strain hardening is less evident, the improvement is lower although results are more accurate.

$$\frac{M_{CSM}}{M_{pl}} = 1 + \frac{E_{sh}}{E}\frac{W_{el}}{W_{pl}}\left(\frac{\varepsilon_{CSM}}{\varepsilon_y} - 1\right) - \left(1 - \frac{W_{el}}{W_{pl}}\right)\cdot\left(\frac{\varepsilon_{CSM}}{\varepsilon_y}\right)^{-2} \tag{6.20}$$

Table 6.9. Assessment of the CSM design approach for bending and comparison with standards.

Grade		M_{CSM}/M_u	M_{EN}/M_u	$M_{EN,rev}/M_u$	$M_{SEI,AS}/M_u$
Austenitic	Mean	0.85	0.74	0.78	0.77
	COV	0.089	0.093	0.097	0.097
Ferritic	Mean	0.94	0.87	0.93	0.93
	COV	0.071	0.096	0.063	0.041
Duplex	Mean	0.88	0.77	0.85	0.84
	COV	0.083	0.105	0.080	0.067
All	Mean	0.90	0.80	0.86	0.85
	COV	0.092	0.122	0.109	0.104

The CSM approach for cross-sectional pure compression and bending resistance has been widely studied in the literature and its accuracy has been demonstrated by several research works. However, more limited investigations have been conducted regarding more general loading conditions such as the combination of axial compression and bending moment. Recent studies on carbon steel cross-sections subjected to combined loading by Liew and Gardner (2015) proposed an interaction expression based on CSM resistances. This approach is based on the equations given in EN1993-1-1 (2005) for Class 1 and 2 cross-sections but considering different power parameters and the pure compression and bending capacities calculated

according to the CSM, as presented in Eq. (6.21). No distinction between principal axes is required for RHS and SHS sections and the power parameters are a*=a+1.2, b=0.8, with $n_{CSM}=N_{Ed}/N_{CSM}$ and $a=A_w/A$, the ratio of the cross-section web area to gross area, as defined in section 6.3.3. However, for $\varepsilon_{csm}/\varepsilon_y$ ratios lower than 3 or slenderness values from 0.5 to 0.68 interaction parameters need to be considered equal to unity, which leads into a linear interaction but with end points calculated according to the CSM.

$$M_{R,CSM}=M_{CSM}\left(1-n_{CSM}^{a^*}\right)^{1/b} \tag{6.21}$$

Alternatively, a simplified CSM approach was proposed for stainless steel cross-sections subjected to combined loading where the interaction expression codified in EN1993-1-1 (2005) for Class 1 and 2 cross-sections is considered with the fundamental capacities determined according to the CSM instead of the squash load and plastic bending moment capacity. The CSM axial and bending capacities can be calculated from the expression presented previously. The same proposal was also suggested by Zhao et al. (2015a, 2015b, 2015c) based on experimental results on austenitic, lean duplex and ferritic stainless steel RHS and SHS, where the accuracy of this CSM method given by Liew and Gardner (2015) was also confirmed. Zhao et al. (2015b) proposed for cross-sections with slendernesses between 0.6 and 0.68 a linear interaction formula with CSM endpoints was proposed, given in Eq. (6.22), while for lower slendernesses Eq. (6.23) is adopted.

$$\frac{N_{Ed}}{N_{CSM}}+\frac{M_{y,Ed}}{M_{y,CSM}}+\frac{M_{z,Ed}}{M_{z,CSM}}\leq 1.0 \tag{6.22}$$

$$M_{N,CSM}=M_{CSM}\frac{1-n_{CSM}}{1-0.5a} \text{ with } n_{CSM}=\frac{N_{Ed}}{N_{CSM}} \tag{6.23}$$

The quantitative evaluation of the CSM based methods for stainless steel RHS and SHS sections subjected to combined loading is reported in Table 6.10, where results corresponding to stocky cross-sections from the design expressions codified in standards are also included. Results relative to the CSM method developed by Liew and Gardner (2015) are denoted as r_{CSM}/r_u ratios, while $r_{CSM,sim}/r_u$ correspond to the simplified CSM proposed herein and also given by Zhao et al. (2015a, 2015b, 2015c). The calculation of the ratios was derived following the procedure described in section 6.3.3. According to these results, the interaction expression proposed by Liew and Gardner (2015) accurately predicts the ultimate resistance of stainless steel RHS and SHS subjected to combined loading conditions. Nevertheless, the predicted capacities by the simplified CSM are closer to those obtained experimentally and numerically, providing excellent results without introducing any new interaction expression but adopting the equations already codified in EN1993-1-1 (2005), and keeping calculations relatively simple for designers.

Table 6.10. Assessment of the CSM design approach for uniaxial combined loading and comparison with standards.

Grade		r_{CSM}/r_u	$r_{CSM,sim}/r_u$	r_{EN}/r_u	$r_{EN,rev}/r_u$	$r_{SEI/AS}/r_u$
Austenitic	Mean	0.85	0.91	0.81	0.82	0.72
	COV	0.080	0.056	0.049	0.055	0.061
Ferritic	Mean	0.89	0.93	0.80	0.84	0.73
	COV	0.077	0.069	0.087	0.100	0.110
Duplex	Mean	0.85	0.91	0.88	0.89	0.76
	COV	0.079	0.072	0.047	0.045	0.045
All	Mean	0.86	0.92	0.82	0.84	0.73
	COV	0.107	0.067	0.071	0.078	0.084

The interaction expressions based on the ultimate capacities calculated according to the CSM are presented Figure 6.6, where experimental and numerical data are depicted for the considered stainless steel families normalized by the CSM compression and bending resistances. Since the CSM interaction expressions also depend on the ratio of the cross-section web area to gross area, only curves corresponding to a=0.5 are shown for simplicity. In contrast with the results observed in Figure 6.5 for the Eurocode 3 approach, results obtained for the CSM show a considerably lower scatter and conservatism, providing better strength predictions for all stainless steel families.

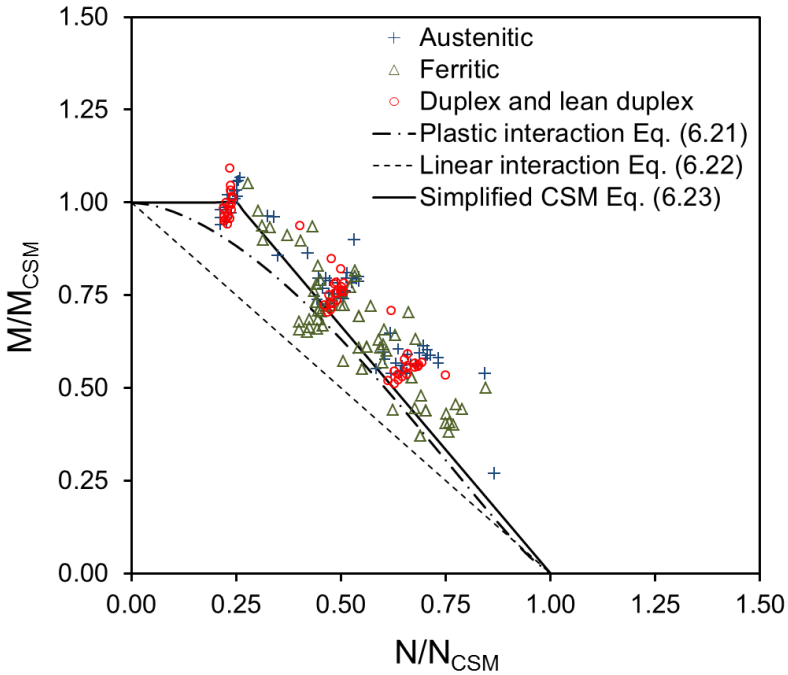

Fig. 6.6. Assessment of the CSM-based approaches for combined loading.

Finally, the reliability of the proposed simplified CSM approach is assessed through the corresponding statistical analyses for stainless steel RHS and SHS subjected to combined loading. The validation has been derived according to EN1990, Annex D (2005) specifications and following the steps described in Tankova et al. (2014). Statistical parameters corresponding to the material and geometrical variations of the different stainless steel grades analysed have been extracted from Afshan et al. (2015). The considered material overstrength ratios are 1.3

for austenitic stainless steel, 1.2 for ferritics and 1.1 for duplex and lean duplex grades, with COVs equal to 0.060, 0.045 and 0.030 respectively, and the COV of the geometric properties was taken as 0.050. The variability due to FE modelling was also included in the analysis thought the procedure described in Bock et al. (2015c), since some deviation between tests and the modelled reality usually occurs, resulting in V_{FE}=0.019.

A summary of the most relevant statistical parameter values is presented in Table 6.11 together with the calculated γ_{M0} factors. b is the mean value of the correction factor, V_δ is the coefficient of variation of the errors of the approach relative to the experimental results and V_r is the combined coefficient of variation.

Table 6.11. Summary of the reliability analysis results for the simplified CSM approach for combined loading.

Grade	b	V_δ	V_r	γ_{M0}
Austenitic	1.113	0.055	0.099	0.86
Ferritic	1.080	0.071	0.101	0.93
Duplex	1.131	0.077	0.100	1.04

According to the results gathered in Table 6.11 the simplified CSM approach for stocky cross-sections subjected to combined loading can be safely applied for all stainless steel grades if the partial safety factor γ_{M0} currently codified in EN1993-1-4 (2006) is considered, which is equal to 1.10, since the calculated γ_{M0} values lay below 1.10. Very similar results were also reported by Zhao et al. (2015b, 2015c).

6.5 Assessment of DSM resistance provisions

The Direct Strength Method (DSM) is a design method developed by Schafer and Pekoz (1998) that allows the consideration of local and distortional buckling effects in an easy manner through the use of software to determine elastic buckling modes in conjunction with strength curves instead of considering the effective width calculations. Although the DSM has been implemented in the North American Specification AISI-S100-12 (2012) for carbon steel structures, it has not yet been included in stainless steel standards.

The Direct Strength Method considers the effect of local buckling by reducing the resistance of the gross section through a simple strength curve without calculating any effective property of the cross-section. According to AISI-S100-12 (2012), the general nominal resistance of a carbon steel cross-section R_{nl} is obtained by reducing the yield load R_y due to the effect of local buckling, as given in Eq. (6.24). For the cross-sectional compression resistance $R_{nl}=N_{c,Rk}$ and $R_y=N_y$ are considered, while for evaluating the bending moment resistance $R_{nl}=M_{c,Rk}$ and $R_y=M_y$ need to be adopted, where N_y is the cross-sectional squash load and M_y is the first yield bending moment. The reduction due to local buckling interaction depends on the local slenderness of the cross-section λ_l calculated from Eq. (6.25), which measures the susceptibility of the cross-section to local buckling through the corresponding critical elastic local buckling

load R_{crl}. R_{crl} can be obtained from a number of numerical methods and related software programs based on finite element and finite strip methods. R_{crl} corresponds to the critical elastic local buckling load N_{crl} for compression and it is equal to the critical elastic local buckling moment M_{crl} for bending.

$$\frac{R_{nl}}{R_y} = \begin{cases} 1 \text{ for } \lambda_l \leq 0.776 \\ \frac{1}{\lambda_l^{0.8}} - \frac{0.15}{\lambda_l^{0.8}} \text{ for } \lambda_l > 0.776 \end{cases} \quad (6.24)$$

$$\lambda_l = \sqrt{\frac{R_y}{R_{crl}}} \quad (6.25)$$

The local buckling strength of stainless steel sections was investigated by Becque et al. (2008) through an experimental programme comprising lipped channel section, I-section and RHS columns. Since no appreciable differences were found among the different stainless steel grades, a single interaction curve was proposed for all families, given by Eq. (6.26). This strength curve is slightly lower than that provided for carbon steel cross-sections and uses a lower limiting slenderness. Niu et al. (2015) demonstrated that the reduction of the bending moment capacity due to local buckling of stainless steel beams can be also conservatively calculated from Eq. (6.26). Therefore, the local buckling behaviour of stainless steel cross-sections can be derived from the same strength curve regardless the considered loading case as for carbon steel specimens.

$$\frac{R_{nl}}{R_y} = \begin{cases} 1 \text{ for } \lambda_l \leq 0.474 \\ \frac{0.95}{\lambda_l^{0.8}} - \frac{0.22}{\lambda_l^{1.6}} \text{ for } \lambda_l > 0.474 \end{cases} \quad (6.26)$$

Rossi and Rasmussen (2013) included the effect of strain hardening in the DSM design approach for stainless steel cross-sections by adopting a linear expression relating the cross-sectional resistance to the slenderness instead of using the classical horizontal yield limit. The ultimate tensile strength σ_u was considered in the definition of the resistance so the ratio between the predicted capacity and the conventional yield limit tends to $\sigma_u/\sigma_{0.2}$ as the slenderness approaches zero, following a linear curve as given in Eq. (6.27). The predicted cross-sectional resistance that considers both strain hardening effects for stocky cross-sections while reducing the resistance due to the local buckling interaction R_{enh_nl} proposed for stainless steel cross-sections is presented in Eq. (6.27). Although this approach was originally proposed for compression and distortional buckling effects, it can be easily extended to different loading conditions such as bending. A simple modification of this expression to be adapted for the carbon steel strength curve is proposed herein (see Eq. (6.28)), considering a different limiting slenderness but following the same procedure described in Rossi and Rasmussen (2013).

$$\frac{R_{enh\_nl}}{R_y} = \begin{cases} 1+\left(1-2.11\lambda_l\right)\left(\frac{\sigma_u}{\sigma_{0.2}}-1\right) & \text{for } \lambda_l \le 0.474 \\ \frac{0.95}{\lambda_l^{0.8}}-\frac{0.22}{\lambda_l^{1.6}} & \text{for } \lambda_l > 0.474 \end{cases} \quad (6.27)$$

$$\frac{R_{enh\_nl}}{R_y} = \begin{cases} 1+\left(1-1.29\lambda_l\right)\left(\frac{\sigma_u}{\sigma_{0.2}}-1\right) & \text{for } \lambda_l \le 0.776 \\ \frac{1}{\lambda_l^{0.8}}-\frac{0.15}{\lambda_l^{0.8}} & \text{for } \lambda_l > 0.776 \end{cases} \quad (6.28)$$

6.5.1 Cross-sections subjected to compression

The evaluation of the local buckling strength curves and the applicability of the enhanced material property approach proposed in Rossi and Rasmussen (2013) for stainless steel RHS and SHS subjected to pure compression are presented in this section. The ferritic, austenitic, duplex and lean duplex stainless steel RHS and SHS tests reported in Table 2.1 and the FE results obtained from the parametric studies have been considered in the study as for previous sections.

Figure 6.7 presents the experimental and numerical ultimate loads N_u normalized by the respective squash loads N_y plotted against the corresponding cross-sectional slenderness λ_l calculated from Eq. (6.25). The strength curves for carbon steel (Eq. (6.24)) and stainless steel (Eq. (6.26)) cross-sections considering local buckling are also presented, together with the enhanced material property approaches for different stainless steel families, Eq. (6.28).

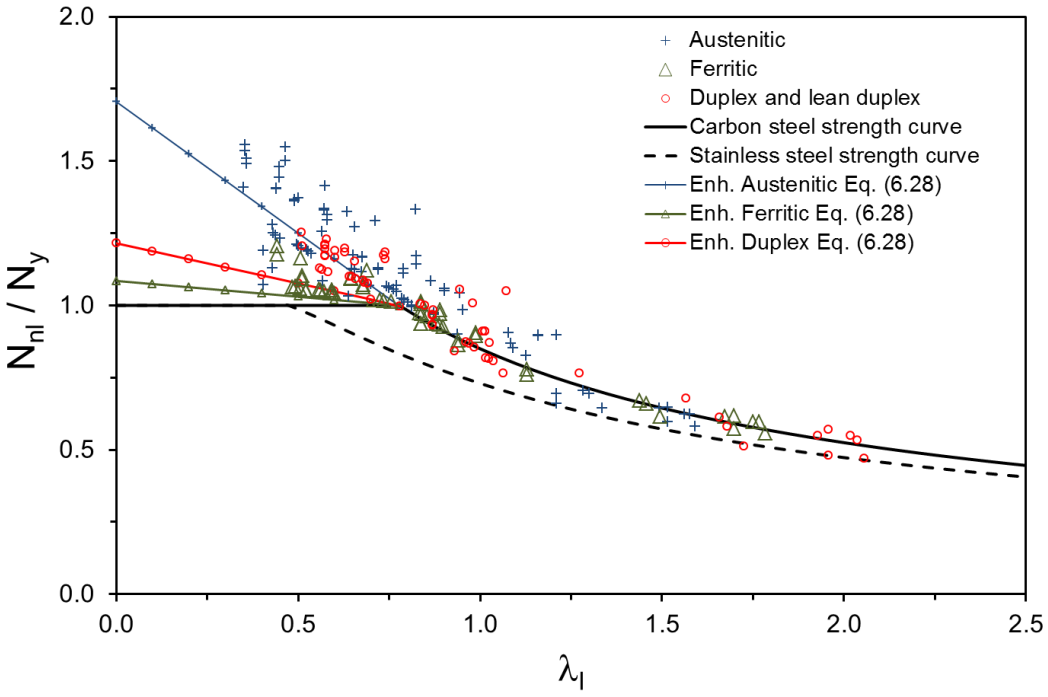

Fig. 6.7. Assessment of DSM approach for stainless steel RHS and SHS in compression.

Each experimental data point presents a different $\sigma_u/\sigma_{0.2}$ ratio and needs to be analysed with that particular value. However, for simplicity, Figure 6.7 only presents the enhanced property curves for the average $\sigma_u/\sigma_{0.2}$ ratios of the considered experimental results. All critical elastic local buckling loads N_{crl} and moments M_{crl} considered in the DSM assessment have been also calculated from a buckling analysis conducted with CUFSM (Schafer and Ádány (2006)).

According to Figure 6.7, the local buckling curve codified for carbon steel cross-sections provides a better estimation of the ultimate capacity of slender stainless steel cross-sections in compression and it also demonstrates the improvement introduced when the enhanced material properties are considered for stocky cross-sections. The reason for the unexpected better agreement between the ultimate strengths and the DSM strength curve for carbon steel rather than the curve for stainless steel is likely related to the fact the stainless steel DSM strength curve is based on research on open sections with substantially smaller thickness than those considered in the present study on closed sections, and hence are likely to have been more detrimentally affected by local geometric imperfections.

Tables 6.12 and 6.13 present the assessment of the DSM strength curves corresponding to stainless steel and carbon steel cross-sections for stainless steel RHS and SHS subjected to compression. The mean values and COVs of the predicted-to-experimental (or FE) capacity ratios N_{DSM}/N_u considering both strength curves are reported for stocky and slender cross-sections and different stainless steel families. Results corresponding to stocky cross-sections are presented in Table 6.12 for the DSM approach including enhanced material properties and N_{pred}/N_u ratios for the design approaches codified in different standards and the Continuous Strength Method (CSM) are also reported. Although these results have already been reported in Table 6.8, they have also been included in Table 6.12 for comparison.

Table 6.12. Assessment of the DSM for stocky cross-sections subjected to compression and comparison with other design approaches.

Grade		N_{DSM}/N_u CS-curve	N_{DSM}/N_u SS-curve	N_{CSM}/N_u	N_{EN}/N_u	$N_{EN,rev}/N_u$	$N_{SEI/AS}/N_u$
Austenitic	Mean	0.88	0.76	0.80	0.76	0.77	0.77
	COV	0.119	0.072	0.082	0.106	0.117	0.122
Ferritic	Mean	0.94	0.84	0.93	0.91	0.92	0.93
	COV	0.053	0.018	0.050	0.049	0.050	0.051
Duplex	Mean	0.89	0.70	0.86	0.83	0.85	0.86
	COV	0.050	0.076	0.056	0.046	0.052	0.056
All	Mean	0.90	0.76	0.85	0.81	0.83	0.83
	COV	0.095	0.076	0.093	0.110	0.116	0.119

According to the results presented in Figure 6.8 and Table 6.12 the best method for the prediction of the compression resistance of stainless steel stocky cross-sections is the proposed DSM approach considering the enhanced material properties based on the carbon steel strength curve given in Eq. (6.28). Very similar and excellent results are obtained for the CSM since both approaches consider strain hardening effects, and as mentioned in the previous section for the CSM, the improvement in strength predictions for the DSM approach is more

notable for austenitic stainless steel cross-sections, where strain hardening effects are more important.

The accuracy of the DSM strength curves for slender cross-sections is evaluated from the data with local slenderness higher than λ_l>0.776. These results are reported in Table 6.13 and are compared with those corresponding to the design methods based on the effective width methods codified in standards, also included in Table 6.3. Results demonstrate that the DSM strength curve corresponding to carbon steel cross-sections given in Eq. (6.24) is the approach that provides both accurate and safe results for slender stainless steel cross-sections subjected to pure compression. As mentioned in the previous section, although highest N_{pred}/N_u ratios are obtained for SEI/ASCE 8-02 (2002) and AS/NZS4673 (2001), the capacity of a number of austenitic and duplex specimens is substantially overestimated.

Table 6.13. Assessment of the DSM for slender cross-sections subjected to compression and comparison with other design approaches.

Grade		N_{DSM}/N_u CS-curve	N_{DSM}/N_u SS-curve	N_{EN}/N_u	$N_{EN,rev}/N_u$	$N_{SEI/AS}/N_u$
Austenitic	Mean	0.94	0.78	0.85	0.89	0.96
	COV	0.093	0.100	0.116	0.105	0.121
Ferritic	Mean	0.99	0.86	0.91	0.95	1.02
	COV	0.033	0.054	0.056	0.053	0.072
Duplex	Mean	0.98	0.83	0.90	0.94	1.02
	COV	0.080	0.082	0.102	0.098	0.117
All	Mean	0.98	0.83	0.89	0.92	1.01
	COV	0.070	0.087	0.094	0.093	0.106

6.5.2 Cross-sections subjected to bending

Stocky RHS and SHS beams have significant inelastic reserve strength, with ultimate bending moments reaching the full plastic moment capacity M_{pl}, fact that is partly incorporated in design standards. EN1993-1-4 (2006) assigns full plastic capacity to cross-sections classified as Class 1 or 2 while AS/NZS4673 (2001) and SEI/ASCE 8-02 (2002) allow the consideration of the inelastic reserve strength by assuming an ideally elastic-plastic stress-strain curve throughout the cross-section as described in “Procedure II” and adopting a compression strain factor C_y to determine the maximum compressive strain, as mentioned in section 6.3.2. AS/NZS4673 (2001) also contains provisions for utilizing the full plastic bending capacity for rectangular and square hollow sections.

Shifferaw and Schafer (2012) proposed a different design approach for cold-formed carbon steel C and Z beams where the inelastic reserve strength was implemented into the DSM formulation. The approach takes advantage of the inelastic reserve strength for members sufficiently locally stable to reach a partial yield of the cross-section, exceeding the elastic bending moment capacity. This new approach has been included in the revised AISI-S100-16 (2016). According to Shifferaw and Schafer (2012), the inelastic reserve is assumed to be a function of the maximum compressive strain as given in Eq. (6.29) with a compression strain factor C_y given in Eq. (6.30), which is different from that codified in “Procedure II” of

AS/NZS4673 (2001) and SEI/ASCE 8-02 (2002). λ_{ly} is the limiting slenderness for carbon steel cross-sections, equal to 0.776. The compression strain factor C_y codified in AS/NZS4673 (2001) and SEI/ASCE 8-02 (2002) is defined in terms of the b/t ratio, but can be easily transformed into Eq. (6.31) by considering the slenderness definition given in Eq. (6.5), equivalent to that codified in AS/NZS4673 (2001) and SEI/ASCE 8-02 (2002).

$$M_{nl} = M_y + (M_{pl} - M_y)\left(1 - \frac{1}{C_y^2}\right) \tag{6.29}$$

$$C_y = \left(\frac{\lambda_{ly}}{\lambda_l}\right)^{0.5} \tag{6.30}$$

$$C_y = \begin{cases} 3 & \lambda_l \le 0.58 \\ 3 - 2\left(\frac{\lambda_l - 0.58}{0.196}\right) & 0.58 \le \lambda_l \le 0.776 \\ 1 & \lambda_l \ge 0.776 \end{cases} \tag{6.31}$$

However, in order to be consistent with the scope of AISI-S100-12 (2012), Shifferaw and Schafer (2012) limited the maximum strain in inelastic bending to $3\varepsilon_y$, where ε_y is the yield strain. No specific limit was provided for stainless steel beams but since “Procedure II" in SEI/ASCE 8-02 (2002) and AS/NZS4673 (2001) also limits the C_y parameter to a maximum value of 3, the same limit has been considered in the following analysis.

The analysis presented in this research concerning stainless steel RHS and SHS beams is only focused on the cross-sectional behaviour since the lateral-torsional strength of hollow sections is high and cross-sectional failure is expected. For stocky cross-sections, where the first yield capacity is significantly exceeded, the effect of strain hardening and the partial yielding of the cross-section have been incorporated into the analysis considering the enhanced material property curves given in Eq. (6.27) and Eq. (6.28) and the inelastic reserve strength expressions with the different definitions of the compression strain factor C_y. The local buckling behaviour of stainless steel beams has also been investigated through the strength curves given by Eq. (6.24) and Eq. (6.26) for carbon steel and stainless steel slender cross-sections, respectively.

Figure 6.8 presents the experimental and numerical bending moment capacities of the studied specimens normalized by the first yield moment M_y and plotted against the corresponding local slenderness. Figure 6.8 also includes the strength curves for carbon and stainless steel cross-sections, and the curves that consider the enhanced material properties for different stainless steel grades. Note again that since each experimental result is characterized by a different $\sigma_u/\sigma_{0.2}$ ratio, the enhanced material property curves corresponding to the average $\sigma_u/\sigma_{0.2}$ ratios are only presented. The results shown in Figure 6.8 suggest that the local buckling strength curve proposed for stainless steel cross-sections underestimates the flexural capacity of the analysed RHS and SHS beams and the curve provided for carbon steel cross-sections is more accurate. It is also appreciated that the consideration of the enhanced material properties

introduces important improvement in the flexural capacity prediction of stocky cross-sections, still showing a considerable conservatism. Therefore, the DSM approach suggested in Shifferaw and Schafer (2012) that considers the inelastic reserve strength M_n has been adopted instead of the first yield moment M_y.

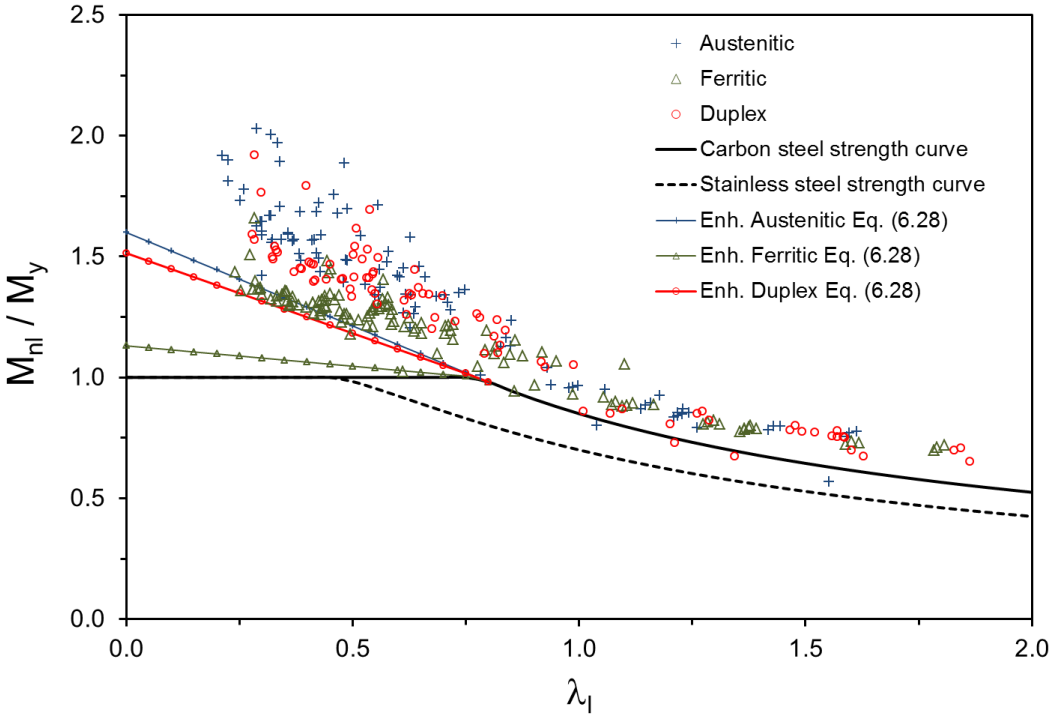

Fig. 6.8. Assessment of DSM approach for stainless steel RHS and SHS beams based on the elastic capacity M_y.

Tables 6.14 and 6.15 present the mean values and COVs of the predicted-to-experimental (or FE) bending moment capacity ratios M_{DSM}/M_u for stocky and slender cross-sections respectively. Regarding stocky cross-sections, Table 6.14 compares results obtained from the DSM-based enhanced material property approaches derived from Eqs. (6.27) and (6.28) with those obtained for different standards and the CSM, also reported in sections 6.3 and 6.4.

Table 6.14. Assessment of the DSM for stocky cross-sections subjected to bending and comparison with other design approaches.

Grade		N_{DSM}/N_u CS-curve	N_{DSM}/N_u CS-curve Proc. II C_y	N_{DSM}/N_u SS-curve	M_{CSM}/M_u	M_{EN}/M_u	$M_{EN,rev}/M_u$	$M_{SEI,AS}/M_u$
Austenitic	Mean	0.80	0.96	0.74	0.85	0.74	0.78	0.77
	COV	0.097	0.075	0.085	0.097	0.093	0.097	0.097
Ferritic	Mean	0.89	0.96	0.88	0.94	0.87	0.93	0.93
	COV	0.064	0.042	0.059	0.072	0.096	0.063	0.041
Duplex	Mean	0.78	0.91	0.77	0.88	0.77	0.85	0.84
	COV	0.045	0.067	0.052	0.085	0.105	0.080	0.067
All	Mean	0.83	0.95	0.80	0.89	0.80	0.86	0.85
	COV	0.094	0.065	0.104	0.096	0.122	0.109	0.104

Comparing DSM results that consider enhanced material properties given in the first and third columns of Table 6.14 with those obtained according to "Procedure II" in SEI/ASCE 8-02 (2002) and AS/NZS4673 (2001), it can be observed that higher M_{pred}/M_u ratios are obtained for the latter even if this approach does not account for strain hardening effects. This suggests that the definition of the compression strain factor C_y proposed by Shifferaw and Schafer (2012) for cold-formed carbon steel beams is too conservative for stainless steel RHS and SHS. Hence, results based on the C_y definition provided in "Procedure II" given in Eq. (6.31) have also been included in Table 6.14. Although all approaches provide reasonable predictions for the bending moment capacity of stocky stainless steel RHS and SHS, according to these results the best method is the DSM approach including the enhanced material properties based on the carbon steel strength curve given in Eq. (6.28) and the C_y definition provided in SEI/ASCE 8-02 (2002) and AS/NZS4673 (2001).

Figure 6.9 shows the experimental and numerical bending moment capacities normalized by the flexural resistance considering the inelastic reserve strength M_n calculated from Eqs. (6.29) and (6.31) considering the compression strain factor C_y given in SEI/ASCE 8-02 (2002) and AS/NZS4673 (2001). Figure 6.9 clearly demonstrates the improvement of the new formulation, reducing considerably the underestimation and scatter of the predicted ultimate bending moment capacities for all stainless steel grades.

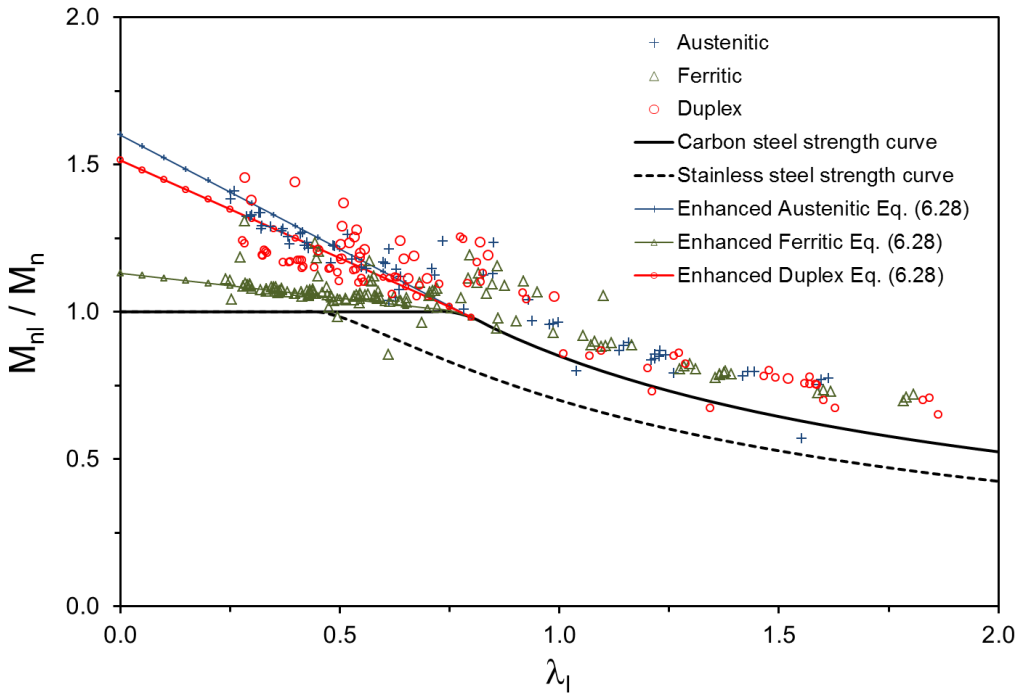

Fig. 6.9. Assessment of DSM approach for stainless steel RHS and SHS beams based on the inelastic reserve strength capacity M_n.

The assessment of the DSM approaches for slender cross-sections in bending is presented in Table 6.15. The mean M_{pred}/M_u ratios closest to unity are obtained for the effective width methods given in standards (EN1993-1-4 (2006), SEI/ASCE 8-02 (2002) and AS/NZS4673 (2001)), although overpredictions lead to highly scattered results. Alternatively, DSM predictions

based on the carbon steel strength curve given in Eq. (6.24) are accurate and less scattered, being an excellent alternative to the effective width method for stainless steel hollow sections in bending.

Table 6.15. Assessment of the DSM for slender cross-sections subjected to bending and comparison with other design approaches.

Grade		M_{DSM}/M_u CS-curve	M_{DSM}/M_u SS-curve	M_{EN}/M_u	$M_{EN,rev}/M_u$	$M_{SEI,AS}/M_u$
Austenitic	Mean	0.88	0.71	0.92	0.93	0.89
	COV	0.079	0.106	0.080	0.076	0.147
Ferritic	Mean	0.87	0.75	0.92	0.93	0.93
	COV	0.054	0.047	0.092	0.085	0.107
Duplex	Mean	0.85	0.71	0.96	0.98	0.96
	COV	0.079	0.085	0.129	0.123	0.165
All	Mean	0.87	0.73	0.93	0.95	0.93
	COV	0.071	0.085	0.106	0.100	0.142

6.5.3 Cross-sections subjected to combined loading

AISI-S100-12 (2012) does not provide any specific expression based on the DSM for the design of beam-columns so the general interaction equation is applicable with the compression and bending resistances calculated according to the DSM. However, Rasmussen (2006) extended the DSM approach for compression members to beam-columns by introducing a member resistance parameter r_{ne} equal to the radial distance in the M/M_y-N/N_y plane. In this approach the beam-column behaviour is directly calculated with a unique strength curve considering the member and section slenderness based on the elastic instabilities of the member subjected to the actual stress distribution. This approach has been adapted in this section to predict the capacity of cross-sections subjected to combined loading conditions and the accuracy of this new method is evaluated. The basis of the approach is the same since the different resistance parameters are calculated as radial distances in the M/M_y-N/N_y plane (see Figure 6.10).

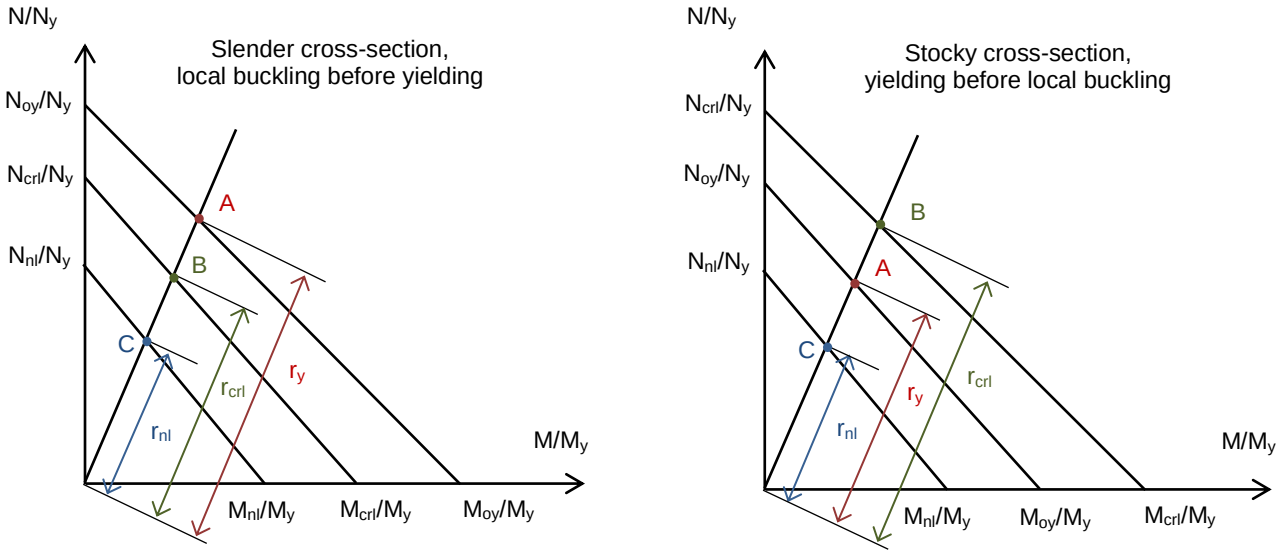

Fig. 6.10. Graphical definition of the extended radial distances for the combined loading approach.

The most notable modification is that the radial distance governing the member behaviour changes to the yielding radial distance r_y calculated from Eq. (6.32) when cross-sections subjected to combined loading are considered, see point A in Figure 6.10. In the Figure, N_{oy} and M_{oy} represent the axial load and bending moment that cause the yielding of the cross-section, respectively, and can be obtained from an interaction expression similar to that given in Eq.(6.33) assuming that $M_{oy}=e \cdot N_{oy}$, where e is the eccentricity of the compression load.

$$r_y = \sqrt{\left(\frac{N_{oy}}{N_y}\right)^2 + \left(\frac{M_{oy}}{M_y}\right)^2} \tag{6.32}$$

$$\frac{N_{oy}}{N_y} + \frac{M_{oy}}{M_y} = 1 \tag{6.33}$$

The local buckling behaviour of the cross-section (point B) is evaluated through the local buckling radial distance r_{crl} calculated from Eq. (6.34) and combined with the yielding parameter r_y to obtain a generalized slenderness λ_n, as per Eq. (6.35). In Eq. (6.34), N_{ocr} and M_{ocr} represent the local buckling compression load and bending moment, respectively, and are calculated from an elastic buckling analysis.

$$r_{crl} = \sqrt{\left(\frac{N_{ocr}}{N_y}\right)^2 + \left(\frac{M_{ocr}}{M_y}\right)^2} \tag{6.34}$$

$$\lambda_n = \sqrt{\frac{r_y}{r_{crl}}} \tag{6.35}$$

Once the slenderness λ_n of the cross-section is known, the resistance of the cross-section r_{enh_nl} is determined from the strength curves given in Eqs. (6.28) and (6.27) for carbon steel and stainless steel sections respectively when $R_{enh\_nl}=r_{enh\_nl}$, $R_y=r_y$ and $R_{crl}=r_{crl}$ are considered. The predicted compression and flexural strengths of the cross-section N_{nl} and M_{nl} can be finally determined from Eq. (6.36). Note that Eqs. (6.27) and (6.28) incorporate the effects of enhanced material properties and local buckling.

$$r_{enh\_nl} = \sqrt{\left(\frac{N_{nl}}{N_y}\right)^2 + \left(\frac{M_{nl}}{M_y}\right)^2} \tag{6.36}$$

The assessment of the proposed DSM-based approach for cross-sections subjected to combined loading conditions is presented comparing the predicted capacities with those obtained from tests and FE parametric studies. Assuming the conclusions presented in the previous section regarding stainless steel RHS and SHS beams, the bending moment capacity M_n considering inelastic strength reserve calculated with the compression strain factor C_y proposed in AS/NZS4673 (2001) and SEI/ASCE 8-02 (2002) has been implemented in the analysis by replacing M_y with M_n in Eq. (6.33). Figure 6.11 shows the assessment of the

proposed method for stainless steel cross-sections subjected to combined compression and uniaxial bending by presenting the normalized experimental and numerical resistance ratios r_u/r_y against the corresponding generalized slenderness λ_n. The enhanced material property curves corresponding to the carbon steel strength curve (Eq. (6.24a)) are also presented, which correspond to the average $\sigma_u/\sigma_{0.2}$ ratios of the experimental specimens.

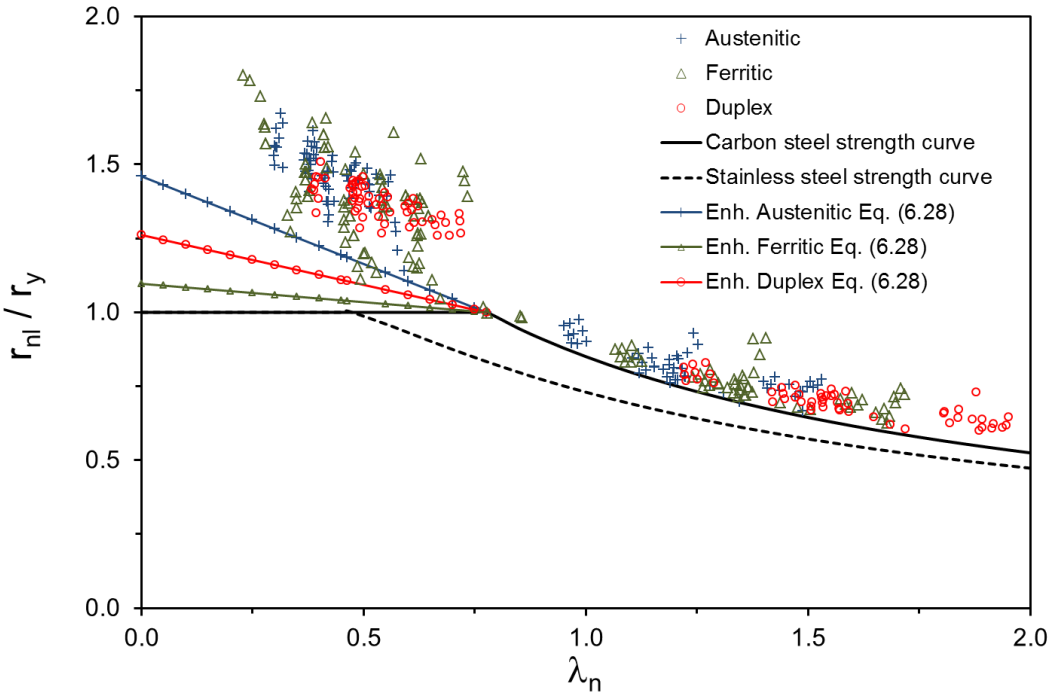

Fig. 6.11. Assessment of DSM approach for stainless steel cross-sections under uniaxial combined loading considering linear interaction in yielding.

Figure 6.11 suggests that the local buckling curve for carbon steel cross-sections accurately predicts the combined loading strength of slender cross-sections, and that the strength curve for stainless steel cross-sections is conservative over the full slenderness range. Regarding stocky cross-sections, it is evident that the consideration of the enhanced material properties introduces important improvement on the ultimate strength predictions when compared to the yield capacity (r_{nl}/r_y=1), but is still conservative. This over-conservatism is higher than for the compression and bending moment loading cases investigated in previous sections due to the assumption made in Eq. (6.33), where a linear interaction is assumed for the yield capacity. The linear interaction is usually accurate for slender cross-sections, but becomes increasingly conservative as the local slenderness decreases.

The influence of the interaction approach assumed for calculating the yield capacity under combined loading has been analysed by considering the interaction expression provided in EN1993-1-1 (2005) for Class 1 and 2 cross-sections, presented in Eq. (6.37), where a plastic response of the cross-section is allowed in the calculation of the reduced bending moment capacity $M_{n,red}$. N_{oy} is calculated from Eq. (6.38) and the parameter $a=a_w=(A-2bt)/A$ needs to be considered when calculating the major axis strength, while for minor axis bending

$a=a_f=(A-2ht)/A$ is defined, where b and h are the internal width and height respectively. This interaction expression is considered as are the enhanced material properties in order to obtain accurate predictions of the ultimate strength of stocky cross-sections under combined loading. However, it is important to note that this interaction expression should only be applied to those cross-sections with a local slenderness lower than 0.776, while for more slender cross-sections the linear interaction equation presented in Eq. (6.33) should be applied.

$$M_{n,red} = M_n \frac{1 - N_{oy}/N_y}{1 - 0.5a} \tag{6.37}$$

$$N_{oy} = \left[\frac{e(1 - 0.5a)}{M_n} + \frac{1}{N_y} \right]^{-1} \tag{6.38}$$

Results corresponding to the final DSM proposal for stocky cross-sections subjected to combined loading have been compared with those obtained from the different standards (EN1993-1-4 (2006), SEI/ASCE 8-02 (2002) and AS/NZS4673 (2001)). Alternative design methods based on the CSM discussed in previous section have also been included in the analysis. Table 6.16 presents the mean values and COVs of the predicted-to-experimental (or FE) resistance ratios reported in Table 6.10 and those corresponding to the DSM approach r_{DSM}/r_u for stocky cross-sections under combined loading. Table 6.16 shows that the best capacity predictions are provided by the approaches considering strain hardening effects while conservative results are obtained for the codified expressions. According to the results presented in Table 6.16, the DSM approach proposed by adapting the procedure given in Rasmussen (2006) provides excellent predictions of the ultimate capacity of stainless steel hollow sections subjected to combined compression and bending when the enhanced material properties corresponding to the proposed carbon steel strength curve (Eq. (6.28)) and the compression strain factor C_y codified in AS/NZS4673 (2001) and SEI/ASCE 8-02 (2002) (Eq. (6.37)) are considered.

Table 6.16. Assessment of the DSM for stocky cross-sections subjected to combined loading and comparison with other design approaches.

Grade		r_{DSM}/r_u CS-curve	r_{DSM}/r_u SS-curve	r_{CSM}/r_u	$r_{CSM,sim}/r_u$	r_{EN}/r_u	$r_{EN,rev}/r_u$	$r_{SEI/AS}/r_u$
Austenitic	Mean	0.96	0.82	0.85	0.91	0.81	0.82	0.72
	COV	0.059	0.070	0.080	0.056	0.049	0.055	0.061
Ferritic	Mean	0.94	0.86	0.89	0.93	0.80	0.84	0.73
	COV	0.067	0.071	0.077	0.069	0.087	0.100	0.110
Duplex	Mean	0.93	0.84	0.85	0.91	0.88	0.89	0.76
	COV	0.051	0.098	0.079	0.072	0.047	0.045	0.045
All	Mean	0.94	0.84	0.86	0.92	0.82	0.84	0.73
	COV	0.062	0.078	0.107	0.067	0.071	0.078	0.084

Finally, design methods based on the effective width method are compared with the DSM approaches in Table 6.17 for slender cross-sections, where results from Table 6.7 are also reported for the codified approaches. The presented results suggest that the proposed DSM-

based approach for combined loading based on the carbon steel strength curve provides the best and less scattered capacity predictions for the analysed data, together with the method codified in AS/NZS 4673 (2001) and SEI/ASCE 8-02 (2002), although the resistance of several specimens is overestimated by the later.

Table 6.17. Assessment of the DSM for slender cross-sections subjected to combined loading and comparison with other design approaches.

Grade		r_{DSM}/r_u CS-curve	r_{DSM}/r_u SS-curve	r_{EN}/r_u	$r_{EN,rev}/r_u$	$r_{SEI/AS}/r_u$
Austenitic	Mean	0.89	0.78	0.85	0.91	0.96
	COV	0.059	0.073	0.127	0.064	0.042
Ferritic	Mean	0.91	0.80	0.82	0.86	0.94
	COV	0.060	0.063	0.159	0.141	0.126
Duplex	Mean	0.87	0.82	0.86	0.93	0.93
	COV	0.052	0.042	0.159	0.113	0.149
All	Mean	0.89	0.80	0.84	0.89	0.94
	COV	0.060	0.061	0.153	0.120	0.118

The assessment of the final approach proposed for the prediction of the resistance of stainless steel RHS and SHS subjected to combined loading is presented in Figure 6.12. The improvement introduced by a more accurate interaction expression in the prediction of the ultimate resistance of stocky cross-sections is remarkable and it is demonstrated that the proposed approach provides good estimation of the ultimate capacity of cross-sections subjected to combined loading for the full slenderness range.

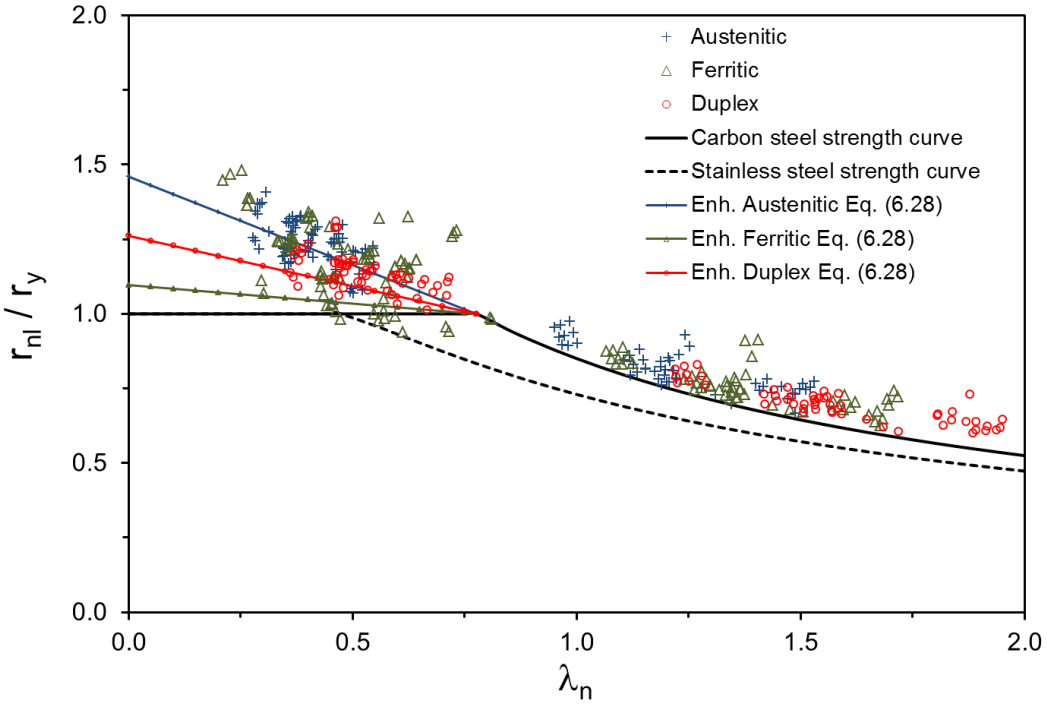

Fig. 6.12. Assessment of the proposed DSM approach for stainless steel cross-sections under uniaxial combined loading.

6.5.4 Reliability analysis

The reliability of the proposed full slenderness range DSM approach is assessed through the corresponding statistical analyses for stainless steel cross-sections subjected to different loading conditions. The procedure provided in section F of the North American Specification AISI-S100-12 (2012) has been followed and the statistical parameters corresponding to the material and geometrical variations of the different stainless steel grades analysed have been extracted from Afshan et al. (2015). The considered material overstrength ratios are 1.3 for austenitic stainless steel, 1.2 for ferritics and 1.1 for duplex and lean duplex grades, with COVs equal to 0.060, 0.045 and 0.030 respectively. The COV of the geometric properties was taken as 0.050. Australian and American codes prescribe resistance factors ϕ equal to 0.9 for tubular cross-sections in compression and bending and the target reliability index is β=2.5. In the calculation of the reliability indexes the load data and factors from the Commentary of AS/NZS4600 (2005) have been considered and a dead-to-live load ratio of 1/5 has been assumed.

Table 6.18 reports the calculated reliability indexes for the full slenderness range DSM approach for austenitic, ferritic and duplex stainless steel RHS and SHS. Considering the resistance factors ϕ prescribed in AS/NZS 4673 (2001) and SEI/ASCE 8-02 (2002) equal to 0.9, results in Table 6.18 demonstrate that the proposed approach can be safely applied to all the studied stainless steel grades and loading conditions since calculated indexes are higher than the target reliability index β=2.5.

Table 6.18. Reliability calibration of the proposed full slenderness range DSM approach.

Grade	Calculated reliability indexes β		
	Compression	Bending	Combined loading
Austenitic	3.43	3.38	3.46
Ferritic	3.09	3.17	3.19
Duplex	2.75	2.99	2.96

6.6 Summary of proposals and concluding remarks

The cross-section behaviour of stainless steel RHS and SHS subjected to different loading conditions has been investigated in this chapter. The strength of experimental and numerical stub columns and beams described in previous chapters allowed the assessment of several design expressions codified in different standards (e.g. EN1993-1-4 (2006), SEI/ASCE 8-02 (2002) and AS/NZS4673 (2001)) and alternative design approaches.

Experimental and FE results demonstrated that while the classification limits codified in EN1993-1-4 (2006) for internal elements are safe, the revised limits proposed by Gardner and Theofanous (2008) provide more accurate Class 3 and Class 2 predictions.

The cross-section capacities of stainless steel RHS and SHS subjected to compression, bending and combined loading conditions have been compared with the predicted capacities

using the codified design provisions in EN1993-1-4 (2006), SEI/ASCE 2-08 (2002) and AS/NZS4673 (2001). Results demonstrated that the codified methods generally provide overconservative results for stocky cross-sections since strain hardening effects are not considered, while the estimation of local buckling in slender cross-sections is more accurate.

The Continuous Strength Method (CSM) is a deformation based design approach that includes strain hardening effects when the compression and bending capacity of stocky cross-sections is estimated, providing considerably better results than the codified design expressions, since no discrete classification is considered and strain hardening effects are included. The CSM approach proposed by Liew and Gardner (2015) was found to provide accurate resistance predictions of stocky cross-sections subjected to combined compression and uniaxial bending loading. However, a simplified CSM method was proposed, together with Zhao et al. (2015a, 2015b, 2015c), where the interaction expressions codified in EN1993-1-1 (2005) are considered with the CSM compression and bending resistances. This method provides accurate strength predictions of stocky cross-sections under combined loading keeping calculations relatively simple and its reliability has been statistically demonstrated.

The Direct Strength Method (DSM) is a design approach that allows the consideration of local and distortional buckling effects in an easy manner through the use of strength curves and can also account for strain hardening effects with the enhanced material property approach proposed by Rossi and Rasmussen (2013). A full slenderness range DSM approach given in Eq. (6.28) which considers the effect of strain hardening and local buckling interaction has been proposed based on the strength curve given for carbon steel structures in AISI-S100-12 (2012). The expression is based on the local cross-section slenderness λ_l defined in Eq. (6.25) and can be used in the design of stainless steel hollow cross-sections subjected to different loading conditions. The accuracy and applicability of the proposed approach has been demonstrated from an exhaustive reliability analysis.

$$\frac{R_{enh\_nl}}{R_y} = \begin{cases} 1+\left(1-1.29\lambda_l\right)\left(\dfrac{\sigma_u}{\sigma_{0.2}}-1\right) & \text{for } \lambda_l \le 0.776 \\ \dfrac{1}{\lambda_l^{0.8}}-\dfrac{0.15}{\lambda_l^{0.8}} & \text{for } \lambda_l > 0.776 \end{cases} \tag{6.28}$$

$$\lambda_l = \sqrt{\frac{R_y}{R_{crl}}} \tag{6.25}$$

For stocky stainless steel RHS and SHS beams the inelastic reserve strength is also contemplated adopting the compression strain factor C_y provided in AS/NZS4673 (2001) and SEI/ASCE 8-02 (2002) through Eqs. (6.29) and (6.31).

$$M_{nl} = M_y + \left(M_{pl} - M_y\right)\left(1-\frac{1}{C_y^2}\right) \tag{6.29}$$

$$C_y = \begin{cases} 3 & \lambda_l \le 0.58 \\ 3 - 2\left(\dfrac{\lambda_l - 0.58}{0.196}\right) & 0.58 \le \lambda_l \le 0.776 \\ 1 & \lambda_l \ge 0.776 \end{cases} \tag{6.31}$$

Finally, a new DSM approach that accurately predicts the ultimate capacity of stainless steel RHS and SHS subjected to combined loading has been proposed based on the design method proposed by Rasmussen (2006) for beam-columns. This approach directly tackles the combined loading behaviour considering a generalized local slenderness calculated from Eq. (6.35) based on the actual stress distribution and provides more accurate results than the methods considering the uncoupled combined loading problem. r_{crl} is the parameter that accounts for the local buckling behaviour of the cross-section, defined in Eq. (6.34), while r_y is the yielding parameter, calculated from in Eq. (6.32) adopting a linear interaction equation for slender cross-sections (Eq. (6.33)) and considering the interaction expression provided in EN1993-1-1 (2005) for Class 1 and 2 cross-sections when stocky cross-sections are analysed (Eq. (6.37)). Finally, the resistance of the cross-section r_{enh_nl} is determined from the strength curves given in Eqs. (6.28) and (6.27) for carbon steel and stainless steel sections respectively and the predicted compression and flexural strengths of the cross-section N_{nl} and M_{nl} can be finally determined from Eq. (6.36).

$$\lambda_n = \sqrt{\frac{r_y}{r_{crl}}} \tag{6.35}$$

$$r_{crl} = \sqrt{\left(\frac{N_{ocr}}{N_y}\right)^2 + \left(\frac{M_{ocr}}{M_y}\right)^2} \tag{6.34}$$

$$r_y = \sqrt{\left(\frac{N_{oy}}{N_y}\right)^2 + \left(\frac{M_{oy}}{M_y}\right)^2} \tag{6.32}$$

$$\frac{N_{oy}}{N_y} + \frac{M_{oy}}{M_y} = 1 \tag{6.33}$$

$$M_{n,red} = M_n \frac{1 - N_{oy}/N_y}{1 - 0.5a} \tag{6.37}$$

$$r_{enh\_nl} = \sqrt{\left(\frac{N_{nl}}{N_y}\right)^2 + \left(\frac{M_{nl}}{M_y}\right)^2} \tag{6.36}$$

CHAPTER 7

Member behaviour of stainless steel RHS and SHS columns and beam-columns

7.1 Introduction

The behaviour of stainless steel Rectangular and Square Hollow Section (RHS and SHS) members subjected to compression and combined loading is investigated in this chapter. Experimental results presented in chapter 4 have been considered, together with additional test data collected from the literature and the strengths obtained from the FE parametric studies. Although the analysis is primarily focused on ferritic stainless steel, considerable data on austenitic and duplex members have also been studied.

First the flexural buckling behaviour of stainless steel columns is studied, where after a brief assessment of the existing design approaches a full slenderness range Direct Strength Method (DSM) approach is proposed. This approach is based on the existing buckling curves and provides accurate resistance predictions for slender and stocky cross-sections since local buckling and strain hardening effects are considered and its reliability has been statistically assessed.

Following the column analysis, the beam-column behaviour of stainless steel members subjected to uniform and non-uniform bending moment distributions is analysed. The assessments of the codified provisions based on the Effective Width Method and alternative design approaches are first presented, and a full slenderness range DSM approach for beam-columns is then proposed. In this approach the beam-column behaviour is directly tackled with a unique strength curve, considering the member and section slendernesses based on the

elastic instabilities of the section subjected to the actual stress distribution, and both strain hardening and local buckling effects are accounted for. The assessment of the proposed DSM approach is then presented; demonstrating that beam-column capacity predictions obtained for the DSM approach improve the results corresponding to traditional methods for stocky and slender cross-sections for different bending distributions. Finally, the proposal is statistically validated for all stainless steel grades.

7.2. Flexural buckling behaviour of stainless steel columns

This section presents the different methodologies that consider the interaction between overall and local buckling effects in stainless steel RHS and SHS members subjected to compression, where the approaches codified in standards and the alternative expressions available in the literature have been considered. Results corresponding to the different methods (the Effective Width Method and the Direct Strength Method) are compared in order to identify the most appropriate and accurate design approach for stainless steel tubular columns.

7.2.1 Flexural buckling curves and design approaches for stainless steel columns

In the different structural stainless steel design standards the strength of stainless steel columns is usually determined by reducing the cross-section capacity due to local buckling and then the effect of flexural buckling is considered based on a certain buckling curve. The codified approaches account for the effect of local buckling through the Effective Width Method (EWM) described in chapter 6 (section 6.2) with the corresponding reduction factors ρ, and then evaluate the overall buckling strength of the member. According to European and Australian standards, EN1993-1-4 (2006) and AS/NZS4673 (2001), the flexural buckling resistance of stainless columns is calculated from Eq. (7.1), where χ is the reduction factor due to flexural buckling defined in Eq. (7.2). A_{eff} is the effective are of the cross-section if required, $\sigma_{0.2}$ corresponds to the 0.2% proof stress conventionally considered as the yield stress and γ_{M1} is the partial safety factor for instability. The member slenderness λ_c can be calculated from $\lambda_c = \sqrt{N_y / N_{cre}}$ where N_{cre} is the minimum of the critical elastic column load for flexural, torsional or flexural-torsional buckling and $N_y=A_{eff}\cdot\sigma_{0.2}$ is the cross-section squash load corresponding to the effective area. AS/NZS4673 (2001) considers a nonlinear expression for the imperfection parameter providing six buckling curves for different stainless steel grades as given in Eq. (7.3) while EN1993-1-4 (2006) establishes that the buckling curve *c* should be considered for hollow sections, considering β=1, λ_0=0 and λ_1=0.4 in Eq. (7.3) for all stainless steel grades. The comparison of these buckling curves is presented in Figure 7.1.

$$N_{b,Rd} = \frac{\chi A_{eff} \sigma_{0.2}}{\gamma_{M1}} \tag{7.1}$$

$$\chi = \frac{1}{\phi + \sqrt{\phi^2 - \lambda_c^2}} \leq 1.0 \tag{7.2}$$

$$\phi = 0.5\left[1+\alpha\left(\left(\lambda_c-\lambda_1\right)^{\beta}-\lambda_0\right)+\lambda_c^2\right] \tag{7.3}$$

Recent research on the flexural buckling response of stainless steel hollow sections conducted by Afshan et al. (2016) proposed some small modifications of the buckling curve provided in EN1993-1-4 (2006) since the partial safety factor γ_{M1}=1.1 was found to be unsafe for the codified curve. The buckling curve *c* was maintained with an imperfection factor α=0.49 but the limiting slenderness λ_0 was decreased. However, since the Afshan et al. (2016) publication was still in the review process when this research work was conducted and the only available information for the new buckling curves was the short summary given in Zhao et al. (2016b), it was decided not to include the approach in this assessment.

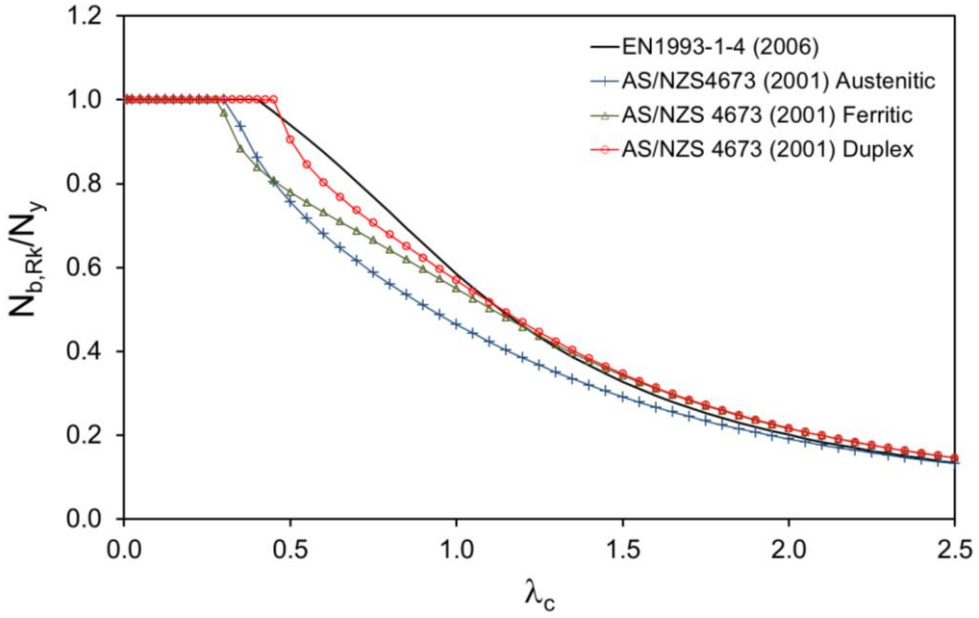

Fig. 7.1. Comparison of buckling curves codified in AS/NZS4673 (2001) and EN1993-1-4 (2006).

Alternatively, SEI/ASCE 8-02 (2002) considers the nonlinear stress-strain response of the material by allowing a gradual yielding through the use of the tangent modulus corresponding to the buckling stress in flexural buckling resistance calculations. The definition of the tangent modulus is based on the Ramberg-Osgood (1942) material model, also provided in different standards and depends on different material parameters.

The assessment of the codified buckling curves is reported in Figures 7.2 and 7.3 for EN1993-1-4 (2006) and AS/NZS4673 (2001) respectively, by presenting the normalized column strengths $N_u/A_{eff}\cdot\sigma_{0.2}$ against the corresponding member slenderness λ_c, where the reduction factors ρ provided in each standard have been adopted in the calculation of the effective areas A_{eff}. Results correspond to austenitic, ferritic and duplex stainless steel RHS and SHS columns obtained from experimental and FE studies. As it can be appreciated in these Figures, the scatter of the results decreases with increasing slendernesses as members behave as elastic columns for both approaches. In the low slenderness range, where no flexural buckling reduction is considered, the overconservatism and scatter of the data is due to strain hardening

effects, being austenitic columns those showing highest $N_u/A_{eff}\cdot\sigma_{0.2}$ ratios. For intermediate slendernesses, few results that lay below the buckling curves can be appreciated, which is more evident for the buckling curve codified in EN1993-1-4 (2006) than for those given in AS/NZS4673 (2001). A more in detail assessment of these approaches and the comparison with alternative design methods is presented in the following section.

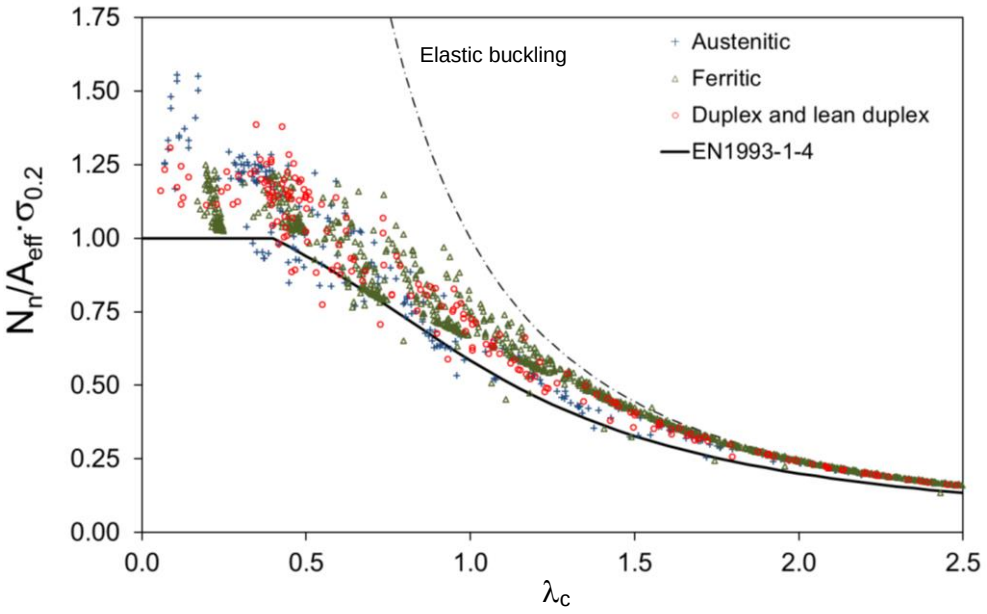

Fig. 7.2. Assessment of the EN1993-1-4 (2006) buckling curve for stainless steel RHS and SHS members in compression.

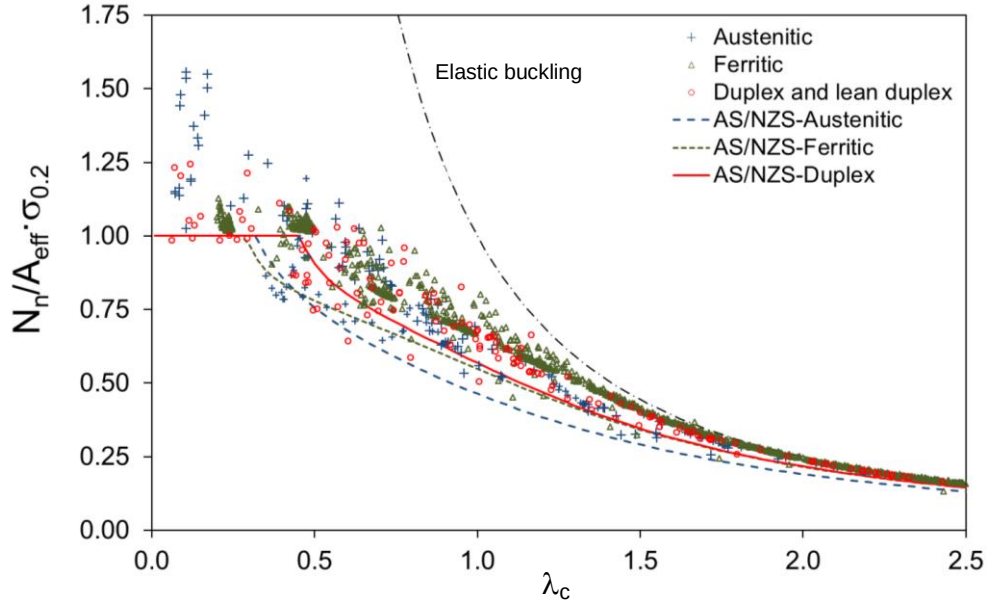

Fig. 7.3. Assessment of the AS/NZS4673 (2001) buckling curves for stainless steel RHS and SHS members in compression.

Alternatively, the Direct Strength Method (DSM) is a design method developed by Schafer and Pekoz (1998) that allows the consideration of local and distortional buckling effects in an easy

manner through the use of software to determine elastic buckling modes in conjunction with strength curves instead of considering the effective width calculations. Regarding column behaviour, the DSM approach first considers the overall buckling of the member with a fully effective cross-section and then introduces the resistance reduction due to local buckling. The North American AISI-S100-12 Specification (2012) for cold-formed carbon steel structures includes a DSM-based approach that determines the capacity of carbon steel members following a different procedure from the buckling curves provided in the EWM approach. Then, the effect of local buckling is considered by reducing the member resistance through a strength curve depending on the local slenderness, which measures the susceptibility of the cross-section to local buckling through the corresponding critical elastic local buckling capacity.

Summarizing, the strength of stainless steel columns is usually determined from a certain buckling curve that provides the strength reduction due to flexural buckling, while the interaction with local buckling effects is differently determined depending on the considered method. Codified standards initially consider the effect of local buckling through the Effective Width Method and then evaluate the overall buckling strength, while the DSM approach reduces the member capacity of a fully effective cross-section due to local buckling. Therefore, the accuracy of both EWM and DSM methodologies are highly dependent on the accuracy of the considered buckling curves.

7.2.2 DSM approach for stainless steel columns

The flexural buckling behaviour of stainless steel SHS and RHS columns is investigated in this section and design recommendations based on the Direct Strength Method are provided for members with stocky and slender cross-sections. A full slenderness approach is thus provided for stainless steel members in compression as suggested for cross-sections in section 6.5 and results are compared to those obtained from the traditional Effective Width Method. The study is based on the strength results from the experimental programme on ferritic stainless steel columns presented in chapter 4, as well as on the experimental results collected from the literature on stainless steel RHS and SHS columns, reported in Table 2.4, and the conducted FE parametric studies described in chapter 5. The analysis considers the different buckling curves codified in AS/NZS4673 (2001) and EN1993-1-4 (2006) in the evaluation of the full slenderness DSM approach.

The local buckling interaction is considered through the same strength curve for both cross-section and members, and the nominal column capacity N_{nl} can be determined from Eq. (7.4) for carbon steel specimens. The cross-section slenderness is calculated from Eq. (7.5), where the flexural buckling resistance of the fully effective cross-section $N_{b,ne}$ is considered instead of the squash load N_y considered for cross-sections. N_{crl} represents the critical elastic local buckling load.

$$\frac{N_{nl}}{N_{b,ne}} = \begin{cases} 1 & \lambda_l \leq 0.776 \\ \dfrac{1}{\lambda_l^{0.8}} - \dfrac{0.15}{\lambda_l^{0.8}} & \lambda_l > 0.776 \end{cases} \quad (7.4)$$

$$\lambda_l = \sqrt{\frac{N_{b,ne}}{N_{crl}}} \tag{7.5}$$

Becque et al. (2008) investigated the local buckling behaviour of stainless steel structures through an experimental programme on lipped channel sections, I-sections and RHS columns. Although no differences were appreciated among the different stainless steel grades, lipped channel and I-section results highlighted the necessity of an alternative strength curve for stainless steels. This curve is presented in Eq. (7.6) and it is slightly lower than that given for carbon steel sections, with a lower limiting slenderness. However, the study also demonstrated that the former strength curve given in Eq. (7.4) for carbon steel cross-sections was still valid for stainless steel SHS and RHS.

$$\frac{N_{nl}}{N_{b,ne}} = \begin{cases} 1 & \lambda_l \leq 0.474 \\ \dfrac{0.95}{\lambda_l^{0.8}} - \dfrac{0.22}{\lambda_l^{1.6}} & \lambda_l > 0.474 \end{cases} \tag{7.6}$$

The study on the local and overall buckling interaction conducted by Becque et al. (2008) was based on the flexural buckling curves codified in AS/NZS4673 (2001) for stainless steel columns. Since the obtained results were accurate, no alternative design approach was proposed for the determination of the member strength as it is provided in the AISI-S100-12 (2012) specification for carbon steel members designed according to the DSM.

Recent research works by Rossi and Rasmussen (2013) on stainless steel cross-sections and members subjected to compression lead into a full slenderness DSM approach, as previously described in chapter 6. This approach was also based on the buckling curves provided in AS/NZS4673 (2001) and accounted for strain hardening effects by proposing a modified expression for the flexural buckling resistance $N_{b,ne}$, presented in Eq. (7.7), where λ_{lim} is the limiting slenderness at which χ becomes equal to unity. The interaction of local and member buckling is accounted for adopting the Becque et al. (2008) approach given in Eq. (7.6).

$$\frac{N_{b,ne}}{N_y} = \begin{cases} 1 + \left(1 - \dfrac{\lambda_c}{\lambda_{lim}}\right)\left(\dfrac{\sigma_u}{\sigma_{0.2}} - 1\right) & \lambda_c \leq \lambda_{lim} \\ \dfrac{1}{\phi + \sqrt{\phi^2 - \lambda_c^2}} & \lambda_c > \lambda_{lim} \end{cases} \tag{7.7}$$

Figures 7.4 to 7.6 present the assessment of the DSM approach for RHS and SHS members in compression for different stainless steel grades by depicting the $N_u/N_{b,ne}$ ratios against the corresponding local slenderness λ_l. For each stainless steel grade results corresponding to the bucking curves provided in AS/NZS4673 (2001) (empty markers) and EN1993-1-4 (2006) (solid markers) have been considered. Member strengths have been normalized by the flexural buckling resistances of the gross-sections $N_{b,ne}$ calculated considering the relevant buckling

curve. Slendernesses have been calculated from Eq. (7.5) and the critical elastic local buckling loads N_{crl} were obtained from CUFSM (Schafer and Ádány, 2006). The DSM strength curve that accounts for local buckling in stainless steel specimens proposed by Becque et al. (2008) and the curve codified in the AISI-S100-12 (2012) specification for carbon steel members are also depicted.

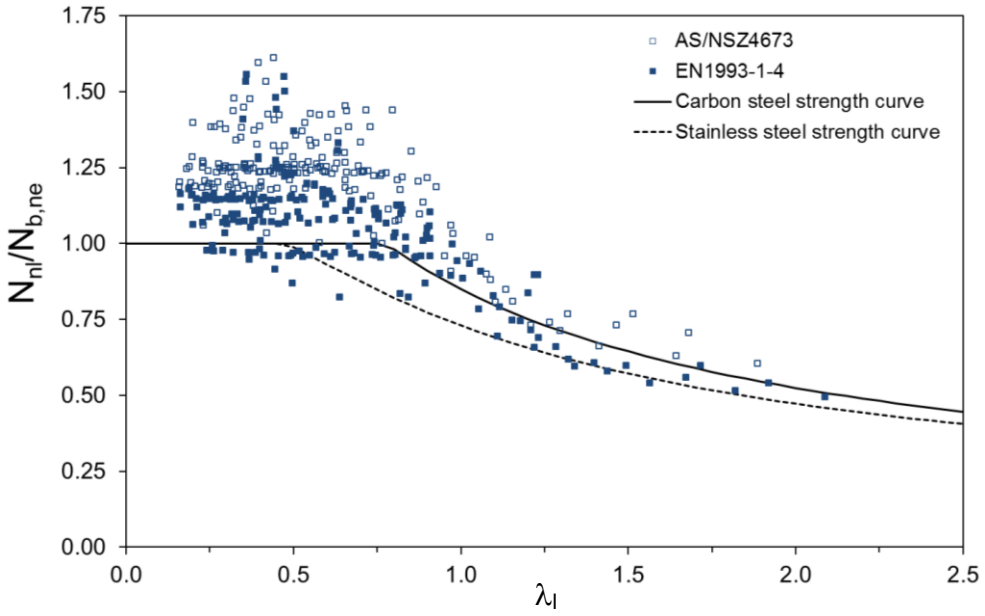

Fig. 7.4. Assessment of the DSM approach for austenitic stainless steel RHS and SHS members in compression for different buckling curves.

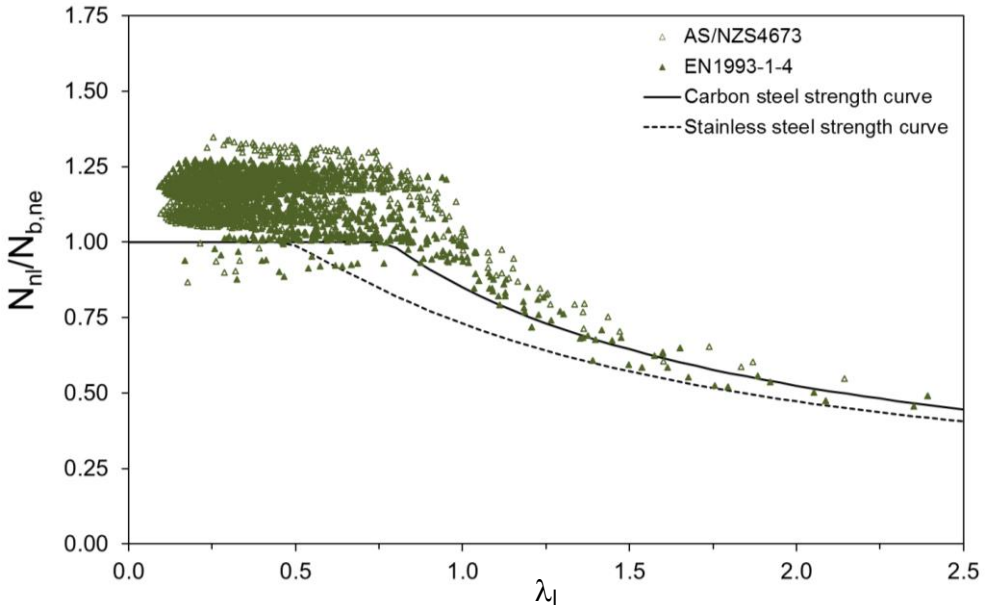

Fig. 7.5. Assessment of the DSM approach for ferritic stainless steel RHS and SHS members in compression for different buckling curves.

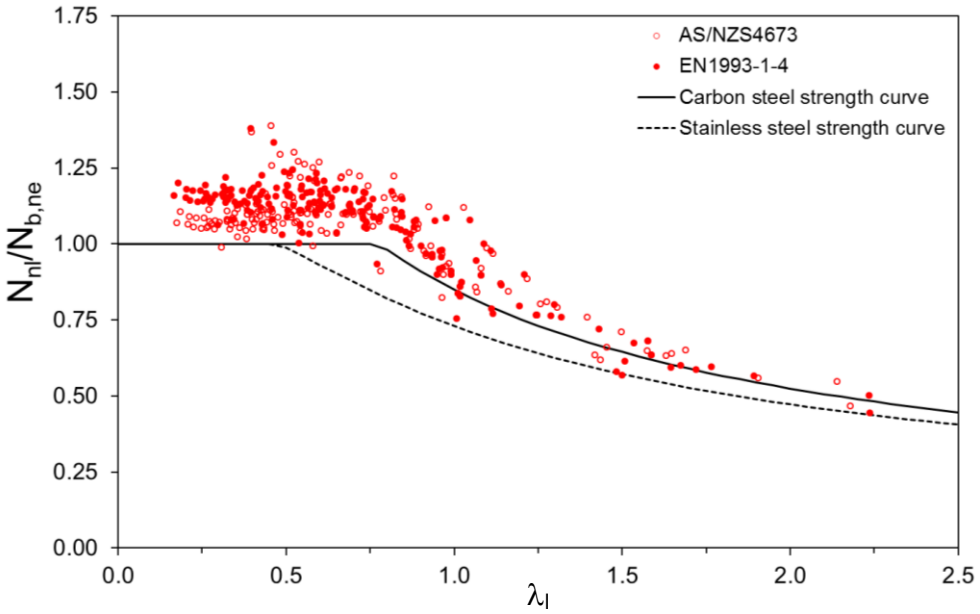

Fig. 7.6. Assessment of the DSM approach for duplex and lean duplex stainless steel RHS and SHS members in compression for different buckling curves.

Figures 7.4, 7.5 and 7.6 demonstrate that results corresponding to the bucking curves in AS/NZS4673 (2001) and EN1993-1-4 (2006) are similar although $N_u/N_{b,ne}$ ratios are slightly lower for EN1993-1-4 (2006), particularly for austenitic and ferritic stainless steel grades, since the buckling curves in AS/NZS4673 (2001) are considerably lower than curve *c* for these materials, as shown in Figure 7.1. For duplex and lean duplex both standards provide similar buckling curves and the differences are notably smaller. However, it is evident from Figures 7.4, 7.5 and 7.6 that no differences are appreciated among the different stainless steel grades for the overall-local buckling interaction and that the DSM approach provides good prediction of the ultimate capacity of stainless steel RHS and SHS columns with slender cross-sections. It can also be appreciated that the most accurate results are obtained for the strength curve provided for carbon steel cross-sections Eq. (7.4), as reported by Becque and Rasmussen (2008), where a better agreement of the carbon steel DSM strength curve was observed for stainless steel RHS and SHS columns. Similar results were also highlighted in chapter 6 regarding cross-sectional behaviour. These Figures also highlight the existence of a considerable strength reserve for some of the specimens showing low cross-section slenderness. This reserve can be partly attributed to the effect of strain hardening and as it can be noticed, highest $N_u/N_{b,ne}$ ratios are observed for austenitic stainless steel columns, followed by duplex and ferritics, as expected from the typical stress-strain behaviour of these grades.

Few results with $N_u/N_{b,ne}$ ratios lower than the unity with low local slenderness λ_l can be appreciated in Figures 7.4 and 7.5 for austenitic members and the buckling curve codified in for EN1993-1-4 (2006), and particularly for ferritic stainless steel columns. These results do not correspond to an unsafe resistance prediction of the DSM approach, but to an overestimated flexural buckling capacity for the considered buckling curves. This is evident from Figures 7.2

and 7.3, where several results that lay below the buckling curves are appreciated. For ferritic stainless steel columns, most of the results found to be unsafe correspond to the experimental data from Afshan and Gardner (2013a), which were attributed to an inaccurate buckling curve.

The assessment of the DSM approach for considering the effect of local buckling in stainless steel RHS and SHS columns is presented in Table 7.1 for the buckling curves provided in AS/NZS4673 (2001) and EN1993-1-4 (2006). The mean values and coefficients of variation (COV) of the predicted-to-experimental (or FE) strengths obtained for the DSM are compared to those obtained through the codified Effective Width Methods for the same buckling curves in order to evaluate the accuracy of each method. N_{EN} represents the predicted column resistance using the EN1993-1-4 (2006) buckling curve, while N_{AS} corresponds to capacity predictions for the AS/NZS4673 (2001) buckling curves. For the DSM approach, strength curves corresponding to carbon steel and stainless steel cross-sections, given in Eqs. (7.4) and (7.6) respectively, have been assessed. Since the interaction between local and overall buckling is investigated, only results corresponding to slender cross-sections have been contemplated. Cross-sections with a cross-sectional slenderness λ_l higher than 0.776 have been considered in the DSM approach for the CS-curve in Table 7.1, while those with a cross-sectional slenderness higher than 0.474 have been included in the results for SS-curve. For the EWM approaches, those cross-sections in which the reduced cross-sectional area needs to be considered have been included in the analysis.

Table 7.1. Assessment of design approaches for members in compression with slender cross-sections.

Grade		DSM CS-curve Eq. (7.4)		DSM SS-curve Eq. (7.6)		EWM approaches	
		N_{EN}/N_u	N_{AS}/N_u	N_{EN}/N_u	N_{AS}/N_u	N_{EN}/N_u	N_{AS}/N_u
Austenitic	Mean	0.98	0.87	0.85	0.74	0.91	0.82
	COV	0.101	0.089	0.110	0.089	0.119	0.132
Ferritic	Mean	0.93	0.88	0.83	0.79	0.85	0.81
	COV	0.080	0.088	0.092	0.095	0.093	0.179
Duplex	Mean	0.93	0.83	0.81	0.81	0.87	0.86
	COV	0.082	0.076	0.081	0.079	0.109	0.134
All	Mean	0.94	0.89	0.83	0.78	0.87	0.83
	COV	0.090	0.087	0.095	0.095	0.107	0.159

According to results presented in Table 7.1 and Figures 7.4 to 7.6, considerably different results are obtained for the carbon steel and stainless steel strength curves for the DSM approach, regardless the adopted buckling curve. Although the stainless steel strength curve can be conservatively applied to the analysed RHS and SHS columns with slender cross-sections, more accurate results are obtained for the carbon steel strength curve given in Eq. (7.4). Comparing these results with the predicted capacities according to the codified EWM approaches, it is evident from Table 7.1 that the adoption of the DSM-based approach with the carbon steel strength curve improves the flexural buckling resistance predictions for all the considered buckling curves and stainless steel grades in addition to avoid effective width

calculations. Therefore, the DSM is highlighted as a simpler and more accurate method for the prediction of the flexural buckling resistance of stainless steel RHS and SHS columns with slender cross-sections. Regarding the most appropriate flexural buckling curves, Table 7.1 demonstrates that the highest predicted-to-experimental (or FE) ratios are obtained for the buckling curve codified in EN1993-1-4 (2006) for both EWM and DSM approaches, although the flexural buckling capacity of some specimens is overpredicted. Accurate results are also obtained for the buckling curves codified in AS/NZS4673 (2001).

However, it is evident from the data with high $N_u/N_{b,ne}$ ratios in Figures 7.4 to 7.6 that some of the members with low cross-section slenderness show an important strength reserve mainly due to strain hardening effects. This fact is, as mentioned previously, more evident for austenitic stainless steels. Therefore, a similar procedure to that presented in chapter 6 to account for strain hardening effects in the resistance of stainless steel RHS and SHS is proposed in this section. Rossi and Rasmussen (2013) suggested an approach that considers the enhanced material properties in stainless steel columns, which has already been introduced. This approach provides an enhanced column capacity calculated from Eq. (7.7), where the adopted level of strain hardening only depends on the member slenderness of the column, without considering the behaviour of the cross-section. For a short column with a slender cross-section the method would therefore provide an enhanced column capacity that would be then reduced according to the corresponding strength curve due to local buckling effects. The approach presented in this section is slightly different and considers both member and cross-section slenderness when determining the level of strain hardening to be assigned to each specimen.

The method is based on the approach presented in chapter 6 for cross-sections, which was also suggested by Rossi and Rasmussen (2013) for cross-sections, and is presented in Eq. (7.8). This expression corresponds to the enhanced material property approach based on the carbon steel strength curve and considering the conclusions extracted in chapter 6 for cross-section behaviour and from Figures 7.4 to 7.6, only results corresponding to this strength curve will be considered. However, this expression only considers the cross-section slenderness and, if no additional restrictions are defined, unsafe predictions of the ultimate capacities would be obtained for slender members.

$$\frac{N_{enh\_nl}}{N_{b,ne}} = 1 + \left(1 - 1.29\lambda_l\right)\left(\frac{\sigma_u}{\sigma_{0.2}} - 1\right) \quad \text{for} \quad \lambda_l \leq 0.776 \tag{7.8}$$

Low cross-section slenderness λ_l values calculated from Eq. (7.5) can correspond to stocky cross-sections with a high local buckling critical load N_{crl}, susceptible of reaching stresses higher than the 0.2 proof stress or yield strength. Hence, the adoption of design approaches that consider strain hardening effects would introduce considerable improvements to the prediction of the capacity of these members. However, when low λ_l values are caused by low flexural buckling resistances $N_{b,ne}$, the member will fail due to overall buckling and the cross-section will only attain low stress levels. For these specimens strain hardening effects should

not be considered, and the adoption of enhanced strengths would result in an overestimation of the actual capacity of the columns. Therefore, the effect of the overall buckling behaviour of the studied member needs to be considered by introducing an additional limitation by imposing that $\chi \cdot \sigma_{DSM} \geq \sigma_{0.2}$, as given in Eq. (7.9), which can also be presented as Eq. (7.10).

$$\frac{N_{enh\_nl}}{A} = \chi\sigma_{0.2}\left[1+\left(1-1.29\lambda_l\right)\left(\frac{\sigma_u}{\sigma_{0.2}}-1\right)\right] \geq \sigma_{0.2} \tag{7.9}$$

$$\chi\left[1+\left(1-1.29\lambda_l\right)\left(\frac{\sigma_u}{\sigma_{0.2}}-1\right)\right] \geq 1 \tag{7.10}$$

The assessment of the proposed modification to the DSM approach based on the carbon steel strength curve that considers the enhanced material properties is presented in Table 7.2. The mean values and COVs of the predicted-to-experimental (or FE) flexural buckling resistances of stainless steel columns with stocky cross-section are reported for the same buckling curves considered for slender cross-sections. Specimens showing a cross-section slenderness λ_l lower than 0.776 have been considered in the evaluation of the DSM approach, and results are compared to those obtained for AS/NZS4673 (2001) and EN1993-1-4 (2006) provisions, denoted as EWM-based although the cross-sections considered now are fully effective. The predicted capacities of EWM-based approaches are limited to the yield stress, while DSM-based methods incorporate strain-hardening effects in those specimens satisfying Eq. (7.10).

Table 7.2. Assessment of design approaches for members in compression with stocky cross-sections.

Grade		DSM CS-curve Eqs. (7.4) and (7.8)		EWM approaches	
		N_{EN}/N_u	N_{AS}/N_u	N_{EN}/N_u	N_{AS}/N_u
Austenitic	Mean	0.96	0.82	0.88	0.77
	COV	0.111	0.100	0.104	0.100
Ferritic	Mean	0.87	0.88	0.85	0.84
	COV	0.076	0.068	0.073	0.095
Duplex	Mean	0.88	0.91	0.85	0.84
	COV	0.050	0.057	0.052	0.102
All	Mean	0.88	0.87	0.85	0.83
	COV	0.085	0.074	0.077	0.100

Table 7.2 demonstrates that the DSM approach for columns with stocky cross-sections based on the carbon steel strength curve provides improved results for all stainless steel grades and considered buckling curves, since higher N_{pred}/N_u ratios, with similar scatter, are obtained. However, as mentioned before, strain hardening effects cannot be included for all specimens with low cross-section slenderness. In order to evaluate the improvement introduced by the new proposal, only specimens with $\lambda_l \leq 0.776$ that also fulfil the limitation given in Eq. (7.10) have been considered in the assessment presented in Table 7.3. Nevertheless, it must be noted that these specimens do not represent a big portion of the analysed experimental and FE data,

since both low member and cross-sectional slenderness are required to consider enhanced material properties.

Table 7.3. Assessment of design approaches for stocky members in compression with stocky cross-sections.

Grade		DSM CS-curve Eq. (7.8)		EWM-based approaches	
		N_{EN}/N_u	N_{AS}/N_u	N_{EN}/N_u	N_{AS}/N_u
Austenitic	Mean	0.97	0.89	0.83	0.77
	COV	0.115	0.076	0.112	0.094
Ferritic	Mean	0.94	0.94	0.92	0.93
	COV	0.069	0.072	0.060	0.062
Duplex	Mean	0.90	0.91	0.87	0.89
	COV	0.036	0.035	0.041	0.041
All	Mean	0.94	0.93	0.90	0.89
	COV	0.081	0.072	0.080	0.097

According to the results presented in Table 7.3, the consideration of the enhanced material properties in the prediction of the ultimate capacity of stocky stainless steel columns improves the obtained results for all buckling curves, although more relevant improvements are obtained for austenitic stainless steel specimens than for duplex and ferritics. In accordance to Table 7.3, best results are observed for the buckling curve codified in EN1993-1-4 (2006) when enhanced material properties are considered, although for duplex grades marginal differences are appreciable since the buckling curves corresponding to both standards are very similar.

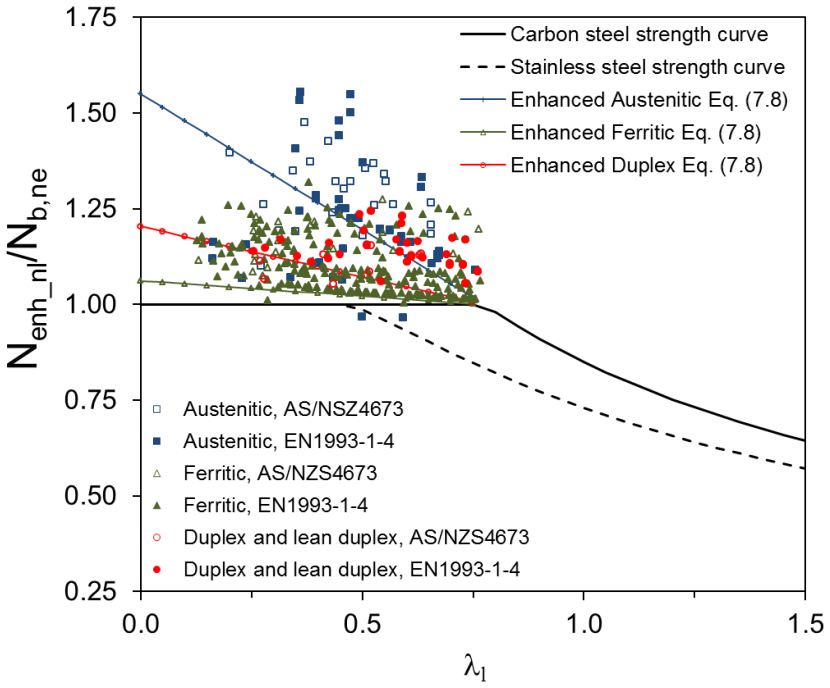

Fig. 7.7. Assessment of the DSM approach for enhanced material properties for stainless RHS and SHS members in compression and different buckling curves.

Similar results are observed in Figure 7.7, where the $N_u/N_{b,ne}$ ratios of the column specimens contemplated in Table 7.3 are presented together with the enhanced material property curves given in Eq. (7.8) for austenitic, ferritic and duplex stainless steel grades. Note that although each data point presents a different $\sigma_u/\sigma_{0.2}$ ratio and needs to be analysed with that particular value, Figure 7.7 only presents the enhanced property curves for the average $\sigma_u/\sigma_{0.2}$ ratios for simplicity.

7.2.3 CSM approach for stainless steel columns

The previous section presents the proposed DSM approach that incorporates enhanced material properties in stainless steel column capacity predictions. The Continuous Strength Method (CSM) is a design method based on the deformation capacity of cross-sections that introduces strain hardening effects, but it is currently limited to cross-sectional resistance predictions. The accuracy of the method has been assessed and demonstrated in chapter 6 for the behaviour of stainless steel cross-sections subjected to compression, bending and combined loading conditions.

The applicability of the CSM to columns with stocky cross-sections to which strain hardening effects are relevant is investigated in this section, based on the research conducted for the DSM approach. The similarities between the DSM approach for stocky cross-sections and the CSM allow a direct extension of the DSM to stainless steel columns, following a similar procedure. Thus, the capacity of stainless steel RHS and SHS columns according to the new CSM approach can be obtained from Eq. (7.11). χ corresponds to the flexural buckling reduction factor for a certain buckling curve, σ_{CSM} is the CSM design stress and A is the gross area of the cross-section. If the definition of σ_{CSM} described in chapter 6 is considered, Eq. (7.11) can be written in terms of the flexural buckling resistance $N_{b,ne}$ without considering strain hardening effects as in Eq. (7.12). The maximum strain that the cross-section can reach ε_{CSM} and the strain hardening modulus E_{sh} can be obtained from the expressions described in chapter 6 for cross-section behaviour, while E and ε_y correspond to the Young's modulus and the yield strain respectively.

$$N_{b,CSM} = \frac{\chi \sigma_{CSM} A}{\gamma_{M1}} \tag{7.11}$$

$$\frac{N_{b,CSM}}{N_{b,ne}} = 1 + \frac{E_{sh}}{E}\left(\frac{\varepsilon_{CSM}}{\varepsilon_y} - 1\right) \tag{7.12}$$

However, the definition of the cross-section slenderness that needs to be considered in the CSM curve should now be calculated from Eq. (7.13), as for the DSM approach, and a similar limitation for slender members needs to be adopted. This limitation is also obtained by imposing that strain hardening effects are only accounted if the stress at which the column fails is higher than the yield stress, $\chi \cdot \sigma_{CSM} \geq \sigma_{0.2}$, which is equivalent to the condition given in Eq. (7.14).

$$\lambda_p = \sqrt{\frac{N_{b,ne}}{N_{crl}}} \tag{7.13}$$

$$\chi\left[1+\frac{E_{sh}}{E}\left(\frac{\varepsilon_{CSM}}{\varepsilon_y}-1\right)\right] \geq 1 \tag{7.14}$$

The accuracy of the proposed CSM approach for stainless steel columns is evaluated in Table 7.4 for the flexural buckling curves provided in AS/NZS4673 (2001) and EN1993-1-4 (2006), where predicted column resistances are compared with experimental and numerical strengths. Specimens showing cross-section slenderness lower that the CSM limit $\lambda_p \leq 0.68$ and fulfilling the condition given in Eq. (7.14) are considered in the assessment and results are compared to resistance predictions obtained from the codified expressions that do not consider strain hardening effects. The dataset considered in Table 7.4 slightly differs from that used in the evaluation of the DSM-based approach in Table 7.3 since the limiting equations are different for both approaches.

Table 7.4. Assessment of design approaches for stocky members in compression with stocky cross-sections.

Grade		CSM approach		EWM-based approaches	
		N_{EN}/N_u	N_{AS}/N_u	N_{EN}/N_u	N_{AS}/N_u
Austenitic	Mean	0.87	0.82	0.82	0.77
	COV	0.117	0.077	0.102	0.094
Ferritic	Mean	0.93	0.94	0.91	0.92
	COV	0.081	0.079	0.067	0.066
Duplex	Mean	0.88	0.85	0.87	0.88
	COV	0.033	0.026	0.040	0.042
All	Mean	0.91	0.90	0.88	0.88
	COV	0.093	0.092	0.087	0.098

The comparison of the mean values and COVs of the predicted-to-experimental (or FE) ratios demonstrates the improvement introduced by the CSM approach in ultimate capacity predictions compared to the results without accounting for strain hardening effects. Similar results are obtained for the AS/NZS4673 (2001) and EN1993-1-4 (2006) buckling curves, appreciating the biggest differences for austenitic columns. As for the DSM approach, results corresponding to the EN1993-1-4 (2006) buckling curve are rather better. Note that the results for EWM in Table 7.4 are marginally different from those reported in Table 7.3 since the data sets of the specimens fulfilling Eqs. (7.10) and (7.14) are slightly different.

7.2.4 Reliability analysis

The reliability of the proposed DSM and CSM approaches is assessed through the corresponding statistical analyses for stainless steel RHS and SHS members subjected to compression. The statistical calibration of the proposed full slenderness range DSM approach has been conducted by following the procedure provided in section F of the North American

Specification AISI-S100-12 (2012), while for the CSM approach the statistical analysis has been derived according to EN1990, Annex D (2005) specifications. Statistical parameters corresponding to the material and geometrical variations of the different stainless steel grades have been extracted from Afshan et al. (2015). The considered material overstrength ratios are 1.3 for austenitic stainless steel, 1.2 for ferritics and 1.1 for duplex and lean duplex grades, with COVs equal to 0.060, 0.045 and 0.030 respectively, and the COV of the geometric properties was taken as 0.050.

Regarding the reliability analysis of the full slenderness range DSM approach, Australian and American codes prescribe a resistance factor ϕ equal to 0.9 for tubular cross-sections in compression and the target reliability index is β=2.5. In the calculation of the different reliability indexes the load data and factors from the Commentary of AS/NZS4600 (2005) have been considered and a dead-to-live load ratio of 1/5 has been assumed. Table 7.5 reports the calculated reliability indexes for the full slenderness range DSM approach for austenitic, ferritic and duplex stainless steel columns considering the buckling curves codified in EN1993-1-4 (2006) and AS/NZS4673 (2001).

Table 7.5. Summary of the reliability analysis results for the full slenderness range DSM for members in compression.

Grade	Calculated reliability indexes β			
	Stocky cross-sections Enhanced mat. properties		Slender cross-sections Local buckling	
	EN1993-1-4	AS/NZS4673	EN1993-1-4	AS/NZS4673
Austenitic	2.98	3.54	3.11	3.64
Ferritic	3.13	3.10	3.16	3.40
Duplex	3.08	3.01	2.79	2.87

Considering the resistance factor ϕ equal to 0.9 prescribed in AS/NZS4673 (2001) and SEI/ASCE 8-02 (2002), results in Table 7.5 demonstrate that the proposed approach can be safely applied to members in compression for all the studied stainless steel grades since the calculated indexes are higher than the target reliability index β=2.5.

The statistical analysis of the CSM approach for stainless steel columns was derived according to EN1990, Annex D (2005) following the steps described in Tankova et al. (2014) and a summary of the most relevant statistical parameter values is presented in Table 7.6 together with the calculated γ_{M1} factors. b is the mean value of the correction factor, V_δ is the coefficient of variation of the error relative to the experimental results and V_r is the combined coefficient of variation. The variability due to FE modelling was also included in the analysis thought the procedure described in Bock et al. (2015c), since some deviation between tests and the modelled reality usually occurs, resulting in V_{FE}=0.019. According to the results gathered in Table 7.6 the proposed CSM approach for stocky members subjected to compression can be safely applied for all stainless steel grades if the partial safety factor γ_{M1} currently codified in

EN1993-1-4 (2006) is considered, which is equal to 1.10, since the calculated γ_{M1} values lay below 1.10.

Table 7.6. Summary of the reliability analysis results for the CSM approach for members in compression.

	Grade	b	V_δ	V_r	γ_{M1}
EN1993-1-4 buckling curve	Austenitic	1.156	0.110	0.137	0.99
	Ferritic	1.021	0.083	0.109	1.09
	Duplex	1.115	0.034	0.070	0.97
AS/NZS4673 buckling curves	Austenitic	1.231	0.078	0.112	0.87
	Ferritic	1.031	0.082	0.108	1.07
	Duplex	1.110	0.036	0.071	0.97

7.3 Beam-column behaviour of stainless steel members

This last section presents the analysis of the beam-column behaviour of RHS and SHS stainless steel members. Test results presented in chapter 4 have been considered, together with the collected experimental data and the FE strengths from the conducted parametric studies. Ferritic, austenitic and duplex stainless steel members subjected to compression and different bending moment distributions have been studied in order to assess the different interaction expressions codified in standards, as well as the alternative approaches available in the literature. In addition, a full slenderness DSM-based approach that includes both enhanced material properties and local buckling effects is proposed for beam-columns, and results are compared to the strength predictions obtained from traditional interaction expressions in standards and the literature.

7.3.1 Design expressions for stainless steel beam-columns

Different approaches can be found in standards and the literature regarding design expressions for the evaluation of stainless steel beam-columns. Nevertheless, beam-column behaviour verifications are usually presented as interaction expressions with the same general expression, given by Eq. (7.15), and a certain interaction factor *k*. The differences among these approaches basically lay on the definition of the interaction factor *k* and the calculation of the basic flexural buckling $N_{b,Rd}$ and bending moment $M_{c,Rd}$ capacities. N_{Ed} and M_{Ed} correspond to the design load and bending moment, respectively, and γ_{M1} is the instability partial safety factor.

$$\frac{N_{Ed}}{N_{b,Rd}} + k\frac{M_{Ed}}{M_{c,Rd}/\gamma_{M1}} \leq 1 \tag{7.15}$$

The interaction expression codified in EN1993-1-4 (2006) is described by Eq. (7.16), where the minimum value of 1.2 is worth mentioning, which usually derives into overconservative capacity predictions since the full bending capacity of the cross-section cannot be reached for low axial compression values. Other standards for stainless steel, such as SEI/ASCE 8-02 (2002) and AS/NZS4673 (2001), consider an interaction factor *k* with an amplification factor that depends

on the critical elastic column load for flexural buckling N_{cre}, given by Eq. (7.17). Alternatively, "Method B" in EN1993-1-1 (2005) for carbon steel provides the interaction factor in Eq. (7.18), which has also been included in the analysis for comparison.

$$k = 1 + 2(\lambda_c - 0.5)\frac{N_{Ed}}{N_{b,Rd}} \quad \text{but} \quad 1.2 \le k \le 1.2 + 2\frac{N_{Ed}}{N_{b,Rd}} \tag{7.16}$$

$$k = \frac{1}{1 - \frac{N_{Ed}}{N_{cre}}} \tag{7.17}$$

$$k = 1 + 0.6\lambda_c \frac{N_{Ed}}{N_{b,Rd}} \le 1 + 0.6\frac{N_{Ed}}{N_{b,Rd}} \tag{7.18}$$

Recent research on experimental and FE stocky stainless steel RHS and SHS beam-columns subjected to different bending moment distributions was carried out by Zhao et al. (2016b). A new expression for the interaction factor *k* which also considers the different behaviour of diverse stainless steel grades was proposed based on the interaction factor suggested by Greiner and Kettler (2008). The proposed interaction factor is given in Eq. (7.19) and the calibrated D_i parameter values for different stainless steel grades can be found in the original publication. This proposal was based on an alternative flexural buckling resistance approach given by Afshan et al. (2016) and the pure bending moment resistance determined according to the Continuous Strength Method (CSM), where the effect of strain hardening is considered. This flexural buckling approach has not been included in the previous stainless steel column investigations since the paper was under the review process when this thesis was written. Since the only available information for the new buckling curves is the short summary given in Zhao et al. (2016b), it was decided not to include the approach in column behaviour but to use the new buckling curves in the assessment of the interaction expression proposed by Zhao et al. (2016b).

$$k = 1 + D_1(\lambda_c - D_2)\frac{N_{Ed}}{N_{b,Rd}} \le 1 + D_1(D_3 - D_2)\frac{N_{Ed}}{N_{b,Rd}} \tag{7.19}$$

As in Zhao et al. (2016b), non-uniform bending moment distributions have also been included in the parametric studies described in chapter 5 in order to assess the different approaches. The effect of the bending moment gradient is usually accounted for by including equivalent moment factors C_m in Eq. (7.15) although EN1993-1-4 (2006) provisions do not account for the effect of the bending moment gradient in the member behaviour and the same interaction expression is provided for uniform and non-uniform bending moment distributions. Two different equivalent moment factors have been assessed, the equivalent uniform moment factor $C_{m,u}$ given in Eq. (7.20) (Austin (1961), Lindner (2003), Greiner and Lindner (2006), Boissonade et al. (2006)) and the sinusoidal reference moment $C_{m,s}$ given in Eq. (7.21) (Boissonade et al. (2002, 2004, 2006)), based on constant and sinusoidal reference moments respectively. The equivalent uniform moment factor $C_{m,u}$ is currently codified in EN1993-1-1 (2005) and it is used in the design of carbon steel beam-columns, as well as in Australian and American specifications

(i.e. AS/NZS 4600 (2005), AISI-S100-12 (2012), AS/NZS4673 (2001) and SEI/ASCE 8-02 (2002)) for carbon steel and stainless steel beam-columns. $\psi=M_1/M_2$ is the ratio of the smaller to the larger moment at the ends, negative when the member is bent in reverse curvature and positive when it is bent in single curvature according to EN1993-1-1 (2005), although AS/NZS4673 (2001) and SEI/ASCE 8-02 (2002) use an opposite sign convention.

$$C_{m,u} = 0.6 + 0.4\psi \geq 0.4 \tag{7.20}$$

$$C_{m,s} = 0.79 + 0.21\psi + 0.36(\psi - 0.33)\frac{N_{Ed}}{N_{cre}} \tag{7.21}$$

7.3.2 Strength of stainless steel beam-columns

Experimental and numerical beam-column data are depicted in Figures 7.8 to 7.10, where the normalized compression loads $N_u/N_{b,Rk}$ are plotted against the normalized moments $M_u/M_{c,Rk}$ for austenitic, ferritic and duplex stainless steel members subjected to combined loading. Results corresponding to the flexural buckling and bending resistances according to EN1993-1-4 (2006) are only presented for simplicity, and the interaction expressions corresponding to member slenderness equal to the minimum, average and maximum slenderness (i.e. λ_c=0.5, λ_c=1.25 and λ_c=2) are also depicted. The image on the left hand side of each Figure shows the results without considering the equivalent moment factors, while Figures on the right have been multiplied by the equivalent uniform moment factor $C_{m,u}$ given by Eq. (7.20), showing $C_m \cdot M_u/M_{c,Rk}$–$N_u/N_{b,Rk}$ results. Although a more in detail study is presented in the following pages, these figures suggest that the equivalent uniform moment factor is a good estimator of the beneficial effect introduced by the bending moment gradient.

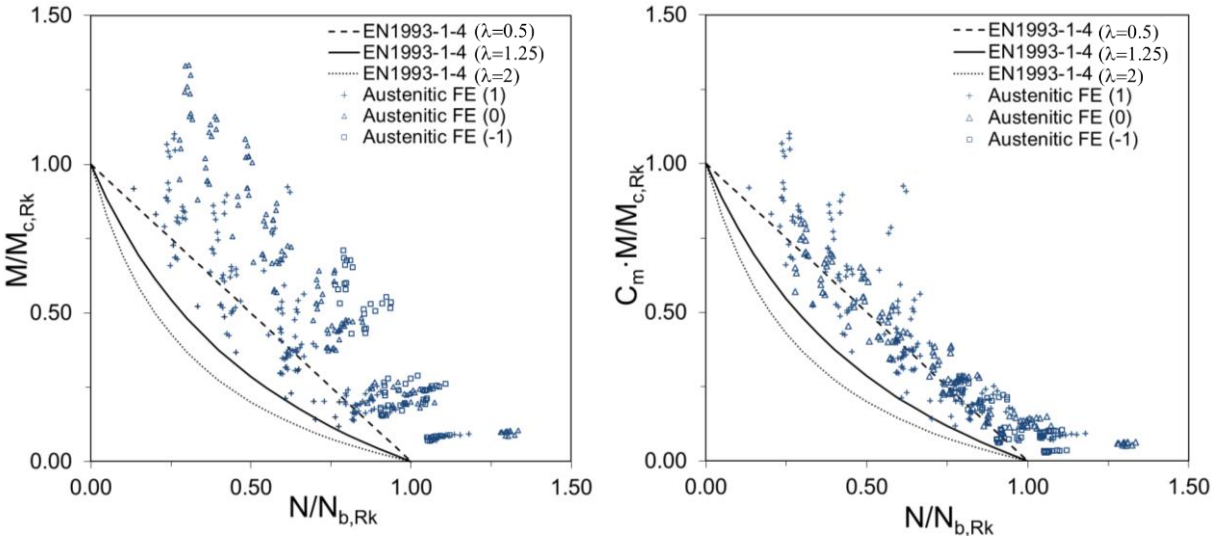

a) Without considering the equivalent moment factor $C_{m,u}$

b) Considering the equivalent moment factor $C_{m,u}$

Fig. 7.8. Austenitic stainless steel beam-column results for different bending distributions.

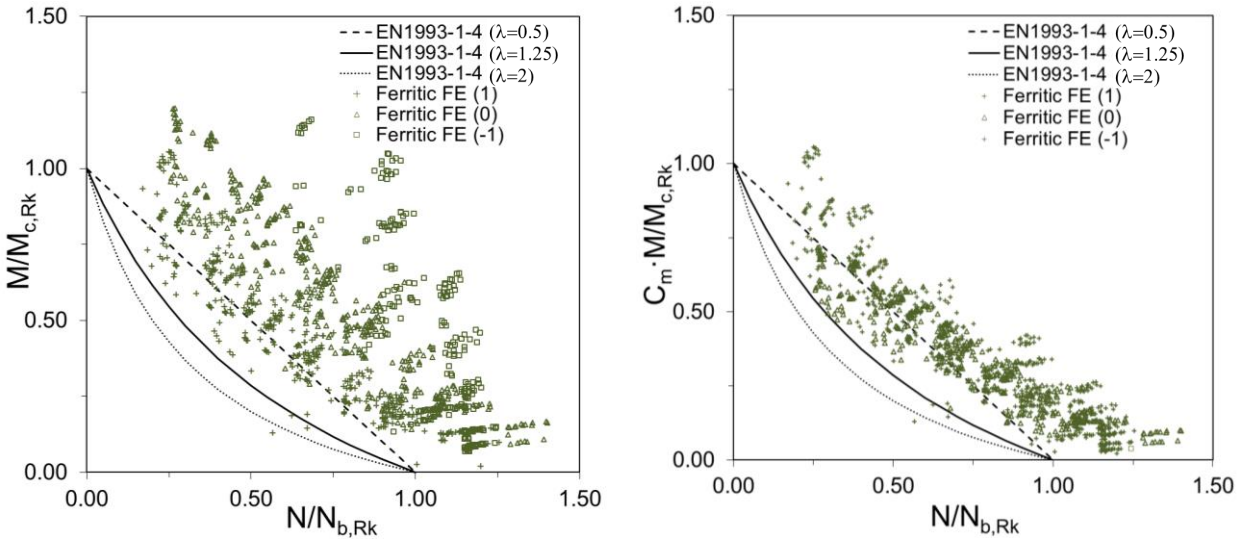

a) Without considering the equivalent moment factor $C_{m,u}$

b) Considering the equivalent moment factor $C_{m,u}$

Fig. 7.9. Ferritic stainless steel beam-column results for different bending distributions.

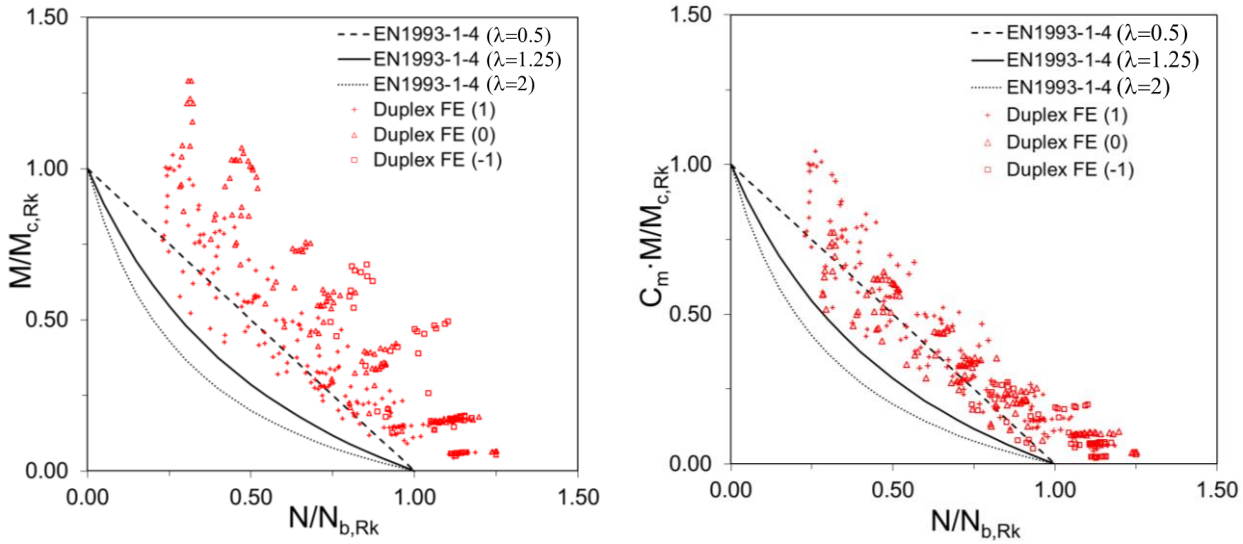

a) Without considering the equivalent moment factor $C_{m,u}$

b) Considering the equivalent moment factor $C_{m,u}$

Fig. 7.10. Duplex stainless steel beam-column results for different bending distributions.

The assessment of the different interaction expressions is presented in Tables 7.7 to 7.10, where the mean values and coefficients of variation (COVs) of the r_{pred}/r_u ratios by which design interaction curves exceed or fall short of the corresponding test (or FE) data are reported for austenitic, ferritic and duplex stainless steel beam-columns, as defined in Figure 7.11. Results corresponding to the experimental results and conducted FE parametric analysis on stainless steel beam-columns have been considered in Tables 7.7-7.8 and Tables 7.9-7.10 for uniform and non-uniform bending moment distributions respectively. In these tables, r_{EN1-4} corresponds to the resistance parameter calculated according to the flexural buckling resistance and interaction expression provided in EN1993-1-4 (2006), while r_{EN1-1} adopts the same column resistance but the interaction expression codified in EN1993-1-1 (2005), given in Eq. (7.18).

$r_{AS/NZS}$ stands for the AS/NZS4673 (2001) approach for beam-columns and r_{Zhao} refers to the design expression proposed by Zhao et al. (2016b) with column resistances obtained from the flexural buckling curves proposed by Afshan et al. (2016). Although Eq. (7.19) was proposed by Zhao et al. (2016b) only for stainless steel beam-columns with stocky cross-section, predicted results have been compared also for slender sections, adopting EN1993-1-4 (2006) provisions for the calculation of the effective cross-section properties. To allow future comparisons, results corresponding to stocky and slender cross-sections are reported in separated Tables, where those cross-sections for which the effective area is different from the gross area have been considered as slender cross-sections.

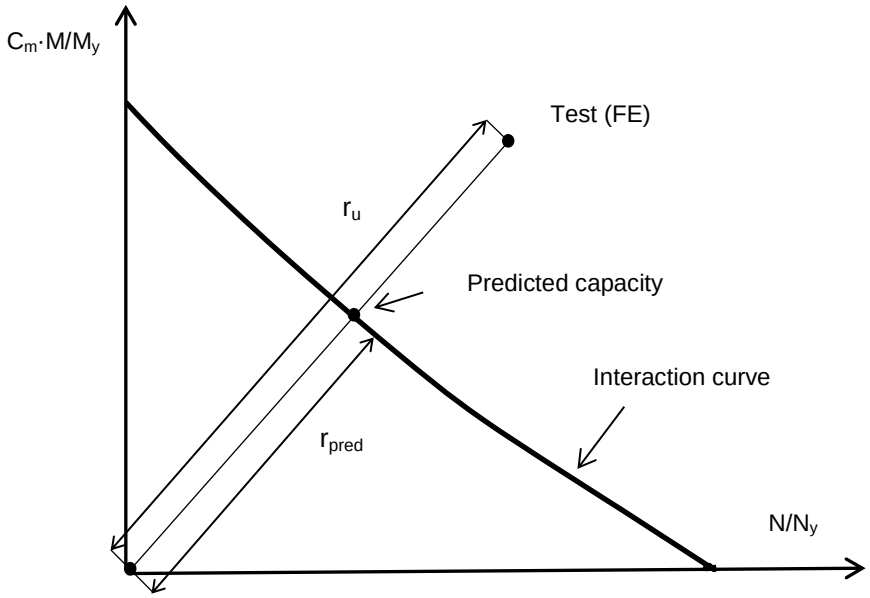

Fig. 7.11. Graphic definition of the r_{pred}/r_u ratios for the assessment of design approaches.

The assessment of the different approaches for slender cross-sections and uniform bending distribution is presented in Table 7.7, where it is appreciated that the most accurate and less scattered results are obtained for the EN1993-1-1 (2005) interaction expression considering the flexural buckling and bending resistances from EN1993-1-4 (2006). However, it is evident that all approaches provide safe and quite conservative strength predictions.

Table 7.7. Assessment of design approaches for beam-column with slender cross-sections under uniform bending distribution.

Grade		r_{EN1-4}/r_u	$r_{AS/NZS}/r_u$	r_{EN1-1}/r_u	r_{Zhao}/r_u
Austenitic	Mean	0.81	0.76	0.85	0.81
	COV	0.086	0.100	0.091	0.081
Ferritic	Mean	0.78	0.78	0.83	0.80
	COV	0.093	0.106	0.082	0.125
Duplex	Mean	0.83	0.82	0.86	0.83
	COV	0.106	0.106	0.091	0.106
All	Mean	0.80	0.78	0.84	0.81
	COV	0.098	0.109	0.087	0.115

Results corresponding to members with stocky cross-sections subjected to compression and uniform bending are presented in Table 7.8 for the same approaches studied in Table 7.7. The most accurate approach for stocky cross-sections corresponds to the EN1993-1-1 (2005) interaction expression given in Eq. (7.18) although no strain hardening effects are considered. However, nearly same results are also obtained for the expression proposed by Zhao et al. (2016b), where the bending capacity of the cross-sections is estimated according to the Continuous Strength Method. This is attributed to the fact that the interaction expression in EN1993-1-1 (2005) is lower and also because the approach by Zhao et al. (2016b) is based on lower flexural buckling curves.

Table 7.8. Assessment of design approaches for beam-column with stocky cross-sections under uniform bending distribution.

Grade		r_{EN1-4}/r_u	$r_{AS/NZS}/r_u$	r_{EN1-1}/r_u	r_{Zhao}/r_u
Austenitic	Mean	0.84	0.82	0.91	0.91
	COV	0.097	0.070	0.093	0.095
Ferritic	Mean	0.83	0.85	0.90	0.85
	COV	0.088	0.061	0.082	0.084
Duplex	Mean	0.81	0.86	0.86	0.87
	COV	0.072	0.036	0.059	0.048
All	Mean	0.83	0.84	0.90	0.87
	COV	0.089	0.061	0.084	0.087

In the design process of a beam-column both cross-sectional and member resistance conditions need to be verified. For those members subjected to combined compression and uniform bending, the behaviour of specimens is governed by member failure. However, as the end moment ratio ψ decreases, the failure can occur at cross-sectional level at the ends of the member and the failure of specimens is no longer due to global buckling. This fact is more likely to occur for members subjected to bitriangular bending distributions (ψ=-1) showing low member slenderness. In design expressions, equivalent moment factors C_m decrease for low end moment ratios ψ and the cross-section failure condition can become more restrictive, determining the ultimate resistance of the considered specimen, since the C_m factor reduces considerably the value of the considered equivalent bending moment. Therefore, both failure conditions have been considered in the assessment of beam-columns subjected to non-uniform moment diagrams, comparing the most restrictive predicted capacity with the corresponding experimental and numerical strengths.

For EN1993-1-4 (2006), EN1993-1-1 (2005) and Zhao et al. (2016b) approaches the cross-section behaviour was determined according to EN1993-1-4 (2006) provisions analysed in chapter 6, while for the AS/NZS4673 (2001) approach expressions in the Australian standard have been considered. Results corresponding to beam-columns subjected to non-uniform bending distributions are reported in Tables 7.9 and 7.10 for slender and stocky cross-sections respectively. The mean values and COVs of the predicted-to-experimental (or FE) strengths are presented for the different approaches and the equivalent uniform and sinusoidal moment factors. Only results corresponding to specimens showing member failure have been

considered in the analysis. It can be observed from these Tables that r_{pred}/r_u results corresponding to the equivalent uniform moment factor $C_{m,u}$ are higher than for the equivalent sinusoidal moment factor $C_{m,s}$ for all materials and interaction approaches.

Table 7.9. Assessment of design approaches for beam-column with slender cross-sections under non-uniform bending distribution.

a) Equivalent uniform moment factor $C_{m,u}$

Grade		r_{EN1-4}/r_u	$r_{AS/NZS}/r_u$	r_{EN1-1}/r_u	r_{Zhao}/r_u
Austenitic	Mean	0.81	0.71	0.84	0.78
	COV	0.073	0.100	0.068	0.069
Ferritic	Mean	0.74	0.73	0.78	0.73
	COV	0.099	0.108	0.082	0.109
Duplex	Mean	0.79	0.79	0.83	0.79
	COV	0.087	0.108	0.086	0.090
All	Mean	0.76	0.74	0.79	0.75
	COV	0.100	0.112	0.087	0.107

b) Equivalent sinusoidal moment factor $C_{m,s}$

Grade		r_{EN1-4}/r_u	$r_{AS/NZS}/r_u$	r_{EN1-1}/r_u	r_{Zhao}/r_u
Austenitic	Mean	0.79	0.69	0.82	0.75
	COV	0.100	0.094	0.079	0.093
Ferritic	Mean	0.73	0.72	0.77	0.72
	COV	0.107	0.104	0.078	0.111
Duplex	Mean	0.78	0.75	0.81	0.77
	COV	0.099	0.112	0.082	0.104
All	Mean	0.75	0.72	0.78	0.73
	COV	0.109	0.107	0.083	0.110

Results in Table 7.9 demonstrate that the most accurate beam-column capacity predictions correspond to the EN1993-1-1 (2005) interaction expression together with the flexural buckling and bending capacities determined from EN1993-1-4 (2006) provisions for slender stainless steel RHS and SHS beam-columns subjected to non-uniform bending distributions. Similar conclusions have also been extracted for beam-columns with uniform bending.

Table 7.10. Assessment of design approaches for beam-column with stocky cross-sections under non-uniform bending distribution.

a) Equivalent uniform moment factor $C_{m,u}$

Grade		r_{EN1-4}/r_u	$r_{AS/NZS}/r_u$	r_{EN1-1}/r_u	r_{Zhao}/r_u
Austenitic	Mean	0.87	0.78	0.90	0.87
	COV	0.078	0.061	0.077	0.090
Ferritic	Mean	0.80	0.78	0.83	0.77
	COV	0.105	0.073	0.090	0.095
Duplex	Mean	0.82	0.81	0.86	0.83
	COV	0.079	0.089	0.065	0.069
All	Mean	0.82	0.79	0.86	0.80
	COV	0.102	0.076	0.090	0.102

b) Equivalent sinusoidal moment factor $C_{m,s}$

Grade		r_{EN1-4}/r_u	$r_{AS/NZS}/r_u$	r_{EN1-1}/r_u	r_{Zhao}/r_u
Austenitic	Mean	0.83	0.75	0.86	0.85
	COV	0.099	0.057	0.083	0.085
Ferritic	Mean	0.78	0.77	0.82	0.76
	COV	0.093	0.057	0.069	0.093
Duplex	Mean	0.80	0.81	0.82	0.80
	COV	0.095	0.067	0.062	0.067
All	Mean	0.80	0.77	0.83	0.79
	COV	0.098	0.062	0.075	0.098

Regarding stainless steel beam-columns with stocky cross-sections subjected to non-uniform bending distributions, results are reported in Table 7.10 and the best capacity predictions are also obtained from the combination of the EN1993-1-1 (2005) interaction curve and the flexural buckling and bending capacities from EN1993-1-4 (2006). Results corresponding to the approach proposed by Zhao et al. (2016b) are also excellent for austenitic and duplex stainless steels, although the low r_{pred}/r_u ratios obtained for ferritic specimens considerably reduce the overall results.

Summarizing, the assessment of the interaction expressions codified in EN1993-1-4 (2006), AS/NZS4673 (2001) and EN1993-1-1 (2005) and proposed by Zhao et al. (2016b) for stainless steel beam-columns under different bending moment distributions has been presented in Tables 7.7 to 7.10. Results demonstrated that the most accurate strength predictions are obtained for the EN1993-1-1 (2005) interaction expression given in Eq. (7.18) with the flexural buckling and bending capacities determined from EN1993-1-4 (2006) provisions in combination with the equivalent uniform moment factor $C_{m,u}$ provided in Eq. (7.20) for the analysed stainless steel grades and cross-sections.

7.3.3 DSM approach for stainless steel beam-columns with uniform bending moment

AISI-S100-12 Specification (2012) does not provide any specific DSM-based expression for the design of beam-columns so the general interaction expressions need to be applied with the flexural buckling and bending resistances calculated from the DSM approaches presented in previous sections. However, Rasmussen (2006) extended the existing DSM approach for flexural buckling to beam-columns by introducing resistance parameters defined as radial distances in the M/M_y-N/N_y plane, as shown in Figure 7.12. In this approach the beam-column behaviour is directly tackled with a unique strength curve, considering the member and cross-section slendernesses based on the elastic instabilities of the specimen subjected to the actual stress distribution. Note that this method would represent the column behaviour when particularized to the vertical N/N_y axis.

According to Rasmussen (2006) the DSM approach for beam-columns first considers the member behaviour through interaction expression similar to that given in Eq. (7.22) from which the overall buckling strengths N_{one} and M_{one} (point A in Figure 7.12) can be obtained. Bending moments are expressed in terms of the axial load through a load eccentricity e, $M=e \cdot N$ and the

resistance parameter r_{ne} corresponding to the member behaviour can be obtained through Eq. (7.23). The method allows the consideration of different interaction factors *k* for beam-columns, several equivalent moment factors C_m, flexural buckling resistances $N_{b,ne}$ and bending moment capacities M_{ne}.

$$\frac{N_{one}}{N_{b,ne}} + k \cdot C_m \frac{M_{one}}{M_{ne}} = 1 \tag{7.22}$$

$$r_{ne} = \sqrt{\left(\frac{N_{one}}{N_y}\right)^2 + \left(\frac{M_{one}}{M_y}\right)^2} \tag{7.23}$$

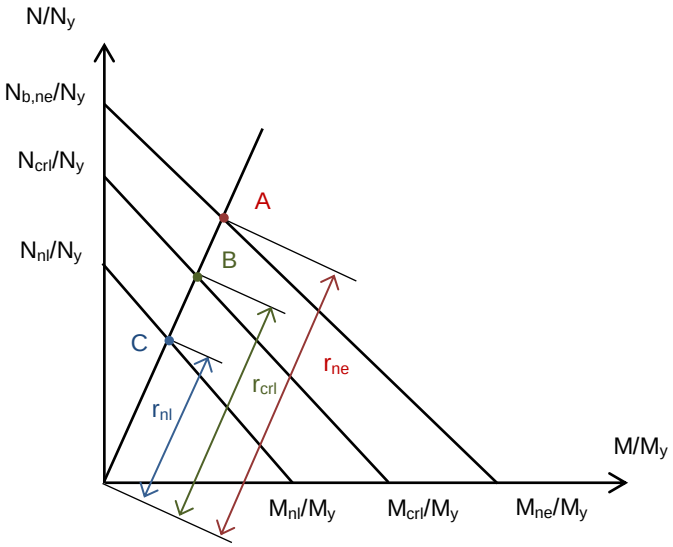

Fig. 7.12. Graphical definition of the radial distances for the beam-column approach by Rasmussen (2006).

The local buckling behaviour of the cross-section is introduced using the r_{crl} parameter defined in Eq. (7.24), where N_{ocr} and M_{ocr} are the axial compression and moment causing the local buckling of the cross-section under combined compression and bending loading conditions, obtained from a buckling analysis (point B). Finally, a generalized local slenderness is calculated from Eq. (7.25).

$$r_{crl} = \sqrt{\left(\frac{N_{ocr}}{N_y}\right)^2 + \left(\frac{M_{ocr}}{M_y}\right)^2} \tag{7.24}$$

$$\lambda_n = \sqrt{\frac{r_{ne}}{r_{crl}}} \tag{7.25}$$

Assuming that the strength equations derived for cross-sectional and column behaviour are also applicable to beam-columns, the nominal resistance parameter r_{nl} can be calculated through Eqs. (7.26) and (7.27), which correspond to the strength curves for carbon steel and stainless steel sections respectively. The predicted axial compression and bending strengths of the member N_{on} and M_{on} (point C) are finally obtained from Eq. (7.28). This DSM-based approach

has been modified and adapted to cross-sections subjected to combined compression and bending loading conditions in chapter 6 by considering that the radial distance governing the member strength changes to the yield radial distance r_y.

$$\frac{r_{nl}}{r_{ne}} = \begin{cases} 1 & \lambda_n \le 0.776 \\ \dfrac{1}{\lambda_n^{0.8}} - \dfrac{0.15}{\lambda_n^{0.8}} & \lambda_n > 0.776 \end{cases} \tag{7.26}$$

$$\frac{r_{nl}}{r_{ne}} = \begin{cases} 1 & \lambda_n \le 0.474 \\ \dfrac{0.95}{\lambda_n^{0.8}} - \dfrac{0.22}{\lambda_n^{1.6}} & \lambda_n > 0.474 \end{cases} \tag{7.27}$$

$$r_{nl} = \sqrt{\left(\frac{N_{on}}{N_y}\right)^2 + \left(\frac{M_{on}}{M_y}\right)^2} \tag{7.28}$$

For the comparison of the experimental and numerical results with the strength capacities predicted by this method the following procedure needs to be considered, as described in Rasmussen (2006). Although the described methodology is an iterative procedure when predicted capacities are compared with experimental (or FE) strengths, this iteration is not required in a design situation where the design action is used to determine the eccentricity and the interaction factors. It should also be noted that in the assessment of the different interaction approaches presented in the previous section the calculation of the predicted beam-column strength also required the resolution of a nonlinear equation.

1) Assume a value for $(N_{on})^i$.
2) Calculate the eccentricity corresponding to $(N_{on})^i$ and determine N_{one} from Eq. (7.22). Then calculate r_{ne} from Eq. (7.23). In a design situation, the eccentricity would be calculated for the design action rather than for $(N_{on})^i$.
3) Calculate the r_{cr} radial distance from a buckling analysis considering the actual stress distribution in the cross-section and Eq. (7.24).
4) Calculate the generalized slenderness λ_n from Eq. (7.25) and the resistance parameter r_{nl} from Eqs. (7.26) or (7.27).
5) Calculate $(N_{on})^{i+1}$ from Eq. (7.29) and compare it with $(N_{on})^i$. If $(N_{on})^i = (N_{on})^{i+1}$, convergence has been reached and $(N_{on})^i$ is the axial compression strength. If $(N_{on})^i \neq (N_{on})^{i+1}$, go to step 2) with $(N_{on})^{i+1}$ until convergence is reached.

$$(N_{on})^{i+1} = \frac{r_n}{\left[\left(\frac{1}{N_y}\right)^2 + \left(\frac{e^i}{M_y}\right)^2\right]^{0.5}} \tag{7.29}$$

As for the traditional methods assessed in the previous section, the accuracy of the DSM approach is highly dependent on the correct estimation of the flexural buckling $N_{b,ne}$ and bending moment M_{ne} capacities, as well as on the considered interaction expression for the

member behaviour *k* and the equivalent moment factor C_m. Based on the previous investigations on RHS and SHS beams reported in chapter 6, the bending moment resistance calculated considering the inelastic capacity reserve with the compression strain factor C_y provided in AS/NZS4673 (2001) and SEI/ASCE 8-02 (2002) has been considered in the analysis. Regarding flexural buckling behaviour, the different approaches contemplated in section 7.2 have been considered.

The DSM-based approach developed by Rasmussen (2006) for beam-columns is herein analysed for austenitic, ferritic and duplex stainless steel RHS and SHS members subjected to compression and uniform bending loading conditions using different flexural buckling resistances $N_{b,ne}$ and interaction expressions *k*. Since the different interaction factors considered were calibrated based on the first order bending moments, implicitly consider second order effects and the $M_{one}=N_{one}\cdot e_0$ relationship, together with $C_m=1$, should be considered in the interaction expressions for uniform bending moment distributions. Although the original proposal only included the capacity reduction due to local buckling effects in slender cross-sections, the method has been investigated as a full cross-sectional slenderness approach that also considers the enhanced material properties for stocky cross-sections. Results obtained using the DSM design approach have been compared to the predicted beam-column strengths obtained from the codified approaches through the traditional Effective Width Method assessed in the previous section to identify the most appropriate approach for stainless steel beam-columns.

Figures 7.13 to 7.15 present the assessment of the DSM approach for experimental and FE results corresponding to beam-columns under uniform bending moment distribution for austenitic, ferritic and duplex stainless steel grades, respectively. Results corresponding to the interaction expressions *k* codified in AS/NZS4673 (2001) and EN1993-1-4 (2006) given in Eqs.(7.17) and (7.16) are first presented for each material, followed by the Zhao et al. (2016b) and EN1993-1-1 (2005) approaches for Eqs.(7.19) and (7.18). All local buckling loads were obtained from CUFSM (Schafer and Ádány, 2006) calculations as for previous DSM approaches. In these Figures r_u/r_{ne} ratios are plotted against the corresponding generalized slenderness λ_n calculated from Eq. (7.25), and carbon steel and stainless steel strength curves are also depicted for comparison. Figures 7.13 to 7.15 suggest that the strength curve given for carbon steel cross-section in Eq. (7.26) provides better results for beam-columns, showing a similar behaviour to that exhibited for columns and cross-sections. The scatter observed in the low slenderness range for all materials and assessed interaction expressions can be partly attributed to strain hardening effects when stocky members and cross-sections are considered, but also to the inaccuracy of the analytic expressions used in the prediction of the flexural buckling and interaction behaviour of the specimens.

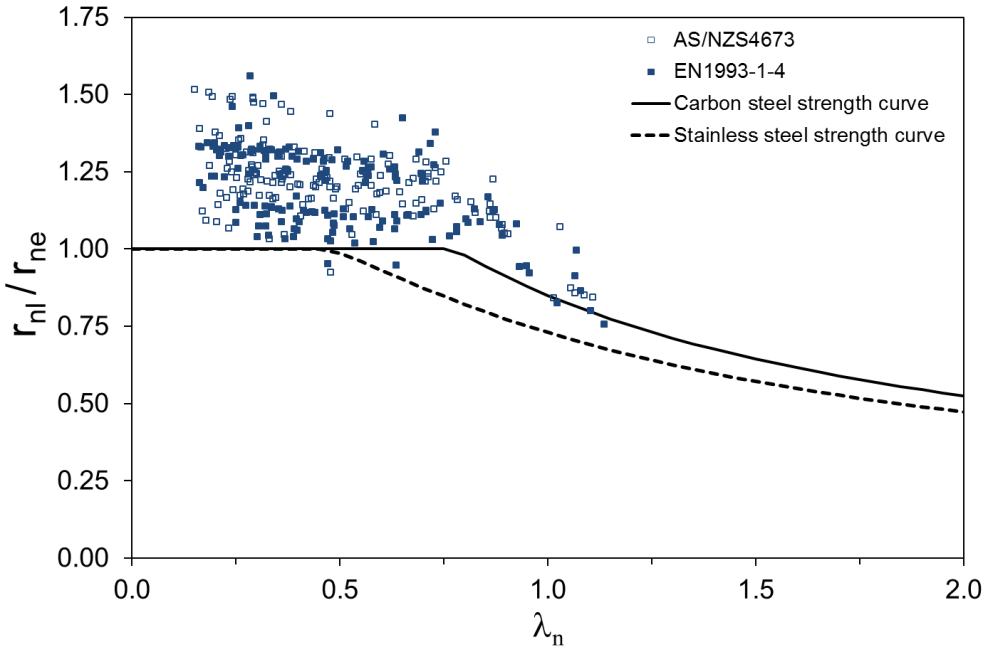

a) AS/NZS4673 and EN1993-1-4 approaches

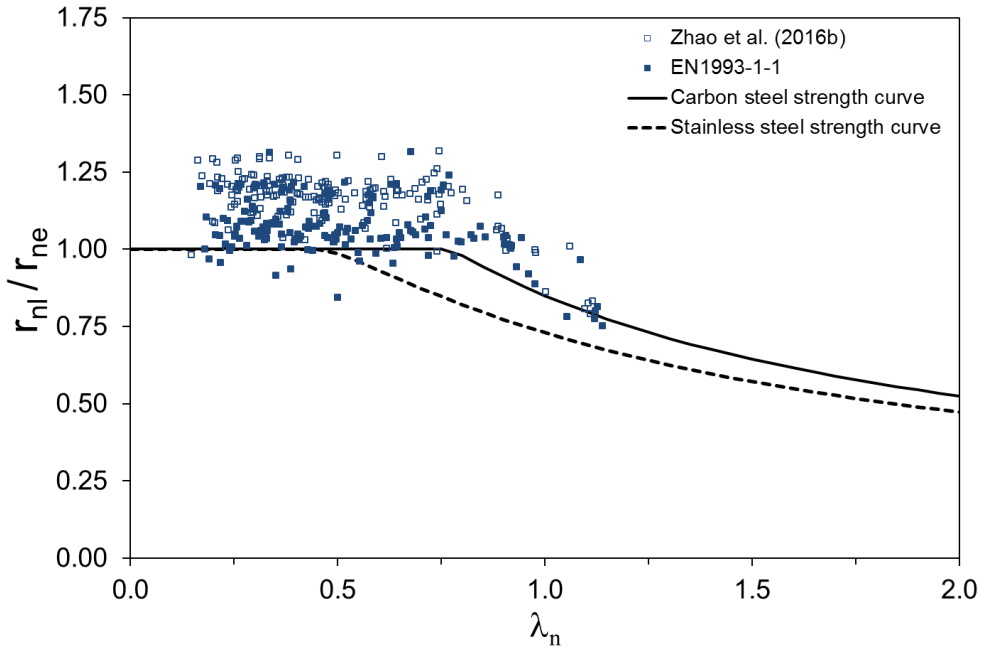

b) Zhao et al. (2016b) and EN1993-1-1 approaches

Fig. 7.13. Assessment of the DSM approach for austenitic stainless steel RHS and SHS beam-columns under uniform bending for different interaction and buckling curves.

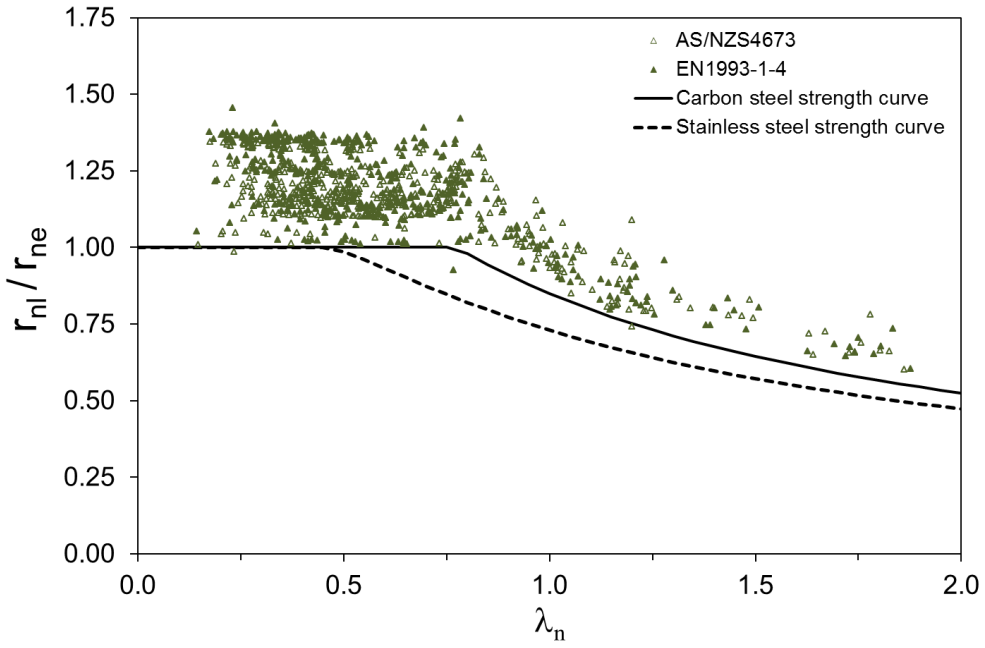

a) AS/NZS4673 and EN1993-1-4 approaches

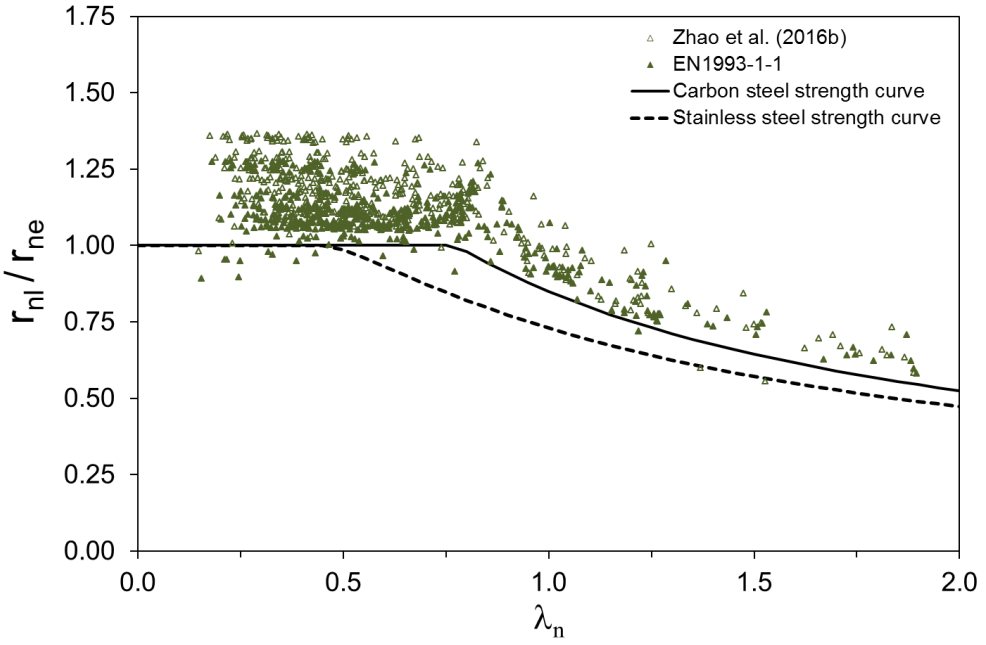

b) Zhao et al. (2016b) and EN1993-1-1 approaches

Fig. 7.14. Assessment of the DSM approach for ferritic stainless steel RHS and SHS beam-columns under uniform bending for different interaction and buckling curves.

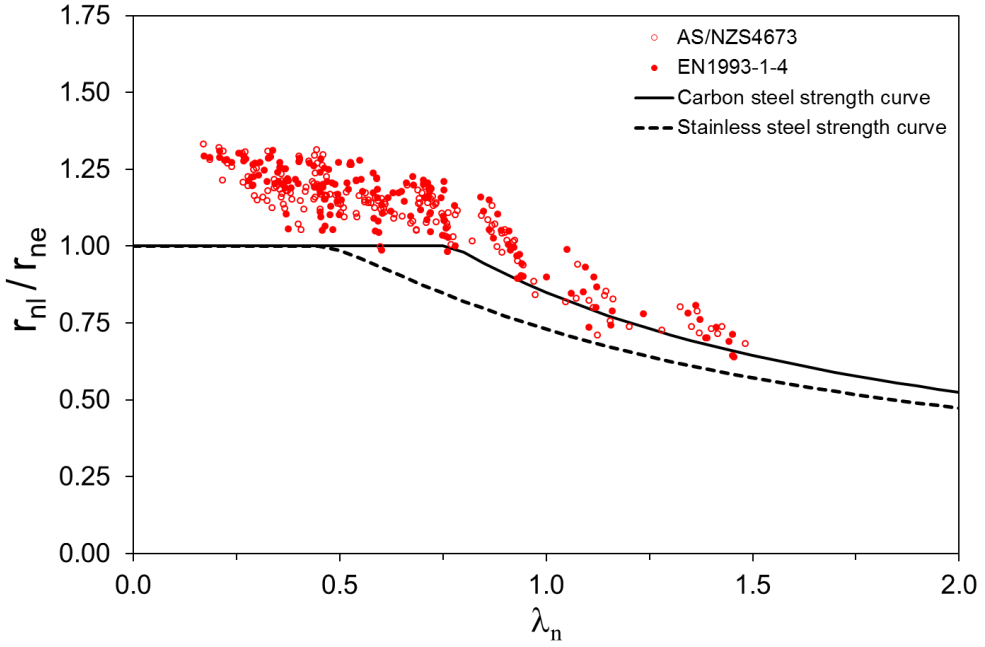

a) AS/NZS4673 and EN1993-1-4 approaches

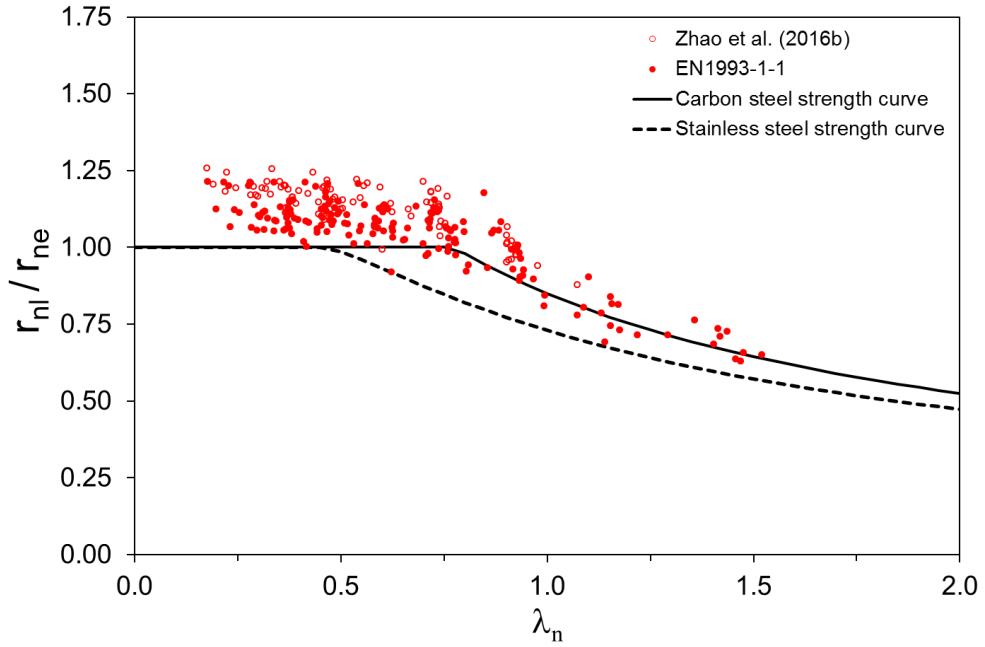

b) Zhao et al. (2016b) and EN1993-1-1 approaches

Fig. 7.15. Assessment of the DSM approach for duplex stainless steel RHS and SHS beam-columns under uniform bending for different interaction and buckling curves.

The assessment of the DSM approach has been derived, as for columns and cross-sections in chapter 6, analysing slender and stocky cross-sections separately in order to evaluate both the overall-local buckling interaction and strain hardening effects. The numerical assessment of the new approach for beam-columns under uniform bending distribution is presented in Tables 7.11 and 7.12 for slender and stocky cross-sections respectively. Based on the conclusions

extracted from cross-sectional and column behaviour and the observations made from Figures 7.13 to 7.15, only results corresponding to the strength curve provided for carbon steel specimens (Eq. (7.26)) are considered and reported in this analysis. These results need to be compared with the r_{pred}/r_u ratios reported in Tables 7.7 and 7.8 in the previous section, which correspond to the same interaction expressions but considering the local buckling effects through the Effective Width Method (EWM) and where no strain hardening effects are introduced except for the Zhao et al. (2016b) approach.

Results reported in Table 7.11 correspond to stainless steel beam-columns with slender cross-sections showing generalized slenderness higher than $\lambda_n \geq 0.776$ subjected to uniform bending moment distribution. According to these results, the most accurate capacity predictions are obtained for the EN1993-1-1 (2005) interaction curve given in Eq. (7.18) with the flexural buckling resistance determined according to EN1993-1-4 (2006) and the bending resistance calculated considering the inelastic capacity reserve as reported in chapter 6. These results are in line with the conclusions extracted from Table 7.7 for the effective width-based methods. The comparison of DSM and EWM results for slender cross-sections demonstrates that the DSM approach improves the capacity prediction of stainless steel beam-columns for all material grades and considered interaction expressions, since the average r_{pred}/r_u ratios presented in Table 7.11 are higher than those in Table 7.7. This improvement is caused by two different factors. First, the fact of considering the actual stress distribution in the cross-section when determining the generalized slenderness λ_n, that provides a better estimation of the susceptibility of the cross-section to local buckling effects; and second, the strength curve adopted for the member capacity reduction due to local buckling is more accurate than the reduction factors ρ codified in standards.

Table 7.11. Assessment of the DSM design approach for beam-columns with slender cross-section and uniform bending distribution for different interaction expressions.

Grade		r_{EN1-4}/r_u	$r_{AS/NZS}/r_u$	r_{EN1-1}/r_u	r_{Zhao}/r_u
Austenitic	Mean	0.90	0.87	0.94	0.89
	COV	0.073	0.070	0.065	0.074
Ferritic	Mean	0.86	0.85	0.89	0.87
	COV	0.066	0.072	0.062	0.089
Duplex	Mean	0.92	0.92	0.96	0.91
	COV	0.087	0.077	0.078	0.077
All	Mean	0.88	0.87	0.92	0.88
	COV	0.078	0.080	0.074	0.086

Beam-columns with stocky cross-section can reach stress levels beyond the established yield stress if members are stable enough to reach a partial yield of the cross-section. As evidenced in the previous section for the consideration of strain hardening effects in columns, low generalized slenderness λ_n values can correspond to stocky cross-sections with the corresponding high r_{cr} parameters, but also to slender members with low r_{ne} parameters. Therefore, the effect of the overall member behaviour needs to be considered in the definition of

an additional limitation. The definition of this limit is not as clear as for columns, where the stress at which the column failed has been limited to the 0.2% proof stress, since compression loads interact with bending moments. However, and following a similar approach to that given for columns, the condition presented in Eq. (7.30) is proposed for beam-columns. This condition establishes that the enhanced member capacity should always be higher than the yielding strength of the cross-section, described by the r_y parameter. This r_y factor corresponds to the cross-section yield behaviour under combined loading conditions already analysed in chapter 6. Hence, the enhanced strength can be obtained from Eq. (7.31) for beam-columns.

$$r_{ne}\left[1+\left(1-1.29\lambda_n\right)\left(\frac{\sigma_u}{\sigma_{0.2}}-1\right)\right]\leq r_y \tag{7.30}$$

$$\frac{r_{enh\_nl}}{r_{ne}}=1+\left(1-1.29\lambda_n\right)\left(\frac{\sigma_u}{\sigma_{0.2}}-1\right) \quad \text{for} \quad \lambda_n\leq 0.776 \tag{7.31}$$

Considering the definitions of r_{ne} and r_y previously introduced in Eq. (7.23) and Eq. (6.30) respectively, Eqs. (7.32) and (7.33) can be obtained, and by combining them with Eq. (7.30), the condition for considering strain hardening effects leads to Eq. (7.34). Considering that for uniform bending distributions C_m is equal to unity, this condition can be re-written as given in Eq. (7.35).

$$r_{ne}=N_{one}\sqrt{\left(\frac{1}{N_y}\right)^2+\left(\frac{eC_m}{M_y}\right)^2} \tag{7.32}$$

$$r_y=N_{oy}\sqrt{\left(\frac{1}{N_y}\right)^2+\left(\frac{e}{M_y}\right)^2} \tag{7.33}$$

$$\frac{N_{one}}{N_y}\left[1+\left(1-1.29\lambda_n\right)\left(\frac{\sigma_u}{\sigma_{0.2}}-1\right)\right]\frac{\sqrt{\left(\frac{1}{N_y}\right)^2+\left(\frac{eC_m}{M_y}\right)^2}}{\sqrt{\left(\frac{1}{N_y}\right)^2+\left(\frac{e}{M_y}\right)^2}}\leq 1 \tag{7.34}$$

$$\frac{N_{one}}{N_y}\left[1+\left(1-1.29\lambda_n\right)\left(\frac{\sigma_u}{\sigma_{0.2}}-1\right)\right]\leq 1 \tag{7.35}$$

The assessment of the DSM approach for beam-columns with stocky cross-sections showing generalized slenderness lower than $\lambda_n \leq 0.776$ is presented in Table 7.12 for the different interaction expressions and uniform bending moment diagram. For those specimens satisfying the condition given in Eq. (7.35) the enhanced material properties from Eq. (7.31) have been considered and results are compared to the r_{pred}/r_u ratios corresponding to the EWM reported in Table 7.8. These Tables demonstrate that DSM predictions are more accurate for all stainless steel grades and interaction expressions, obtaining excellent results for the EN1993-1-1 (2005) interaction curve as for beam-columns with slender cross-sections. As highlighted for stainless

steel columns, the improvement introduced in the beam-column capacity prediction is more evident for austenitic and duplex stainless steel grades. For ferritics the differences are again smaller since these specimens are characterized by a low $\sigma_u/\sigma_{0.2}$ ratio.

Table 7.12. Assessment of the DSM design approach for beam-columns with stocky cross-section and uniform bending distribution for different interaction expressions.

Grade		r_{EN1-4}/r_u	$r_{AS/NZS}/r_u$	r_{EN1-1}/r_u	r_{Zhao}/r_u
Austenitic	Mean	0.89	0.87	0.98	0.88
	COV	0.138	0.108	0.107	0.110
Ferritic	Mean	0.82	0.85	0.91	0.88
	COV	0.089	0.060	0.065	0.080
Duplex	Mean	0.85	0.87	0.92	0.86
	COV	0.063	0.050	0.052	0.044
All	Mean	0.84	0.86	0.93	0.85
	COV	0.106	0.073	0.083	0.083

7.3.4 DSM approach for stainless steel beam-columns with non-uniform bending moment

Once the full slenderness DSM approach for beam-columns presented in Rasmussen (2006) has been validated for stainless steel members subjected to compression and uniform bending, the method has been extended and adapted to non-uniform bending diagrams. The beneficial effect introduced by the bending moment gradient has been investigated by assessing the two equivalent moment factors introduced in section 7.3.1, the equivalent uniform moment factor $C_{m,u}$ and the equivalent sinusoidal moment factor $C_{m,s}$ given in Eqs. (7.20) and (7.21) respectively. The method proposed in the previous section has been extended to beam-columns subjected to non-uniform bending moment distributions by assuming a small modification in the procedure described in Eqs. (7.22) to (7.29). In all equations an equivalent load eccentricity as given by $e_{eq}=C_m e_0$ needs to be adopted in order to obtain accurate and safe capacity predictions of stainless steel beam-columns.

As highlighted in section 7.3.2, the cross-sectional and member resistance conditions need be verified when designing a beam-column. For those members subjected to combined compression and uniform bending the member verification is more restrictive. However, for non-uniform bending distributions the failure mechanism is not clear and both failure conditions need to be considered and the most restrictive capacity compared with the corresponding strength. In the assessment of the DSM approach, the cross-section capacity of the considered specimens has been determined according to the full slenderness range DSM approach proposed in chapter 6 for cross-sections subjected to combined loading. Therefore, the specimens considered in the following analysis only correspond to those showing overall or combined overall-local failure modes.

The assessment of the full slenderness range DSM approach for beam-columns subjected to non-uniform bending diagrams is presented in Tables 7.13 and 7.14 for slender and stocky cross-sections respectively, where the strength curve corresponding to carbon steel cross-sections given in Eq. (7.26) has been considered. The same interaction expressions assessed

in previous sections have been considered in the analysis (i.e. equations codified in AS/NZS4673 (2001) and EN1993-1-4 (2006), the EN1993-1-1 (2005) interaction approach and the Zhao et al. (2016b) proposal). Results corresponding to the two equivalent moment factors are also reported. It can be appreciated that, as in section 7.3.2 for EWM, the adoption of the equivalent uniform moment factor $C_{m,u}$ provides higher r_{pred}/r_u ratios and more accurate strength predictions for stocky and slender cross-sections, regardless the considered stainless steel grade. Therefore, it is recommended that the equivalent uniform moment factor $C_{m,u}$ is considered in the design of stainless steel beam-columns subjected to non-uniform bending diagrams when both EWM and DSM approaches are considered, since more accurate predictions are obtained and apart from being a more simple expression, there is no need of including new expressions in the standards.

The numerical assessment of the DSM approach for stainless steel beam-columns with slender cross-sections is presented in Table 7.13 where the mean values and COVs of the predicted-to-experimental (or FE) ratios are reported. Results demonstrate that the DSM approach improves the strength prediction of stainless steel beam-columns with slender cross-sections if results are compared with the corresponding values for the EWM in Table 7.9 for different interaction expressions and materials. As for uniform bending moment, this is due to the fact that the actual stress distribution is considered when the generalized slenderness is calculated and the adoption of a more accurate strength curve for local buckling. In addition, the best capacity prediction is also obtained for the EN1993-1-1 (2005) interaction curve with the flexural buckling curve codified in EN1993-1-4 (2006), as for the analyses presented before.

Table 7.13. Assessment of the DSM design approach for beam-columns with slender cross-section and non-uniform bending distribution for different interaction expressions.

a) Equivalent uniform moment factor $C_{m,u}$

Grade		r_{EN1-4}/r_u	$r_{AS/NZS}/r_u$	r_{EN1-1}/r_u	r_{Zhao}/r_u
Austenitic	Mean	0.87	0.81	0.91	0.84
	COV	0.081	0.104	0.077	0.089
Ferritic	Mean	0.80	0.80	0.83	0.80
	COV	0.093	0.084	0.075	0.097
Duplex	Mean	0.88	0.88	0.92	0.88
	COV	0.096	0.098	0.086	0.079
All	Mean	0.82	0.82	0.86	0.82
	COV	0.101	0.094	0.091	0.100

b) Equivalent sinusoidal moment factor $C_{m,s}$

Grade		r_{EN1-4}/r_u	$r_{AS/NZS}/r_u$	r_{EN1-1}/r_u	r_{Zhao}/r_u
Austenitic	Mean	0.86	0.79	0.87	0.82
	COV	0.083	0.094	0.086	0.105
Ferritic	Mean	0.80	0.79	0.83	0.78
	COV	0.098	0.064	0.075	0.090
Duplex	Mean	0.85	0.86	0.89	0.84
	COV	0.135	0.107	0.115	0.127
All	Mean	0.81	0.80	0.84	0.80
	COV	0.108	0.083	0.092	0.104

For beam-columns with stocky cross-sections showing a generalized slenderness lower than $\lambda_n \leq 0.776$, the assessment of the DSM approach for the different interaction expressions is presented in Table 7.14. Results correspond to beam-columns subjected to non-uniform bending diagrams, where enhanced material properties have been considered when Eq. (7.34) is satisfied. Table 7.14 demonstrates that the most accurate results are obtained for the EN1993-1-1 (2005) interaction curve, although the capacity of few austenitic specimens is overestimated for the equivalent uniform moment factor. However, these overestimations will be overcomed by the reliability analysis presented in the next section. When these results are compared with those reported in Table 7.10 for the same interaction expressions based on the EWM, it can be appreciated that the DSM approach improves the capacity predictions for all stainless steel grades as for slender cross-sections and uniform bending moment distributions.

Table 7.14. Assessment of the DSM design approach for beam-columns with stocky cross-section and non-uniform bending distribution for different interaction expressions.

a) Equivalent uniform moment factor $C_{m,u}$

Grade		r_{EN1-4}/r_u	$r_{AS/NZS}/r_u$	r_{EN1-1}/r_u	r_{Zhao}/r_u
Austenitic	Mean	0.94	0.88	1.02	0.92
	COV	0.169	0.146	0.154	0.143
Ferritic	Mean	0.79	0.82	0.87	0.77
	COV	0.129	0.090	0.087	0.126
Duplex	Mean	0.84	0.86	0.90	0.86
	COV	0.127	0.120	0.127	0.116
All	Mean	0.83	0.83	0.90	0.81
	COV	0.155	0.114	0.132	0.150

b) Equivalent sinusoidal moment factor $C_{m,s}$

Grade		r_{EN1-4}/r_u	$r_{AS/NZS}/r_u$	r_{EN1-1}/r_u	r_{Zhao}/r_u
Austenitic	Mean	0.93	0.85	1.00	0.90
	COV	0.157	0.105	0.113	0.131
Ferritic	Mean	0.79	0.80	0.86	0.77
	COV	0.125	0.081	0.068	0.124
Duplex	Mean	0.82	0.84	0.88	0.82
	COV	0.082	0.064	0.058	0.067
All	Mean	0.82	0.82	0.89	0.80
	COV	0.145	0.087	0.101	0.136

The assessment of the full slenderness range DSM approach for beam-columns under non-uniform bending distributions is also presented in Figures 7.16 to 7.18 for austenitic, ferritic and duplex stainless members. Experimental and FE capacities are normalized r_u/r_{ne} and plotted against the corresponding generalized slenderness λ_n, and compared with the strength curves for carbon and stainless steel cross-sections. Interaction expressions codified in AS/NZS4673 (2001) and EN1993-1-4 (2006) are first presented for each material, followed by the Zhao et al. (2016b) and EN1993-1-1 (2005) results. Considering the conclusions extracted from previous Tables, only results corresponding to the equivalent uniform moment factor $C_{m,u}$ are provided. As for beam-columns under uniform bending diagram, these Figures highlight that

the strength curve given for carbon steel cross-section provides better results than that proposed for stainless steels. This strength curve was also found to be more accurate for RHS and SHS members in compression and cross-sections under different loading conditions throughout this thesis.

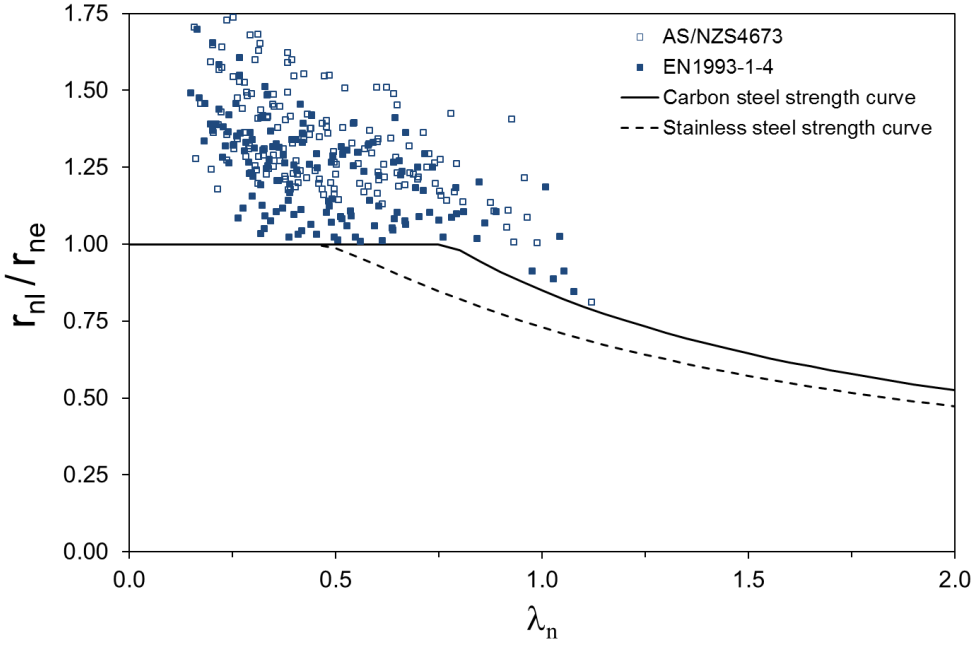

a) AS/NZS4673 and EN1993-1-4 approaches

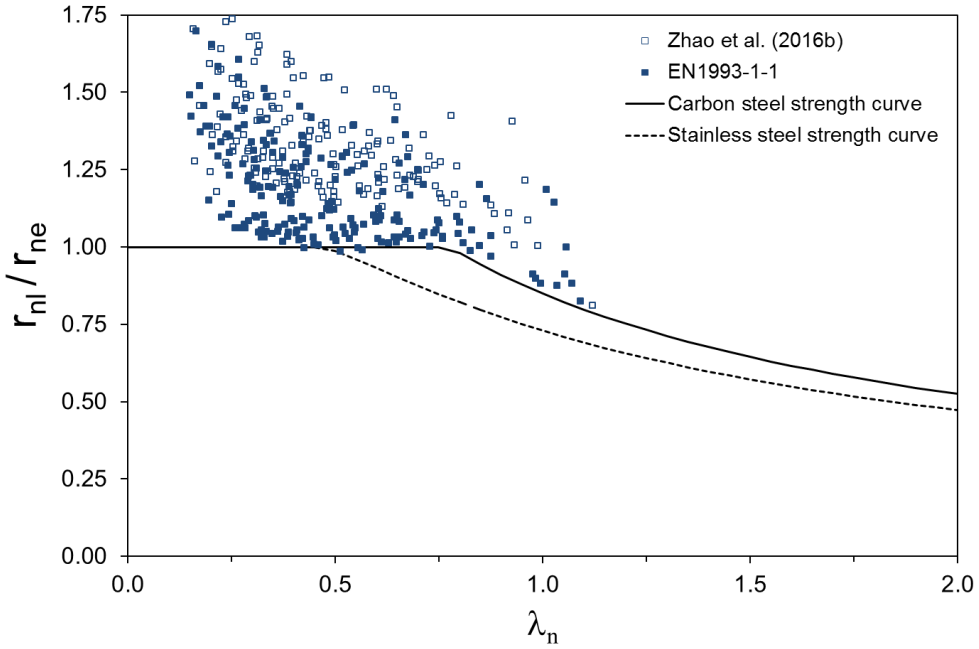

b) Zhao et al. (2016b) and EN1993-1-1 approaches

Fig. 7.16. Assessment of the DSM approach for austenitic stainless steel RHS and SHS beam-columns with non-uniform bending for different interaction and buckling curves.

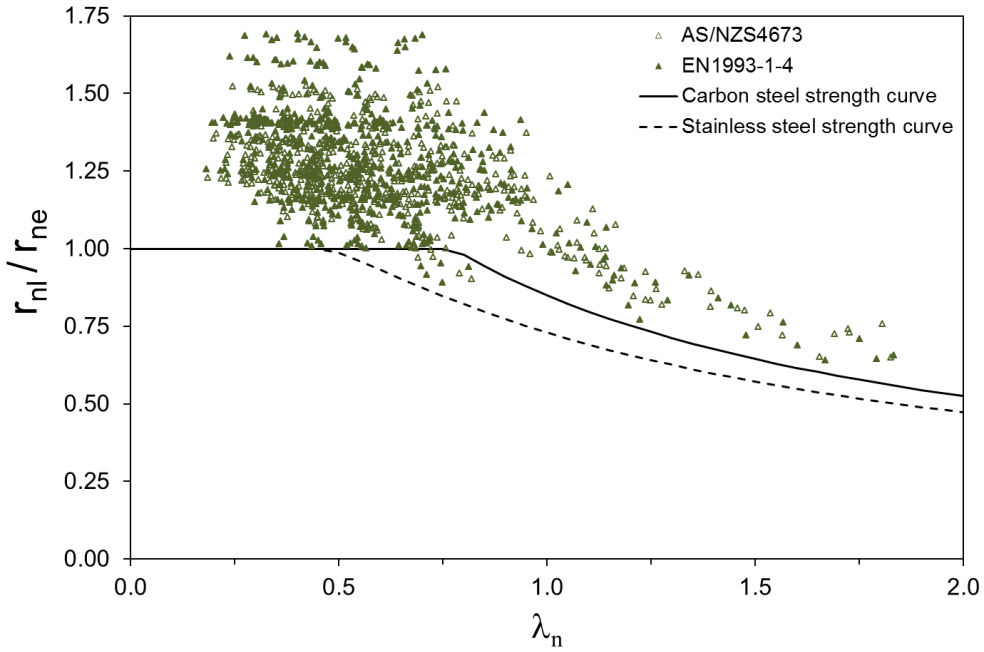

a) AS/NZS4673 and EN1993-1-4 approaches

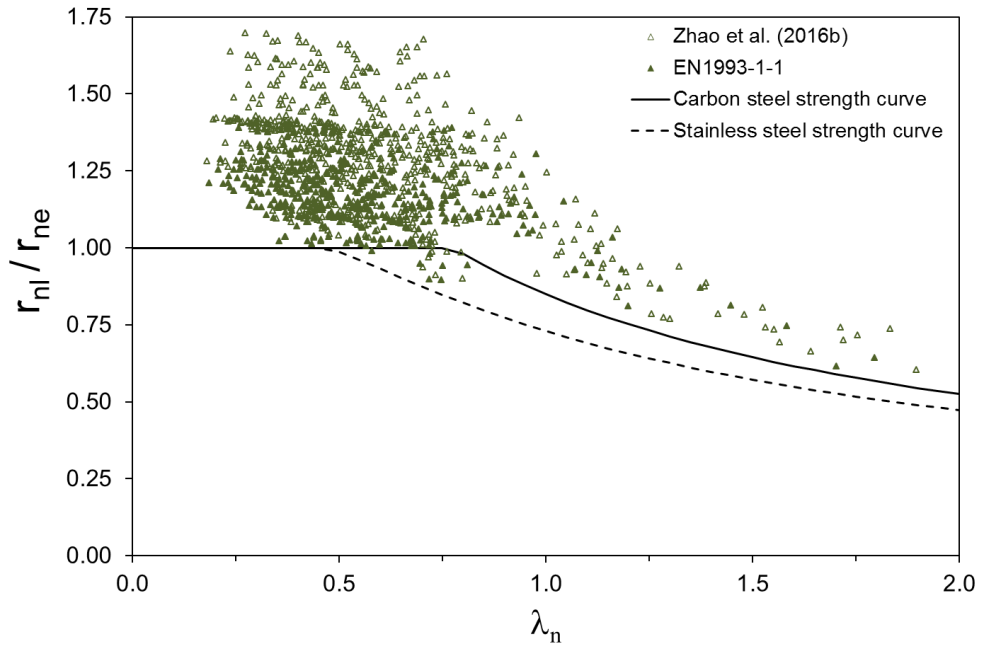

b) Zhao et al. (2016b) and EN1993-1-1 approaches

Fig. 7.17. Assessment of the DSM approach for ferritic stainless steel RHS and SHS beam-columns with non-uniform bending for different interaction and buckling curves.

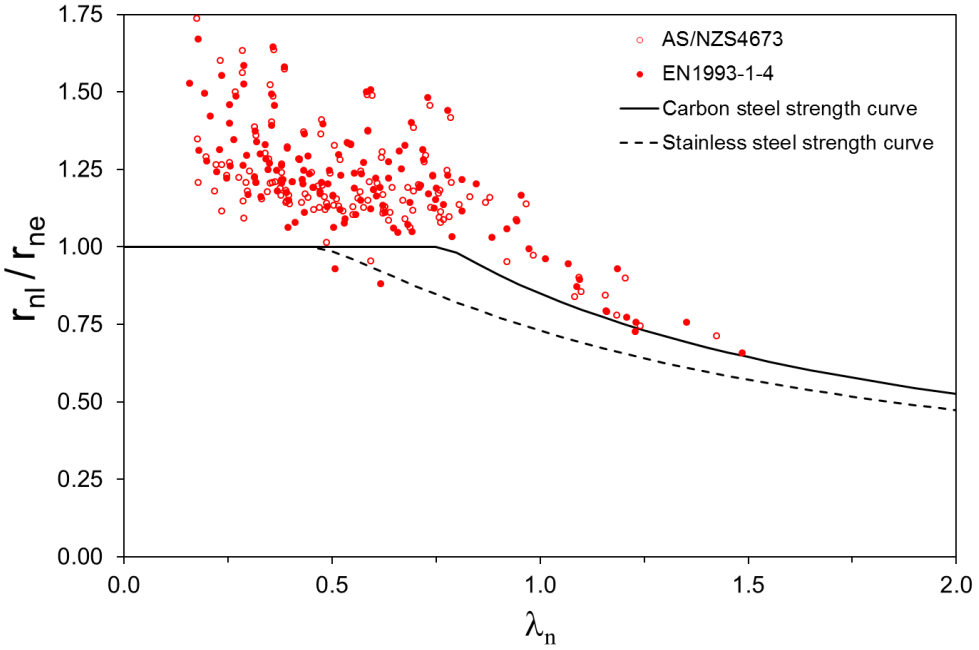

a) AS/NZS4673 and EN1993-1-4 approaches

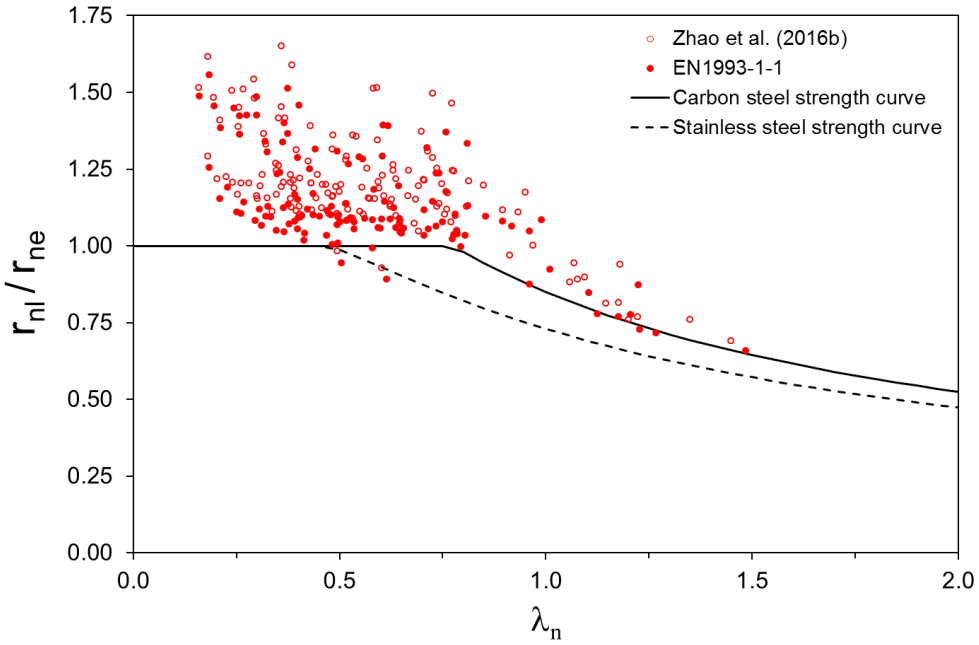

b) Zhao et al. (2016b) and EN1993-1-1 approaches

Fig. 7.18. Assessment of the DSM approach for duplex stainless steel RHS and SHS beam-columns with non-uniform bending for different interaction and buckling curves.

7.3.5 CSM approach for stainless steel beam-columns

Results and analyses presented in previous sections demonstrated that the interaction equation that better predicts the beam-column behaviour of stainless steel RHS and SHS members is the approach codified in EN1993-1-1 (2005) together with the column resistance obtained from the flexural buckling curve provided in EN1993-1-4 (2006). For non-uniform bending distributions, the equivalent uniform moment factor $C_{m,u}$ was found to provide accurate estimation of the effect of moment gradient. It has also been demonstrated that the incorporation of strain hardening effects in the proposed Direct Strength Method (DSM) approach notably improves the resistance prediction of those beam-columns stable enough to reach partial yielding of the cross-section if compared to the traditional Effective Width Methodology (EWM).

Therefore, and before this chapter is closed, a preliminary assessment of the beam-column behaviour is presented based on the methodology introduced in section 7.3.2 but considering the end points calculated according to the Continuous Strength Method (CSM). The analysis of the CSM approach for stainless steel beam-columns is based on the general interaction equation given in Eq. (7.15), but adopting the bending moment resistances determined in accordance with the CSM provisions described in chapter 6 and the flexural buckling resistances obtained from the expressions proposed in section 7.2.3.

The assessment has been conducted analysing experimental and FE beam-column strengths corresponding to members stable enough to reach partial yielding satisfying the limitation established in Eq. (7.14) for columns, which corresponds to a subset of the data considered in previous sections. Since the parametric studies described in chapter 5 were not specifically conceived for the assessment of a CSM-based approach, the number of available data is limited for austenitic and ferritic grades, and no data is feasible for duplex stainless steel. This study is thus presented as a preliminary assessment of the CSM approach for stainless steel beam-columns.

Considering all the conclusions extracted from previous sections, the approach will only be analysed considering the interaction expression provided EN1993-1-1 (2005) and given in Eq. (7.18), with the CSM approach for columns based on the flexural buckling curve provided in EN1993-1-4 (2006). The assessment of the approach for stainless steel beam-columns under uniform bending distributions is presented in Table 7.15 as mean values of the predicted-to-experimental ratios r_{pred}/r_u and COVs for austenitic and ferritic stainless steel grades, and results corresponding to the DSM and the EWM for the same subset of the analysed data are provided for comparison. Similar results but for beam-columns with non-uniform bending distributions are presented in Table 7.16, where the equivalent uniform moment factor $C_{m,u}$ given in Eq. (7.20) has been adopted.

Table 7.15. Assessment of the CSM approach for beam-columns with uniform bending distribution and comparison with alternative methods.

Grade		r_{pred}/r_u		
		CSM	DSM	EWM
Austenitic	Mean	0.97	1.09	0.87
	COV	0.064	0.045	0.077
Ferritic	Mean	0.98	0.92	0.93
	COV	0.040	0.039	0.034
All	Mean	0.97	1.02	0.89
	COV	0.055	0.092	0.072

Table 7.16. Assessment of the CSM approach for beam-columns with non-uniform bending distribution and comparison with alternative methods.

Grade		r_{pred}/r_u		
		CSM	DSM	EWM
Austenitic	Mean	1.04	1.19	0.95
	COV	0.036	0.028	0.022
Ferritic	Mean	1.03	1.02	0.98
	COV	0.017	0.009	0.006
All	Mean	1.03	1.09	0.96
	COV	0.025	0.087	0.024

Although the considered database only permitted a preliminary analysis, results demonstrate that the adoption of accurate end points together with an adequate interaction expression provides excellent resistance predictions of the member strength of stainless steel beam-columns also for the traditional methodology provided in standards. Thus, the adoption of the CSM column and beam resistances is presented as a promising design approach for stocky beam-columns where strain hardening effects are relevant. However, a more in detail study should be conducted considering a more representative database and including also duplex stainless steel specimens.

7.3.6 Reliability analysis

The reliability of the proposed full slenderness range DSM approach for beam-columns is assessed through the corresponding statistical analyses. The statistical calibration has been also conducted by following the procedure provided in section F of the North American Specification AISI-S100-12 (2012) and the statistical parameters corresponding to the material and geometrical variations of the different stainless steel grades analysed have been extracted from Afshan et al. (2015). The considered material overstrength ratios are, as for the column analysis in section 7.2.4, 1.3 for austenitic stainless steel, 1.2 for ferritics and 1.1 for duplex and lean duplex grades, with COVs equal to 0.060, 0.045 and 0.030 respectively, and the COV of the geometric properties was taken as 0.050.

The Australian and American codes prescribe a resistance factor ϕ equal to 0.9 for tubular cross-sections in compression and bending and the target reliability index is β=2.5. In the

calculation of the different reliability indexes the load data and factors from the Commentary of AS/NZS4600 (2005) have been considered and a dead-to-live load ratio of 1/5 has been assumed. Table 7.17 presents the reliability indexes calculated for the full slenderness range DSM approach for austenitic, ferritic and duplex stainless steel beam-columns subjected to uniform bending distributions, while Table 7.18 reports the indexes corresponding to non-uniform distributions.

Table 7.17. Summary of the reliability analysis results for the full slenderness range DSM for beam-columns with uniform bending distribution.

Grade	Calculated reliability indexes β			
	Stocky cross-sections Enhanced mat. properties		Slender cross-sections Local buckling	
	AS/NZS4673	EN1993-1-1 and EN1993-1-4	AS/NZS4673	EN1993-1-1 and EN1993-1-4
Austenitic	3.62	3.07	3.77	3.47
Ferritic	3.62	3.30	3.47	3.33
Duplex	3.14	2.91	2.84	2.59

Table 7.18. Summary of the reliability analysis results for the full slenderness range DSM for beam-columns with non-uniform bending distribution.

Grade	Calculated reliability indexes β			
	Stocky cross-sections Enhanced mat. properties		Slender cross-sections Local buckling	
	AS/NZS4673	EN1993-1-1 and EN1993-1-4	AS/NZS4673	EN1993-1-1 and EN1993-1-4
Austenitic	3.26	2.66	3.83	3.48
Ferritic	3.67	3.43	3.76	3.67
Duplex	2.85	2.69	2.95	2.79

Considering the resistance factors ϕ prescribed in AS/NZS4673 (2001) and SEI/ASCE 8-02 (2002) equal to 0.9, results in Tables 7.17 and 7.18 demonstrate that the proposed approach for beam-columns can be safely applied to all the studied stainless steel grades and bending distributions since calculated indexes are higher than the target reliability index β=2.5.

7.4 Summary of proposals and concluding remarks

A full slenderness range Direct Strength Method (DSM) approach has been proposed in this chapter for stainless steel RHS and SHS members subjected to compression and combined loading conditions with different bending distributions. The proposal is based on the strength curve provided for carbon steel cross-sections in the AISI-S100-12 (2012) specification for local buckling interaction and on the basis established by Rossi and Rasmussen (2013) for enhanced material properties. The new approach was found to be more accurate for both columns and beam-columns than the codified specifications for stocky and slender cross-sections, since

strain hardening effects are incorporated and due to the fact that the actual stress distribution of the cross-section is considered when determining the slenderness, what provides a better estimation of the susceptibility of the cross-section to local buckling effects. The adopted strength curve for the member capacity reduction due to local buckling was also found to be more accurate than the reduction factors codified in standards. Although some additional limitations need to be imposed before strain hardening effects are included in member behaviour, it has been demonstrated that the same strength curve proposed for cross-sectional behaviour is applicable for stainless steel columns and beam-columns. The reliability of the proposed DSM approaches was assessed through the corresponding statistical analyses for columns and beam-columns following the procedures provided in section F of the North American Specification AISI-S100-12 (2012) and EN1990, Annex D (2005) and it was demonstrated that they can be safely applied.

The full slenderness range DSM approach for RHS and SHS stainless steel columns is given in Eqs. (7.8) and (7.4), where the strength of the column is determined from the flexural buckling resistance of the fully effective cross-section $N_{b,ne}$, and the cross-section slenderness is determined from Eq. (7.5). It has also been demonstrated that the most accurate capacity predictions are obtained when the buckling curve codified in EN1993-1-4 (2006) is considered for the determination of the basic flexural buckling resistance $N_{b,ne}$ for all the studied stainless steel grades. The effect of strain hardening can also be included in the calculation of the column resistance for those members with local slenderness lower than $\lambda_l \leq 0.776$ and satisfying the condition stated in Eq. (7.10).

$$\frac{N_{enh\_nl}}{N_{b,ne}} = \begin{cases} 1+\left(1-1.29\lambda_l\right)\left(\dfrac{\sigma_u}{\sigma_{0.2}}-1\right) & \lambda_l \leq 0.776 \quad (7.8) \\ \dfrac{1}{\lambda_l^{0.8}}-\dfrac{0.15}{\lambda_l^{0.8}} & \lambda_l \geq 0.776 \quad (7.4) \end{cases}$$

$$\lambda_l = \sqrt{\frac{N_{b,ne}}{N_{crl}}} \quad (7.5)$$

$$\chi\left[1+\left(1-1.29\lambda_l\right)\left(\frac{\sigma_u}{\sigma_{0.2}}-1\right)\right] \geq 1 \quad (7.10)$$

Based on the previous DSM proposal for stocky cross-sections, a new expression based on the Continuous Strength Method (CSM) has also been proposed for stainless steel columns. This proposal is given in Eq. (7.12) and considers strain hardening effects for those members stable enough to reach partial yielding of the cross-section, members satisfying Eq. (7.14). The method is based on the maximum strain ε_{CSM} and strain hardening modulus E_{sh} obtained from the CSM equations given for cross-sectional resistance. The best predictions are also obtained for the flexural buckling resistance $N_{b,ne}$ obtained from the buckling curve codified in EN1993-1-4 (2006).

$$\frac{N_{b,CSM}}{N_{b,ne}} = 1 + \frac{E_{sh}}{E}\left(\frac{\varepsilon_{CSM}}{\varepsilon_y} - 1\right) \tag{7.12}$$

$$\chi\left[1 + \frac{E_{sh}}{E}\left(\frac{\varepsilon_{CSM}}{\varepsilon_y} - 1\right)\right] \geq 1 \tag{7.14}$$

A full slenderness range DSM approach has also been proposed for RHS and SHS stainless steel members subjected to combined loading conditions with different bending diagrams based on the original method by Rasmussen (2006). The proposed strength curve, given in Eqs. (7.31) and (7.26), considers strain hardening and local buckling effects and is the same curve adopted for columns and cross-sectional resistance predictions and it is based on radial resistance parameters calculated in the M/M_y-N/N_y diagram. The generalized slenderness λ_n is based on the r_{ne} and r_{crl} parameters governing the member and local buckling behaviour of the specimen as for Eq. (7.25). The method has been extended to non-uniform bending moment distributions by assuming an equivalent load eccentricity as given by $e_{eq}=C_m e_0$ and adopting the equivalent uniform moment factor $C_{m,u}$ already included in EN1993-1-1 (2005), AS/NZS4673 (2001) and SEI/ASCE 8-02 (2002). The most accurate capacity predictions are obtained for the EN1993-1-1 (2005) interaction curve given in Eq. (7.18) with the flexural buckling resistance determined according to EN1993-1-4 (2006) and the bending resistance calculated considering the inelastic capacity reserve as reported in chapter 6. In order to guarantee that members are stable enough and incorporate strain hardening effects in beam-column resistance predictions, an equivalent condition to that imposed for columns, given in Eq. (7.30), needs to be satisfied.

$$\frac{r_{enh\_nl}}{r_{ne}} = \begin{cases} 1 + (1 - 1.29\lambda_n)\left(\frac{\sigma_u}{\sigma_{0.2}} - 1\right) & \lambda_n \leq 0.776 \quad (7.31) \\ \frac{1}{\lambda_n^{0.8}} - \frac{0.15}{\lambda_n^{0.8}} & \lambda_n \geq 0.776 \quad (7.26) \end{cases}$$

$$\lambda_n = \sqrt{\frac{r_{ne}}{r_{crl}}} \tag{7.25}$$

$$k = 1 + 0.6\lambda_c \frac{N_{Ed}}{N_{b,Rd}} \leq 1 + 0.6\frac{N_{Ed}}{N_{b,Rd}} \tag{7.18}$$

$$r_{ne}\left[1 + (1 - 1.29\lambda_n)\left(\frac{\sigma_u}{\sigma_{0.2}} - 1\right)\right] \leq r_y \tag{7.30}$$

Finally, a preliminary assessment of the CSM approach for stainless steel stocky beam-columns has been presented, where bending moment and column strengths calculated according to CSM provisions are considered. Results indicated that the adoption of accurate end points provides excellent resistance predictions of beam-column strengths as strain hardening effect are incorporated. However, a more in detail study is needed in order to validate the accuracy and reliability of the approach considering a more representative database and including also duplex stainless steel specimens.

CHAPTER 8

Behaviour of stainless steel RHS and SHS continuous beams

8.1 Introduction

Development of efficient design guidance for stainless steel structures is key for the increased use of this corrosion-resistant material by considering both nonlinear behaviour and strain hardening effects into resistance prediction expressions, together with the moment redistribution in indeterminate structures. With the aim of analysing the bending moment redistribution capacity and assessing the applicability of plastic design methods to stainless steel structures, a comprehensive study on continuous beams is presented in this chapter.

First current Class 1 limits are assessed from the experimental results on ferritic stainless steel Rectangular and Square Hollow Section (RHS and SHS) beams reported in chapter 4, followed by a brief assessment of the design methods based on global elastic analysis. The analysis demonstrates that these capacity predictions are considerably overconservative due to strain hardening effects and the bending moment redistribution capacity of the beams. Thus, the assessment of the different design approaches based on global plastic analysis is then presented, where the traditional plastic design method is investigated together with an alternative approach based on the Continuous Strength Method (CSM). The accuracy and reliability analyses of these approaches are investigated.

Finally, a Direct Strength Method (DMS) approach is proposed based on the CSM for indeterminate structures for stainless steel continuous beams. This approach is based on the DSM bending capacity approach suggested in chapter 6 and provides marginally better results

than the CSM for indeterminate structures. The reliability of the method is also demonstrated by means of statistical analyses.

8.2 Assessment of limits for Class 1 cross-sections

The European standard EN1993-1-4 (2006) for the design of structural stainless steel elements accounts for the effect of local buckling through the cross-section classification concept given in EN1993-1-1 (2005), as mentioned in chapter 6. The Class is assigned to each cross-section depending upon its susceptibility to local buckling by comparing predetermined limits with the $c/\varepsilon t$ value of the most slender constituent plate element, considering both geometrical and material properties of the studied element. c is the width or depth of the relevant part of a cross-section, t is the element thickness and ε considers the material properties, defined as $\varepsilon=[(235/\sigma_{0.2})\cdot(E/210000)]^{0.5}$, where $\sigma_{0.2}$ is the 0.2% proof stress traditionally considered as the yield stress for stainless steels and E is the Young's modulus. Class limits are currently codified in EN1993-1-4 (2006), although revised limits were proposed by Gardner and Theofanous (2008) for austenitic and duplex stainless steel cross-sections due to the over-conservatism of the codified limits.

The assessment of the Class 3 and Class 2 limits for both classifications has already been presented in chapter 6 for stainless steel RHS and SHS, since these limits depend on cross-section response. It was found that while EN1993-1-4 (2006) limits provide safe results, the revised limits proposed by Gardner and Theofanous (2008) are more accurate for the analysed cross-sections. However, Class 1 cross-sections are associated with the global behaviour of structures and the assessment of this limit cannot be dissociated from the study of stainless steel indeterminate structures.

The distinction between Class 2 and Class 1 is traditionally derived from the rotation capacity developed by the beams and it is related to the $c/\varepsilon t$ slenderness parameter. The rotation capacity R is a measure of rotation between the point at which the moment-curvature curves reach the plastic bending capacity M_{pl} and the point at which the moment falls below M_{pl} (see Figure 8.1). Carbon steel cross-sections are considered to be Class 1 if $R\geq3$, and as no specific definition is currently available for stainless steels, the same condition is usually considered. However, some research works such as Theofanous et al. (2014) suggest that a minimum deformation capacity limit should be established to guarantee sufficient moment redistribution instead of the classical rotation capacity definition.

For four-point bending tests, the rotation capacity R is determined from $R=\kappa_u/\kappa_{pl}-1$, where κ_u is the curvature corresponding to the ultimate load and given in Eq. (8.1) and κ_{pl} is the elastic curvature corresponding to M_{pl} in the ascending branch, defined as $\kappa_{pl}=M_{pl}/EI$. I is the relevant second moment of area, u_{av} is the average value of the deflections at the loading sections, u_2 is the deflection at the midspan section and L^* is the distance between applied loads, as previously defined in Figure 4.14 in chapter 4.

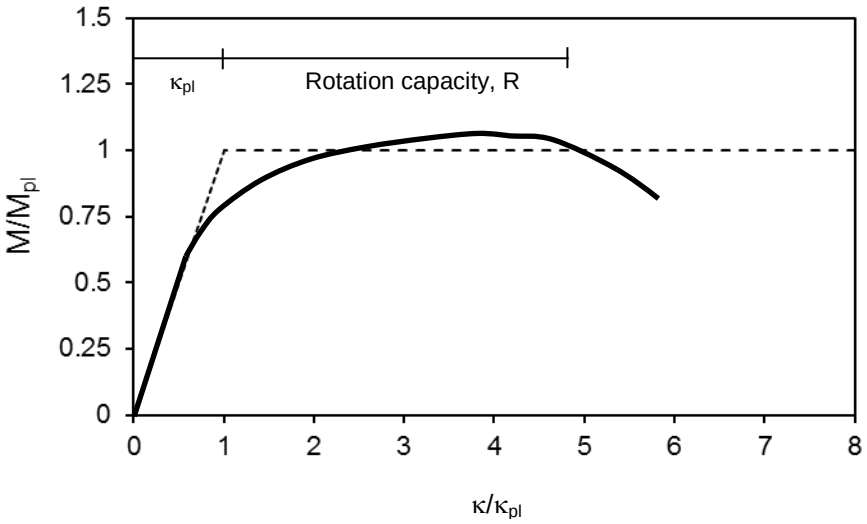

Fig. 8.1. Graphic definition of the rotation capacity, R.

$$\kappa = \frac{8 \cdot (u_2 - u_{av})}{4 \cdot (u_2 - u_{av})^2 + L^{*2}} \tag{8.1}$$

To assess the Class 1 limit, the rotation capacity R is plotted against the c/εt slenderness in Figure 8.2 for the four-point bending tests conducted on ferritic stainless steel RHS and SHS beams showing M_u/M_{pl} ratios greater than unity and described in chapter 4. As mentioned previously, a minimum rotation capacity of R≥3 is typically adopted for stainless steel Class 1 cross-sections since no specific limit is provided.

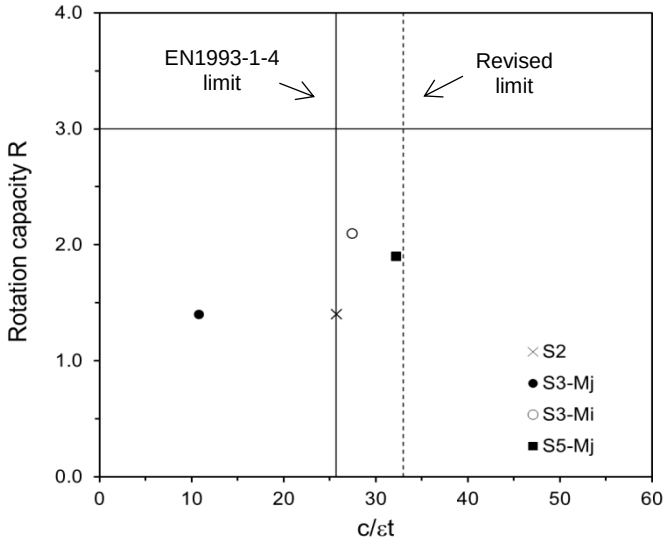

Fig. 8.2. Class 1 limit assessment for simply supported beams.

Figure 8.2 indicates that both Class 1 cross-sectional classification limits appear to be unsafe for the tested specimens, since none of them reach the required rotation limit expected from their c/εt slenderness. This can be attributed to the less ductile behaviour of ferritic stainless

steel grades compared to austenitic and duplex grades, and it is in line with results reported by Afshan and Gardner (2013a). Nevertheless, it should be noted that these conclusions are based on a single experimental specimen with a c/εt ratio lower that the corresponding Class 1 limit for the codified classification. The plastic moment capacity of these cross-sections is not clearly defined due to their nonlinear stress-strain behaviour and consequently the R≥3 criterion should be revised when stainless steel cross-sections are considered. Theofanous et al. (2014) proposed alternative criteria based on cross-sectional deformation capacity for determining whether global plastic design can be considered, which will be analysed in the following sections.

Figure 8.3 presents the measured experimental load-end rotation curves for the ferritic stainless steel continuous beam tests reported in chapter 4. Measured loads have been normalized by the collapse loads determined according to conventional plastic design F_{coll} calculated following the procedures described in the following sections. This Figure demonstrates that the consideration of plastic design overestimates the capacity of all the tested beams, since none of the cross-sections has the sufficient rotation capacity to develop a full plastic mechanism and reach the corresponding collapse load. Therefore these specimens cannot be experimentally considered as Class 1 cross-sections. These results reinforce the conclusions presented above, highlighting that both analysed classifications provide unsafe Class 1 predictions for cold-formed ferritic RHS and SHS.

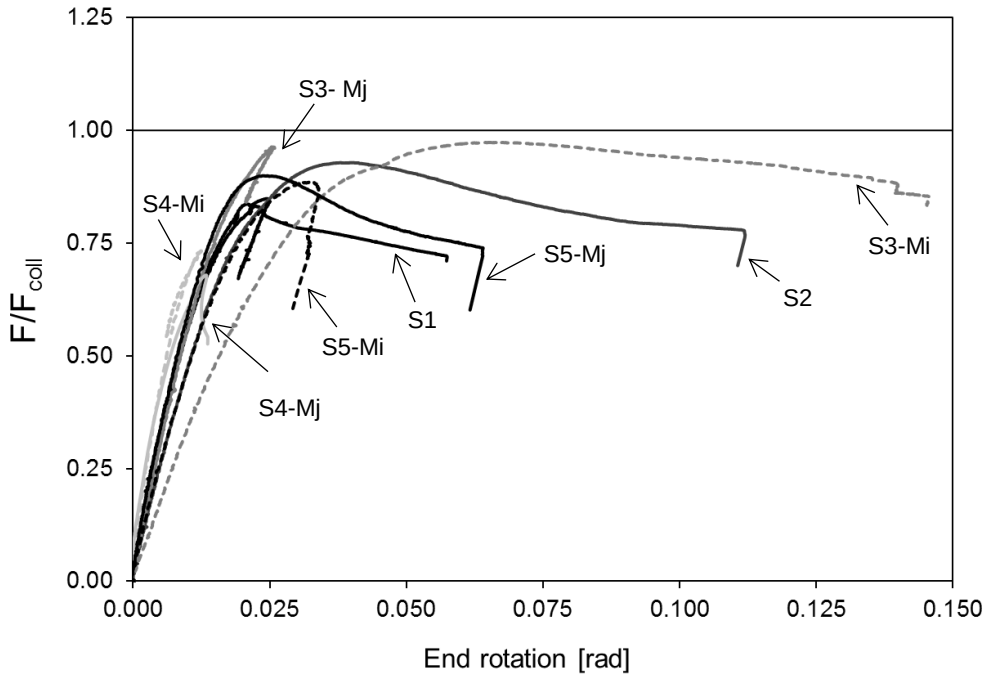

Fig. 8.3. Normalized load-end rotation experimental curves for continuous beam tests.

8.3 Assessment of design methods based on global elastic analysis

Various metallic alloys such as stainless steel exhibit a nonlinear stress-strain relationship, even for low strain values, together with pronounced gradual yielding and this material response needs to be considered when proposing specific design expressions. European design guidance for stainless steel EN1993-1-4 (2006), based on EN1993-1-1 (2005) specification for carbon steel, considers four cross-sectional Classes depending on their local buckling susceptibility, and a different resistance is assigned to each Class. Nevertheless, no plastic design is allowed for stainless steel elements in EN1993-1-4 (2006) despite their high ductility, which, with the fact that strain hardening effects are not considered when stainless steel structures are designed, leads to overly conservative load carrying capacity predictions.

For the continuous beams analysed in this chapter, EN1993-1-4 (2006) states that the entire beam fails when the first plastic hinge is formed at the $M_{c,Rd}$ bending capacity obtained from the equations presented in chapter 6. For Class 1 and 2 cross-sections the plastic bending capacity M_{pl} is considered, while for Class 3 cross-sections the elastic bending capacity M_y is assigned and for Class 4 sections effective section properties need to be calculated. However, the analysis conducted in chapter 6 for cross-sectional resistance demonstrated that including strain hardening effects into bending capacity predictions considerably improves the obtained results, particularly for austenitic and duplex stainless steel beams. Therefore, the assessment of design methods based on global elastic analysis presented in this section will consider all the different approaches investigated in chapter 6 for bending moment resistance predictions, including the Continuous Strength Method (CSM) and the Direct Strength Method (DSM).

The assessment of design methods based on global elastic analysis is reported in Table 8.1 for austenitic, ferritic and duplex stainless steel continuous beams comparing experimental and FE strengths with the loads at which the first plastic hinge is formed F_{h1}. In the analysis test results reported in chapter 4 have been considered, together with the collected experimental data presented in chapter 2 and the results derived from the parametric study presented in chapter 5. For each stainless steel grade the mean values and coefficients of variation (COVs) of the predicted-to-experimental (or FE) ratios $F_{h1,pred}/F_u$ corresponding to the different bending capacity predictions are provided.

Table 8.1. Assessment of design methods based on global elastic analysis.

Grade		$F_{h1,EN}/F_u$	$F_{h1,EN,rev}/F_u$	$F_{h1,CSM}/F_u$	$F_{h1,DSM}/F_u$
Austenitic	Mean	0.63	0.64	0.74	0.83
	COV	0.134	0.139	0.106	0.122
Ferritic	Mean	0.74	0.76	0.79	0.78
	COV	0.107	0.131	0.121	0.125
Duplex	Mean	0.69	0.70	0.74	0.77
	COV	0.106	0.149	0.101	0.123
All	Mean	0.69	0.70	0.76	0.79
	COV	0.132	0.157	0.114	0.127

$F_{h1,EN}$ corresponds to the bending capacity predictions according to the codified classification limits in EN1993-1-4 (2006), while $F_{h1,EN,rev}$ stands for the revised limits proposed by Gardner and Theofanous (2008). $F_{h1,CSM}$ and $F_{h1,DSM}$ correspond to the bending capacities calculated according to the CSM provisions and the DSM approach proposed in chapter 6, respectively. According to the results reported in Table 8.1 the ultimate load predictions tend to be highly conservative and scattered when design methods based on global elastic analysis are considered, regardless the predicted bending moment capacity. However, higher $F_{h1,pred}/F_u$ ratios are observed for the approaches that consider strain hardening effects, such as the CSM and the DSM. Since most of the analysed cross-sections show considerably low cross-section slendernesses, this overconservatism can be attributed partly to strain hardening effects but mainly to the bending moment redistribution capacity of the beams. As it can be observed, the most conservative results are obtained for austenitic and duplex stainless steel beams, followed by ferritic beams. This is in line with the typical stress-strain diagrams shown by these grades, where austenitics exhibit the highest $\sigma_u/\sigma_{0.2}$ ratios and ferritics have the less enhanced material response. Thus, it is essential for an efficient use of stainless steel structures to provide design guidance where both strain hardening and bending moment redistribution are considered.

Similar results can be observed in Figure 8.4, where the predicted-to-experimental (and FE) load ratios are depicted against the corresponding local slenderness for the bending resistances determined according to EN1993-1-4 (2006) and the DSM approach proposed in chapter 6. The local cross-section slendernesses were calculated from $\lambda_l = \sqrt{\sigma_{0.2}/\sigma_{cr}}$, where σ_{cr} is the critical buckling stress obtained from a buckling analysis conducted with CUFSM (Schafer and Ádány (2006)). In the Figure corresponding to EN1993-1-4 (2006) resistance provisions, Class 1, Class 2 and Class 3 limits have also been depicted for comparison.

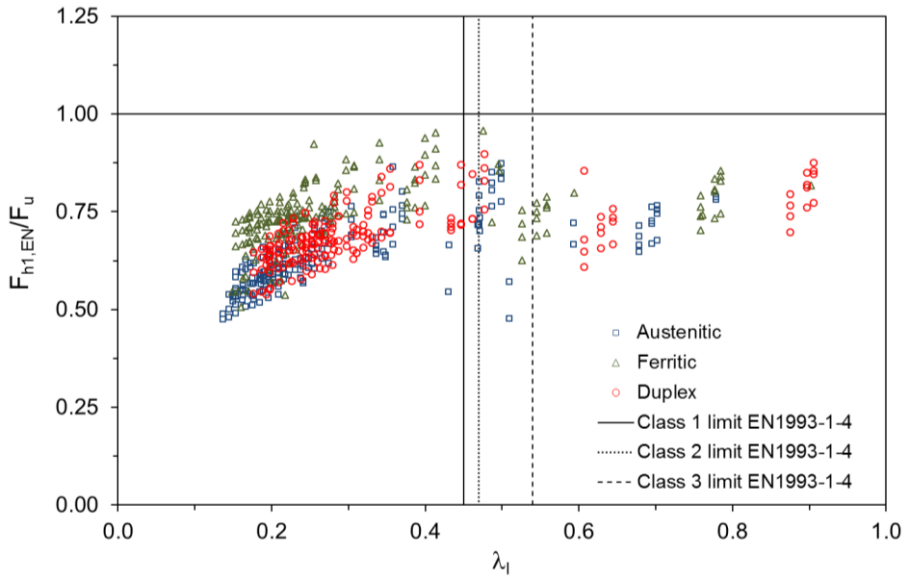

a) Bending resistance according to EN1993-1-4 provisions

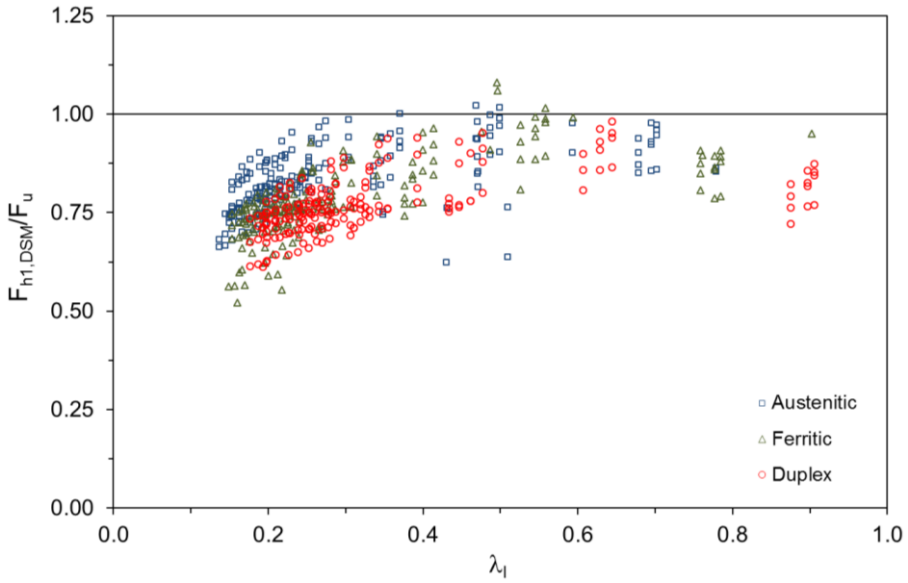

b) Bending resistance according to DSM provisions

Fig. 8.4. Assessment of design methods based on elastic analysis for different approaches.

As it is demonstrated in Figure 8.4a, the most conservative results corresponding to the EN1993-1-4 (2006) approach are obtained for the stockiest cross-sections. These predictions become more accurate as the local slenderness λ_l increases, as cross-sections become more slender and get closer to the Class 2 limit so the redistribution is less evident. The drop in the $F_{h1,pred}/F_u$ ratios for specimens with slendernesses higher than the Class 3 limit corresponds to the prediction of the effective section properties for Class 4 cross-sections. For the DSM approach assessed in Figure 8.4b the predicted capacities are found to be closer to the experimental and numerical strengths as strain hardening effects are accounted for and since no discrete transition in the bending moment capacity is considered, the transition in result accuracy is smoother.

8.4 Assessment of design methods based on global plastic analysis

The results presented in the previous section for stainless steel RHS and SHS continuous beams with stocky cross-sections demonstrated that the adoption of design methods based on global elastic analyses, as currently codified in EN1993-1-4 (2006), provides overly conservative strength predictions. As demonstrated in section 8.3, including strain hardening effects in the formulation improves the obtained results but they are still overly conservative, which indicates that bending moment redistribution also needs to be accounted for in the design of stainless steel structures. Although EN1993-1-4 (2006) does not currently allow plastic design for stainless steel elements in despite their high ductility, the assessment of the different design methods based on global plastic analysis is presented in this section and their possible application to stainless steel structures is investigated.

8.4.1 Traditional global plastic design

European standard for carbon steel structures EN1993-1-1 (2005) allows the traditional global plastic design method to be adopted for those structures with stocky cross-sections by considering a plastic collapse mechanism similar to that shown in Figure 8.5 and a rigid-plastic material response based on the formation of plastic hinges. L_s corresponds to the considered span length, while L_1 is the distance between the applied load and the internal support, as previously defined in Figure 5.8 in chapter 5.

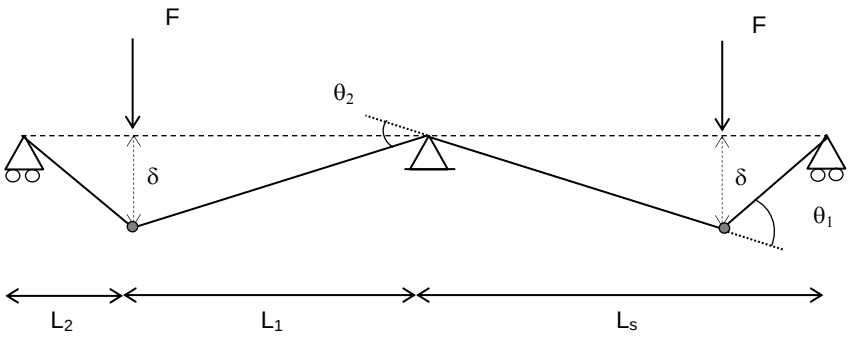

Fig. 8.5. Plastic collapse mechanism for two span continuous beams.

The collapse load is calculated through the virtual work principle, where the external work done by the applied loads F_k acting through virtual displacements δ_k is equated to the internal work resulting from the hinge rotations θ_i as given in Eq. (8.2).

$$\sum_k F_k \delta_k = \sum_i M_i \theta_i \tag{8.2}$$

Plastic design is limited to those cross-sections showing a sufficient rotation capacity to allow moment redistribution in the structure. EN1993-1-1 (2005) and EN1993-1-4 (2006) consider these cross-sections as Class 1. However, and in order to assess the applicability of global plastic design to stainless steel RHS and SHS continuous beams, Figure 8.6 presents the comparison of the calculated collapse loads F_{coll} with the experimental and numerical strengths for all specimens regardless the cross-section Class. F_{coll}/F_u ratios are plotted against the analytically calculated cross-section slenderness λ_l for the considered loading configurations through the L_1/L ratios. Codified EN1993-1-4 (2006) and revised Class 1 limits are also shown in Figure 8.6. The reason why the analytical slendernesses are considered is that when a cross-section is classified, $c/\varepsilon t$ ratios are analytically calculated without considering any element interaction. Hence, the definition of Class 1 limit should be inferred from this calculated slenderness.

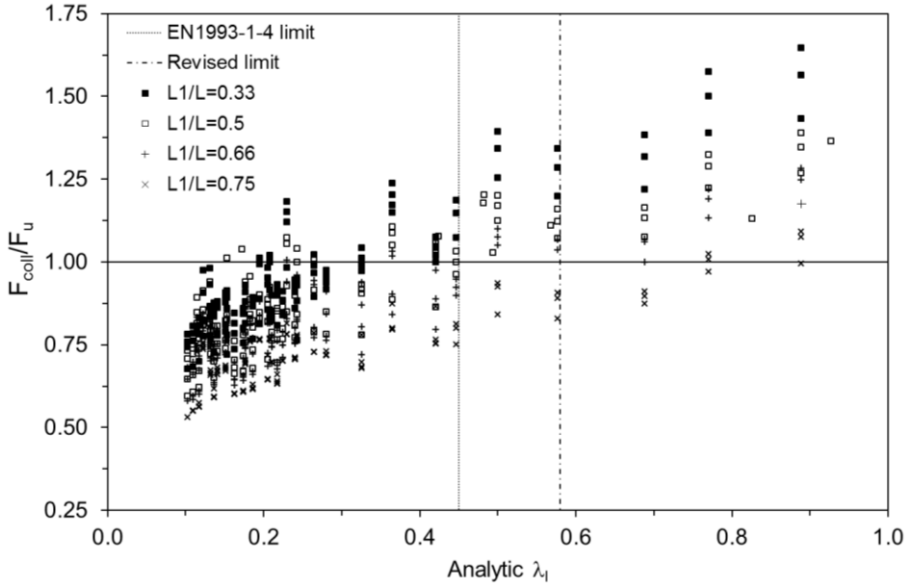

Fig. 8.6. Assessment of the traditional plastic design method for different loading configurations.

Figure 8.6 demonstrates that although the Class 1 limit currently codified in EN1993-1-4 (2006) provides a reasonable distinction between those specimens where global plastic design is applicable, results also depend on the considered structural configuration. The highest F_{coll}/F_u results are obtained for specimens with L_1/L=0.33 and decrease as the L_1/L ratio increases. The same tendency is observed for all three stainless steel grades and this suggests that the interaction between the bending moment and the local transverse forces influence the strength of the beam.

Figure 8.7 presents similar results corresponding to the traditional global plastic design F_{coll}/F_u but for the different stainless steel grades analysed and where local slendernesses determined from CUFSM (Schafer and Ádány (2006)) have been considered, as for Figure 8.4. Codified EN1993-1-4 (2006) and revised Class 1 limits are also shown.

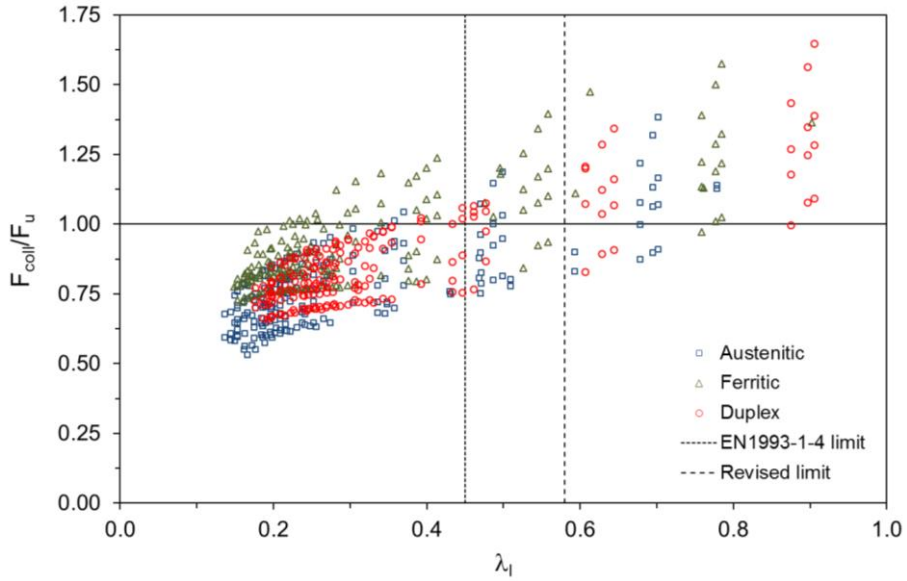

Fig. 8.7. Assessment of the traditional plastic design method for different stainless steel grades.

As it is appreciated in Figure 8.7, the capacity of the most slender specimens is overpredicted when global plastic design is considered, while the predictions get more accurate for cross-sections showing an intermediate slenderness. For the stockiest cross-sections, where the effect of strain hardening is more influential, the consideration of an elastic-perfectly plastic material results in overconservative predictions. A similar behaviour is observed for all the analysed materials, although predictions for austenitic stainless steel continuous beams are found to be the most conservative, followed by duplex and ferritic grades. However, Figure 8.7 shows that the strength of several ferritic specimens with low local slenderness and loading configurations with $L_1/L=0.33$ is overestimated when traditional plastic design is considered. This is caused by the less ductile behaviour typically exhibited by these stainless steel grades, although the statistical analyses presented in the following section will overcome these few unsafe results.

8.4.2 CSM for indeterminate structures

The assessment of the traditional plastic design approach demonstrated that for continuous beams showing low cross-section slendernesses conservative strength predictions are obtained, since only the yielding of the cross-sections is considered without accounting for strain hardening effects. Similar conclusions were also reported by Theofanous et al. (2014) from an experimental programme where austenitic and lean duplex stainless steel continuous beams with RHS, SHS and I-sections were investigated. Theofanous et al. (2014) assessed the applicability of an alternative approach developed by Gardner et al. (2011) for carbon steel indeterminate structures to different stainless steel grades. The Continuous Strength Method (CSM) for indeterminate structures is also based on global plastic design but bending moment capacities including enhanced material properties are assigned to the plastic hinges instead of the plastic moment capacities M_{pl}. This modification of the traditional plastic analysis assigns the full CSM cross-sectional resistance to the critical plastic hinge and allows a degree of strain hardening for the rest of the hinges.

The critical hinge is that showing the largest rotation capacity demand relative to the deformation capacity of the cross-section. The rotation demand of each hinge is calculated using Eq. (8.3), where θ_i is the rotation derived from kinematic considerations for the collapse mechanism considered, h_i is the section height at the considered location and $(\varepsilon_{CSM}/\varepsilon_y)_i$ is the corresponding normalized CSM strain ratio at the i^{th} hinge.

$$\alpha_i = \frac{\theta_i \cdot h_i}{\left(\varepsilon_{CSM} / \varepsilon_y\right)_i} \tag{8.3}$$

Once the critical hinge is identified, the rest of relative rotation demands are obtained from Eq. (8.4), and the corresponding bending capacities are calculated. The limits designated in Eq. (8.4) represent the CSM applicability limits stated in Afshan and Gardner (2013b) and Bock et al. (2015a) due to material ductility requirements in EN1993-1-1 (2005) and to avoid

overpredictions through the adopted bilinear material models. According to the method, the full deformation capacity is exploited for the first plastic hinge obtaining M_{CSM} from Eq. (8.5), while for subsequent plastic hinges deformations are reduced in proportion to the plastic hinge rotation ratios through the calculated ε_{CSM} values. The collapse load is calculated through the virtual work principle as in conventional plastic design but adopting the predicted bending capacities at each plastic hinge instead of the traditional plastic moment capacity M_{pl}.

$$\left(\frac{\varepsilon_{CSM}}{\varepsilon_y}\right)_i = \frac{\alpha_i}{\alpha_{crit}}\left(\frac{\varepsilon_{CSM}}{\varepsilon_y}\right)_{crit} \leq \left(\frac{\varepsilon_{CSM}}{\varepsilon_y}\right)_{i,limit} \tag{8.4}$$

$$\frac{M_{CSM}}{M_{pl}} = 1 + \frac{E_{sh}}{E}\frac{W_{el}}{W_{pl}}\left(\frac{\varepsilon_{CSM}}{\varepsilon_y} - 1\right) - \left(1 - \frac{W_{el}}{W_{pl}}\right)\cdot\left(\frac{\varepsilon_{CSM}}{\varepsilon_y}\right)^{-2} \tag{8.5}$$

According to Eq. (8.3), the relative rotation demand α_i of each hinge is proportional to the absolute rotation demands θ_i shown in Figure 8.5, since the cross-section height h_i and basic $(\varepsilon_{CSM}/\varepsilon_y)_i$ ratios are constant along the member length for the analysed specimens. Therefore, the capacities of the plastic hinges with reduced deformation can be determined from the absolute rotation demands θ_i. For those loading configurations where the distance between the internal support and the load is lower than the half of the span $L_1 \leq L_s/2$, the critical hinge is that formed in the support section, while for $L_1 \geq L_s/2$ configurations the critical hinge is formed in the loading section. For $L_1 = L_s/2$ all three plastic hinges require the same relative rotation demands.

Sufficient deformation capacity for moment redistribution to occur is usually guaranteed by ensuring a rotation capacity of $R \geq 3$. However, as previously highlighted, this criterion should be revised when considering stainless steels as the plastic moment capacity of these cross-sections is not clear. Gardner et al. (2011) proposed a new criterion based on deformation capacity in order to guarantee that a cross-section is capable of moment redistribution in indeterminate structures with a minimum value of $\varepsilon_{CSM}/\varepsilon_y \geq 3$ for I-sections and 3.6 for box sections, where ε_{CSM} is the CSM strain and ε_y is the yielding strain.

This limit corresponds to the $\varepsilon_{CSM}/\varepsilon_y$ ratio at which the calculated CSM bending capacity M_{CSM} equals the plastic bending moment M_{pl}, which happens at a local slenderness $\lambda_l = 0.47$ according to the CSM curve given in chapter 6. If the M_{CSM}/M_{pl} ratios of the considered cross-sections are plotted against the corresponding local slenderness λ_l as in Figure 8.8, it can be appreciated that $M_{CSM}/M_{pl} = 1$ values are observed for slenderness values approximately equal to 0.5 for the different stainless steel grades.

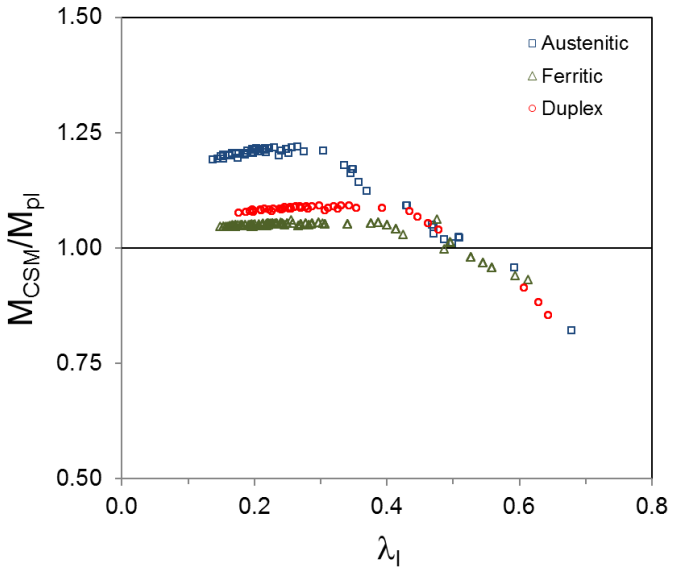

Fig. 8.8. Assessment of the applicability limit for the CSM for indeterminate structures.

Figure 8.9 presents the predicted capacities calculated using the CSM for indeterminate structures $F_{coll,CSM}$ normalized by the experimental and numerical strengths for austenitic, ferritic and duplex stainless steel continuous beams. Results are again plotted against the corresponding local slenderness determined from CUFSM calculations. Only results corresponding to local slendernesses lower than $\lambda_l \leq 0.47$ are considered in the analysis, since for more slender cross-sections the CSM would predict bending moments between the elastic and plastic bending capacities and the calculated collapse loads would not be comparable with traditional design plastic design results.

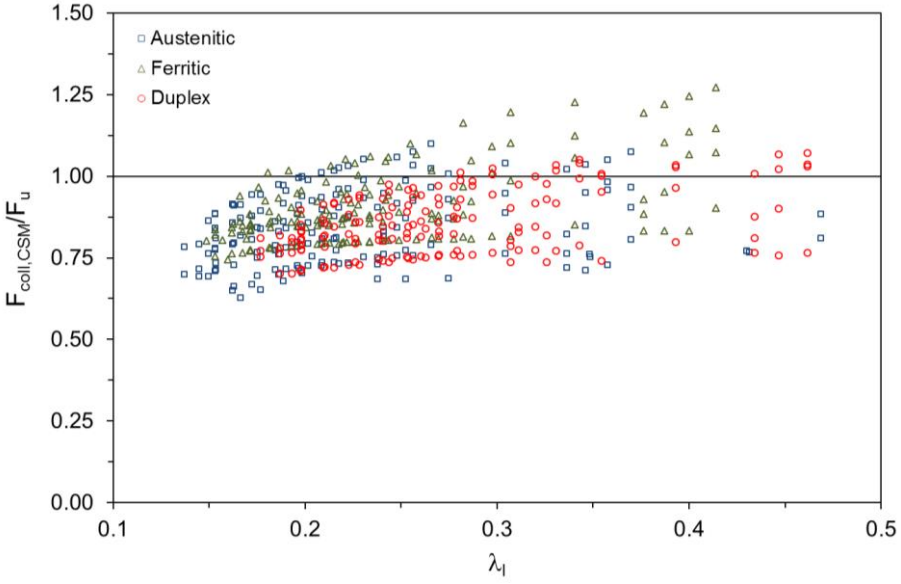

Fig. 8.9. Assessment of the CSM for indeterminate structures for different stainless steel grades.

The comparison between Figures 8.7 and 8.9 demonstrates that the strength prediction of stainless steel continuous beams is clearly improved when the strain hardening effects are

incorporated to the strength calculation along with the redistribution of bending moments. This improvement is more evident for austenitic specimens, while only slight modifications are appreciated for ferritics, stainless steel grades showing lowest $\sigma_u/\sigma_{0.2}$ ratios.

8.4.3 Assessment of design methods based on global plastic analysis

The numerical assessment and comparison of the analysed plastic design methods is presented in Table 8.2. The mean values and coefficients of variation (COVs) of the predicted-to-experimental (or FE) ratios are reported for the different design approaches and stainless steel grades. The assessment of the traditional plastic design is investigated for those cross-sections classified as Class 1 according to the classification limit codified in EN1993-1-4 (2006) and the revised limit proposed by Gardner and Theofanous (2008), denoted as $F_{coll,EN}/F_u$ and $F_{coll,EN,rev}/F_u$ respectively. Results corresponding to the CSM for indeterminate structures $F_{coll,CSM}/F_u$ showing local slendernesses lower than $\lambda_l \leq 0.47$ are also reported.

According to the results reported in Table 8.2, it is evident that allowing plastic design in stainless steel structures considerably improves the ultimate capacity prediction of continuous beams. However, and as mentioned previously, the adoption of an elastic-perfectly plastic material response results in still considerably conservative capacity predictions for stainless steel grades characterized by high strain hardening effects. Including enhanced material properties together with global plastic design methods in design approaches provides much more accurate capacity predictions, as shown for the CSM in Table 8.2. Thus, the CSM for indeterminate structures is found to be the best design approach for all analysed materials from the mean F_{pred}/F_u ratios with marginally lower scattered previsions.

Table 8.2. Assessment of design methods based on global plastic design.

Grade		$F_{coll,EN}/F_u$	$F_{coll,EN,rev}/F_u$	$F_{coll,CSM}/F_u$
Austenitic	Mean	0.75	0.75	0.84
	COV	0.169	0.166	0.132
Ferritic	Mean	0.87	0.89	0.90
	COV	0.128	0.153	0.126
Duplex	Mean	0.81	0.83	0.86
	COV	0.126	0.155	0.113
All	Mean	0.81	0.82	0.87
	COV	0.153	0.172	0.127

Although results reported in Table 8.2 provide mean F_{pred}/F_u ratios lower than unity, the capacity of several specimens is overpredicted, as highlighted in Figures 8.6, 8.7 and 8.9, particularly for loading configurations with low L_1/L ratios ($L_1/L=0.33$). Hence, the reliability of these design approaches is assessed by conducting the relevant statistical analyses for the traditional global plastic design approach (considering both cross-section classification limits) and the CSM approach for indeterminate structures.

The validation has been derived, as in previous chapters, according to EN1990, Annex D (2005) specifications and following the steps described in Tankova et al. (2014). Statistical parameters corresponding to the material and geometrical variations of the different stainless steel grades analysed have been extracted from Afshan et al. (2015). The considered material overstrength ratios are 1.3 for austenitic stainless steel, 1.2 for ferritics and 1.1 for duplex and lean duplex grades, with COVs equal to 0.060, 0.045 and 0.030 respectively, and the COV of the geometric properties was taken as 0.050. The variability due to FE modelling was also included in the analysis thought the procedure described in Bock et al. (2015c), since some deviation between tests and the modelled reality usually occurs, resulting in V_{FE}=0.015.

A summary of the most relevant statistical parameters is presented in Table 8.3, where b is the mean value of the correction factor, V_δ is the coefficient of variation of the errors of each approach relative to the experimental results and V_r is the combined coefficient of variation. Finally γ_{M0} corresponds to the calculated partial safety factor for each stainless steel grade.

Table 8.3. Summary of the reliability analysis results for current global plastic design methods for continuous beams.

	Grade	b	V_δ	V_r	γ_{M0}
Traditional plastic design for EN1993-1-4 limits	Austenitic	1.336	0.164	0.182	0.95
	Ferritic	1.144	0.121	0.131	1.03
	Duplex	1.229	0.123	0.138	1.05
Traditional plastic design for revised limits	Austenitic	1.318	0.162	0.181	0.96
	Ferritic	1.085	0.143	0.152	1.18
	Duplex	1.196	0.147	0.159	1.16
CSM-based plastic design	Austenitic	1.175	0.131	0.154	0.95
	Ferritic	1.097	0.120	0.130	1.07
	Duplex	1.155	0.112	0.127	1.08

According to the results reported in Table 8.3 and the partial safety factor γ_{M0} currently provided in EN1993-1-4 (2006) for cross-sectional resistance, equal to 1.10, the traditional plastic design approach can be safely applied for all stainless steel grades if the Class 1 limit codified in EN1993-1-4 (2006) is considered. Same conclusions can be derived for the CSM approach for indeterminate structures since the calculated γ_{M0} values also lay below the provided γ_{M0}=1.10 value. However, according to the partial safety factors γ_{M0} reported in Table 8.3 for the traditional plastic design approach considering the revised Class 1 limit proposed by Gardner and Theofanous (2008), strength predictions are too optimistic for the considered ferritic and duplex stainless steel grades. Consequently, and although the revised classification limits suggested by Gardner and Theofanous (2008) for stainless steel Class 3 and Class 2 cross-sections were found to be more accurate than the codified limits in chapter 6, the limit provided for Class 1 cross-sections cannot be safely used according to the analysed data.

8.5 New proposal for global plastic design based on DSM provisions

The design approaches based on global plastic design assessed in previous section, particularly the CSM for indeterminate structures, have been found to be an excellent alternative for the design of stainless steel continuous beams, since strain hardening effects and bending moment redistribution are considered. The approaches have also been demonstrated to satisfy the reliability requirements for the safe application of the CSM for indeterminate structures and the traditional plastic analysis approach for the EN1993-1-4 (2006) Class 1 limit. However, and since alternative design expressions have been proposed in chapter 6 based on the Direct Strength Method (DSM), a modification of the CSM for indeterminate structures is proposed in this last section adapting it to DSM provisions.

8.5.1 Development and assessment of the new DSM approach for plastic design

The CSM method assigns, as described in the previous section, the full CSM deformation capacity to the critical hinge, and deformations are reduced for subsequent plastic hinges in proportion to the relative rotation ratios. Thus, the full CSM bending moment capacity is assigned to the first plastic hinge while reduced capacities based on the absolute rotation demands θ_i are assigned to the rest. The same principle can be adopted for a modified DSM approach for indeterminate structures, where the full DSM bending capacity M_{DSM} is assigned to the critical hinge and reduced capacities are adopted for the subsequent plastic hinges. The analysed specimens present a constant cross-section along the length so these reductions can be determined from the absolute rotation demands θ_i. The DSM approach for stainless steel RHS and SHS beams proposed in chapter 6 is based on the cross-section slenderness of the specimen, from which the bending capacity M_{DSM} is calculated. In the proposed method, the bending resistance associated to each plastic hinge is determined from an equivalent local slenderness λ_l^* determined from Eq. (8.6), being θ_{crit} the absolute rotation demand of the critical hinge.

$$\lambda_{l,i}^* = \frac{\theta_{crit}}{\theta_i}\lambda_l \tag{8.6}$$

Once the equivalent local slenderness λ_l^* of each particular hinge is determined, the corresponding bending capacity is calculated from the equations proposed in chapter 6 and the collapse load is calculated through the virtual work principle as in conventional plastic design. In order to verify that the member presents sufficient deformation capacity for moment redistribution to occur, a criterion based on deformation capacity is also proposed. For simplicity, the c/εt limit adopted for the Class 1 cross-sections in EN1993-1-4 (2006) has been adopted, which corresponds to a slenderness equal to $\lambda_l \leq 0.45$ for internal elements in pure compression. Note that this limit is almost the same adopted by the CSM approach for indeterminate structures, as described in section 8.4.2 and Figure 8.8.

Figure 8.10 plots the numerical and experimental strengths against the predicted capacities for the global plastic design approaches assessed in Tables 8.2 and 8.4, including the proposed DSM-based approach. The different Figures clearly show the improvement introduced by the approaches at which enhanced material properties are included (see Figures 8.10c and 8.10d) compared to those only including bending moment redistribution (Figures 8.10a and 8.10b).

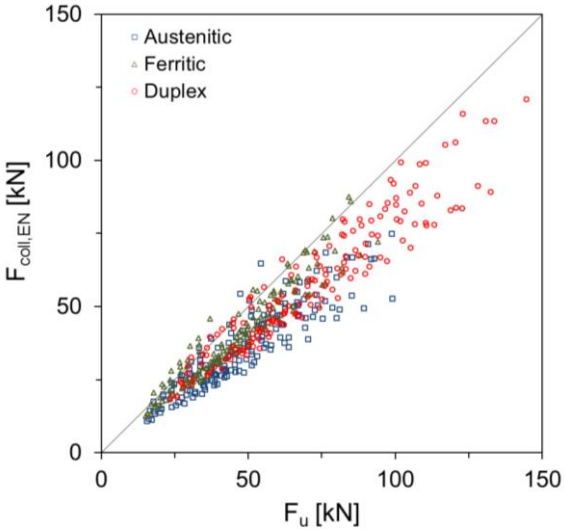

a) Traditional plastic design for codified classification limits

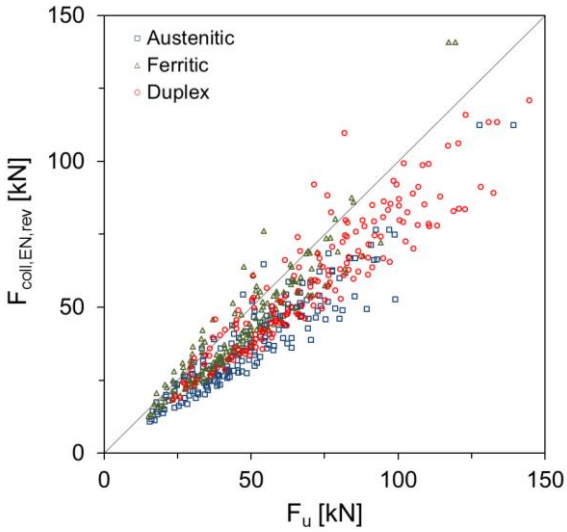

b) Traditional plastic design for revised classification limits

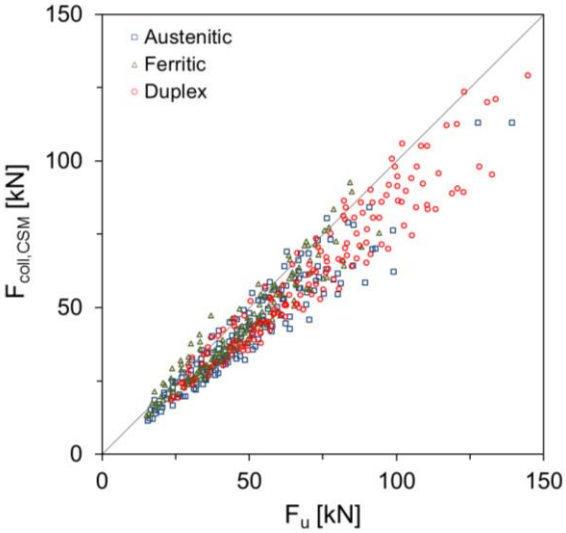

c) CSM for indeterminate structures

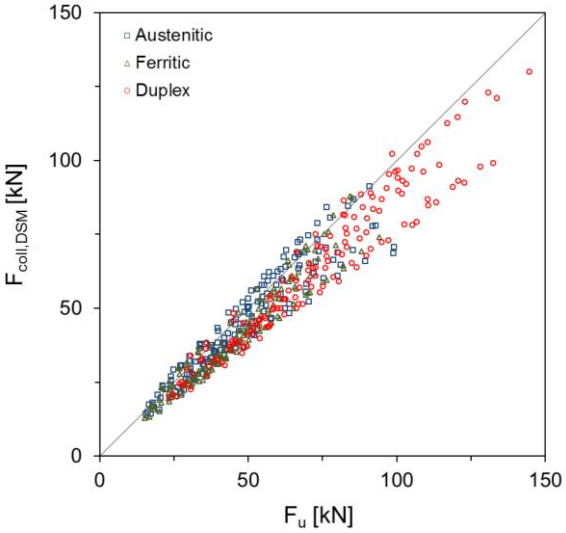

d) Proposed DSM approach for indeterminate structures

Fig. 8.10. Assessment of design methods based on global plastic analysis for different stainless steel grades.

The assessment to the proposed approach is reported in Table 8.4, where mean values and COVs of the predicted-to-experimental (or FE) ratios are presented. Results indicate that, as strain hardening effects and bending moment redistribution are considered, the adapted DSM approach for continuous beams provides excellent strength predictions for all grades. Although

mean values are slightly higher than those reported in Table 8.3 for the CSM, particularly for austenitic specimens, both methods are essentially the same.

Table 8.4. Assessment of the proposed DSM design approach.

Grade		$F_{coll,DSM}/F_u$
Austenitic	Mean	0.94
	COV	0.118
Ferritic	Mean	0.88
	COV	0.109
Duplex	Mean	0.87
	COV	0.100
All	Mean	0.89
	COV	0.115

8.5.2 Reliability analysis

Finally, the reliability of the proposed DSM plastic design approach is demonstrated through the corresponding statistical analysis for stainless steel RHS and SHS continuous beams. The validation has been derived according to EN1990, Annex D (2005) specifications as described in section 8.4.3 in order to allow the comparison among the different methods and the summary of the most relevant statistical parameters is presented in Table 8.5. According to the results gathered in Table 8.5 the proposed DSM-based approach can also be safely applied for all stainless steel grades if the partial safety factor γ_{M0} currently codified in EN1993-1-4 (2006) is considered, since the calculated γ_{M0} values lay below 1.10.

Table 8.5. Summary of the reliability analysis results for the proposed DSM approach for continuous beams according to Annex D in EN1990.

Grade	b	V_δ	V_r	γ_{M0}
Austenitic	1.067	0.119	0.144	1.07
Ferritic	1.127	0.106	0.127	1.04
Duplex	1.141	0.100	0.116	1.06

Nevertheless, and since the new proposal adopts the bending moment capacities calculated from the DSM approach proposed in chapter 6, additional reliability analyses have been conducted. The procedure provided in section F of the North American Specification AISI-S100-12 (2012) has been followed and the same statistical parameters corresponding to the material and geometrical variations have been adopted. Australian and American codes prescribe resistance factors ϕ equal to 0.9 for tubular cross-sections in bending with a target reliability index of β=2.5. In the calculation of the reliability indexes the load data and factors from the Commentary of AS/NZS4600 (2005) have been considered and a dead-to-live load ratio of 1/5 has been assumed. The calculated reliability indexes for the DSM approach for austenitic, ferritic and duplex stainless steel RHS and SHS continuous beams are reported in Table 8.6.

Table 8.6. Summary of the reliability analysis results for the proposed DSM approach for continuous beams according to AISI-S100-12.

Grade	Calculated reliability index β
Austenitic	3.21
Ferritic	3.30
Duplex	3.03

Considering the resistance factors ϕ prescribed in AS/NZS 4673 (2001) and SEI/ASCE 8-02 (2002) equal to 0.9, results in Table 8.6 demonstrate that the proposed approach can be also safely applied to all the studied stainless steel grades according to AISI-S100-12 (2012) since calculated indexes are higher than the target reliability index β=2.5.

8.6 Summary of proposals and concluding remarks

This chapter provides a comprehensive analysis on stainless steel RHS and SHS continuous beams. Current EN1993-1-4 (2006) provisions do not allow global plastic design in stainless steel structures despite their high ductility, and the failure of the structure is limited to the load at which the first plastic hinge is formed. The analysis of experimental and numerical stainless continuous beam strengths demonstrated that ultimate capacity predictions calculated based on the first hinge formation result in a considerable overconservatism due to strain hardening effects and the bending moment redistribution capacity of the beams.

The assessment of the traditional global plastic design methods with the Class 1 cross-section limits provided in EN1993-1-4 (2006) and suggested by Gardner and Theofanous (2008) has been presented. It has been concluded through relevant reliability analyses in accordance with EN1990, Annex D (2005) that although the Class 1 limit codified in EN1993-1-4 (2006) can be safely applied for the partial safety factor γ_{M0} currently provided in EN1993-1-4 (2006), the revised limit is too optimistic for ferritic and duplex stainless steel grades. However, including bending moment redistribution in capacity predictions is not enough since strain hardening effects play an important role when stocky cross-sections are analysed. Thus, the CSM for indeterminate structures has also been assessed and it has been found to be the best design approach for all analysed materials, and has also been statistically validated.

In addition, a new method has been proposed for stainless steel RHS and SHS continuous beams based on the DSM bending capacity approach suggested in chapter 6. The method adopts the basis of the CSM approach for indeterminate structures, where the full DSM bending capacity is assigned to the critical hinge while reduced capacities are adopted for the subsequent plastic hinges. This reduction is determined from an equivalent local slenderness determined from Eq. (8.6), being θ_{crit} and θ_i the absolute rotation demand of the critical hinge and the i^{th} hinge respectively, and the collapse load is calculated through the virtual work principle. The proposed method provides marginally better results than the CSM approach for indeterminate structures and its reliability has been assessed through the corresponding

statistical analyses following the procedures provided in AISI-S100-12 (2012) and EN1990, Annex D (2005).

$$\lambda_{l,i}^{*} = \frac{\theta_{crit}}{\theta_i}\lambda_l \tag{8.6}$$

Further research is necessary to extend this study to different and more complicated indeterminate structural configurations such as frames to validate the analysed and proposed expressions for more general stainless steel structures.

CHAPTER 9

Conclusions and suggestions for future research

9.1 General conclusions

Key conclusions extracted from the several research works presented in this thesis are summarized in this last chapter. The most general findings are first presented, while more specific and in detail conclusions extracted from the different chapters can be found in the next section. The chapter is concluded with few recommendations for future research building on that carried out in this thesis.

The efficient design of structures is one of the mainstays in design practise, regardless the considered construction material. This efficiency will depend on the adopted structural typology and general design, which rely on the engineers' capacity of searching for optimum solutions. However, the efficiency of a structure also depends on the design provisions codified in the different standards. Given the high material cost of stainless steel in comparison to carbon steel, the development of efficient design expressions that include all specific features of this corrosion-resistant material is crucial to incorporate it in the normal engineering practise. With design expressions that account for the nonlinear stress-strain response and strain hardening effects, stainless steels would lead to more efficient, economic and sustainable structural designs.

Therefore, the different research topics considered in this thesis had the main objective of understanding the behaviour of stainless steel Rectangular and Square Hollow Section (RHS and SHS) elements in order to identify the shortcomings of the current design specifications and develop more efficient guidance that overcome these limitations.

The research works on the structural behaviour of stainless steel element has traditionally been based on the most common austenitic and duplex stainless steel grades, although considerable investigation efforts have also been made in the study of lean duplex grades. However, ferritic stainless steels, showing substantially lower initial material cost due to the little nickel content, have only been investigated as structural material during the last years.

Therefore, the experimental programme presented in chapter 4 focused on the behaviour of ferritic stainless steel RHS and SHS elements in order to supplement the existing experimental database and provide comprehensive evidence of this stainless steel grade. The experimental programme consisted of several tests on five different cross-sections. The actual geometry and initial geometric imperfections were carefully measured and the material response of flat and corner regions of each section were characterized by conducting 20 tensile coupon tests. 10 stub column tests were performed under pure compression and 16 subjected to combined loading conditions, while 8 beams were tested under four-point bending configuration and 4 subjected to three-point bending loading conditions. The bending moment redistribution capacity of ferritic continuous beams was investigated by conducting 9 five-point bending tests. Finally, 12 tests were carried out on ferritic stainless steel RHS and SHS columns to determine the behaviour of members subjected to concentric and eccentric compression loads.

Nevertheless, and in order to present a comprehensive investigation, austenitic and duplex grades were also contemplated in the different analyses through Finite Element parametric studies described in chapter 5.

In general, the behaviour of ferritic stainless steel RHS and SHS elements is more similar to that shown by carbon steel structures, since the nonlinear stress-strain behaviour and strain hardening are less evident for these grades. The developed expressions for the description of the material behaviour of ferritic grades were therefore different from those given for the most ductile austenitic and duplex grades. However, no relevant differences were found in the prediction of strengths among the different stainless steel grades analysed in this thesis regarding the development of new design expressions, which is a very positive conclusion to be highlighted.

Chapter 3 presents a comprehensive study of the nonlinear stress-strain response of different stainless steel alloys and the modelling thereof. Over 600 experimental stress-strain curves including austenitic, ferritic and duplex grades were collected and analysed. The material model proposed by Rasmussen (2003), and currently included in Annex C of EN1993-1-4 (2006), was found to accurately represent the measured stress-strain curves for the different stainless steel grades and material types, including ferritic stainless steels for which the model had not previously been fully verified. Revised predictive equations for the strain hardening parameters n and m were recommended and expressions for ultimate tensile stress and strain for ferritic stainless steels were also proposed and are recommended for inclusion in EN1993-1-4 (2006).

Despite the nonlinear stress-strain behaviour of various metallic alloys such as stainless steel, European design guidance EN1993-1-4 (2006) considers four cross-sectional Classes depending on their local buckling susceptibility, and a different resistance is assigned to each Class. Class limits are currently codified in EN1993-1-4 (2006), although revised limits were proposed by Gardner and Theofanous (2008) for austenitic and duplex stainless steel cross-sections due to the overconservatism of the codified limits. The throughout investigations conducted in chapter 6 and chapter 8 demonstrated that although the revised classification limits were found to be more accurate than the codified limits for austenitic, ferritic and duplex stainless steel Class 3 and Class 2 cross-sections, the revised limit provided for Class 1 cross-sections cannot be safely used according to the analysed data. Therefore, it is recommended that only Class 3 and Class 2 limits proposed in Gardner and Theofanous (2008) are included in future revisions of the EN1993-1-4 (2006) specification.

The extensive analysis of the cross-section and member behaviour of austenitic, ferritic and duplex stainless steel RHS and SHS elements conducted in chapter 6, chapter 7 and chapter 8 demonstrated that the adoption of an elastic-perfectly plastic material response results in overly conservative strength predictions since enhanced material properties are ignored. The same shortcoming were identified for the compression, bending and combined loading behaviour of stainless steel cross-sections and members, and this fact was more evident for stainless steels characterized by important strain hardening effects, such as austenitics, while for ferritic grades, with low $\sigma_u/\sigma_{0.2}$ ratios, differences were not that relevant. Therefore, a full slenderness range Direct Strength Method (DSM) approach that accounts for strain hardening and local buckling effects was proposed in chapter 6 and chapter 7 for an efficient design of stainless steel cross-section and members, respectively. The approach is based on the same strength curve for all different loading conditions although some additional expressions and limitations need to be considered for each particular case, and provides more accurate strength predictions for all considered grades and loading situations than codified expressions.

Chapter 7 also presents a new CSM approach that includes strain hardening effects in the strength prediction of stocky stainless steel columns. The adoption of this new proposal in beam-column design was assessed and although the considered database only permitted a preliminary analysis, results demonstrated that the adoption of accurate end points together with an adequate interaction expression provides excellent resistance predictions of the member strength of stainless steel beam-columns. Thus, the adoption of the CSM column and beam resistances is presented as a promising design approach for stocky beam-columns where strain hardening effects are relevant. However, a more in detail study should be conducted considering a more representative database and including also duplex stainless steel specimens.

Finally, the behaviour of indeterminate stainless steel structures was investigated through a comprehensive analysis on stainless steel RHS and SHS continuous beams. Although current EN1993-1-4 (2006) provisions do not allow plastic design in stainless steel structures despite

their high ductility, the analysis conducted in chapter 8 demonstrated that strength predictions calculated based on global elastic calculations result in a considerable overconservatism due to strain hardening effects and bending moment redistribution being ignored. Thus, the Continuous Strength Method (CSM) for indeterminate structures was found to be the best design approach for all analysed materials. In addition, a DSM method that adopts the basis of the CSM approach was proposed based on the previously proposed DSM approach for beams. The proposed method provides marginally better results and its reliability was assessed through the corresponding statistical analyses. Therefore, it is concluded that the inclusion of design approaches based on plastic analysis in EN1993-1-4 (2006) provisions should be considered for a more efficient design of simple stainless steel indeterminate structures and the adoption of approaches that also include strain hardening effects is also highly recommended.

9.2 Specific conclusions

This section reports the specific conclusions derived from this thesis regarding the behaviour of stainless steel RHS and SHS cross-section and members. Although the conclusions have also been highlighted at the end of each chapter, it was considered that a gathered summary of the proposed design approaches would provide the reader a general overview of the conducted research works.

9.2.1 Description of stress-strain curves for stainless steel alloys

The study of the modelling of the stress-strain response of stainless steel alloys was investigated through an extensive database of experimental stress-strain curves, including austenitic, ferritic and duplex grades. The material model proposed by Rasmussen (2003), and currently included in Annex C of EN1993-1-4 (2006), was found to accurately represent the measured stress-strain curves for the different stainless steel grades and material types. Based on the assembled data set, values and predictive expressions for the key material parameters of the Rasmussen (2003) model were re-evaluated. A revised predictive equation (Eq. (9.1)) and revised numeric values for the strain hardening parameter *n* were recommended for all stainless steel families. A new expression for the prediction of the second strain hardening parameter *m* for all stainless steel grades presented in Eq. (9.2) was also proposed. Finally, revised predictive expressions for ultimate tensile stress and strain for ferritic stainless steels were proposed, given in Eqs. (9.3b) and (9.4b) respectively. It is recommended that these proposals are incorporated into future revisions of EN1993-1-4 (2006). Additionally, the revised values for the first strain hardening parameter *n*, presented in Table 3.12, are recommended for inclusion in EN1993-1-4 (2006). The numeric values of Young's modulus for stainless steel proposed by Afshan et al. (2013) are also recommended herein. The proposed predictive expressions and the recommended modifications to made to Annex C of EN1993-1-4 (2006) are summarised as follows:

$$n = \frac{\ln 4}{\ln\left(\frac{\sigma_{0.2}}{\sigma_{0.05}}\right)} \quad \text{for all grades} \tag{9.1}$$

$$m = 1 + 2.8\frac{\sigma_{0.2}}{\sigma_u} \quad \text{for all grades} \tag{9.2}$$

$$\frac{\sigma_{0.2}}{\sigma_u} = \begin{cases} 0.20 + 185\frac{\sigma_{0.2}}{E} & \text{for austenitic, duplex and lean duplex} \quad (9.3a) \\ 0.46 + 145\frac{\sigma_{0.2}}{E} & \text{for ferritic grades} \quad (9.3b) \end{cases}$$

$$\varepsilon_u = \begin{cases} 1 - \frac{\sigma_{0.2}}{\sigma_u} & \text{for austenitic, duplex and lean duplex} \quad (9.4a) \\ 0.6 \cdot \left(1 - \frac{\sigma_{0.2}}{\sigma_u}\right) & \text{for ferritic grades} \quad (9.4b) \end{cases}$$

9.2.2 Full slenderness DSM approach for cross-sections and members

The Direct Strength Method (DSM) is a design approach that allows the consideration of local and distortional buckling effects in an easy manner through the use of strength curves and can also account for strain hardening effects considering the enhanced material property approach proposed by Rossi and Rasmussen (2013). A full slenderness range DSM approach that considers both strain hardening and local buckling interaction effects was proposed for stainless steel RHS and SHS based on the strength curve given for carbon steel structures in AISI-S100-12 (2012) and shown in Eq. (9.5). The method was developed for cross-sections in chapter 6 and for members in chapter 7. The accuracy and applicability of the proposed approaches were demonstrated from exhaustive reliability analyses for the considered loading conditions and stainless steel grades.

$$\frac{R_{enh\_nl}}{R_0} = \begin{cases} 1 + (1 - 1.29\lambda_n)\left(\frac{\sigma_u}{\sigma_{0.2}} - 1\right) & \text{for } \lambda_n \le 0.776 \\ \frac{1}{\lambda_n^{0.8}} - \frac{0.15}{\lambda_n^{0.8}} & \text{for } \lambda_n > 0.776 \end{cases} \tag{9.5}$$

$$\lambda_n = \sqrt{\frac{R_0}{R_{crl}}} \tag{9.6}$$

R_{enh_nl} is the parameter representing the predicted strength of the considered loading condition and R_0 is the reference resistance that needs to be enhanced due to strain hardening effects or reduced due to local buckling interaction. The expression is based on a local cross-section slenderness λ_n that considers the actual stress distribution of the cross-section and thus provides a better estimation of its susceptibility to local buckling effects. The generalized slenderness is calculated from Eq. (9.6), where R_{crl} represents the critical elastic local buckling load and can be obtained from a number of numerical methods and related software

programmes based on finite element and finite strip methods. Strain hardening effects are contemplated through the $\sigma_u/\sigma_{0.2}$ ratio, where σ_u and $\sigma_{0.2}$ are the tensile strength and the proof strength corresponding to the 0.2% plastic strain. The nominal R_{nl_enh}, reference resistances R_0 and critical elastic local buckling loads R_{crl} to be considered for the different loading cases are summarized in Table 9.1 and are defined as given below.

Table 9.1. Definition of R_{nl_enh}, R_0 and R_{crl} parameters for different loading cases.

	Loading condition	R_{enh_nl}	R_0	R_{crl}
Cross-section behaviour	Compression	$N_{c,Rk}$	N_y	N_{crl}
	Bending	$M_{c,Rk}$	M_n	M_{crl}
	Combined loading	$r_{c,Rk}$	r_y	r_{crl}
Member behaviour	Compression	$N_{b,Rk}$	$N_{b,ne}$	N_{crl}
	Combined loading	$r_{b,Rk}$	r_{ne}	r_{crl}

$N_{c,Rk}$ and N_y are the nominal cross-sectional compression resistance and squash load respectively, while N_{crl} corresponds to the critical elastic local buckling compression load. $M_{c,Rk}$ is the nominal bending resistance, M_{crl} corresponds to the critical elastic local buckling moment and M_n is the bending capacity of the cross-section that also contemplates the inelastic reserve strength, as given in Eq. (9.7). The compression strain factor C_y provided in "Procedure II" of AS/NZS4673 (2001) and SEI/ASCE 8-02 (2002) and defined in Eq. (9.8) needs to be adopted for stainless steel RHS and SHS beams. M_y and M_{pl} are the elastic and plastic bending capacities respectively.

$$M_n = M_y + (M_{pl} - M_y)\left(1 - \frac{1}{C_y^2}\right) \tag{9.7}$$

$$C_y = \begin{cases} 3 & \lambda_n \le 0.58 \\ 3 - 2\left(\frac{\lambda_n - 0.58}{0.196}\right) & 0.58 \le \lambda_n \le 0.776 \\ 1 & \lambda_n \ge 0.776 \end{cases} \tag{9.8}$$

When combined loading conditions are contemplated, the analysis is conducted in the N/N_y-M/M_y diagram and radial distances are considered. The nominal combined loading resistance $r_{c,Rk}$ is determined from Eq. (9.9), where N_{on} and M_{on} are the predicted cross-section compression and flexural strengths and the r_{crl} parameter that accounts for the local buckling behaviour can be obtained from Eq. (9.10), where N_{ocr} and M_{ocr} represent the compression and bending moments that cause the local buckling of the cross-section. The yielding parameter r_y is obtained from Eq. (9.11), where N_{oy} and M_{oy} are the compression and bending moments when the yielding of the cross-section occurs. For stocky cross-sections the yielding is evaluated from the interaction expression provided in EN1993-1-1 (2005) for Class 1 and Class 2 cross-

sections (Eq. (9.12)), while for slender cross-sections a linear interaction, given in Eq. (9.13), is adopted.

$$r_{c,Rk} = \sqrt{\left(\frac{N_{on}}{N_y}\right)^2 + \left(\frac{M_{on}}{M_y}\right)^2} \tag{9.9}$$

$$r_{crl} = \sqrt{\left(\frac{N_{ocr}}{N_y}\right)^2 + \left(\frac{M_{ocr}}{M_y}\right)^2} \tag{9.10}$$

$$r_y = \sqrt{\left(\frac{N_{oy}}{N_y}\right)^2 + \left(\frac{M_{oy}}{M_y}\right)^2} \tag{9.11}$$

$$\frac{M_{oy}}{M_n} = \frac{1 - N_{oy}/N_y}{1 - 0.5a} \tag{9.12}$$

$$\frac{N_{oy}}{N_y} + \frac{M_{oy}}{M_y} = 1 \tag{9.13}$$

Regarding member behaviour, similar parameter definitions need to be considered. The nominal flexural buckling strength $N_{b,Rk}$ is obtained through the flexural buckling resistance of the fully effective cross-section $N_{b,ne}$. The additional limitation given in Eq. (9.14) needs to be considered for those members with local slenderness lower than $\lambda_n \leq 0.776$ to guarantee that members are stable enough for cross-sections to reach partial yielding. It was also demonstrated that the most accurate capacity predictions were obtained when the buckling curve codified in EN1993-1-4 (2006) is considered for the determination of the basic flexural buckling resistance $N_{b,ne}$.

$$\chi\left[1 + (1 - 1.29\lambda_n)\left(\frac{\sigma_u}{\sigma_{0.2}} - 1\right)\right] \geq 1 \tag{9.14}$$

Finally, when the nominal member resistance $r_{b,Rk}$ of stainless steel members subjected to combined loading conditions is calculated, the r_{ne} parameter governing the member behaviour (Eq. (9.15)) is obtained from the classical interaction expression given in Eq. (9.16) and adopting the interaction factor *k* provided in EN1993-1-1 (2005) for carbon steel members, presented in Eq. (9.17). N_{one} and M_{one} correspond to the overall buckling strengths. The local buckling parameter r_{crl} is determined from Eq. (9.10). In order to guarantee that members are stable enough and allow incorporating enhanced material properties in beam-column resistance predictions, an equivalent condition to that imposed for columns, given in Eq. (9.18), needs to be satisfied. The method was extended to non-uniform bending moment distributions by assuming an equivalent load eccentricity as given by $e_{eq}=C_m e_0$ and the equivalent uniform moment factor $C_{m,u}$.

$$r_{ne} = \sqrt{\left(\frac{N_{one}}{N_y}\right)^2 + \left(\frac{M_{one}}{M_y}\right)^2} \tag{9.15}$$

$$\frac{N_{one}}{N_{b,ne}} + k \cdot C_m \frac{M_{one}}{M_n} = 1 \tag{9.16}$$

$$k = 1 + 0.6\lambda_c \frac{N_{one}}{N_{b,ne}} \leq 1 + 0.6 \frac{N_{one}}{N_{b,ne}} \tag{9.17}$$

$$r_{ne}\left[1 + (1 - 1.29\lambda_n)\left(\frac{\sigma_u}{\sigma_{0.2}} - 1\right)\right] \leq r_y \tag{9.18}$$

9.2.3 DSM approach for indeterminate structures

Chapter 8 provides a comprehensive analysis on stainless steel RHS and SHS continuous beams. Current EN1993-1-4 (2006) provisions do not allow plastic design in stainless steel structures despite their high ductility, and the failure of the structure is limited to the load at which the first plastic hinge is formed. The analysis of experimental and numerical stainless continuous beam strengths demonstrated that ultimate capacity predictions calculated based on the first hinge formation result in a considerable overconservatism due to strain hardening and the bending moment redistribution effects.

The assessment of the traditional plastic design methods with the Class 1 cross-section limits provided in EN1993-1-4 (2006) and suggested by Gardner and Theofanous (2008) was presented. It was concluded through relevant reliability analyses conducted in accordance with EN1990, Annex D (2005) that although the Class 1 limit codified in EN1993-1-4 (2006) can be safely applied for the partial safety factor γ_{M0} currently provided in EN1993-1-4 (2006), the revised limit is too optimistic for ferritic and duplex stainless steel grades. However, it was also highlighted that including bending moment redistribution in capacity predictions is not enough since strain hardening effects play an important role when stocky cross-sections are analysed. Thus, the Continuous Strength Method (CSM) for indeterminate structures was also assessed and it was found to be the best design approach for all analysed materials after relevant statistical validations.

Finally, a DSM method was proposed for stainless steel RHS and SHS continuous beams based on the DSM bending capacity approach previously suggested. The method adopts the basis of the CSM approach for indeterminate structures, where the full DSM bending capacity is assigned to the critical hinge while reduced capacities are adopted for the subsequent plastic hinges. This reduction is determined from an equivalent local slenderness determined from Eq. (9.19), being θ_{crit} and θ_i the absolute rotation demand of the critical hinge and the i^{th} hinge respectively, and the collapse load is calculated through the virtual work principle. The proposed method provides marginally better results than the CSM approach for indeterminate structures

and its reliability was assessed through the corresponding statistical analyses following the procedures provided in AISI-S100-12 (2012) and EN1990, Annex D (2005).

$$\lambda_{n,i}^{*} = \frac{\theta_{crit}}{\theta_i}\lambda_n \tag{9.19}$$

9.2.4 CSM approach for stocky cross-sections, columns and beam-columns

The Continuous Strength Method (CSM) is a deformation based design approach that includes strain hardening effects in the prediction of the compression and bending capacities of stocky cross-sections. It was proved to provide considerably better results than codified design expressions for cross-sections subjected to pure compression and pure bending. For the combined compression and uniaxial loading conditions, the CSM approach proposed by Liew and Gardner (2015) was found to provide accurate resistance predictions. However, a simplified CSM method was proposed in chapter 6, together with research works reported by Zhao et al. (2015a, 2015b, 2015c), where the interaction expressions codified in EN1993-1-1 (2005) are considered with the CSM compression and bending resistances, N_{CSM} and M_{CSM}, as given in Eqs. (9.20) and (9.21). This method provides accurate predictions of stocky cross-sections under combined loading keeping calculations relatively simple and its reliability was statistically demonstrated.

$$\frac{N_{Ed}}{N_{CSM}} + \frac{M_{y,Ed}}{M_{y,CSM}} + \frac{M_{z,Ed}}{M_{z,CSM}} \leq 1.0 \tag{9.20}$$

$$M_{N,CSM} = M_{CSM}\frac{1-n_{CSM}}{1-0.5a} \text{ with } n_{CSM} = \frac{N_{Ed}}{N_{CSM}} \tag{9.21}$$

Based on the DSM proposal for columns with stocky cross-sections presented in the previous section, a new expression based on the CSM was also proposed for stainless steel columns. This proposal is given in Eq. (9.22) and considers strain hardening effects for those members stable enough to reach partial yielding of the cross-section, members satisfying Eq. (9.23). The method is based on the maximum strain ε_{CSM} and strain hardening modulus E_{sh} obtained from the CSM equations given for cross-sectional resistance. The best predictions were also obtained for the flexural buckling resistance $N_{b,ne}$ obtained from the buckling curve codified in EN1993-1-4 (2006).

$$\frac{N_{b,CSM}}{N_{b,ne}} = 1 + \frac{E_{sh}}{E}\left(\frac{\varepsilon_{CSM}}{\varepsilon_y} - 1\right) \tag{9.22}$$

$$\chi\left[1 + \frac{E_{sh}}{E}\left(\frac{\varepsilon_{CSM}}{\varepsilon_y} - 1\right)\right] \geq 1 \tag{9.23}$$

An alternative CSM-based approach for beam-column design was finally assessed by assuming an interaction equation where the end points were determined according to CSM provisions for beams and the new approach proposed for columns. Preliminary results demonstrated that considering CSM-based beam and column resistances together with an adequate interaction expression provides excellent resistance predictions for stocky beam-columns where strain hardening effects are relevant. This new method was found to be a promising design approach although a more in detail study considering a more representative database is required.

9.3 Suggestions for future research

The suggestions and ideas emerged throughout the development of this thesis are proposed in this last section. Suggestions are divided in three different paths, focused on material behaviour, extension of the proposed full slenderness approach to open cross-sections and the analysis of more complicated but realistic structural configurations in order to evaluate the overall behaviour of stainless steel structures.

The expressions proposed in chapter 3 for the analytical modelling of the nonlinear behaviour of the different stainless steel grades was based on an extensive coupon test results including cold-formed and sheet materials tested in rolling and transverse directions, tension and compression. Therefore, the behaviour of stainless steel cold-formed and sheet materials are considerably well characterized. However, several stainless steel product types, such as stainless steel reinforcing bars, have not been included in the analysis. A constitutive material model definition for these elements is required in order to introduce stainless steel rebars in Eurocode 2, extending the horizons of the applicability of these corrosion resistant materials. It is expected that the two-stage material model proposed for cold-formed and sheet materials will also be applicable to stainless steel rebars, although it is possible that n values and some of the coefficients in the predictive expressions may be different and will need to be characterized. Finally, it would also be necessary to revise the constitutive model for stainless steel codified in EN1993-1-2 (2005) for elevated temperatures in order to provide a comprehensive material model for all stainless steel products in different situations.

Building on the research carried out on the full slenderness range Direct Strength Method (DSM), presented in chapters 6 and 7 of this thesis, suggestions for expanding the method to cover the design of open stainless steel cross-sections are made. The investigations derived in this thesis concluded that the strength curve currently codified for carbon steel cross-sections in AISI-S100-12 (2012) provides a better estimation of the ultimate capacity of slender stainless steel cross-sections although a different local buckling curve was proposed for these grades. The reason for the unexpected better agreement is likely related to the fact the stainless steel DSM strength curve was based on research on open sections with substantially smaller thickness than those considered in the present study on closed sections. Further research should be conducted in open sections, such as I-sections and channel sections, in order to identify the strength curve that better predicts the local buckling interaction in the different loading cases analysed in this thesis. The proposed approach that contemplates strain

hardening effects at cross-section and member level should also be assessed for these sections.

From the experimental programme described in chapter 4, and considering the available experimental data on stainless steel member behaviour, the research should be complemented by analysing not only different boundary conditions, such as fixed-fixed and pinned-fixed end restrains, but also the interaction between minor axis buckling and major axis bending. The k_{yz} and k_{zy} interaction coefficients provided in EN1993-1-1 (2005) for carbon steel members are not contemplated in EN1993-1-4 (2006). Only the axis at which the bending moment is actuating is considered with the smallest value of the flexural buckling resistances about both principal axes, resulting in overly conservative predictions. The study of the k_{yz} and k_{zy} interaction coefficients for stainless steel members through experimental and numerical strengths would allow evaluating the interaction between minor axis buckling and major axis bending and calibrating the coefficients.

The applicability of the alternative CSM-based approach proposed for beam-column design in chapter 7 should also be more extensively investigated through a more representative database that includes the most usual stainless steel grades and cross-section types. Preliminary results found this approach to be a promising design method for stocky beam-columns where strain hardening effects are relevant but it requires further investigations and reliability analyses.

Considerable research works have been conducted during the last years on hollow stainless steel specimens and the behaviour of both cross-sections and members have been widely investigated. Moreover, several new approaches that consider strain hardening and local buckling effects have been proposed. Since the behaviour of isolated elements has been considerably well captured, the research should move on to more complex but realistic structural configurations, such as stainless steel frames. Investigations should first focus on room temperature and static loading conditions and the interaction between local, member and overall frame imperfections should be studied, as well as second order effects. The analysis of the frames would allow the assessment of the CSM and DSM-based approaches for indeterminate structures for more general structural applications. The research should after be extended to fire situations and dynamic loading conditions, where the excellent elevated temperature strength retention of stainless steels would be exploited and their high ductility would be decisive in the design of structures in areas with high earthquake risk.

References

ABAQUS. (2012) ABAQUS/Standard user's manual volumes I-III and ABAQUS CAE manual. Version 6.12. Hibbitt, Karlsson & Sorensen, Inc., Pawtucket, USA.

Afshan S. and Gardner L. (2013a). Experimental study of cold-formed ferritic stainless steel hollow sections. *Journal of Structural Engineering (ASCE)*, 139(5), 717–728.

Afshan S. and Gardner L. (2013b). The continuous strength method for structural stainless steel design. *Thin-Walled Structures*, 68, 42–49.

Afshan S., Rossi B. and Gardner L. (2013). Strength enhancements in cold-formed structural sections – Part I: Material testing. *Journal of Constructional Steel Research,* 83, 177–188.

Afshan S., Francis P., Baddoo N.R. and Gardner L. (2015). Reliability analysis of structural stainless steel design provisions. *Journal of Constructional Steel Research*, 114, 293–304.

Afshan S., Zhao O. and Gardner L. (2016). Buckling curves for the design of stainless steel columns. *Journal of Constructional Steel Research*, submitted.

AISI. (1974). American Iron and Steel Institute, Specification for the design of cold-formed stainless steel structural members, Washington, D.C., 1974.

AISI. (2012). AISI- S100-12. North American specification for the design of cold-formed steel structural members. American Iron and Steel Institute (AISI). Washington, D.C., 2012.

AISI. (2016). AISI- S100-16. Revised North American specification for the design of cold-formed steel structural members. American Iron and Steel Institute (AISI). Washington, D.C., 2016.

Arrayago I. and Real E. (2015). Experimental study on ferritic stainless steel RHS and SHS cross-sectional resistance under combined loading. *Structures*, 4, 69–79.

Arrayago I. and Real E. (2016). Experimental study on ferritic stainless steel simply supported and continuous beams. *Journal of Constructional Steel Research,* 119, 50–62.

Arrayago I., Real E. and Mirambell E. (2013). Constitutive equations for stainless steels: experimental tests and new proposal. *Proceedings of The Fifth International Conference on Structural Engineering, Mechanics and Computation*, Cape Town, South Africa, 1435–1440.

Arrayago I., Bock M. and Real E. (2014). Preliminary study on the resistance of ferritic stainless steel cross-sections under combined loading. *Proceedings of the Eurosteel 2014 7th European Conference on Steel and Composite Structures*, Napoli (Italy).

Arrayago I., Real E. and Gardner L. (2015). Description of stress–strain curves for stainless steel alloys. *Materials and Design*, 87, 540–552.

Arrayago I., Real E. and Mirambell E. (2016a). Experimental study on ferritic stainless steel RHS and SHS beam-columns. *Thin-Walled Structures,* 100, 93–104.

Arrayago I., Rasmussen K.J.R. and Real E. (2016b). Full slenderness range DSM approach for stainless steel hollow cross-sections. *Eighth International Conference on Steel and Aluminium Structures*. Hong Kong, China. Submitted.

AS/NZS4600. (2005). Cold-formed steel structures. Sydney: Standards Australia; 2005.

AS/NZS4673. (2001). Cold-formed stainless steel structures. Sydney: Standards Australia; 2001.

Austin W.J. (1961). Strength and design of metal beam-columns. *Journal of the Structural Division*, 87(4), 1–34.

Becque J. and Rasmussen K.J.R. (2008). Numerical investigation and design methods for stainless steel columns failing by interaction of local and overall buckling. Research Report No. R888. Centre for Advanced Structural Engineering, School of Civil Engineering, The University of Sydney, Australia.

Becque J. and Rasmussen K.J.R. (2009a). Experimental investigation of local-overall interaction buckling of stainless steel lipped channel columns. *Journal of Constructional Steel Research*, 65, 1677–1684.

Becque J. and Rasmussen K.J.R. (2009b). A numerical investigation of local-overall interaction buckling of stainless steel lipped channel columns. *Journal of Constructional Steel Research*, 65, 1685–1693.

Becque J. and Rasmussen K.J.R. (2009c). Experimental investigation of the interaction of local and overall buckling of stainless steel I-columns. *Journal of Structural Engineering (ASCE)*, 135(11), 1340–1348.

Becque J., Lecce M. and Rasmussen K.J.R. (2008). The direct strength method for stainless steel compression members. *Journal of Constructional Steel Research*, 64, 1231–1238.

Bock M., Arrayago I., Real E. and Mirambell E. (2013). Study of web crippling in ferritic stainless steel cold formed sections. *Thin-Walled Structures*, 69, 29–44.

Bock M., Gardner L. and Real E. (2015a). Material and local buckling response of cold-formed ferritic stainless steel sections. *Thin-Walled Structures*, 89, 131–141.

Bock M., Arrayago I. and Real E. (2015b). Experiments on cold-formed ferritic stainless steel slender sections. *Journal of Constructional Steel Research,* 109, 13–23.

Bock M., Miranda F.X. and Real E. (2015c). Statistical evaluation of a new resistance model for cold-formed stainless steel cross-sections subjected to web crippling. *International Journal of Steel Structures*, 15, 1–18.

Boissonnade N., Jaspart J.P., Muzeau J.P. and Villette M. (2002). Improvement of the interaction formulae for beam columns in Eurocode 3. *Computers & structures*, 80(27), 2375–2385.

Boissonnade N., Jaspart J.P., Muzeau J.P. and Villette M. (2004). New interaction formulae for beam-columns in Eurocode 3: The French–Belgian approach. *Journal of Constructional Steel Research*, 60, 421–431.

Boissonnade N., Greiner R., Jaspart J.P. and Lindner J. (2006). Rules for Member Stability in EN 1993-1-1: Background documentation and design guidelines. ECCS European Convention for Constructional Steelwork.

Centre for Advanced Structural Engineering. Compression tests of stainless steel tubular columns. Investigation Rep. S770, 1990. University of Sydney, Australia.

Cruise R.B. and Gardner L. (2008a). Strength enhancements induced during cold forming of stainless steel sections. *Journal of Constructional Steel Research*, 64(11), 1310–1316.

Cruise R.B. and Gardner L. (2008b). Residual stress analysis of structural stainless steel sections. *Journal of Constructional Steel Research*, 64(3), 352–366.

Dawson R.G. and Walker A.C. (1972). Post-buckling of geometrically imperfect plates. *Journal of the Structural Division (ASCE)*, 98(1), 75–94.

Ellobody E. and Young B. (2005). Structural performance of cold-formed high strength stainless steel columns. *Journal of Constructional Steel Research*, 61, 1631–1649.

Ellobody E. and Young B. (2006). Experimental investigation of concrete-filled cold-formed high strength stainless steel tube columns. *Journal of Constructional Steel Research*, 62, 484–492.

Estrada I., Real E. and Mirambell E. (2005). Stainless steel girders longitudinally stiffened: behaviour in shear. Experimental and numerical analysis. *Proceedings of the Eurosteel 2005, 4th European Conference on Steel and Composite Structures*. Maastrich, Netherlands, 215–220.

Euro Inox (1994). Design Manual for Stainless Steel. Second Edition.

Euro Inox (2006). Design Manual for Structural Stainless Steel. Third Edition.

Euro Inox (2007). Design Manual for Structural Stainless Steel. Third Edition. Commentary

European Committee for Standardization (CEN). (2009). EN10088–4. Stainless steels: Part 4: Technical delivery conditions for sheet/plate and strip of corrosion resisting steels for general purposes. Brussels, Belgium.

European Committee for Standardization (CEN). (2009). ENISO 6892-1. Metallic materials - Tensile testing - Part 1: Method of test at room temperature. Brussels, Belgium.

European Committee for Standardization. (2005). EN1990. European Committee for Standardization Eurocode. Basis of structural design. Brussels, Belgium.

European Committee for Standardization. (2005). EN1993–1–1. European Committee for Standardization Eurocode 3. Design of steel structures. Part 1–1: General rules and rules for buildings. Brussels, Belgium.

European Committee for Standardization. (2005). EN1993-1-2. European Committee for Standardization Eurocode 3. Design of steel structures. Part 1-2: General rules. Structural fire design. Brussels, Belgium.

European Committee for Standardization. (2006). EN1993-1-3. European Committee for Standardization Eurocode 3. Design of steel structures. Part 1-3: General rules. Supplementary rules for cold formed members and sheeting. Brussels, Belgium.

European Committee for Standardization. (2006). EN1993-1-4. European Committee for Standardization Eurocode 3. Design of steel structures. Part 1–4: General rules. Supplementary rules for stainless steels. Brussels, Belgium.

European Committee for Standardization. (2006). EN1993-1-5. European Committee for Standardization Eurocode 3. Design of steel structures. Part 1-5: Plated structural elements. Brussels, Belgium.

Fan S., Liu F., Zheng B., Shu G. and Tao Y. (2014). Experimental study on bearing capacity of stainless steel lipped C section stub columns. *Thin-Walled Structures*, 83, 70–84.

Gardner L. (2002). A New Approach to Structural Stainless Steel Design. Doctoral Thesis. Imperial College London.

Gardner L. (2008). The Continuous Strength Method. *Proceedings of the Institution of Civil Engineers – Structures and Buildings*, 161(3), 127–133.

Gardner L. and Ashraf M. (2006). Structural design for non-linear metallic materials. *Engineering Structures,* 28(6), 926–934.

Gardner L. and Nethercot D.A. (2004a). Experiments on stainless steel hollow sections – Part 1: Material and cross-sectional behaviour. *Journal of Constructional Steel Research*, 60(9), 1291–1318.

Gardner L. and Nethercot D.A. (2004b). Experiments on stainless steel hollow sections – Part 2: Member behaviour of columns and beams. *Journal of Constructional Steel Research*, 60(9), 1319–1332.

Gardner L. and Nethercot D.A. (2004c). Numerical modelling of stainless steel structural components – A consistent approach. *Journal of Structural Engineering (ASCE)*, 130(10), 1586–1601.

Gardner L. and Nethercot D.A. (2004d). Structural stainless steel design: A new approach. *Structural Engineer*, 82(21), 21–28.

Gardner L. and Thoufanous M. (2008). Discrete and continuous treatment of local buckling in stainless steel elements. *Journal of Constructional Steel Research*, 64, 1207–1216.

Gardner L., Talja A. and Baddoo N. R. (2006). Structural design of high-strength austenitic stainless steel, *Thin-Walled Structures*, 44(5), 517–528.

Gardner L., Insausti A., Ng K.T. and Ashraf M. (2010). Elevated temperature material properties of stainless steel alloys. *Journal of Constructional Steel Research*, 66(5), 634–647.

Gardner L., Wang F.C., and Liew A. (2011). Influence of strain hardening on the behaviour and design of steel structures. *International Journal of Structural Stability and Dynamics*, 11(5), 855–875.

Greiner R. and Kettler M. (2008). Interaction of bending and axial compression of stainless steel members. *Journal of Constructional Steel Research*, 64, 1217–1224.

Greiner R. and Lindner J. (2006). Interaction formulae for members subjected to bending and axial compression in EUROCODE 3 – the Method 2 approach. *Journal of Constructional Steel Research*, 62(8), 757–770.

Han L.H., Chen F., Liao F.Y., Tao Z. and Uy B. (2013). Fire performance of concrete filled stainless steel tubular columns. *Engineering Structures*, 56, 165–181.

Hill H.N. (1944). Determination of stress-strain relations from "offset" yield strength values, Technical Note No. 927.

Hradil P. and Talja A. (2013). Investigating the role of gradual yielding in stainless steel columns and beams by virtual testing. *Proceedings of The Fifth International Conference on Structural Engineering, Mechanics and Computation*, Cape Town, South Africa, 1459–1464.

Hradil P., Fülöp L. and Talja A. (2012). Global stability of thin-walled ferritic stainless steel members. *Thin-Walled Structures*, 61, 106–114.

Hradil P., Talja A., Real E., Mirambell E. and Rossi B. (2013). Generalized multistage mechanical model for nonlinear metallic materials. *Thin-Walled Structures*, 63, 63–69.

Huang Y. and Young B. (2012). Material properties of cold-formed lean duplex stainless steel sections. *Thin-Walled Structures*, 54, 72–81.

Huang Y. and Young B. (2013a). Experimental and numerical investigation of cold-formed lean duplex stainless steel flexural members, *Thin-Walled Structures*, 73, 216–228.

Huang Y. and Young B. (2013b). Tests of pin-ended cold-formed lean duplex stainless steel columns. *Journal of Constructional Steel Research*, 82, 203–215.

Huang Y. and Young B. (2014a). Experimental investigation of cold-formed lean duplex stainless steel beam-columns. *Thin-Walled Structures*, 76, 105–117.

Huang Y. and Young B. (2014b). The art of coupon tests. *Journal of Constructional Steel Research*, 96, 159–175.

Huang Y. and Young B. (2014c). Structural performance of cold-formed lean duplex stainless steel columns. *Thin-Walled Structures*, 83, 59–69.

Hyttinen V. (1994). Design of cold-formed stainless steel SHS beam-columns. Report 41. University of Oulu, Oulu, Finland.

Islam S.M.Z. and Young B. (2012). Ferritic stainless steel tubular members strengthened with high modulus CFRP plate subjected to web crippling. *Journal of Constructional Steel Research*, 77, 107–118.

Jandera M. and Machacek J. (2014). Residual stress influence on material properties and column behaviour of stainless steel SHS. *Thin-Walled Structures*, 83, 12–18.

Jandera M. and Syamsuddin D. (2014). Interaction formula for stainless steel beam-columns. *Proceedings of the Seventh European Conference on Steel and Composite Structures (EUROSTEEL)*, Napoli, Italy.

Jandera M., Gardner L. and Machacek J. (2008). Residual stresses in cold-rolled stainless steel hollow sections. *Journal of Constructional Steel Research*, 64(11), 1255–1263.

Johnson A.L. and Winter G. (1966). Behaviour of stainless steel columns and beams. *Journal of the Structural Division (ASCE)*, 92(5), 97–118.

Kuwamura H. (2003). Local buckling of thin-walled stainless steel members. *Steel Structures,* 3(3), 191–201.

Lecce M. and Rasmussen K.J.R. (2006). Distortional buckling of cold-formed stainless steel sections: experimental investigation. *Journal of Structural Engineering (ASCE)*, 132(4), 497–504.

Liew A. and Gardner L. (2015). Ultimate capacity of structural steel cross-sections under combined loading. *Structures*, 1, 2–11.

Lindner J. (2003). Design of beams and beam columns. *Progress in Structural Engineering and Materials*, 5(1), 38–47.

Liu Y. and Young B. (2003). Buckling of stainless steel square hollow section compression members. *Journal of Constructional Steel Research*, 59(2), 165–177.

Lopes N., Vila Real P. and Simões da Silva L. (2007). Numerical modelling of the flexural buckling of axially loaded stainless steel members. *Proceedings of the Third International Conference on Steel and Composite Structures ICSCS07*, Manchester, UK.

Lui W.M., Ashraf M. and Young B. (2014). Tests of cold-formed duplex stainless steel SHS beam-columns. *Engineering Structures*, 74, 111–121.

Manninen T. (2011). Structural Applications of Ferritic Stainless Steels (SAFSS): WP1 End-user Requirements and Material Performance. Task 1.3 Characterization of stress-strain behaviour: Technical Specifications for Room-Temperature: Tensile and Compression Testing.

Mirambell E. and Real E. (2000). On the calculation of deflections in structural stainless steel beams: an experimental and numerical investigation. *Journal of Constructional Steel Research*, 54(4), 109–133.

Nip K.H., Gardner L. and Elghazouli A.Y. (2010). Cyclic testing and numerical modelling of carbon steel and stainless steel tubular bracing members. *Engineering Structures*, 32(2), 424–441.

Niu S., Rasmussen K.J.R. and Fan F. (2014). Distortional–global interaction buckling of stainless steel C-beams: Part I: Experimental investigation. *Journal of Constructional Steel Research*, 96, 127–139.

Niu S., Rasmussen K.J.R. and Fan F. (2015). Local–Global Interaction Buckling of Stainless Steel I-Beams. II: Numerical Study and Design, *Journal of Structural Engineering (ASCE)*, 141(8): 04014195.

Quach W.M, Teng J.G and Chung K.F. (2008). Three-stage full-range stress-strain model for stainless steels. *Journal of Structural Engineering (ASCE)*, 134(9), 1518–1527.

Ramberg W. and Osgood W.R. (1943). Description of stress-strain curves by three parameters. Technical Note No. 902. Washington, D.C., USA: National Advisory Committee for Aeronautics.

Rasmussen K.J.R. (2000). Recent research on stainless steel tubular structures. *Journal of Constructional Steel Research*, 54(3), 75–88.

Rasmussen K.J.R. (2001). Full-range stress-strain curves for stainless steel alloys. Research report No. R811. Department of Civil Engineering. The University of Sydney.

Rasmussen K.J.R. (2003). Full-range stress–strain curves for stainless steel alloys. *Journal of Constructional Steel Research*, 59(1), 47–61.

Rasmussen K.J.R. (2006). Design of slender angle section beam-columns by the Direct Strength Method, *Journal of Structural Engineering (ASCE)*, 132(2), 204–211.

Rasmussen K.J.R. and Hancock G.J. (1993a). Design of cold-formed stainless steel tubular members. I: Columns. *Journal of Structural Engineering (ASCE)*, 119(8), 2349–2367.

Rasmussen K.J.R. and Hancock G.J. (1993b). Design of cold-formed stainless steel tubular members. II: Beams. *Journal of Structural Engineering (ASCE)*, 119(8), 2368–2386.

Rasmussen K.J.R. and Hasham A.S. (2001). Tests of X- and K- joints in CHS stainless steel tubes. *Journal of Structural Engineering (ASCE)*, 127(10), 1183–1189.

Rasmussen K.J.R. and Young B. (2001). Tests of X- and K- joints in SHS stainless steel tubes. *Journal of Structural Engineering (ASCE)*, 127(10), 1173–1182.

Rasmussen K.J.R., Burns T., Bezkorovainy P. and Bambach M.R. (2003). Numerical modelling of stainless steel plates in compression. *Journal of Constructional Steel Research*, 59, 1345–1362.

Real E. and Mirambell E. (2005). Flexural behaviour of stainless steel beams. *Engineering Structures* 28(6), 926–934.

Real E., Mirambell E. and Estrada I. (2007). Shear response of stainless steel plate girders. *Engineering Structures*, 29(7), 1626–1640.

Real E., Mirambell E., Arrayago I. and Marimon F. (2012). Structural Application of Ferritic Stainless Steels (SAFSS): WP3: Structural and thermal performance of steel-concrete composite floor systems. Task 3.2: Decking tests in the construction stage. Internal report.

Real E., Arrayago I., Mirambell E. and Westeel R. (2014). Comparative study of analytical expressions for the modelling of stainless steel behaviour. *Thin-Walled Structures*, 83, 2–11.

Rossi B. (2010). Mechanical behaviour of ferritic grade 3Cr12 stainless steel. Part 1: Experimental investigations. *Thin-Walled Structures*, 48, 553–560.

Rossi B. and Rasmussen K.J.R. (2013). Carrying capacity of stainless steel columns in the low slenderness range, *Journal of Structural Engineering (ASCE)*, 139, 1088–1092.

Saliba N. and Gardner L. (2013a). Cross-section stability of lean duplex stainless steel welded I-sections. *Journal of Constructional Steel Research*, 80, 1–14.

Saliba N. and Gardner L. (2013b). Experimental study of the shear response of lean duplex stainless steel plate girders. *Engineering Structures*, 46, 375–391.

Schafer B. and Ádány S. (2006). Buckling analysis of cold-formed steel members using CUFSM: conventional and constrained finite strip methods, *Proceedings of the 18th International Specialty Conference on Cold-formed Steel Structures*, 39–54.

Schafer B. and Pekoz T. (1998). Direct strength prediction of cold-formed steel members using numerical elastic buckling solutions. *Thin-Walled Structures, Research and Developments,* New York, Elsevier, 127–44.

SEI/ASCE 8-02. (2002). Specification for the design of cold-formed stainless steel structural members. American Society of Civil Engineers (ASCE), Reston, US, 2002.

Shifferaw Y. and Schafer B.W. (2012). Inelastic bending capacity of cold-formed steel members, *Journal of Structural Engineering (ASCE)*, 138(4), 468–480.

Talja A. (1997). Development of the use of stainless steel in construction. Test report on welded I and CHS beams, columns and beam-columns. WP 3.1, 3.2 and 3.3. Final Report. VTT Technical Research Centre of Finland.

Talja A. (2002). Structural design of cold-worked austenitic stainless steel. Test results of RHS, top-hat and sheeting profiles. WP 3.1, 3.2 and 3.3. Final Report. VTT Technical Research Centre of Finland, Espoo, Finland.

Talja A. and Hradil P. (2011). Structural performance of steel members: Model calibration tests. SAFSS-WP2 Internal Report. VTT Technical Research Centre of Finland, Espoo, Finland.

Talja A. and Salmi P. (1995). Design of stainless steel RHS beams, columns and beam-columns. VTT Research Notes 1619. VTT Technical Research Centre of Finland, Espoo, Finland.

Tankova T., Simoes da Silva L., Marques L., Rebelo C. and Taras A. (2014). Towards a standardized procedure for the safety assessment of stability design rules. *Journal of Constructional Steel Research*, 103, 290–302.

Theofanous M. and Gardner L. (2009). Testing and numerical modelling of lean duplex stainless steel hollow section columns. *Engineering Structures*, 31(12), 3047–3058.

Theofanous M. and Gardner L. (2010). Experimental and numerical studies of lean duplex stainless steel beams. *Journal of Constructional Steel Research*, 66(6), 816–825.

Theofanous M., Chan T.M. and Gardner L. (2009). Structural response of stainless steel oval hollow section compression members. *Engineering Structures*, 31, 922–934.

Theofanous M., Saliba N., Zhao O., and Gardner L. (2014). Ultimate response of stainless steel continuous beams. *Thin-Walled Structures*, 83, 115–127.

Tondini N., Rossi B. and Franssen J.M. (2013). Experimental investigation on ferritic stainless steel columns in fire. *Fire Safety Journal*, 62, 238–248.

Uy B., Tao Z. and Han L.H. (2011). Behaviour of short and slender concrete-filled stainless steel tubular columns. *Journal of Constructional Steel Research*, 67, 360–378.

Xu M. and Szalyga M. (2011). Comparative investigations on the load-bearing behaviour of single lap joints with bolts stressed in shear and bearing-experimental and simulation. Master Project. University of Duisburg-Essen, Institute for Metal and Lightweight Structures.

Young B. and Ellobody E. (2006). Experimental investigation of concrete-filled cold formed high strength stainless steel tube columns. *Journal of Constructional Steel Research*, 62(5), 484–492.

Young B. and Liu Y. (2003). Experimental investigation of cold-formed stainless steel columns. *Journal of Structural Engineering (ASCE)*, 129(2), 169–176.

Young B. and Lui W.M. (2005). Behaviour of cold-formed high strength stainless steel sections. *Journal of Structural Engineering (ASCE)*, 131(11), 1738–1745.

Young B. and Lui W.M. (2006). Tests on cold formed high strength stainless steel compression members, *Thin-Walled Structures*, 44(2), 224–234.

Yousuf M., Uy B., Tao Z., Remennikov A. and Liew J.Y.R. (2013). Transverse impact resistance of hollow and concrete filled stainless steel columns. *Journal of Constructional Steel Research*, 82, 177–189.

Zhao O., Rossi B., Gardner L. and Young B. (2015a). Behaviour of structural stainless steel cross-sections under combined loading – Part I: Experimental study. *Engineering Structures*, 89, 236–246.

Zhao O., Rossi B., Gardner L. and Young B. (2015b). Behaviour of structural stainless steel cross-sections under combined loading – Part II: Numerical modelling and design approach. *Engineering Structures*, 89, 247–259.

Zhao O., Rossi B., Gardner L. and Young B. (2015c). Experimental and numerical studies of ferritic stainless steel tubular cross-sections under combined compression and bending. *Journal of Structural Engineering (ASCE)*, 10.1061/(ASCE)ST.1943-541X.0001366, 04015110.

Zhao O., Gardner L. and Young B. (2016a). Buckling of ferritic stainless steel members under combined axial compression and bending. *Journal of Constructional Steel Research*, 117, 35–48.

Zhao O., Gardner L. and Young B. (2016b). Behaviour and design of stainless steel SHS and RHS beam-columns, *Journal of Constructional Steel Research*, 106, 330–345.

Zhao O., Gardner L. and Young B. (2016c). Experimental study of ferritic stainless steel tubular beam-column members subjected to unequal end moments. *Journal of Structural Engineering (ASCE)*, 10.1061/(ASCE)ST.1943-541X.0001563, 04016091.

Zheng B., Hua X. and Shu G. (2015). Tests of cold-formed and welded stainless steel beam-columns. *Journal of Constructional Steel Research*, 111, 1–10.

Zhou F. and Young B. (2005). Tests of cold-formed stainless steel tubular flexural members. *Thin-Walled Structures*, 43(9), 1325–1337.

Zhou F. and Young B. (2007). Experimental and numerical investigations of cold-formed stainless steel tubular sections subjected to concentrated bearing load. *Journal of Constructional Steel Research*, 63, 1452–1466.

UNIVERSITAT POLITÈCNICA DE CATALUNYA
BARCELONATECH
Escola de Doctorat

Acta de calificación de tesis doctoral

Curso académico:

Nombre y apellidos

Programa de doctorado

Unidad estructural responsable del programa

Resolución del Tribunal

Reunido el Tribunal designado a tal efecto, el doctorando / la doctoranda expone el tema de la su tesis doctoral titulada _____

_____.

Acabada la lectura y después de dar respuesta a las cuestiones formuladas por los miembros titulares del tribunal, éste otorga la calificación:

☐ NO APTO ☐ APROBADO ☐ NOTABLE ☐ SOBRESALIENTE

(Nombre, apellidos y firma) Presidente/a	(Nombre, apellidos y firma) Secretario/a	
(Nombre, apellidos y firma) Vocal	(Nombre, apellidos y firma) Vocal	(Nombre, apellidos y firma) Vocal

_____, _____ de _____ de _____

El resultado del escrutinio de los votos emitidos por los miembros titulares del tribunal, efectuado por la Escuela de Doctorado, a instancia de la Comisión de Doctorado de la UPC, otorga la MENCIÓN CUM LAUDE:

☐ SÍ ☐ NO

(Nombre, apellidos y firma) Presidente de la Comisión Permanente de la Escuela de Doctorado	(Nombre, apellidos y firma) Secretario de la Comisión Permanente de la Escuela de Doctorado

Barcelona a _____ de _____ de _____